Mid technology potential for RF passive components and antennas

Divya Unnikrishnan

UNIVERSITÉ DE GRENOBLE

THÈSE

Pour obtenir le grade de

DOCTEUR DE L'UNIVERSITÉ DE GRENOBLE

Spécialité : **Optique et Radiofréquences**

Arrêté ministériel : 7 août 2006

Présentée par

Divya Unnikrishnan

Thèse dirigée par **Smail Tedjini** et
codirigée par **Darine Kaddour**

préparée au sein du **Laboratoire LCIS**
dans **l'École Doctorale EEATS**

Potentiel de la technologie MID pour les composants passifs et des antennes

Thèse soutenue publiquement le **26 février 2015**
devant le jury composé de :

M. Didier VINCENT
Pr., Université Jean Monnet, Rapporteur
M. Tchanguiz RAZBAN
Pr., Université de Nantes, Rapporteur
Mme, Odile PICON
Pr., Université Paris-Est Marne-la-Vallée, Examinateur
Mme. Darine Kaddour
MCF, Grenoble INP, Co-directeur
M. Smail Tedjini
Pr., Grenoble INP, Directeur

UNIVERSITÉ DE GRENOBLE

THÈSE

Pour obtenir le grade de

DOCTEUR DE L'UNIVERSITÉ DE GRENOBLE

Spécialité : **Optique et Radiofréquences**

Arrêté ministériel : 7 août 2006

Présentée par

Divya Unnikrishnan

Thèse dirigée par **Smail Tedjini** et
codirigée par **Darine Kaddour**

préparée au sein du **Laboratoire LCIS**
dans **l'École Doctorale EEATS**

Potentiel de la technologie MID pour les composants passifs et des antennes

Thèse soutenue publiquement le **26 février 2015**
devant le jury composé de :

M. Didier VINCENT
Pr., Université Jean Monnet, Rapporteur
M. Tchanguiz RAZBAN
Pr., Université de Nantes, Rapporteur
Mme, Odile PICON
Pr., Université Paris-Est Marne-la-Vallée, Examinateur
Mme. Darine Kaddour
MCF, Grenoble INP, Co-directeur
M. Smail Tedjini
Pr., Grenoble INP, Directeur

Acknowledgements

It is my pleasure and privilege to thank the many people who made this thesis a reality. First and foremost I would like to thank Prof. Smail Tedjini, director of the thesis, for providing me an opportunity to work for a PhD in the laboratory LCIS, Grenoble INP, France.

I would like to express my sincere gratitude towards the co-director of my thesis Dr. Darine Kaddour, for her invaluable assistance, support and enthusiastic guidance with constructive suggestions during my tenure as a PhD candidate. Besides for the academic support, I thank from the bottom of my heart for her generosity and amicable friendship. She has always been patient and encouraging in times of difficulties and supported me with immense care.

I would like to thank my PhD thesis reviewers, Prof. Didier Vincent, Université Jean Monnet and Prof. Tchanguiz Razban, Université de Nantes for reviewing my thesis and helping me improve its quality.

I express my deep gratitude to all the project partners in PLASTRONICS project, for their valuable discussions and time.

I thank Carole Sevyet, Jennyfer Duberville, Florence Galli and Laurent Lefevre for helping me to go through administrative papers and Cedric Carlotti for his IT support. I would like to thank all my colleagues from LCIS, ESISAR and Grenoble INP for their support. I extend my special thanks to Romain Siragusa, Etienne Perret, Yvan Duroc, Pierre Lemaître-Auger, Raji Nair, Gianfranco Andia Vera, Ngoc Minh Trang Vu, Duy Thong Nguyen, Tsitoha Andriamiharivolamena, Mosaab Daiki, Shankar Nawale, Raquel Rodrigues, Marco Garbati, David Hotte and Olivier Rance for the happy moments at work.

I extend my heartfelt thanks to my dear friends, Deepak Baby, Twinkle Joy, Sreekala P.S, Anoob T.A, Divya R, Sujith Raman and Vipin V for their constant encouragement and sincere support throughout my research career.

Last but not the least, I sincerely thank my family and all my teachers for their unconditional support and love without which this wonderful journey would not have been real.

Divya Unnikrishnan

26 February, 2015

Valence, France.

Résumé

Le développement rapide et à grande échelle des systèmes électroniques dans le domaine de l'automobile, du médical, de la logistique, et des télécommunications a engendré de nouvelles contraintes sur les circuits RF (Radio Fréquence) en termes de performances électriques, de fiabilité, de coût, et de taille.

Aujourd'hui, la technologie MID (Molded Interconnect Devices) offre par sa grande souplesse une voie prometteuse dans le domaine des circuits RF. Les composants moulés interconnectés sont des substrats thermoplastiques injectés avec des pistes conductrices directement intégrées à la surface. Les avantages de cette intégration directe sont indéniables: conception de circuits en 3D assurant ainsi une réduction de poids, de taille et de temps d'assemblage, le tout avec une augmentation de la qualité et de la fiabilité des circuits.

Jusqu'à présent, peu de travaux ont été publiés sur les applications de la technologie MID dans le domaine RF. Le travail présenté dans cette thèse est dédié à l'étude du potentiel de la technologie MID pour les applications RF.

Dans ce manuscrit, une introduction brève à la technologie MID, ses méthodes de fabrication, et un état de l'art de ses applications dans différents domaines: l'automobile, le médical, et les télécommunications sont présentés.

Ensuite, un travail dédié à la caractérisation des différents matériaux thermoplastiques en termes de leurs propriétés thermiques et diélectriques a été réalisé. Les résultats de caractérisation ont montré que le thermoplastique LCP (Liquid Crystal Polymer) Vectra E820i offre une très bonne stabilité thermique et les plus faibles pertes diélectriques parmi les autres thermoplastiques caractérisés. La conductivité des métallisations MID des différentes méthodes de fabrication, Laser Direct Structuring (LDS), impression jet d'encre et LSS (Laser Subtractive Structuring) a été également caractérisée. La conductivité mesurée est dix fois inférieure que celle du cuivre massif.

A partir des résultats de caractérisation, un travail de conception et de développement de circuits RF passifs (lignes de transmission, filtres, coupleurs) et d'antennes en MID, réalisés avec trois différentes méthodes de fabrication: LDS, impression à jet d'encre et LSS a été réalisé. Comme les contraintes de fabrication sont différentes d'une méthode à une autre, trois thermoplastiques moulés différents: LCP Vectra E820i, LCP E130i et ABS PC (Acrylonitrile Butadiene Styrene Poly Carbonate) ont été considérés dans l'étude. Les mesures en bon accord avec les simulations sont présentées dans ce manuscrit.

Afin d'évaluer les différentes technologies de réalisation, des lignes de transmission en topologie CPW (coplanaire), microruban et stripline, sont comparées en termes de pertes et de facteur de qualité. Les mesures montrent que les technologies LDS et LSS offrent de très bonnes performances électriques et mettent en évidence le potentiel de la technologie pour les applications RF. En ce qui concerne LSS, un travail sur des thermoplastiques chargés permet d'améliorer le facteur de qualité et de réduire la taille des circuits RF. L'impression jet d'encre présente quant à elle des pertes conductrices plus importantes et serait plus adaptée pour la réalisation des antennes.

Abstract

In recent years, the demand of device miniaturization along with the improved functionality and flexibility in device manufacturing in the field of automotive electronics, medical, logistics, telecommunication, etc. is growing rapidly. The development of MID (Molded Interconnect Devices) technology has extensively opened up a new path to meet this concept to real devices by proving large-scale integration of mechanical and electronic functions in devices. This constant evolution of MID has led to some new constraints to the RF (Radio Frequency) and microwave domain in terms of less number of components and fabrication process steps. This thesis work focused at the study of the compatibility of MID for RF applications by exploiting its advantages for transmission lines, passive filters, directional couplers and antennas realization. So far, few works had been published in the field of RF in combination with MID technology and certainly little work had been done in the study of the performance of the above mentioned RF components based on various MID fabrication technologies.

The thesis begins with a brief introduction to the MID technology and its importance in RF domain. After presenting some published related works on this domain, the thesis work starts with the characterization of various MID substrate materials based on their thermal and dielectric properties. Molded thermoplastic LCP (Liquid Crystal Polymer) Vectra E820i provides good thermal stability and low loss among the other characterized thermoplastics. In addition, characterizations of conductivities of circuit metallization of MID devices were also carried out and MID metallizations shows conductivities which is ten times less than that of copper conductivity.

By exploiting the characterized results of MID materials, the research is proceeded with the design and development of various RF devices such as transmission lines, filters, couplers and antennas on three different molded thermoplastics such as LCP Vectra E820i, LCP E130i and ABS PC (Acrylonitrile butadiene Styrene Poly Carbonate). Three fabrication techniques of MID such as LDS (Laser Direct Structuring), inkjet printing and LSS (Laser Subtractive Structuring) were also taken into study. Choice of substrate materials, fabrication details and design policies of various devices are presented. MID transmission line losses and quality factor based on CPW (coplanar waveguide), microstrip and stripline technologies are studied and compared. LDS in combination with LCP Vectra E820i provides good performances with lower signal loss and high quality factors among others whereas inkjet printed MID circuits presents higher losses. However, inkjet printing technique offers a great potential for MID antennas applications and LDS and LSS offer better electrical performances for propagating devices providing lower losses. Finally, some approaches for the improvement of the dielectric permittivity of MID thermoplastics are presented.

In this PhD work, a high number of RF devices were designed, fabricated and measured. All measurement results are in good agreement with simulations.

Dedicated to my brother

Contents

List of Figures

List of Tables

Résumé étendu en français

Chapitre-1

Introduction

Cette thèse s'inscrit dans le projet de recherche national "PLASTRONICS" dont l'objectif est le développement de la "Technologie d'interconnexion & de report des composants sur pièces plastiques". Ce projet FUI, est labellisé par les pôles de compétitivité : Minalogic, et Plastipolis. Le projet Plastronics est porté par l'industrie ARaymond, et regroupe 11 partenaires industriels et trois laboratoires de recherche. PLASTRONICS vise le développement de composants plastiques injectés intégrant directement des fonctions électroniques sur la surface de la matière plastique. Avec cet objectif, le projet s'articule autour de l'amélioration et la fiabilité des technologies d'interconnexion, le développement d'un outil d'aide à la conception et l'évolution des composants plastroniques existants dans différents domaines d'application tels que l'automobile, télécommunications, la santé, etc. Le fort développement des systèmes de transmission sans fil engendre des contraintes toujours plus fortes sur la taille et les performances des circuits RF (RadioFréquences). C'est dans ce contexte que ce sujet de cette thèse s'intègre. L'objectif de cette thèse est l'étude du potentiel de la technologie MID pour les applications RF.

La technologie MID (Molded Interconnect Devices) permet l'intégration directe de pistes conductrices électroniques sur la surface 2D ou 3D de substrats thermoplastiques moulés. De ce fait, elle offre une voie prometteuse dans le domaine des circuits RF puisqu'elle permet une liberté totale de conception au contraire des circuits imprimés classiques. Aujourd'hui, à part quelques antennes 3D, peu de travaux ont été publiés sur les propriétés et les applications de cette technologie innovante dans le domaine RF, d'où l'objet et la motivation de cette thèse.

Le travail de thèse a donc débuté par un état de l'art sur la technologie MID, ses méthodes de fabrications et ses applications dans différents domaines dans le Chapitre 2 de ce manuscrit. Différents méthodes de fabrication de circuits MID existent et la technologie LDS (Laser Direct Structuring), LSS (Laser subtractive Structuring) et l'impression jet d'encre sont étudiés dans ce manuscrit. Dans le domaine RF, le choix du substrat MID est une étape importante pour la réalisation des circuits électroniques. Ce choix repose sur les propriétés mécaniques, thermiques, et diélectriques du thermoplastique et dépend surtout de la méthode de fabrication. Les propriétés thermiques, diélectriques des thermoplastiques ainsi que les

propriétés électriques des traces métalliques ont fait l'objet du Chapitre 3. A partir de ces résultats de caractérisations, la circuits RF (lignes de transmission, filtres, coupleurs, antennes) en technologie MID ont été conçus, réalisés et mesurés. Ces circuits ont été réalisés avec les différentes méthodes de fabrication: LDS, LDS et jet d'encre. Ce travail est présenté dans les chapitres 4, 5 et 6.

Le chapitre 4 est dédié à la technologie de fabrication LDS. Le thermoplastique LCP (Liquid Crystal Polymer) Vectra E820i a été considéré pour la conception et la réalisation de lignes de transmission, de filtres et d'antennes. La réalisation des lignes de transmission permet de qualifier la technologie en termes de pertes et de facteur de qualité. Les résultats de mesures des lignes de transmission en bon accord avec les simulations donnent des facteurs de qualité 30, 78, and 100 à 1GHz respectivement pour les topologies coplanaire (CPW), microruban et stripline. Ces résultats illustrent le potentiel de la technologie LDS qui donne des résultats comparables à des substrats RF classiques. Par la suite, les résultats de mesure des filtres et des antennes qui assurent un très bon accord avec la simulation sont présentés. A la fin du chapitre, une réalisation d'une antenne PIFA (Planar Inverted F Antenna) intégrée sur une coque 3D avec les résultats de mesure est présentée. Dans le chapitre 5, les circuits réalisés sur ABS PC (Acrylonitrile Butadiene Styrene Poly Carbonate) et LCP E130i par impression jet d'encre sont présentés. Alors que thermoplastique ABS PC présente un bon état de surface, le thermoplastique LCP E130i nécessite une première étape de planarisation avant l'impression à cause de sa rugosité élevée. Les lignes de transmission réalisées par impression jet d'encre présentent dans le meilleur des cas un facteur de qualité 37 à 2 GHz. L'impression jet d'encre présente donc un facteur de qualité plus faible que celui de la technologie LDS, à cause de la faible épaisseur de la métallisation. Malgré ces pertes, les filtres et les antennes réalisées assurent un très bon accord entre les mesures et les simulations.

Le chapitre 6 est consacré à la technologie LSS. Tout d'abord, le thermoplastique classique LCP E130i est considéré pour la réalisation de lignes de transmission. Ces lignes présentent un facteur de qualité 56 à 2 GHz. Afin d'améliorer encore le facteur de qualité en augmentant la permittivité, de nouvelles matières thermoplastiques chargées de charges minérales sont considérées. Avec cette technique, la permittivité obtenue est de l'ordre 8.56 qui permet donc l'augmentation des facteurs de qualité 117 à 2 GHz et la miniaturisation des circuits RF. Les résultats de simulation et de mesure de coupleurs RF sur cette nouvelle matière sont présentés. En dernier, le chapitre 7 présente la conclusion de la thèse. Il résume la thèse avec une description et les perspectives du travail.

Chapitre -2

Etat de l'art

Ce chapitre passe en revue l'état de l'art de la technologie MID. Aujourd'hui, la technologie MID est présente dans différents domaines d'applications comme l'électronique, le médical, et l'automobile. Cette technologie innovante permet l'intégration directe de pistes conductrices électroniques sur la surface 2D ou 3D de substrats thermoplastiques moulés[1]. De ce fait, elle offre une voie prometteuse dans le domaine des circuits électroniques puisqu'elle permet une liberté totale de conception au contraire des circuits imprimés classiques. Fig. 2.1 présente le principe de la technologie MID.

Fig. 2.1 : Principe de la technologie MID[1].

Le concept de cette technologie a été introduit tout d'abord aux Etats-Unis en 1983 et son intérêt industriel développé en 1985[2]. Initialement, le concept de MID n'a pas bien réussi à cause des difficultés de production, mais l'exigence de ce type de produit a continué à augmenter. Dans les années suivantes, certains pays développés comme l'Allemagne et le Japon ont participé au développement des MIDs[1]. Aujourd'hui, le marché MID se développe énormément et beaucoup de grandes entreprises comme BMW, Volkswagen, Siemens ont déjà intégré MID à leurs produits. Dans la littérature, différents composants MID ont déjà introduits sur le marché dans le domaine de l'automobile, le médical et les telecommunications.

Différentes méthodes de fabrication pour la réalisation de circuits en MID existent; la technologie LDS, LSS, l'impression jet d'encre, Micro-tamponnage, Bi-Injection etc. Dans ce manuscrit, la technologie LDS, LSS et l'impression jet d'encre sont étudiés. Le choix du substrat MID est une étape importante pour la réalisation des circuits électroniques. Ce choix repose sur les propriétés mécaniques, thermiques, et diélectriques du thermoplastique et dépend surtout de la méthode de fabrication. Alors que la technologie LDS nécessite

l'utilisation d'un thermoplastique chargé, l'impression jet d'encre requiert un thermoplastique qui présente une faible rugosité. LSS ne présente pas de contraintes particulières.

Comme la thèse a pour objectif l'étude des applications de la technologie MID dans le domaine de la RF, une étude de l'art des composants RF en technologie MID a été menée. Dans la littérature, quelques antennes réalisées en MID ont été publiées. C. Orlob et al[3,4] a présenté plusieurs antennes 3D MID réalisées par LDS tels qu'une antenne patch, et une antenne log-périodique. Ces antennes ont été réalisées sur du Pocan TP 710-003 LDS. Un bon accord entre les mesures et les simulations du coefficient de réflexion et du diagramme de rayonnement a été obtenu pour les antennes réalisées. J. Thevenard et al[5] a présenté ou comparée en termes de performances une antenne vivaldi 3D pour l'application WLAN (wireless local area network) sur le substrat Pocan Poly- Butylene Terephthalate (PBT) et antenne sur substrat classique comme FR4. L'antenne MID présente une large bande passante et un gain supérieur à celui de l'antenne classique.

Ainsi, le potentiel de la technologie MID pour les applications de l'antenne est bien mis en évidence grâce aux réalisations qui viennent d'être cités. Cependant, peu d'informations sur les propriétés diélectriques dans le domaine RF existent. De plus, à part les antennes, et une ligne de transmission, aucun circuit RF en technologie n'a été publié. L'absence ou le peu d'information en termes des propriétés diélectriques des thermoplastiques dans le domaine RF, et le nombre réduit des circuits MIDs RF publiés a motivé ce travail de thèse. Pour toute la conception de circuits RF, la connaissance des propriétés diélectriques des substrats thermoplastiques moulés est vraiment primordiale la caractérisation de divers échantillons MID est présenté in chapitre 3.

---

[1]W.Xu, " Research on key technology of MID," 2nd Pacific-Asia Conference on Circuits, '10.

[2]K. Feldmann et. al, "Three-Dimensional Automatic Routing in Design of Molded Interconnect Devices (MID)," Production Engineering, pp. 65-68, 2003.

[3]D. Kornek et. al, "Experimental Investigation of Bent Patch Antennas on MID Substrate," European Conference on Antennas and Propagation, '10.

[4]C. Orlob et. al, "Dual- Polarized Log.- Periodic Antenna on a Conical MID Substrate," Proceedings of 5th European Conference on Antennas and Propagation, '11.

[5]J. Thevenard et.al, "Switched Beam 3D-Vivaldi Antennas for WLAN Applications," Int. Symposium on Antennas and Propagation '07.

Chapitre-3

Propriétés électriques des matériaux MID

Ce chapitre est consacré à la caractérisation diélectrique et thermique de substrats thermoplastiques et aux mesures des propriétés électriques des métallisations utilisées pour définir les pistes électroniques.

3.1. Caractérisations thermiques et électriques des matériaux MID

Les performances électriques et la fiabilité des circuits RF dépendent fortement des propriétés du substrat et la conductivité de traces métalliques. Dans la plupart des cas, les substrats n'ont pas de propriétés magnétiques et donc leur perméabilité est considérée comme similaire à celui du vide (μ_r = 1). Pour ceci, la caractérisation de la permittivité électrique du substrat est nécessaire.

Le choix des matériaux thermoplastiques comme substrat RF exige des contraintes au niveau des propriétés diélectriques, thermiques et mécaniques. La sélection du thermoplastique dépend de l'application et de la technique de fabrication. Plusieurs thermoplastiques ont été caractérisés dans ce travail : LCP Vectra E820i, LCP E130i, ABS PC Cycoloy C1200HF, ABS PC Xantar LDS 3710, PC LDS Xantar 3730, PBT (PolyButylene Terephthalate) Pocan 7102 LDS, PBT Ultradur B4520, PPA (PolyPhthalAmide) LDS RTP 4099* 117359D et PA (PolyAmide) 66 Ultramid A3K.

3.1.1. Propriétés thermiques des thermoplastiques

L'analyse thermique des thermoplastiques a été réalisée à l'Ecam (Ecole Catholique d'Arts et Métiers) située à Lyon. La 0 (a) représente le banc de test utilisé pour l'analyse thermique par TGA (Thermal Gravimetric Analysis).

L'étude est réalisée sous une atmosphère inerte de travail (N_2) ou le débit d'air de 25°C à 1000 °C pour une masse de l'échantillon de 10 mg. Ici, les échantillons thermoplastiques sont utilisés pour l'analyse thermique et sont fournis par la société Radiall. La 0 (b) montre la dégradation de la masse des échantillons MID LDS en fonction de la température. On peut voir que LCP Vectra E820i présente une stabilité thermique élevée parmi les échantillons testés. Sa température de dégradation est à 511 ^{0}C alors que tous les

autres échantillons se dégradent à des températures inférieures à 450 ^{0}C. Le PBT Pocan 7102 dégrade facilement au 348 ^{0}C. Aussi, LCP Vectra présente moins de pourcentage de la dégradation de la masse par rapport aux autres échantillons. Il garde 60% de masse après la dégradation jusqu'à 1000 ^{0}C, alors que PA66 Ultramid A3K ne détient que 1% de sa masse après dégradation jusqu'à 1000 ^{0}C.

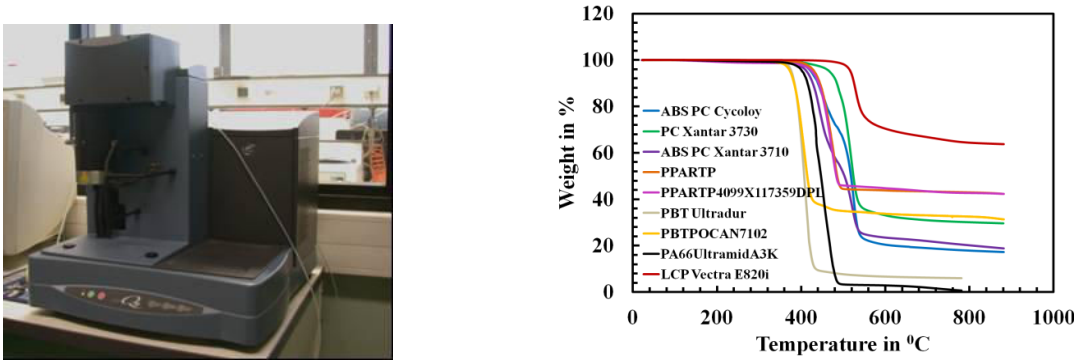

(a) (b)

Fig. 3.1 : L'analyse thermique des matières thermoplastiques LDS MID sous N_2, à 10 ° C / min, (a) photographie de l'équipement de mesure TGA et (b) ses résultats.

3.1.2. Les propriétés diélectriques des thermoplastiques

De nombreuses méthodes pour mesurer la permittivité complexe de matériaux existent. La méthode de la cavité résonante a été choisie pour sa bonne précision. Tous les substrats thermoplastiques sous forme de plaques de dimensions de 10 x 10 x 0.2 cm^3 ont été fournis par le PEP. Les matières LDS moulées considérées (Fig. 3.2) sont faible coût.

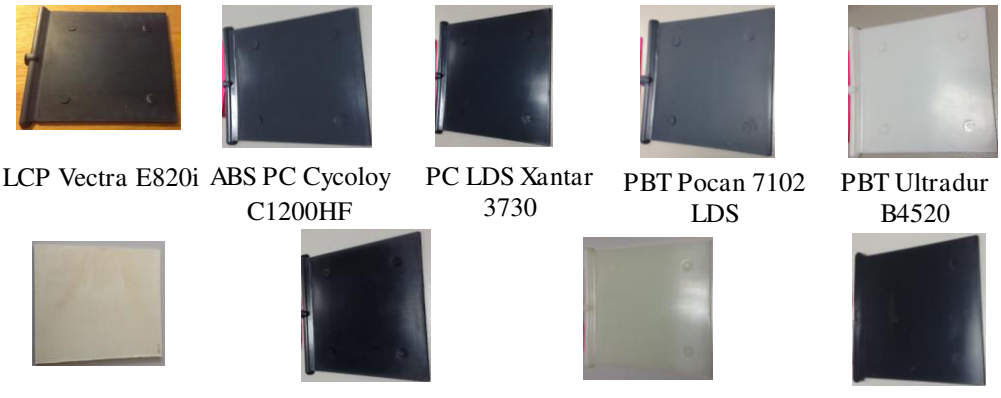

Fig. 3.2 : Photos des plaques des thermoplastiques caractérisés.

La Fig. 3.3 présente la photo de la cavité résonnante. Les substrats ont été caractérisées pour les sept premiers modes impairs TE_{10n} de la cavité résonnante : 0,808 GHz, 1,265 GHz, 1,870 GHz, 2,519 GHz, 3,184 GHz, 3,862 GHz et 4,538 GHz.

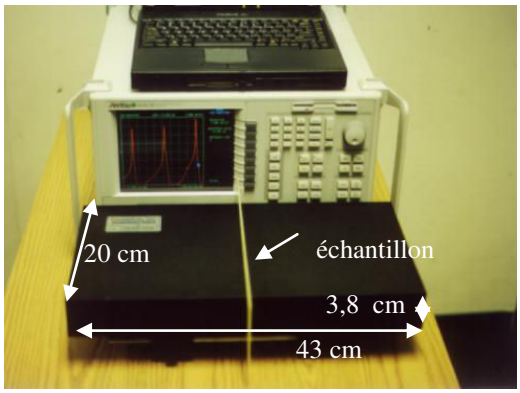

Fig. 3.3 : Photo de la cavité Damaskos.

La Fig. 3.4 présente les propriétés diélectriques de tous les thermoplastiques caractérisés en termes de sa permittivité relative et tangente de pertes. Les valeurs de la permittivité diélectrique des thermoplastiques mesurées montrent une bonne précision de l'extraction jusqu'à 4 GHz. Pour les plus hautes fréquences, la précision de la mesure diminue à cause de la taille des plaques qui ne couvrent pas la section transverse de la cavité. D'après ces mesures, LCP E820i présente la plus faible tangente de pertes de l'ordre de 0,004 avec la plus haute permittivité de l'ordre 4,3. Comme ce substrat possède de faibles pertes et de bonnes propriétés thermiques, il présente un très bon potentiel pour les applications RF.

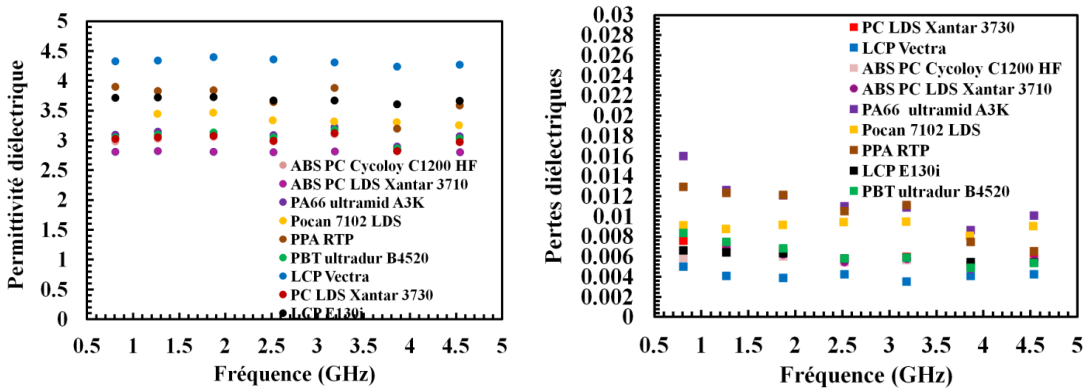

Fig. 3.4 : Propriétés diélectriques des thermoplastiques.

Le paragraphe suivant présente les mesures de conductivité des métallisations des technologies MID.

3.2. Caractérisation électrique des métallisations

La méthode des quatre pointes a été utilisée pour la caractérisation des métallisations. Deux types de métallisations ont été mesurées: encre d'argent pour l'impression jet d'encre et un empilement de Cuivre/Nickel/Or pour les technologies LDS et LSS. La caractérisation électrique de la métallisation en encre d'argent a été réalisée au

EMSE (Ecole Nationale Supérieure des Mines de Saint-Étienne) avec un système de sonde de Jandel et la caractérisation de l'empilement Cuivre/Nickel/Or ont été mesurées par la société Mind.

Le Tableau 3.1 présente la conductivité des d'argent et Cuivre/Nickel/Or pour différentes épaisseurs. La conductivité mesurée est dix fois plus faible que celle du cuivre massif. Si nous considérons les deux fréquences 1 et 2,45 GHz, la profondeur de la peau calculée pour d'argent est de 7,1 μm et 4.5 μm respectivement. Ces valeurs sont supérieures à l'épaisseur de métallisation, ce qui entrainera des pertes conductrices élevées.

Table 3.1: Caractérisation électrique de la métallisation en encre argent et Cuivre/Nickel/Or en fonction de l'épaisseur.

Metallization	**Epaisseur du métal** ***(μm)***	**Résistance carrée** ***(Ω/□)***	**Résistivité** ***(μΩ.cm)***	**Conductivité** **(10^6 S/m)**
Cuivre/Nickel/Or	8	22,8	18	5,48
	10	17	17	5,88
encre d'argent	0,7	150	13,5	7,41
	1,4	98	17,64	5,67
	2,1	45	12,15	4,23

3.3. Bilan

Ce chapitre présente la caractérisation des propriétés thermiques et diélectriques de 9 différents thermoplastiques. Ces mesures ont montré que le LCP vectra E820i présente les plus faibles pertes dielectriques (0.004) et la meilleure stabilité thermiques. Les métallisations des MIDs ont été également caractérisées. Les valeurs optimales mesurées sont de l'ordre de 5 x 10^6 S/m pour la métallisation en encre d'argent avec l'impression jet d'encre et de 5.88 x 10^6 S/m pour l'empilement de Cuivre/Nickel/Or pour les technologies LDS et LSS. Ces caractérisations ont été considérées pour la conception des circuits RF présentés dans les chapitres suivants.

Chapitre-4

Performances RF de circuits MIDs réalisés par LDS

Dans ce chapitre, différents circuits RF (lignes de transmission, filtres, antennes) réalisés sur LCP Vectra E820i avec la méthode LDS sont présentés. Les facteurs de qualité des lignes de transmission réalisées en technologie CPW, microruban et stripline extraits des paramètres S mesurés sont respectivement 31, 75 et 101 à 1 GHz. Comme la technologie LDS permet la réalisation de vias métalisés, le *modèle d'un* via LDS a été developpé. Par la suite, des filtres planaires et trois antennes sont conçus et validés avec des mesures.

4.1. Introduction

A part les antennes, la technologie LDS n'a pas été utilisée pour d'autres applications RF. Ainsi, l'objet de ce chapitre est principalement sur l'étude des propriétés de RF de lignes de transmission LDS, en particulier leurs pertes et leurs facteur de qualité. De plus, l'étude du modèle du via microruban sur LDS est également considérée. Par la suite, des filtres et des antennes RF ont été conçus, fabriqués sur une épaisseur de 2 mm LCP Vectra E820i et mesurés.

4.2. Lignes de transmission LDS

La Fig. 4.1 montre les photographies des lignes de transmission MID sur LCP Vectra E820i réalisés par LDS dans trois topologies différentes : CPW, microruban et stripline.

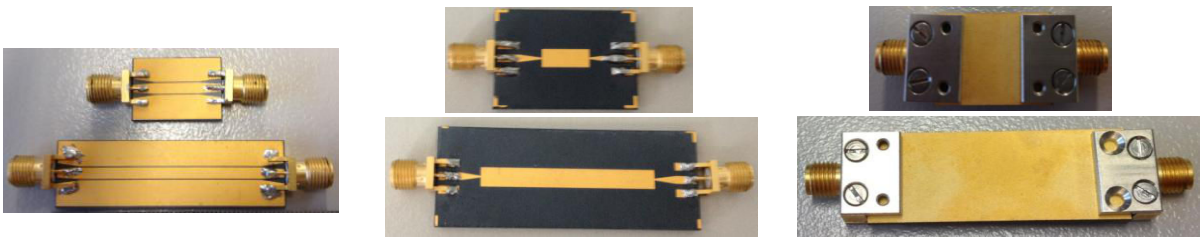

(a) (b) (c)

Fig. 4.1: Lignes de transmission MID sur LCP Vectra E820i, (a) CPW, (b) microruban et (c) stripline.

Les mesures avec calibration electronique ont été réalisées avec l'analyseur vectoriel Agilent N5222A PNA. Pour chaque topologie, deux lignes de transmission de longueurs différentes sont réalisées. Pour les configurations de CPW et microruban, des lignes de

longueur 1 cm et 4 cm sont conçuse alors que pour la configuration stripline, deux lignes de longueur 2 cm et 4 cm sont considérées. Les mesures des paramètres S sont en bon accord avec les simulations. Cette première études confirment le potentiel de la technologie LDS pour la réalisation de lignes de transmission RF. Les propriétés électriques des lignes réalisées comme la constante de propagation, les pertes, facteur de qualité, etc et sont présentés dans les paragraphes suivants.

4.2.1. Performances électriques mesurées

Pour l'extraction précise des propriétés électriques des lignes de transmission, la méthode des deux méthode a été adoptée[1]. Cette méthode permet de s'affranchir des effets des connecteurs et des accés. Comme les lignes de transmission CPW, technologies microruban et stripline de longueur 4 cm présentent respectivement leurs résonances à 3,4 GHz, 3,1 GHz et 2,2 GHz, les résultats extraits sont présentés jusqu'à 4 GHz, parce qu'au delà de la fréquence de résonnance les résultats ne sont pas exploitables.

Les constantes diélectriques effectives extraites des lignes CPW, microruban et de stripline sont respectivement de l'ordre de 2,56, 3,26 et 4,5. Des permittivités relatives de 4,28 et 4,34 ont été extraites à partir des mesures des lignes microruban et CPW à 1 GHz.

A partir des paramètres RLGC, les pertes conductrices et diélectriques sont extraites. Les pertes totales des lignes de transmission LDS mesurées sont inférieures à 0,5 Np/m à 1 GHz (Fig. 4.1(a)). Les lignes de transmission de LDS présentent donc des pertes acceptables et peuvent être utilisés sans problèmes pour les applications RF. Les lignes de transmission MID réalisés par LDS sur LCP Vectra E820i présente un facteur de qualité de 30, 75 et 101 à 1 GHz respectivement pour les topologies CPW, microruban et stripline (Fig. 4.2 (b)).

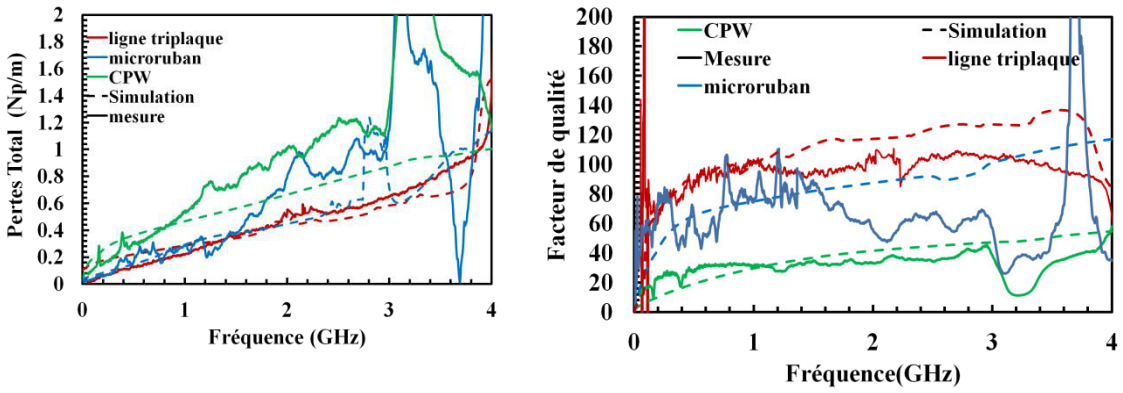

(a) (b)

Fig. 4.2 : (a) Constante d'atténuation (Np/m) et (b) facteur de qualité de lignes de transmission LDS.

En comparant avec les lignes de transmission microruban sur des substrats classiques comme le Rogers RO4003 et un substrat FR4 faible coût, les lignes de transmission LDS microruban présentent un facteur de qualité supérieur les lignes FR4 et plus faible que facteur celui des lignes sur Rogers (Fig. 4.3).

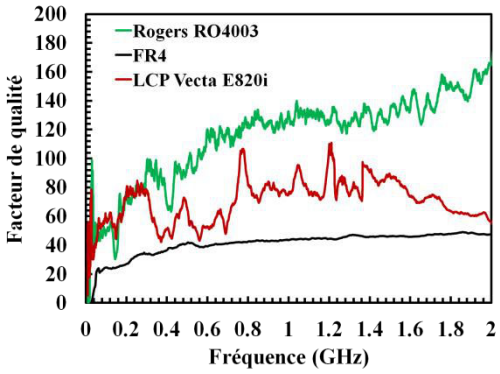

Fig. 4.3 : Comparaison des facteurs de qualité des lignes microruban sur FR4, Rogers RO4003 et LDS LCP Vectra E820i.

À partir de tous ces résultats, la technologie LDS sur LCP Vectra E820i présente un bon potentiel pour les dispositifs RF. Le travail se concentre alors sur la conception et l'analyse de circuits RF sur substrat LDS LCP Vectra E820i tels que les filtres et les antennes. Avant de passer à cette partie, un modèle pour décrire le comportement d'un via LDS qui est élément clé en technologie microruban est developpé dans le paragraphe suivant.

4.3. Modèle du via LDS

Le composant THRU de la méthode de calibrage TRL est considéré comme dispositif sous test (DST) pour l'étude du modèle du via LDS (see Fig. 4.4). Le THRU présente une longueur electrique nulle.

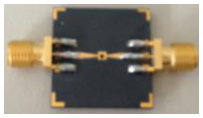

Fig. 4.4 : Photo du DST avec le via LDS.

Un via peut être modélisé par une inductance en série avec une résistance[2]. L'effet de l'inductance parasite augmente avec l'augmentation des fréquences. L'inductance dépend essentiellement du diamètre et de l'épaisseur du via. La résistance parasite théorique calculée varie entre 0,1 à 5,2 Ω de DC à 10 GHz et une valeur de l'inductance théorique de 0,5 nH. La Fig. 4.5 (a) représente le modèle électrique du modèle du DST. Le graphique de la Fig. 4.5 (b) représente la réponse en fréquence du modèle électrique avec une valeur Rvia =2.5 Ω. Comme prévu, le via agit comme un circuit ouvert en basse fréquences avec

une réflexion proche de -5 dB et une mauvaise transmission de -20 dB jusqu'à 1 GHz. Quand fréquence augmente, la réponse du dispositif dégrade.

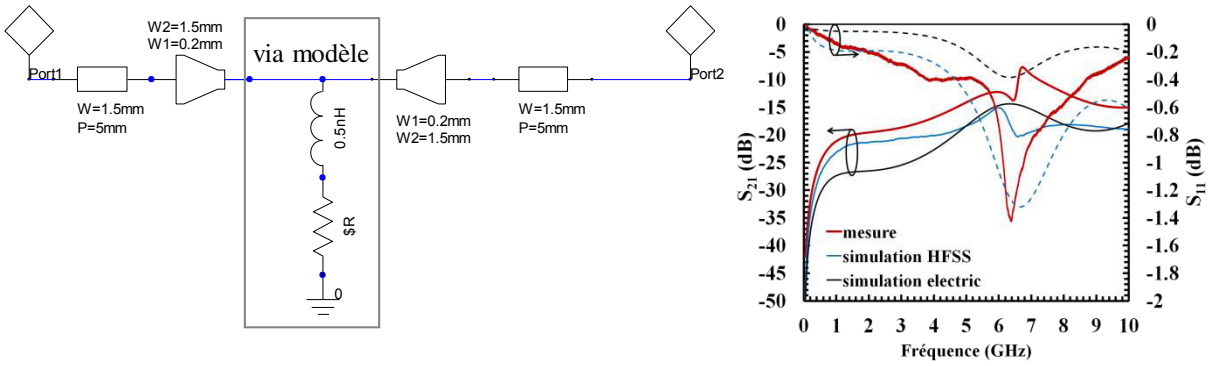

(a) (b)

Fig. 4.5 : (a) Modèle électrique de LDS microruban via and (b) sa réponse en fréquence du S_{21} et S_{11}.

Les résultats de mesures montre que le via LDS présente une bonne qualité et une bonne fiabilité.

4.4. Filtres passifs LDS

4.4.1. Filtres passe-bas

Pour valider le potentiel de MID pour les applications RF, la conception de filtres passe-bas distribués (DLPF) et hybrides (HLPF) sur LCP Vectra E820i dans les deux est menée. Le filtre distribué est un filtre à saut d'impédance basée sur la cascade de tronçons de lignes de haute et de basse impédance. Pour le filtre hybride, la ligne basse impédance est remplacée par des capacités localisés permettant la miniaturisation de la taille du filtre. Les Fig 4.6 (a) et (b) présentent respectivement les photoes du DLPF ($F_{coupure}$ = 2.2 GHz) et HLPF ($F_{coupure}$ = 1.1 GHz) en topologie CPW. Les Fig.4.6 (c) et (d) présentent les photographies des filtres distribués et hybrides en technologie microruban.

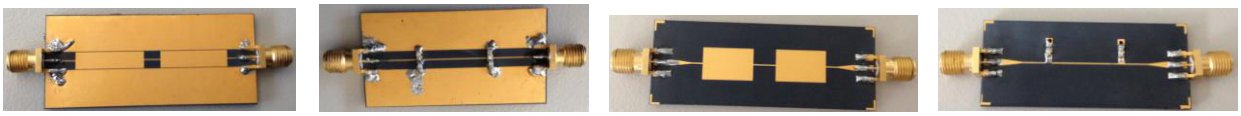

(a) (b) (c) (d)

Fig. 4.6 : Photographie d'un LDS filtres passe-bas sur LCP Vectra E820i, (a) CPW DLPF, (b) CPW HLPF, (c) microruban DLPF and (d) microruban HLPF.

La Fig. 4.7 représente les réponses fréquentielles mesurées des filtre passe-bas sur LDS LCP Vectra E820i en topologie microruban et CPW. Toutes les simulations sont réalisées avec Ansoft HFSS et Ansys. La Fig. 4.7 (a) montre que le DLPF présente une fréquence de coupure de -3 dB à 2,24 GHz, la perte par reflexion sont meilleures que -9 dB, avec des pertes d'insertion de l'ordre 0,6 dB dans la bande passante. L'adaption peut etre améliorée avec une mesure TRL qui permet de s'affranchir des accés et des connecteurs. Les tracés en vert de la Fig 4.7.(a) montrent en effet que l'adaptation est meilleure que -15 dB dans la bande passante. Les lobes secondaires à -20 dB aparaissent à 4,7 GHz.

La Fig. 4.7 (b), le filtre hybride en CPW présente une fréquence coupure de 1,1 GHz, adaptation meilleure que -12 dB, et des pertes de 0,3 dB dans la bande passante. L'adaptaion mesurée avec le calibrage TRL (graphes en vert) montre que l'adaptation est meilleure que -17 dB. Les lobes secondaires sont rejetés plus loin que 5 GHz.

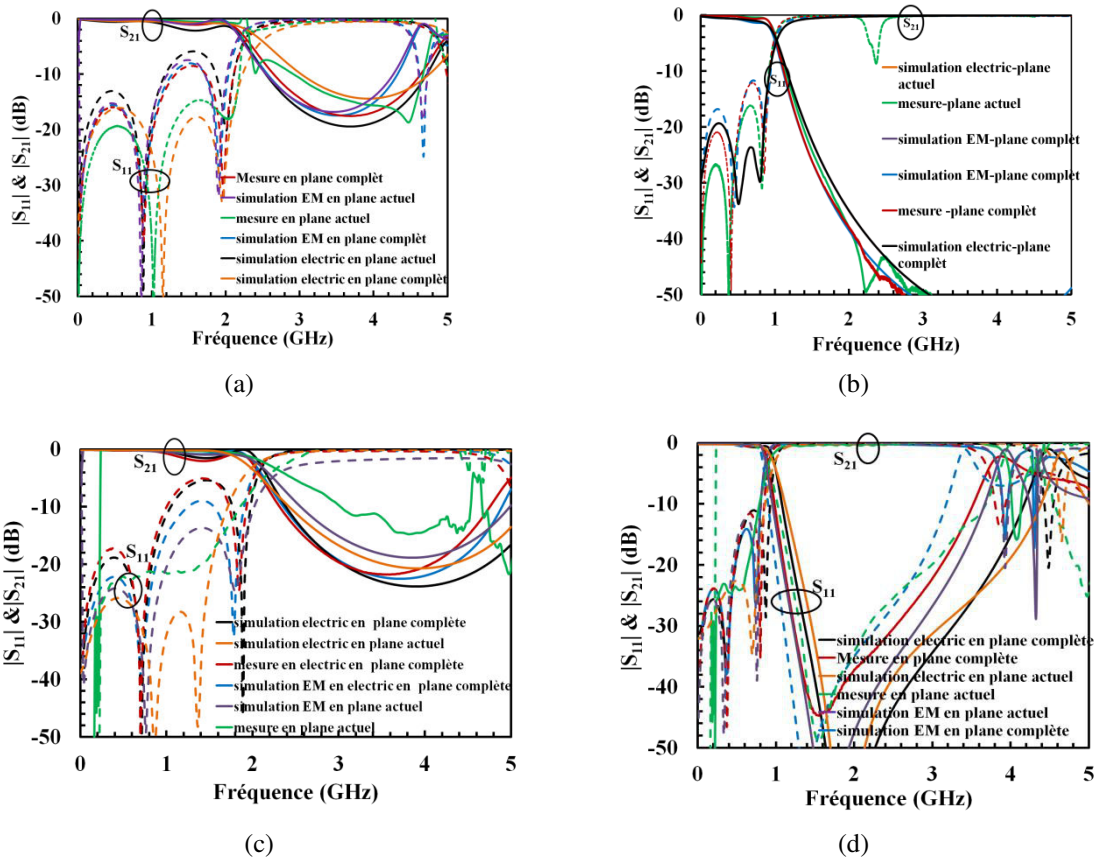

Fig. 4.7 : S paramètres de filtres CPW (a) CPW DLPF, (b) CPW HLPF, (c) microruban DLPF and microruban HLPF.

Pareil, pour le filtre microruban distribué, les résultats de mesure présentés sur la Fig. 4.7 (c), montrent une adaptation de -5 dB et des pertes d'insertion de 2 dB. En appliquant le calibrage TRL (graphes en vert) afin de se placer dans les bons plans du filtre, la

fréquence de coupure mesurée est de 1,9 GHz. Avec le calibrage TRL, une adapatation de -20 dB est obtenue tout au long de la fréquence avec des pertes d'insertion de 0,26 dB.

Les résultats de mesure du filtre microruban distribué de fréquence de coupure 1 GHz sont montrés sur la Fig. 4.7 (d). Avec le calibrage électronique, les pertes de réflexion de -15 dB et des pertes d'insertion de 0,62 dB sont mesurées. Les mesures TRL de ce filtre (en vert) présentent une adaptation meilleure que -25 dB et les lobes parasites sont rejetés à -20 dB à 3,5 GHz, qui est 3,5 fois la fréquence de coupure.

4.4.2. Filtres passe-bande

Les filtres passe-bandes étudiées sont basés sur les topologies suivantes : Dual Behavior Resonator (DBR) et hair pin filter.

Le principe du filtre DBR est basé sur l'association en parallèle de deux tronçons de ligne de transmission. Cette topologie permet de contrôler les zéros de transmission autour de la bande passante recherchée. Un filtre DBR centré à 5,2 GHz a été conçu et fabriqué par LDS sur un substrat LCP E820i (Fig. 4.8 (a)). La simulation et la mesure sont présentése sur la Fig. 4.8 (b). Un bon accord entre la simulation et la mesure est obtenu avec une léger décalage de la fréquence centrale ce qui peut être dû à l'effet des connecteurs et à la précision de la réalisation. Les pertes d'insertion mesurées sont de -1,78 dB et les pertes de reflexion sont de -18 dB. Les zéros de transmission sont mesurés à 4.68 GHz et à 7,03 GHz.

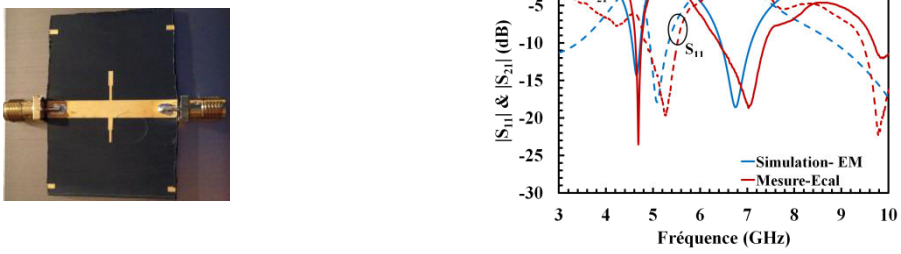

(a) (b)

Fig. 4.8 : Filtre DBR sur LCP Vectra E820i, (a) photo and (b) réponse en fréquence.

Le filtre passe bande du quatrième ordre en topologie hair pin centré à 5,8 GHz est conçu et fabriqué sur LDS LCP Vectra E820i (Fig. 4.9 (a)).

Ce filtre est basé sur le principe des résonateurs demi-onde couplés. Le principal avantage de ce filtre est l'utilisation optimale de l'espace. La réponse de ce filtre dépend de la longueur de la zone couplée, l'espace entre chaque bras et la largeur de ligne. Les réponses de simulation et de mesures sont présentées sur la Fig. 4.9 (b). Le filtre présente une fréquence

centrale de 5,8 GHz et une bande passante de 150 MHz. Les pertes d'insertion sont de -1,93 dB et les pertes de reflexion de -10 dB sont mesurées.

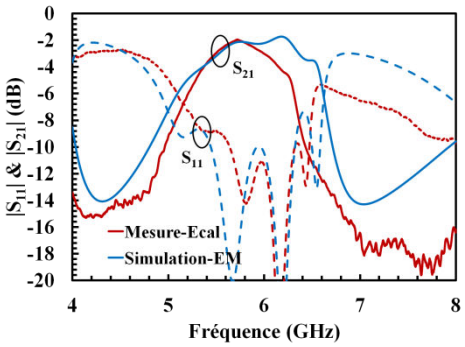

(a) (b)

Fig. 4.9 : Filtre passe-bande on LCP E820i, (a) photo and (b) réponse en fréquence.

La technologie MID est donc validée pour des circuits tels que les filtres. La section suivante présentera des circuits rayonnants en MID.

4.5. Antennes LDS

Après une brève étude d'une antenne patch microruban planaire sur substrat LDS LCP Vectra E820i, une étude d'intégration en 3D a été considérée. L'étude est concentrée sur la conception d'une antenne patch 3D en deux parties et une véritable antenne tridimensionnelle PIFA (Planar Inverted F Antenna).

En raison du coût élevé des moules 3D, une simple antenne patch réalisée en 2 parties a été considérée. Les 2 parties planaires ont été collées ensemble en utilisant du ruban de cuivre avec des angles 0^0 et 45^0 (Fig. 4.10).

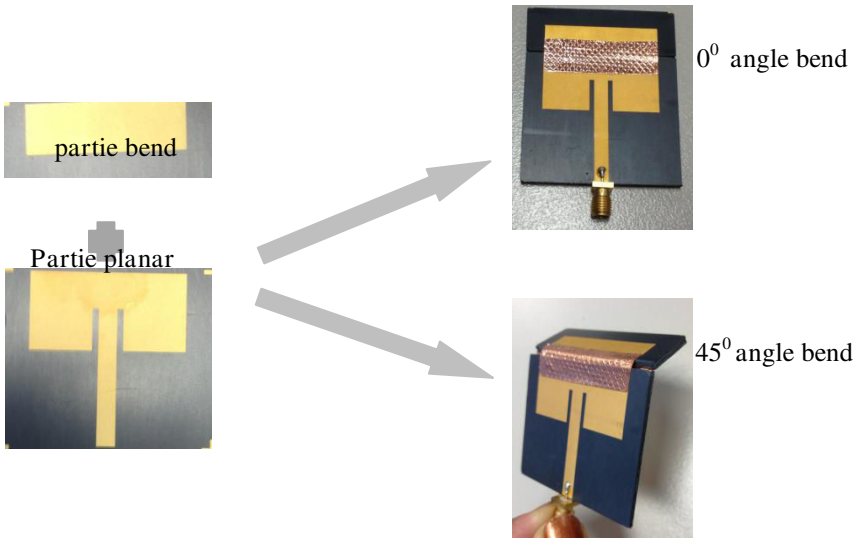

Fig. 4.10 : Antenne bend patch microruban sur LCP Vectra E820i.

La Fig. 4.11 présente la réponse du coefficient de reflexion mesurée dans les angles 0^0 et 45^0. Le coefficient de réflexion présente un bon accord entre la mesure et des simulations pour les deux angles de pliage. En effet, l'augmentation l'angle conduit à un décalage de la résonance à des fréquences plus élevées en raison de la présence de la capacité localisée au niveau du coude. Les résultats de mesure du diagramme de rayonnement montrent un écart de 0,3 dB et 1 dB respectivement pour les angles 0^0 et 45^0. Cet écart peut etre expliqué par la sensibilité de cette configuration lorsque l'antenne tourne.

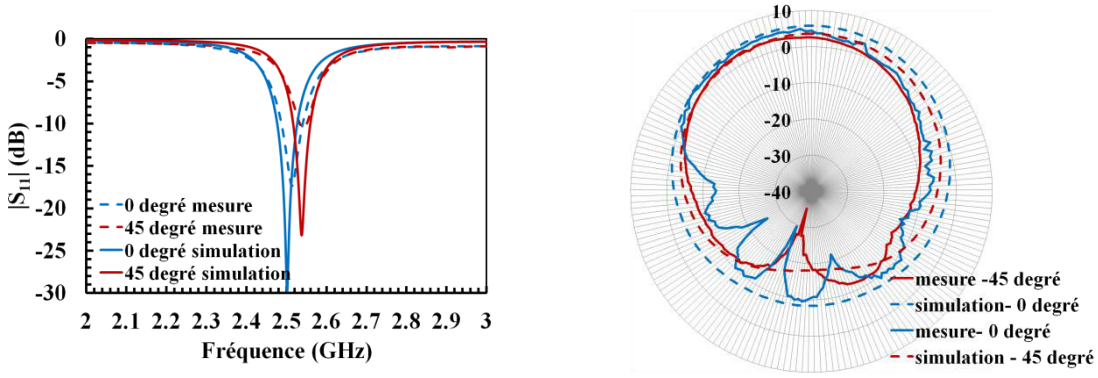

(a) (b)

Fig. 4.11 : Microruban bend antennes patch réponse, (a) coefficient de réflexion en dB and (b) leur diagramme de rayonnement.

Une première réalisation en 3D de l'antenne MID a été étudiée à travers les antennes patch microruban ci-dessus. Une conception originale d'une antenne 3D PIFA a par la suite été réalisée. L'antenne PIFA est placée sur la face externe d'une coque thermoplastique LCP Vectra E820i et le plan de masse est placé à la face interne du thermoplastique comme indiqué dans Fig. 4.12.

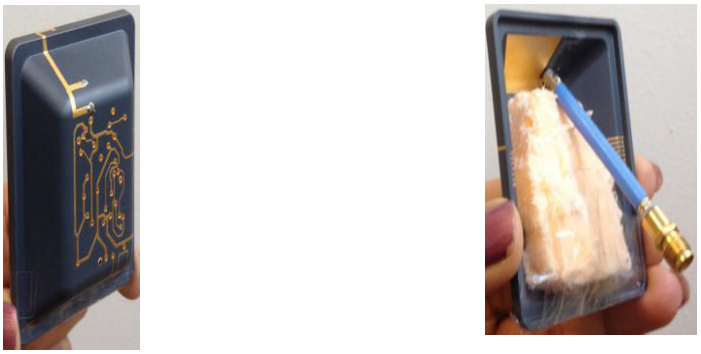

Fig. 4.12 : Antenne PIFA en trois dimensions sur LCP Vectra E820i

Les simulations ont été réalisées avec Ansoft HFSS et les mesures ont été effectuées en utilisant le calibrage Ecal. Comme le montre la Fig. 4.13, la fréquence de résonance

mesurée est décalée vers les basses fréquences par rapport à la simulation. L'antenne a été initialement conçue pour 2,45 GHz et les résultats de mesure montrent une fréquence de réponse à 2,185 GHz avec meilleurs une adaptation meilleure 15 dB. Cette variation entre la simulation et la mesure peut être dû à l'effet de connecteur et à la présence du circuit électronique dense à proximité de l'antenne, étant donné que dans la simulation, l'antenne a seulement été prise en compte. La fréquence de résonance mesurée est considérée pour la mesure du diagramme de rayonnement. L'antenne fabriquée fournit un gain maximum de 1,2 dB avec un diagramme de rayonnement omnidirectionnel. Les résultats des mesures confirment donc la validation de la technologie MID dans la conception des antennes trois dimensions.

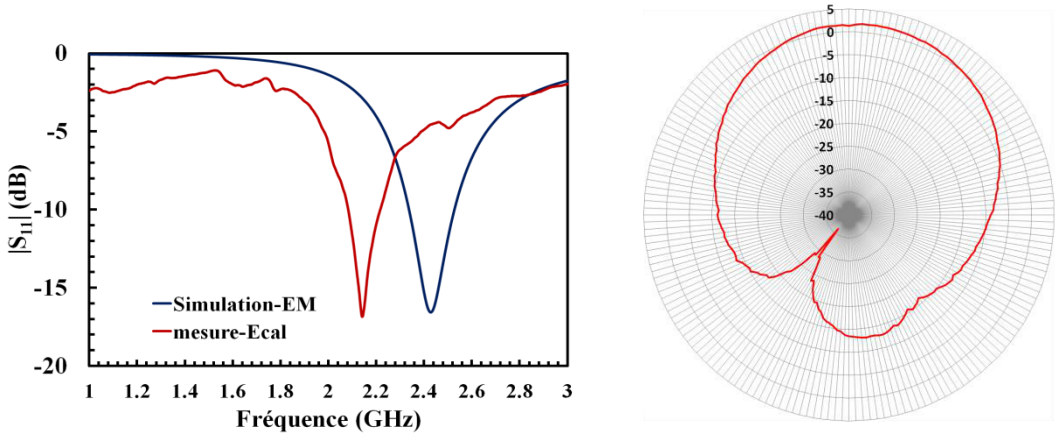

(a) (b)

Fig. 4.13 : Réponse simulée et mesurée de l'antenne PIFA 3D sur LCP Vectra E820i LDS par la fabrication, (a) coefficient de réflexion en dB and (b) diagramme de rayonnement mesuré.

A partir des résultats présentés dans ce chapitreon peut facilement conclure que la technologie MID en association avec la technique de fabrication LDS est bien compatible avec la conception de circuits RF.

4.6. Conclusion

Dans ce chapitre, le thermoplastique LCP Vectra E820i a été choisi en raison de sa stabilité haute température, forte permittivité relative (ε_r = 4,3) parmi tous les autres substrats testés et de faibles pertes diélectriques (tan δ = 0,004). Des lignes de transmission MID sont conçues et fabriqués en topologies CPW, microruban et stripline. Une extraction continue de fréquence de la permittivité relative, les pertes et les facteurs de qualité ont été réalisés. Les résultats de mesure extraits donnent une permittivité effective de 2,56, 3,26 et 4,5 de CPW,

microruban et stripline respectivement et la permittivité relative de 4,28 et 4,34 respectivement CPW et lignes microruban. Les mesures montrent que la ligne CPW présente un faible facteur de qualité de 31, alors que microruban et le stripline présentent des facteurs de qualité de 75 et de 101 respectivement à 1 GHz. De plus, le modèle d'un via microruban a été étudié. Ensuite, des filtres RF planairees et des antennes planaires et 3D ont été conçus et fabriqués sur LCP Vectra E820i. Tous les dispositifs réalisés assurent bon accord avec les résultats de simulation et des propriétés comparables à celles des circuits RF classiques mettant ainsi en évidence le potentiel de la technologie LDS pour les applications RF.

---

[1]A. M. Mangan, S. P. Voinigescu, M. T. Yang and M. Tazlauanu, "De-Embedding Transmission Line Measurements for Accurate Modeling of IC Designs," IEEE Transactions on Electron Devices, vol. 53, pp. 235-241, February 2006.

[2]M. E. Goldfarb and R.A. Pucel, "Modelling Via Holes Ground in Microstrips,"IEEE Microwave and Guided Wave Letters, vol.1, no.6, June 1991.

Chapitre-5

Circuits *MID RF réalisés par impression jet d'encre*

Ce chapitre présente les performances de circuits RF réalisés par impression jet d'encre sur MID utilisant deux thermoplastiques différents: ABS PC et LCP E130i planarisé. La première partie de ce chapitre est consacrée à l'étude des pertes et du facteur de qualité des lignes de transmission microruban et CPW *imprimées par jet d'encre* sur ABS PC. Les pertes conductrices sont dominantes pour les deux topologies en raison de la faible épaisseur de la métallisation qui entraine un effet de peau. Par la suite, une antenne coplanaire large bande est conçue et réalisée par impression jet d'encre sur ABS PC. Les mesures sont en bon accord avec les simulations. La deuxième partie de ce chapitre démontre la compatibilité du substrat LCP pour l'électronique imprimée après une étape de planarisation sur la base des performances des lignes de transmission et des filtres passe-bas sur LCP planarisés .

5.1. Introduction

Ce chapitre est consacré à l'étude de la technologie d'impression jet d'encre sur deux thermoplastiques différents: l'ABS PC et le LCP E130i. La bonne résistance thermique du PC ajoutée la flexibilité de l'ABS font de l'ABS PC qui est un thermoplastique faible coût un bon candidat pour les applications MID. De plus, l'ABS PC présente un très bon état de surface compatible avec les techniques d'impression. Par contre, le LCP E130i présente une rugosité plus importante et nécessite une étape de planarisation pour le rendre compatible avec les techniques d'impression. Tous les circuits ont été fabriqués par EMSE.

5.2. Circuits RF sur ABS PC

Impression jet d'encre

La technique d'impression jet d'encre est effectuée avec imprimante (Ceraprinter, série X) avec des têtes d'impression de 30 pl. Une encre avec des particules d'argent 40% de Sun Chemicals (Réf 5714) est utilisée. Trois couches d'encre conductrices ont été nécessaires pour améliorer les performances électriques. Entre deux couches successives, une étape de séchage dans un four classique à 130°C pendant 10 minutes a été nécessaire. L'étape de frittage final est réalisée à 130°C pendant 30 minutes et la couche métallique finale sur ABS PC présente une conductivité électrique de $5x10^6$ S/m pour une épaisseur totale de 4,5 um.

Lignes de transmission imprimées par jet d'encre

Des lignes de transmission en CPW et microruban ont été réalisées sur ABS PC d'épaisseur 2 mm. Les mesures de toutes les lignes de transmission ont été faites avec un calibrage électronique utilisant l'analyseur vectoriel de réseaux: Agilent N5222A PNA. Les Fig. 5.1 (a) et (b) représentent respectivement les photographies de deux lignes de transmission d'impédance 50 Ω de longueurs 2 et 4 cm en topologie CPW et microruban.

(a) (b)

Fig. 5.1: Lignes de transmission sur MID ABS PC.

La méthode des deux lignes utilisée dans le chapitre 4 a été pareil adoptée pour l'extraction de paramètres électriques. Les paramètres S mesurés des lignes de transmission ont été pris en compte afin d'en extraire la permittivité relative du substrat dans le domaine fréquentiel continu. La permittivité relative de l'ABS PC extraite des paramètres S dans une plage de fréquence allant de 0,5 GHz à 5 GHz est tracée sur la Fig. 5.2. L'extraction de la cavité de mesure est limitée à des fréquences supérieures à 5 GHz à cause de la taille réduite des échantillons. La comparaison entre la valeur de permittivité obtenue à partir des mesures des lignes CPW et microruban et les résultats obtenus à partir de la cavité résonnante est présentée un bon accord avec une valeur moyenne de la permittivité de 2,8 et une variation qui ne dépasse pas 3% sur la gamme de fréquence (Fig. 5.2).

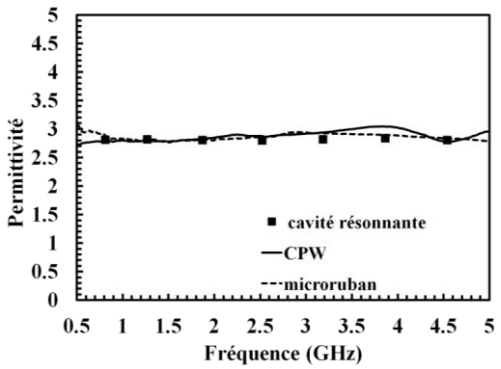

Fig. 5.2: Permittivité diélectrique de l'ABS PC obtenue par la méthode de la cavité résonante et des paramètres S des lignes de transmission CPW et microruban.

Les paramètres S mesurés des lignes en CPW et microruban ont été utilisés pour l'extraction des pertes et du facteur de qualité. La Fig. 5.3 (a) montre que les pertes conductrices sont prédominantes par rapport aux pertes diélectriques. Les pertes diélectriques augmentent proportionnellement avec la fréquence et 0,28 Np/m et 0,2 Np/m obtenues à 2 GHz respectivement pour la ligne CPW et microruban, alors que les pertes conductrices atteignent 2 Np/m et 0,7 Np/m. Les pertes conductrices peuvent être réduites en augmentant l'épaisseur du métal. En effet, l'épaisseur de peau est de 7 µm à 2 GHz (Fig. 5.3 (b)) alors que l'épaisseur de la métallisation est de 4,5 µm ce qui explique les pertes conductrices élevées de la ligne de jet d'encre imprimée. La Fig. 5.3 (c) montre que le extrait facteur de qualité à 2 GHz est de 10,5 et 32 respectivement pour la ligne CPW et lignes microruban qui est inférieur à celui de la ligne LDS.

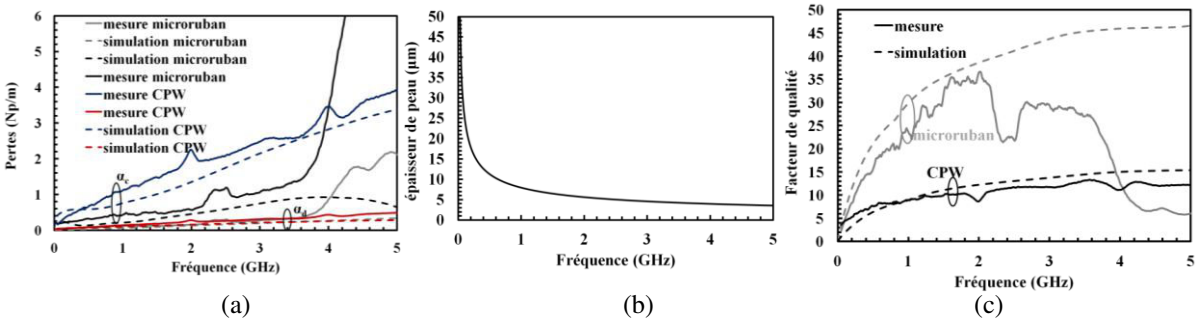

(a) (b) (c)

Fig. 5.3: (a) Les pertes extraites des mesures et des simulations des lignes imprimées CPW et microruban (b) l'épaisseur de la peau, (c) Facteur de qualité.

Antennes MID imprimées par jet d'encre sur ABS PC

Après l'étude des performances des lignes imprimée et une antenne patch classique sur ABS PC, une antenne CPW ULB (ultra large bande) a été conçue, réalisée et mesurée sur ABS PC d'épaisseur 2 mm (Fig. 5.4 (a)). L'antenne se compose d'un demi-disque circulaire avec des pas tapérisés pour améliorer l'adaptation d'impédance dans toute la bande passante.

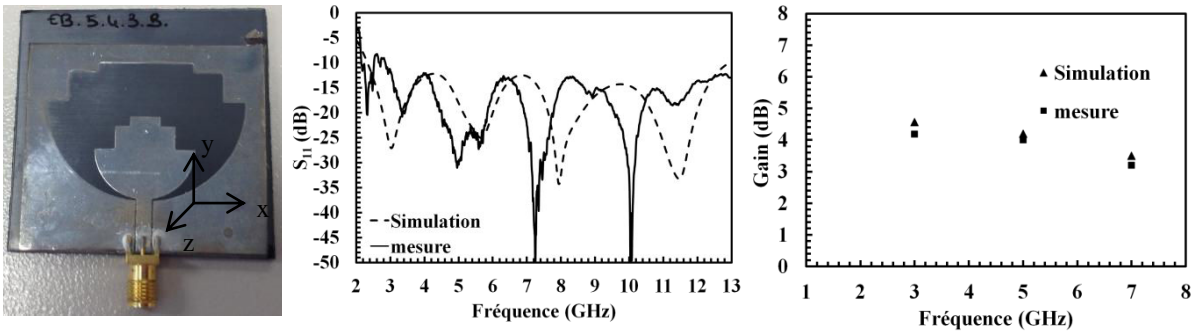

(a) (b) (c)

Fig. 5.4 : Antenne ULB sur ABS PC, (a) photo, (b) coefficient de réflexion, and (c) gain.

Le coefficient de réflexion mesuré (Fig. 5.4 (b)) est meilleur que -10 dB sur toute la bande allant de 3 GHz à 13 GHz couvrant ainsi la totalité de la bande de fréquence ULB. L'écart entre les mesures et les simulations est dû à l'effet de connecteur et de la précision de réalisation. Quatre résonances qui sont directement reliées à la distribution du courant sont observées dans la réponse. Les diagrammes de rayonnement mesurés sont omnidirectionnels dans le plan H et présente un minimum dans le plan E et gain maximal obtenu est de 4,2 dB (Fig. 5.4 (c)). Lorsque la fréquence augmente, les modes d'ordre supérieur sont excités qui se traduit par une déformation au niveau du diagramme de rayonnement. Ces résultats prouvent donc que l'impression jet d'encre offre un grand potentiel pour les antennes ULB.

5.3. Circuits RF sur LCP E130i

5.3.1. Planarisation du LCP E130i

Comme le thermoplastique LCP E130i présente une rugosité de surface importante (jusqu'à 8-9 µm), une étape de planarisation de surface est nécessaire pour réussir à imprimer un circuit électrique de bonne qualité. Différentes étapes ont été effectuées pour réduire la rugosité de surface. La planarisation du substrat permet d'avoir une bonne qualité de la ligne et d'éviter les coupures. La Fig. 5.5 montre des photographies de motifs imprimés sur LCP avec et sans planarisation.

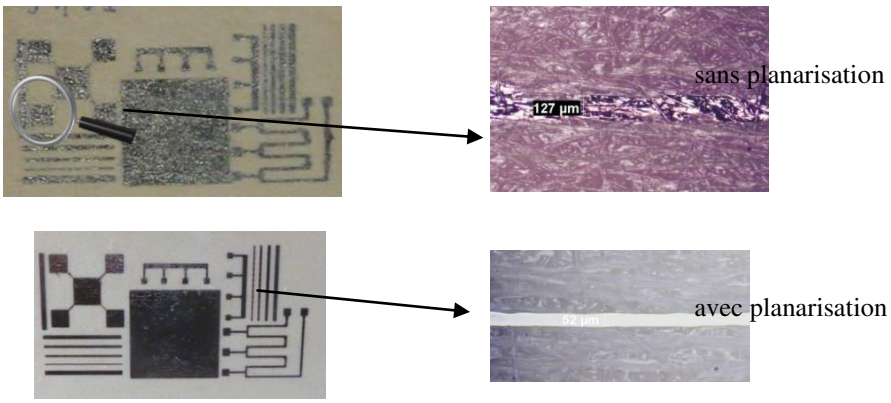

Fig. 5.5 : Photographies d'un LCP imprimée avec et sans planarisation.

5.3.2. Lignes de transmission sur LCP E130i planarisé

Fig. 5.6 (a) et (b) respectivement montre deux séries de 50 Ω lignes de transmission microruban avec un simple couche et double couches de métallisation de longueurs de 5 cm et 2 cm. Chaque couche a une épaisseur de 700 nm. La température choisie pour le séchage de l'encre conductrice d'argent est de 200 °C pendant 30 min. Pour étudier l'origine des pertes, les pertes diélectriques et conductrices ont été calculées à partir des paramètres RLGC

extraits des paramètres S mesurés. La Fig. 5.7 (a) montrent que les pertes conductrices contribuent sont prédominantes. En effet, les lignes de transmission avec une et deux couches présentent) respectivement des pertes conductrices de 1,5 Np/m et 1 Np/m à 2 GHz. De plus, ces lignes de transmission présentent des pertes conductrices élevées par rapport à ceux des lignes microruban LDS LCP Vectra E820i (0,25 Np/m à 2 GHz) et des lignes de transmission imprimées par jet d'encre sur ABS PC (0,7 Np/m à 2 GHz).

(a) (b)

Fig. 5.6 : Des lignes de transmission microruban sur LCP E130i planarisé avec différentes épaisseurs de métallisation (a) avec 0,7 µm, et (b) avec 1,4 um.

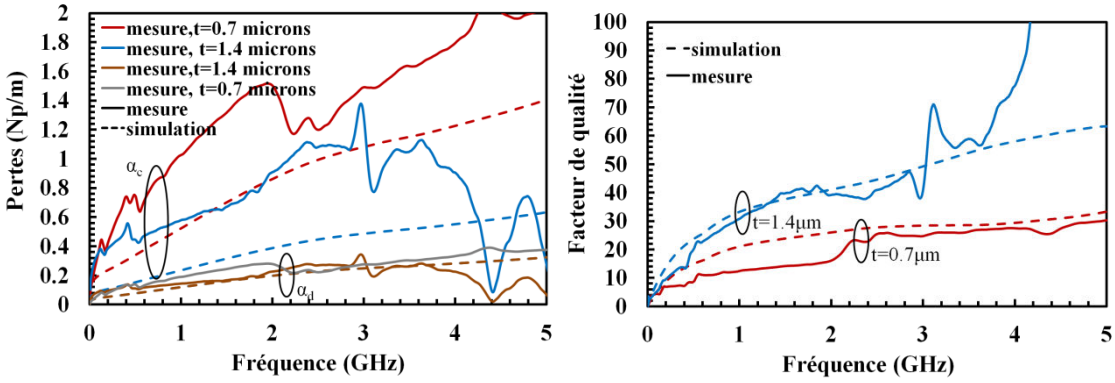

(a) (b)

Fig. 5.7 : (a) Pertes and (b) facteur de qualité des lignes de transmission microruban imprimées sur LCP E130i planarisé avec une épaisseur de métal de 0.7µm et 1,4 um.

La Fig. 5.7 (b) présente les facteurs de qualités extraits des lignes réalisées. Les valeurs mesurées à 2 GHz sont de 17 et 37 respectivement pour les lignes de transmission simple et double couche. Le facteur de qualité peut être amélioré avec des couches plus épaisses de métallisation.

5.3.3. Filtre passe-bas sur LCP E130i planarisé

La Fig. 5.8 (a) montre la photographie du filtre passe-bas (surface 38 x 34 mm^2) à saut d'impédance réalisé est fabriqué LCP planarisé. La mesure a été effectuée à l'aide de l'analyseur vectoriel PNA N5222A d'Agilent avec un calibrage électronique et les

simulations ont été effectués avec Ansys HFSS. Les pertes de réflexion mesurées dans le plan des connecteurs sont meilleures que -12 dB (Fig. 5.8 (b)). La simulations dans le plan du filtre permet d'améliorer l'adaptation de -17 dB. Ces résultats des mesures prouvent à compatibilité de la technologie d'impression à jet d'encre pour la réalisation des circuits RF.

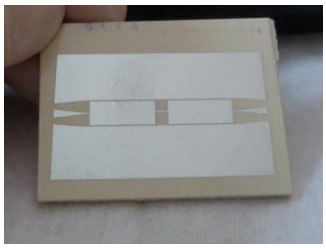

(a)

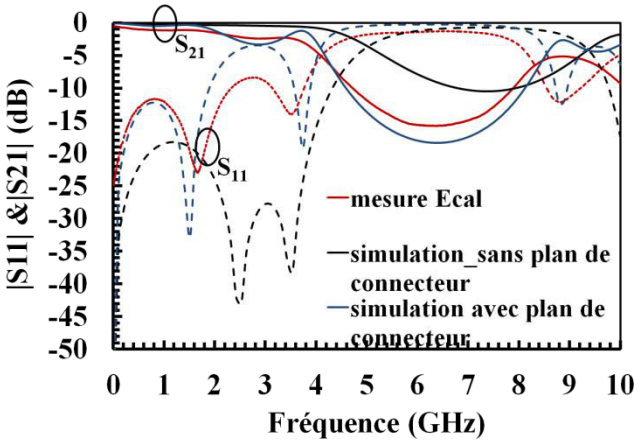

(b)

Fig. 5.8 : Filtre passe-bas Distribué sur planarisée LCP E130i, (a) photo and (b) paramètres S mesurés et simulés.

5.4. Conclusion

Dans ce chapitre, le potentiel de l'impression jet d'encre pour les applications RF en utilisant deux substrats ABS PC et LCP E130i planarisé a été mis en évidence. La caractérisation RF des lignes de transmission CPW et microruban sur ABS PC permettent d'extraire une permittivité relative de l'ordre de 2,8. Les pertes conductrices sont plus importantes que les pertes diélectriques à cause de la faible épaisseur de métallisation. Les facteurs de qualité mesurés à 2 GHz des lignes le CPW et le microruban sont de 10 et 32. Par la suite, une antenne ULB imprimée sur ABS PC a été conçue et réalisée. L'antenne présente un coefficient de réflexion meilleur que -10 dB dans la bande de fréquence allant de 3 GHz à 13 GHz avec un gain maximum de 4,2 dB. La deuxième partie de ce travail de recherche porte sur la planarisation du substrat LCP E130i pour le rendre compatible avec la technologie de l'impression jet d'encre. Des lignes de transmission et un filtre passe-bas à saut d'impédance réalisés sur le substrat LCP planarisé présentent un bon accord entre les mesures et les simulation. Les lignes de transmission sur LCP planarisé présente un facteur de qualité de 37 à 2 GHz (pour une double couche de métallisation). Les résultats présentés dans ce chapitre prouvent ainsi le potentiel de l'impression jet d'encre pour la réalisation de circuits RF démonstrateurs (avec plus de pertes que les autres technologies) et surtout des antennes RF.

Chapitre-6

Dispositifs RF réalisés par LSS sur MID

Ce chapitre présente la conception, la fabrication et la caractérisation de circuits RF réalisés avec la technique d'ablation laser (LSS) sur deux substrats *différents. Tout d'abord, le* thermoplastique LCP E130i est considéré pour la réalisation de lignes de transmission afin *d'étudier les performances électriques de l'ablation laser. Les* lignes de transmission microruban *d'impédance caractéristique de 50 Ω sur LCP E130i* présentent des pertes conductrices inférieures de 0,35 Np/m à 2 GHz ce qui conduit à un facteur de qualité élevé de 56 à 2 GHz. Ensuite, une étude de l'amélioration de la permittivité des matières thermoplastiques en ajoutant des charges complexes. Avec cette technique, un nouveau matériau avec une permittivité de 8,5 a été fabriqué et a servi de support pour la réalisation de lignes de transmission et de coupleur directionnel. Le facteur de qualité des lignes de transmission sur ce nouveau matériau atteint 117 à 2 GHz. Ces bonnes performances électriques font de ce substrat un excellent candidat pour les circuits RF miniatures.

6.1. Introduction

L'ablation laser nécessite l'utilisation d'un substrat entièrement métallisé et permet d'éliminer la métallisation au moyen d'un faisceau laser pour former le motif souhaité. Ce procédé de fabrication est approprié pour les circuits à haute densité métallique. Comme le LCP tient la stabilité thermique la plus élevée, le LCP E130i est utilisé pour la réalisation de lignes de transmission à l'aide de la méthode d'ablation laser. La deuxième partie de ce chapitre introduit la méthode d'addition de charges complexes dans un matériau pour augmenter sa permittivité. Avec cette méthode, un nouveau matériau de permittivité 8,5 a été créé et a été utilisé pour la réalisation de lignes et de coupleurs miniaturisés.

6.2. Propriétés de ligne de transmission microruban sur LCP E130i

Deux lignes de transmission microruban d'impédance 50 Ω ont été conçus et mesurés sur LCP E130i (Fig. 6.1 (a)). La permittivité du LCP E130i de 3,65 et sa tangente de perte de $6{,}10^{-3}$ obtenus avec la cavité résonante ont été utilisés pour la conception initiale. Les paramètres S mesurés des deux lignes de longueur 2 et 4 cm sont utilisés pour l'extraction des

propriétés électriques. La permittivité diélectrique effective extraite de l'ordre de 2,8 ce qui donne une valeur de la permittivité diélectrique relative de 3,7 (Fig. 6.1 (b)). Un écart de 5% entre la valeur mesurée à l'aide de la cavité résonnante, et la valeur extraite à partir des mesures des paramètres S peut être observé au-delà de 3 GHz. Cet écart est peut être dû à l'erreur de la mesure avec la cavité à cause de la taille de la plaque de LCP.

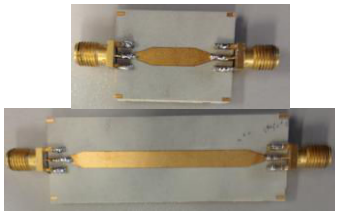

(a)

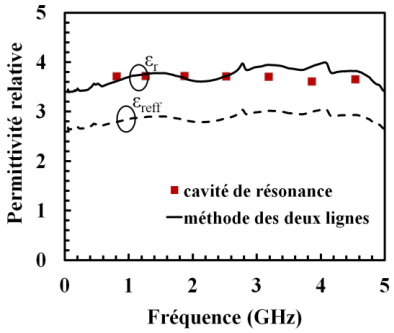

(b)

Fig. 6.1: (a) Lignes de transmission sur LCP E130i réalisées par ablation laser et (b) permittivité du LCPE130i.

Les pertes diélectriques (0,35 Np/m à 2 GHz) mesurées sont plus élevées que les pertes conductrices (0,24 Np/m à 2 GHz) (Fig. 6.2 (a)). La Fig. 6.2 (b) présente le facteur de qualité extrait par rapport à la fréquence. Un facteur de qualité de 56 est observé à 2 GHz. Ce facteur de qualité est légèrement inférieur à celui des lignes de transmission microruban LDS sur LCP Vectra E820i (facteur Q = 61 à 2 GHz). En effet, le LCP E130i présente des pertes diélectriques plus élevés et une plus faible permittivité que le LCP Vectra E820i.

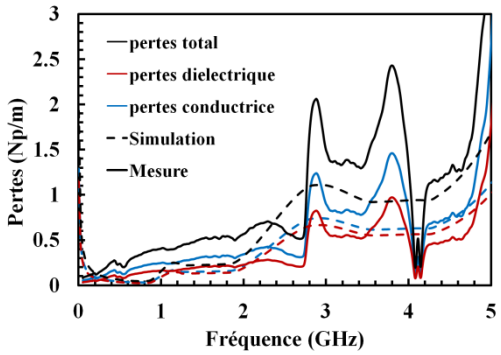

(a)

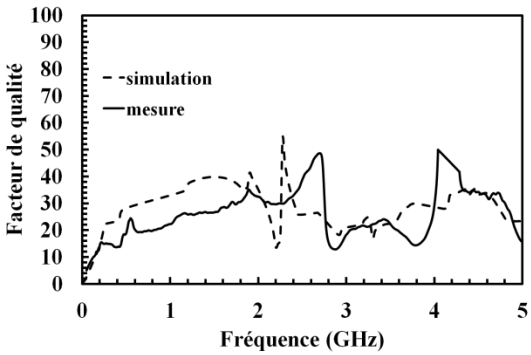

(b)

Fig. 6.2: Propriétés électriques des lignes de transmission sur LCP E130i réalisées par ablation laser (a) pertes (b) facteur de qualité.

6.3. Amélioration de la permittivité de matériaux thermoplastiques

Cette partie présente la caractérisation de trois matériaux thermoplastiques comme le PS (polystyrène), et le PE (polyéthylène) dont la permittivité a été améliorée en ajoutant des charges minérales. Afin d'augmenter la permittivité du PE et PS, des charges d'alumine (Al_2O_3) sont utilisés. Les propriétés diélectriques du thermoplastiques PS et PE avec un pourcentage de 15% et 30% d'Al_2O_3 ont été mesurées. La Fig. 6.3 montre les échantillons de PE et PS.

(a) (b)

(c) (d)

Fig. 6.3: Matériaux thermoplastiques caractérisées (a) PE avec15% d'Al_2O_3, (b) PE avec 30% d'Al_2O_3, (c) PS avec 15% d' Al_2O_3 et (d) PS avec 30% d'Al_2O_3.

Les caractérisations diélectriques ont été faites pour les trois premières fréquences de résonances: 0,815 GHz, 1,280 GHz et 1,891GHz. Pour l'échantillon de PE, la permittivité passe de 2,31 à 3,12 à la troisième fréquence de résonance lorsque la concentration des charges passe de 15% à 30% (Fig. 6.4 (a)). De même, pour l'échantillon PS, les permittivités mesurées sont de 2,88 et 3,22 respectivement pour 15% et 30% d'Al_2O_3 (Fig. 6.4 (b)). L'augmentation de la permittivité est ainsi pouvée pour l'addition des charges d'Al_2O_3.

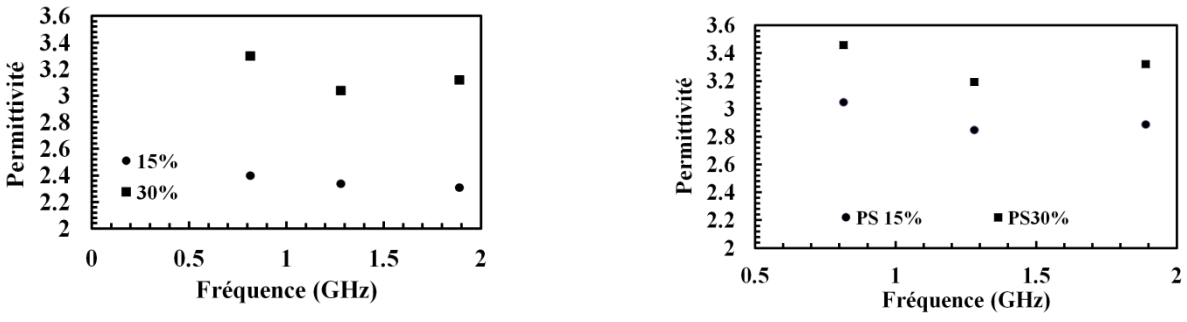

(a) (b)

Fig. 6.4: Permittivités diélectriques de matériaux thermoplastiques avec les charges d'Al_2O_3, (a) PE et (b) PS.

Un nouveau matériau dont la nature doit rester confidentielle a été créé pour le projet Plastronics. La Fig. 6.5 (a) montre une vue d'une plaque de 10 x10 x0.2 cm^3 de dimensions. La partie réelle de la permittivité mesurée de ce nouveau matériau en utilisant la méthode la cavité résonante présente une valeur de 8,5 (Fig. 6.5 (b)). La tangente de pertes mesurée ne dépasse $7x10^{-3}$ dans la bande de fréquences de 0,8 à 1,89 GHz. Cet échantillon présente une valeur de permittivité élevée par rapport à tous les autres substrats thermoplastiques présentés dans cette thèse. Ces propriétés diélectriques mesurées font de ce nouveau polymère un excellent candidat pour la conception des circuits RF miniatures. Ces propriétés diélectriques de l'échantillon ont été exploitées et sont considérées pour la conception de lignes de transmission en microruban et coupleurs miniaturisés.

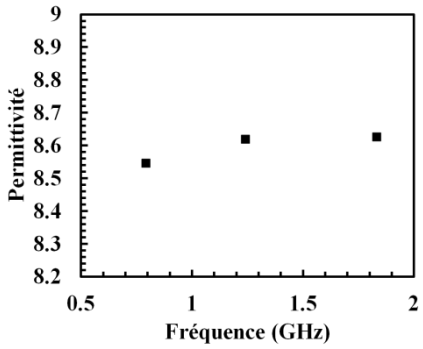

(a) (b)

Fig. 6.5 : Le substrat thermoplastique, (a) la plaque caractérisée (b) partie réelle de la permittivité relative.

6.3.1. Lignes de transmission

La Fig. 6.6 (a) montre deux lignes de transmission microruban de 50 Ω de longueur 2 cm et 5 cm réalisées sur le nouveau substrat de haute permittivité par ablation laser. A partir des paramètres S mesurés, la permittivité, les pertes et le facteur de qualité ont été extraits à l'aide de la méthode des deux lignes de transmission. La permittivité diélectrique effective extraite est de l'ordre de 5,5 ce qui donne une permittivité diélectrique relative de 8,6. En comparaison avec le substrat LCP Vectra LDS classique, avec une permittivité effective pour des lignes microruban de 2,48, une miniaturisation de 55% peut être obtenue avec ce nouveau substrat.

La Fig. 6.6 (b) présente les pertes des lignes de transmission mesurées et simulées sur ce nouveau thermoplastique. Vers la fréquence de résonance, l'extraction des pertes est moins précise. Les pertes diélectriques sont prédominantes sur les pertes conductrices en raison de la tangente de pertes. Les pertes conductrices sont de 0,33 Np/m alors que les pertes diélectriques de 0,36 Np/m sont extraites à 2 GHz. Le facteur de qualité mesuré à

1 GHz est de 117 (Fig. 6.6 (c)). Ce facteur de qualité est le meilleur obtenu pour les lignes microruban en technologie MID. En effet, les lignes de transmission microruban réalisées par LDS sur LCP Vectra E820i et par ablation laser sur LCP E130i présentent un facteur de qualité respectivement 61 et 56 à 1 GHz . En raison de l'augmentation des pertes au-dessus de 3 GHz, le facteur de qualité est réduit en conséquence.

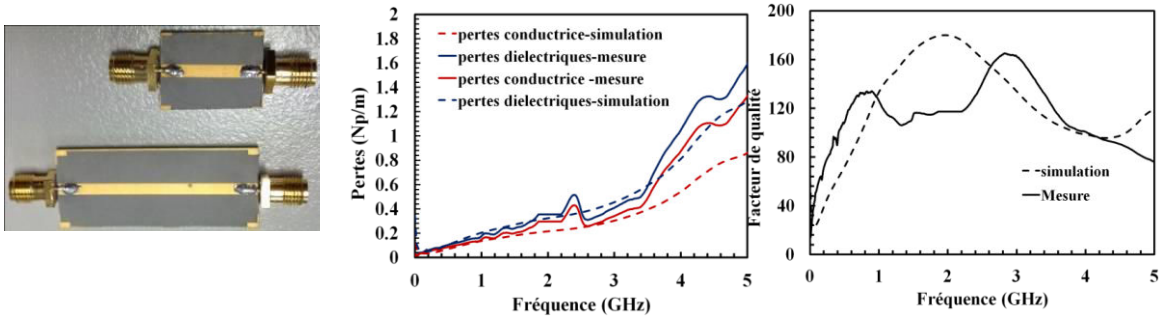

(a) (b) (c)

Fig. 6.6 : Lignes de transmission microruban sur le nouveau thermoplastique, (a) photo, (b) pertes (c) facteur de qualité.

Par conséquence, la technique d'ablation laser combinée avec ce nouveau thermoplastique de haute permittivité offre un bon potentiel pour la conception de circuits RF miniatures. Afin d'exploiter ce bon facteur de qualité, des coupleurs RF sont conçus et réalisés.

6.3.2. Coupleurs directionnels sur MID

Deux coupleurs directionnels à -10 dB avec une fréquence centrale de 1 GHz à 1 section et 3 sections sont réalisés sur le thermoplastique de haute permittivité. La topologie considérée est celle des lignes couplées (Fig. 6.7)

(a) (b)

Fig. 6.7 : (a) Coupleur 1 section et (b) Coupleur 3 sections

Les mesures des coupleurs sont en bon accord avec les résultats de simulation HFSS Ansys. Un facteur de couplage de -10,7 dB et -10,82 dB est obtenu à 1 GHz respectivement pour le coupleur à une section et trois sections. L'écart par rapport au couplage de -10 dB peut être dû à la tolérance de fabrication et à l'effet des connecteurs. Les deux coupleurs

présentent une bonne adaptation d'impédance avec un coefficient de réflexion meilleure que -20 dB. Les pertes d'insertion principalement dues à des pertes diélectriques n'excèdent pas 0,7 dB à 1 GHz dans les deux cas. L'isolation mesurée pour les deux coupleurs est meilleure que -15 dB sur toute la bande de fréquence complète de 0,2 GHz à 2 GHz. Si nous comparons la taille du coupleur à une section avec un coupleur simulé sur LCP Vectra E820i LDS, une miniaturisation de 21% de la longueur et 43% de largeur peut être réalisée. Ainsi, ces résultats ont mis en évidence le potentiel de la technique d'ablation laser avec des substrats haute permittivité.

6.4. Conclusion

Ce chapitre a été consacré à l'étude la compatibilité de la technique d'ablation laser pour les applications RF. Tout d'abord, des lignes de transmission microruban d'impédance 50 Ω sur LCP E130i présentent un facteur de qualité de 56 à 2 GHz. Par la suite, l'amélioration de la permittivité des thermoplastiques comme le PE et le PS par l'addition de charges minérale a été démontrée. Avec cette technique, un nouveau thermoplastique avec une permittivité de 8,5 et une perte de tangente de $7x10^{-3}$ a été introduit. Deux lignes de transmission microruban de 50 Ω ont été réalisées par ablation laser sur ce nouveau matériau. Le facteur de qualité mesuré est de 117 à 1 GHz. Ce substrat fournit un facteur Q par rapport à toutes les autres lignes réalisées, prouvant ainsi le fort potentiel de cette technologie. Par la suite, deux coupleurs directionnels centrés à 1GHz avec un couplage de l'ordre de -10 dB ont été réalisés et évalués. Un bon accord est obtenu entre mesure et de simulation des résultats, validant ainsi le potentiel de ce nouveau matériau compatible avec l'ablation laser pour la réalisation de composants RF MID miniaturisés.

Chapitre-7

Conclusion

L'objectif de cette thèse est l'étude de la compatibilité de la technologie MID dans le domaine de la RF. Cette thèse a permis de réaliser un état de l'art sur la technologie MID, ses méthodes de fabrication et ses applications dans le domaine différent.

Un premier travail de caractérisation des thermoplastiques moulés est présenté dans le chapitre 3. Les thermoplastiques caractérisés pour les propriétés diélectriques et thermiques sont les suivants: LCP Vectra E820i, LCP E130i, ABS PC Cycoloy C1200HF, ABS PC Xantar LDS 3710, PC LDS Xantar 3730, PBT Pocan 7102 LDS, PBT Ultradur B4520, PPA LDS RTP 4099* 117359D et PA 66 Ultramid A3K. Parmi tous ces thermoplastiques, c'est le LCP Vectra E820i qui présente les pertes diélectriques les plus faibles (0,004) et la plus haute permittivité de autour de 4,4 tout en assurant une grande stabilité thermique. Une brève étude de la conductivité des métallisations MID, une combinaison de nickel, de l'or et du cuivre et de l'encre d'argent, a également été réalisée. Les mesures montrent que la conductivité est de l'ordre de 10^{06} S/ m, ce qui est dix fois plus faible que la conductivité du cuivre massif.

Toutes ces propriétés électriques et thermiques des thermoplastiques se sont révélées très intéressantes pour concevoir les circuits RF. Par la suite, le travail a été entrepris dans l'étude de la compatibilité de la technologie MID avec trois méthodes de fabrication MID différentes : LDS, l'impression jet d'encre et LSS. Le Chapitre 4 a été consacré à l'étude des performances RF de la technologie LDS. Le LCP Vectra E820i, en raison de sa haute stabilité thermique et ses bonnes propriétés électriques, a été choisi pour la conception de circuits RF. Des facteurs de qualité de 31, 75 et 101 sont respectivement obtenus à 1 GHz pour des lignes 50 Ω en topologies CPW, microruban et stripline. Les lignes LDS montrent facteur de qualité supérieur à celui des lignes classiques sur FR4 et inférieur à celui du substrat RF de le Rogers RO4003. Par la suite, conception et l'analyse des dispositifs passifs tels que des 2D antennes, une antenne PIFA 3D et les filtres en technologie LDS ont été réalisés. Tous les circuits réalisés en LDS présentent un très bon accord avec les simulations.

Le Chapitre 5 est dédié à la technique d'impression jet d'encre. Le thermoplastique faible coût ABS PC a été sélectionné pour ses propriétés mécaniques et thermiques prometteurs. Les mesures des lignes de transmission 50 Ω CPW et microruban ont permis l'extraction de la permittivité relative, les pertes de RF et le facteur de qualité. Les pertes

conductrices mesurées sont supérieures aux pertes diélectriques. Afin de réduire les pertes par conduction, l'épaisseur de la métallisation doit être augmentée. Par la suite, une antenne patch microruban et une antenne ULB ont été conçues et réalisées. Les mesures sont en bon accord avec les simulations électromagnétiques. Ensuite, le travail s'est consacré à l'étude de la compatibilité du thermoplastique LCP E130i avec la technique d'impression par jet d'encre. Or, la rugosité de surface du LCP est élevée (8-9 μm). Pour ceci, une étape de planarisation a été nécessaire avant de passer à l'impression des circuits électriques. Cette technique a permis de réaliser des lignes de transmission et des filtres passe-bas dont les réponses fréquentielles se sont révélées en très bon accord avec les simulations. La méthode LSS a été également étudiée dans ce travail de thèse. Le chapitre 6 présente les circuits RF réalisés par ablation laser sur le substrat LCP E130i. Les lignes microruban réalisées par LSS sur le substrat LCP E130i résultats présentent un facteur de qualité de 56 à 2 GHz. Dans ce chapitre, une étude de l'amélioration de la permittivité diélectrique des thermoplsatique par l'addition de charges minérale a été considérée. Avec cette technique, un nouveau thermoplastique avec une permittivité de 8,5 et une perte de tangente de $7x10^{-3}$ a été introduit. Ce nouveau matériau a permis la conception réussie de lignes de transmission et coupleurs directionnels miniaturisés.

En conclusion, ce travail de thèse a mis en évidence le potentiel de la technologie MID qui ouvre grâce à sa souplesse une nouvelle voie prometteuse pour les applications RF. L'impression jet d'encre peut offrir malgré ses pertes élevées une solution pour la réalisation de démonstrateurs rapides et faibles coût. Cette technique reste bien adaptée pour la réalisation des structures réfléchissantes comme les antennes. Pour les circuits dans lesquels il y a de la propagation, il vaut mieux privilégier les méthodes LDS et LSS qui présentent un meilleur facteur de qualité. Ce travail a permis de quantifier les performances electriques des MIDs dans le domaine RF à travers des circuits basiques comme les lignes de transmission, les filtres, les coupleurs et les antennes. A la suite de ce travail, de nombreuses perspectives peuvent être envisagées. Nous pouvons citer :

1. le développement de connecteurs intégrés en MID afin d'éviter l'étape de soudure et de report de connecteur qui peut être un frein au développement de la technologie MID.
2. la création d'une bibliothèque de composants MID suivant les différentes méthodes pour faciliter la conception des systèmes RF complets.
3. l'utilisation d'encres conductrices de meilleure qualité et l'impression de couches plus épaisses pour amélioer les performances électriques.
4. le développement de matériaux de haute permittivité compatibles avec la technologie de fabrication LDS afin de miniaturiser les circuits RF 2D et 3D.

PhD Thesis

Chapter-1

Introduction and Motivation

1.1. Background

This PhD thesis comes under a national research project titled PLASTRONICS, supported by PLASTIPOLIS, MINALOGIC and FEDER led by the industry ARaymond, in collaboration with 11 industries and 3 research labs. PLASTRONICS aims at making intelligent injected plastic components by directly integrating electrical or electronic functions onto the plastic surface. The project provides the French industry, the solution of design and production of MID (Molded Interconnect Devices) systems with high added values in commercial market. With this objective, the project revolves around the improvement and reliability of interconnect technologies and innovative extension of existing components, development of a tool to support the design and validation of the industrial production of PLASTRONICS, validation of these technology in market applications such as automotive, telecommunication, health etc. The topic of this thesis is to meet one of those tasks which come under the telecommunication domain, more precisely in RF (Radio Frequency) domain.

The rapid and large scale development of wireless communication systems has put forward some constraints in the RF domain in terms of electrical performances, reliability, cost and size. Within this framework, MID technology is very relevant for the integration of electrical and mechanical functions into a single element of device thereby reducing cost and size with improved system functionality. A review of the development of MID in the field of RF identifies the need of research in several areas: study of the electrical and thermal behavior of thermoplastic materials in RF and study of the integration of RF functions on to the family of thermoplastic substrates within the limits imposed by the manufacturing techniques of MIDs. RF functions can be listed as the development of passive RF devices on MID. MID researchers have already paid attention in a narrower way of analyzing the MID technology in the field of RF by developing three dimensional antennas on molded thermoplastics.

Researches can be enhanced more the study of the performances of RF devices in MID technology, the thesis thus proposes a collective study of RF performances of MID

based on most of passive devices. The idea is to present the RF compatibility with MID technology in two main approaches: 1) analysis of the RF and thermal behavior of molded thermoplastic and 2) the analysis of RF devices manufactured in three different MID fabrication technologies; LDS (Laser Direct Structuring), ink jet printing and LSS (Laser Subtractive Structuring). Though the MID technology offers three dimensional circuits design, the thesis mostly follows the design, development and analysis of planar RF circuits, due to the absence of these information in literature. The thesis thus aims to prove the RF compatibility in most of passive RF components such as transmission lines, filters, couplers and antennas. Study on RF behavior of MID devices based on CPW (coplanar waveguide), microstrip and stripline technologies are considered and compared. The whole studies unfold in this thesis deals with the theoretical aspects, simulations as well as practical implementations of MID devices. The studies also triggers onto the design and evaluation of three dimensional devices.

1.2. Outline of the thesis

The goal of this PhD thesis is to study the potential and limitations of MID in RF domain. The issues related to this PhD work is thus organized and presented in chapter 2 to chapter 6.

In chapter 2, the thesis briefly explains the MID technology to the reader; its history, advantages and applications. This chapter also describes the state-of-art that reviews the contribution of MID to the RF field. A brief review of MID technology in other application fields such as automotive, medical and electronics are presented.

Chapter 3 deals with the study of the behavior of thermoplastic materials and circuit metallization which would be intended to utilize for the design of MID RF circuits. The main idea of this chapter is to characterize the dielectric and thermal properties of various molded thermoplastic substrates. A brief review of various methods of dielectric characterization is done. Along with this, the conductivity measurement of metallization used for defining the circuits of MID are also presented.

From chapter 4 to chapter 6, the research work is divided based on the fabrication techniques of MID circuits. In chapter 4, design of various RF circuits based on LDS fabrication is presented. The low cost low loss thermoplastic LCP (Liquid Crystal Polymer) Vectra E820i is chosen as the substrate for the design of transmission lines, filters and antennas. The properties of LDS transmission lines such as RF losses, quality factor etc. are

studied based on CPW, microstrip and stripline technologies. The study of LDS microstrip via model is also incorporated in this chapter. Finally, the study and implementation of three dimensional PIFA (Planar Inverted-F Antenna) antenna is carried out.

In chapter 5, the work focuses on the performance of inkjet printed circuits in combination with MID technology. Molded ABS PC (Acrylonitrile Butadiene Styrene Poly Carbonate) and LCP E130i are the thermoplastics of interest in this study. The chapter is divided into two sections. In the first section, inkjet printed transmission lines on ABS PC on both CPW and microstrip technologies are studied based on their RF losses and quality factors. Further, MID inkjet printed antennas (Ultra Wide Band antenna and microstrip patch) are designed, realized and measured in terms of their reflection coefficient and radiation pattern. In the second section of this chapter, the compatibility of LCP thermoplastic in printed electronics is studied. Performance of ink jet printed conductive pattern on LCP is investigated. Electrical resistivity of the printed pattern on LCP substrates with and without planarization is compared. Finally, transmission lines and Low Pass Filters are designed and verified with their RF properties.

In chapter 6, the compatibility of two different MID substrates along with LSS method of fabrication is demonstrated. A classical LCP E130i substrate and a synthetized charged High K thermoplastic material have been studied. The study of the improvement in the dielectric permittivity of thermoplastics by the addition of mineral charges is presented. Several other thermoplastics such as PS (PolyStyrene) and PE (PolyEthylene) are also used. The permittivity of High K material with additive charges shows highest improvement in dielectric permittivity among the other experimented thermoplastics, which in turns allow the miniaturization of RF circuits. Thus, High K material is chosen for the analysis of RF performances by designing transmission lines. Along with the study of their RF properties, design of LSS directional couplers on the improved High K material is studied and verified.

Chapter 7 presents the conclusion of the thesis. It summarizes the thesis with a description of the important work provided in it and the future scope of MID technology in the RF domain.

Chapter-2

State-of-art

This chapter introduces the thesis to the reader. The chapter reviews the state of art of Molded Interconnect Devices (MID) technology. In this chapter, different MID fabrication techniques are presented. Several RF devices on MID published in the literature are reviewed with illustrations. This state of art will clearly highlight the objective of the thesis to the readers.

2.1. Molded Interconnect Devices: Basic Concept

MID technology opened a new path for electronic circuits design by the direct integration of electrical conductor patterns onto molded thermoplastic substrates on either two or three dimensional surfaces [1]. Fig. 2.1 illustrates the concept of MID.

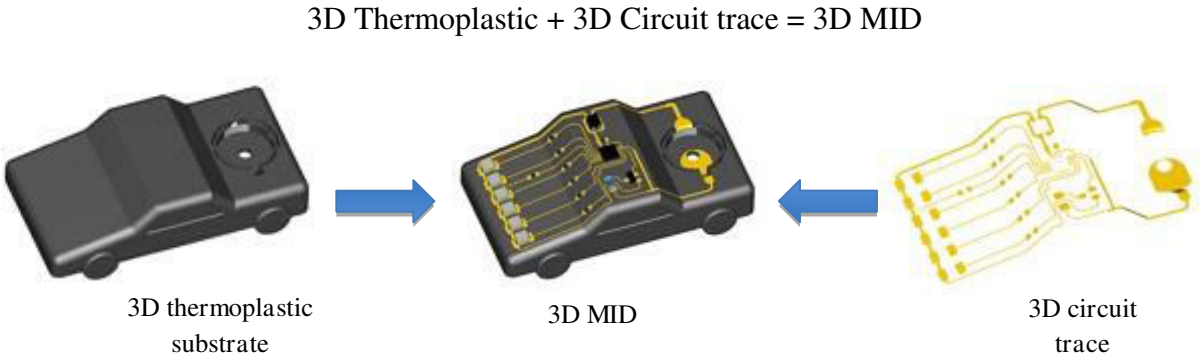

Fig. 2.1 : Molded Interconnect devices: basic concept [2].

The concept of MCB (molded circuit board) was introduced in the USA in 1983 and its industrial interest made the development of MID technology in 1985 [3][4]. MCB follows the printing processes used in classical PCB (printed circuit board) combined with the injection molding. Initially, the concept of MID was unsuccessful due to their production difficulty [5], but the market for this type of product was still growing [6][8]. During 1980's, USA was in the leading role in this field and in the following years the western advanced countries especially Germany and Japan took over its leading role [2]. Nowadays, MID market is developing enormously and many leading companies such as BMW, Volkswagen, Siemens have already integrated MIDs to their products. The details of these MID applications will be given in section 2.3.

In comparison to conventional PCB, MID provides significant environmental, economical and technological advantages [12]. Table 2.1 shows the selection guidelines for using MID or PCB as a choice of design [11]. Indeed, thermoplastic materials used in MIDs can be easily recycled. In addition, components number and fabrication cost can be reduced, thanks to the implanted connectors, switches, wires etc. Fig. 2.2 clearly illustrates the comparison between an MID and a classical circuit [11].

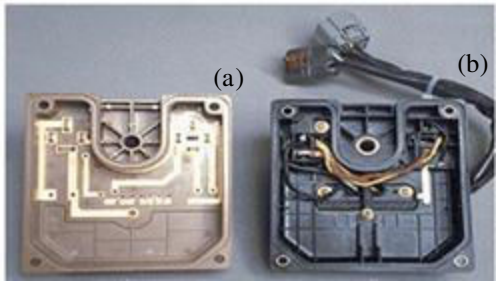

Fig. 2.2 : (a) An MID with reduced number of components and (b) in comparison with a classical devices.

Table 2.1: Selection guidelines of MIDs and classical devices as a choice of circuit design.

MIDs	**Classical devices**
For three dimensional circuitry	For two dimensional circuitry
Reduced weight and volume	Low cost circuit fabrication with mass quantity production
Low circuit density	High circuit density with more than 2 layers of interconnects
Integration of electrical and mechanical functions such as switches, wires, protection case etc.	Permanent method of producing circuit, can't be modified

Smaller size, lower complexity, reduced weight and assembling time are achieved with MIDs providing thus a low cost of fabrication. Several MID fabrication techniques exist and are explained in the following section.

2.2. MID fabrication methods

There are various steps for MID fabrication. Most of MID productions start with the injection molding of thermoplastic. Injection molding is a fabrication process for producing required thermoplastic by injecting their granulates into a mould. Molded thermoplastics are produced either by single or two shot molding. In single shot molding, a single injection molding process with a thermoplastic material is required for the production of MID, whereas in two shot molding, two successive injection molding processes of thermoplastics are used, out of which only one is platable. Further steps of MID production are circuits structuring and selective metallization. Each fabrication process requires a different method of integrating the metallic circuit tracks on the substrate such as LDS (Laser Direct Structuring),

LSS (Laser Subtractive Structuring), inkjet printing, hot stamping, etc. The details of these fabrication techniques are given below.

2.2.1. Laser Direct Structuring (LDS)

It is widely used and well known method of MID fabrication, where the thermoplastic molded parts are manufactured in single shot injection molding. The molded part is subjected for laser activation, a process to activate the surface of the molded thermoplastic and to further undergo selective metallization. Fig. 2.3 shows the process steps of LDS fabrication. LPKF-LDS® process from LPKF Laser and Electronics AG, Garbsen, Germany is followed for MID LDS structuring [6].

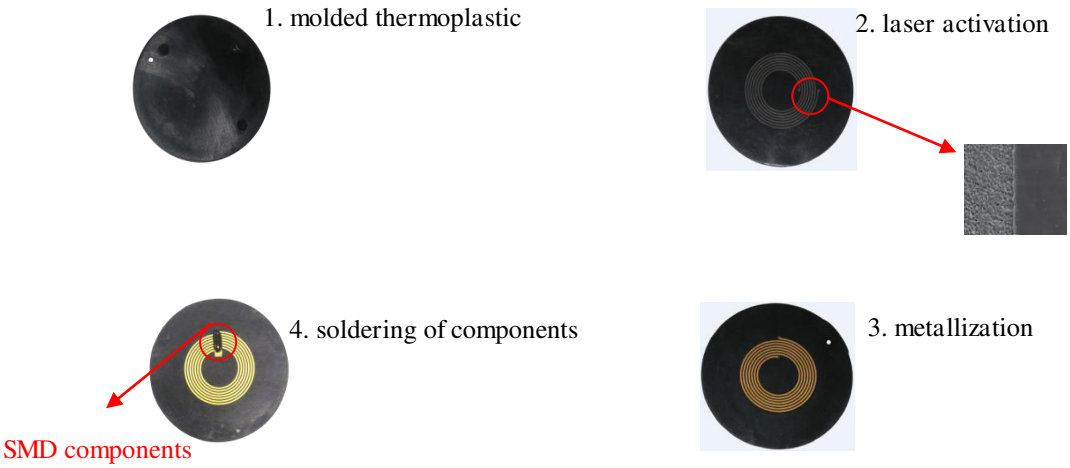

Fig. 2.3 : Process steps of LDS fabrication.

Some of the advantages of this method are great flexibility for design changes, possibility of making circuits on 3D surface, higher level of product integration with improved quality and reduced costs etc. It can implement ultra fine structures of width and gap of less than 100 µm [14]. There are several important considerations for determining LDS thermoplastic such as thermal stability, mechanical characteristics, solderability etc. Special thermoplastics doped with an organic metal complex are required for the LDS fabrication [15]. Some of the LDS compatible thermoplastics are ABS PC (Acrylonitrile Butadiene Styrene Poly Carbonate), PBT (PolyButylene Terephthalate), PPA (PolyPhthalAmide), PPE (Polyethylenimine), LCP (Liquid Crystal Polymer), PEEK (Polyether ether ketone), PEI (PolyEtherImide) etc. [16]. Another major advantage of this MID fabrication is that via holes can be directly implemented.

2.2.2. Laser Subtractive Structuring (LSS)

This method is also known as laser ablation. It is another widely used subtractive fabrication method of MID. Here, the whole molded substrate is chemically activated and coated with metal and then selective laser ablation is used to define the circuit layout and thus to remove the unwanted metal areas [18]. Fig. 2.4 shows the fabrication steps of LSS. Dimension resolution is same as in LDS method. It is more suitable for high density metallization which had been originally developed for two dimensional PCB prototyping [19]. The method involves many additional steps which results in higher cost and lower yield. The advantage of this method of fabrication is that it does not require any special kind of thermoplastics.

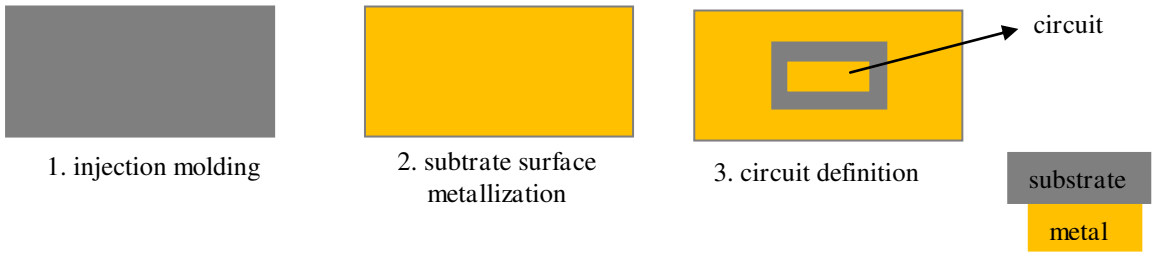

Fig. 2.4 : Process steps of LSS fabrication.

2.2.3. Hot stamping

It is another fast and economic fabrication process applied for the production of MID. Here, the metallic circuit pattern is directly hot pressed on the surface of the thermoplastic substrate [17]. The required circuit pattern is coated with a heated stamp. A copper or metallic foil is kept in between the molding stamp and the thermoplastic substrate. The copper/metallic foil gets heated up by pressing the molding stamp and the copper/metallic lines remains on the substrate surface. The unwanted copper/metallic foil can be removed mechanically. Fig. 2.5 demonstrates the hot stamping method of circuit fabrication.

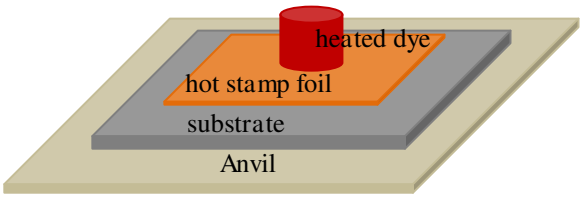

Fig. 2.5 : Process steps of hot stamping fabrication.

The fabrication cost of hot stamping is less compared to two shot molding (method explained below). This method is mainly used for the production of larger parts where high

precision is not a strong requirement. Hot stamping does not allow ultra fine circuitry compared to LDS technology. The minimum acquired dimension for a width is 1000 μm [18]. The above mentioned three MID fabrication methods are come under single component injection molding.

2.2.4. Two shot molding

It is the most complicated three dimensional method of circuit design which requires two molds for thermoplastic molding. Complex and expensive molding tools are used in this method. It is used for high volume production, large plating surface and complex layouts. In this method, two successive injection molding processes are done with two different plastic materials to form the circuit trace on the substrate surface [2]. One of the two plastic materials is platable. The process involves injection of primary molded part where the plastic used is more mechanically stable and gets over-molded with the second plastic. Further, metallization is performed on the platable polymer to make the conductive circuit tracks. Fig. 2.6 shows a three dimensional MID antenna using two shot molding by Nokia and Hitachi cable Ltd [21].

Fig. 2.6 : 2 shot molded 3D MID antenna by Nokia and Hitachi cable Ltd.

There are two types of two shots molding [22][23]; (i) in the first shot, circuit trace is molded in the form of recesses in the non platable plastic and in the second shot, these recesses are filled with the platable plastic (Fig. 2.7 (a)) and (ii) platable plastic is used in first shot and in the second shot, the areas between the conductors are filled with the non platable plastic (Fig. 2.7 (b)). Two shot molding provides a dimensional width of less than 400μm. One of the disadvantages of this method is that in case of design change of the circuit trace, expensive and time consuming modifications are required [18].

(a) (b)

Fig. 2.7 : Different types of 2 shot molding process in MID device (a) type 1 and (b) type 2.

2.2.5. Inkjet printing

It is a recently evolved direct write additive technology which allows printing the circuit pattern directly onto the molded substrate [24]. This method is an economical fabrication solution with reduced cost and without waste, because the consumption of ink can be saved by jetting ink droplets through the nozzle of inkjet system to the desired position. Basically, metal ink with conductive nano particles is inkjet printed on a single shot thermoplastic. Fig. 2.8 illustrates the fabrication process of inkjet printing technology of RF circuit fabrication.

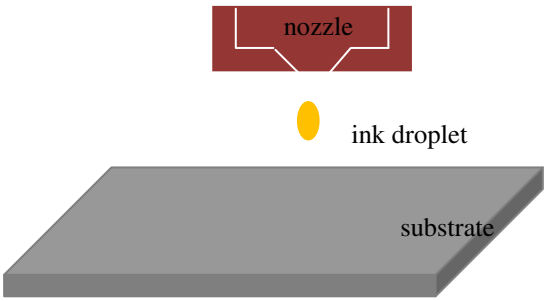

Fig. 2.8 : Inkjet printing fabrication demonstration.

Surface treatment, uniform conductivity and thickness of printed metal lines are major concerns when it comes in printed RF circuits [25]. Substrates with low surface roughness allow to achieve good conductivities in printed electronics. Therefore, inkjet printing conditions such as surface treatment based on planarization, thermal treatment by subsequent curing and sintering step, dot size of ink droplet, and multilayer printing of metal lines are performed to improve the conductivity and metal thickness.

2.2.6. Photo imaging

It is another widely used MID fabrication technique which usually follows flat circuit patterning but also being used for 3D circuit design using 3D mask. The method is

challenging to realize 3D circuits and the fabrication method involved is not environmentally friendly [22].

Based on the above mentioned fabrication techniques in particular LDS, various MID devices are already introduced in the market based on the application requirements. A description of these existing MID components which stimulate the present thesis work is given in the following sections.

2.3. Industrial applications of MID

MID exhibits an enormous potential for technical innovation and are more environmental friendly than conventional PCBs, which they are intended to supplement but not replace. Areas of applications of MIDs include medical equipment, automotive electronics, telecommunications, and domestic appliances. From a product perspective, MIDs are utilized in applications ranging from cars to airplanes, joysticks to cell phones, and flashlights to antennas. Existing MID products in each application domain are described below. The details of each innovation are presented in section 2.4.

2.3.1. Medical domain

Fig. 2.9 presents examples of MID implemented in the medical application domain [6][7][26]. Fig. 2.9 (a) shows the evolution of hearing aids using MID technology developed by Siemens audiologische Technik GmbH, Germany. Fig. 2.9 (b) shows a miniaturized 3D switch element that reduces the assembly time of the dental decay detection device from 5 minutes 30 seconds to 20 seconds. The high performance LED diode is yet another successful development of LDS process towards medical field like dental technology. These LED provides 6 times more life time and considerable increase in its brilliancy with less consumption of energy. Fig. 2.9 (c) shows the MID LED developed by 2E Mechatronic GmbH & Co. KG in Germany.

(a) (b) (c)

Fig. 2.9 : MID medical applications, (a) hearing aids in medical (source: Seimens Audiologische Technik GmbH, Germany, (b) dental decay detection device, and (c) 3D MID LED (source: 2E Mechatronic GmbH & Co. KG, Germany).

2.3.2. Automobile domain

Various contributions towards automobile field have been given by MID technology and are listed in Fig. 2.10. Fig. 2.10 (a) shows a miniaturized multi functional steering wheel introduced by Volkswagen by replacing all wiring from the previous design. Mercedes Benz has also implemented this innovative technology in their car keys (Fig. 2.10 (b)). Fig. 2.10 (c) shows the use of MID in an automotive user interface that incorporates circuit board, wires, connectors, housing etc. appeared in traditional products into a fully functional compact part.

(a) (b)

(c)

Fig. 2.10 : MID automobile applications, (a) multi functional steering wheel, (b) MID car key, and (c) automotive user interface (source: 2E Mechatronic GmbH & Co. KG, Germany).

2.3.3. Telecommunication domain

Due to the advantage of using reduced number of components and its flexible design, the idea of MID has been implemented in various mobile phone designs as seen in Fig. 2.11.

Fig. 2.11 : Various types of MID internal antennas in mobile phones.

The smallest on-ground LDS MID antenna working at 2.4 GHz is commercialized by Molex [27]. The antenna realized on LCP substrate weighs only 0.03g and its size is 3 x 3 x 4 mm^3 on an LCP substrate. Though it supports SMD components soldering, the antenna requires a stripline matching on the PCB and does not require any discrete matching components. It is usable as a standalone device without the need of cable connection. This light weight component is used in portable electronic devices for bluetooth, zigbee, wifi and other wireless standards. Fig. 2.12 illustrates the photo of the Molex antenna and its return loss measurement. It is a monopole antenna with omni directional radiation pattern with a maximum gain of 3 dBi as shown in Fig. 2.13.

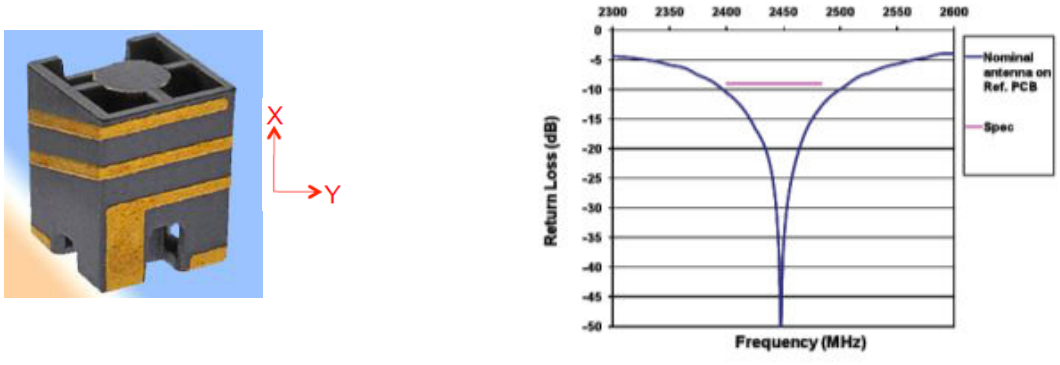

(a) (b)

Fig. 2.12 : Smallest on-ground MID antenna, (a) fabricated antenna prototype, and (b) its reflection coefficient.

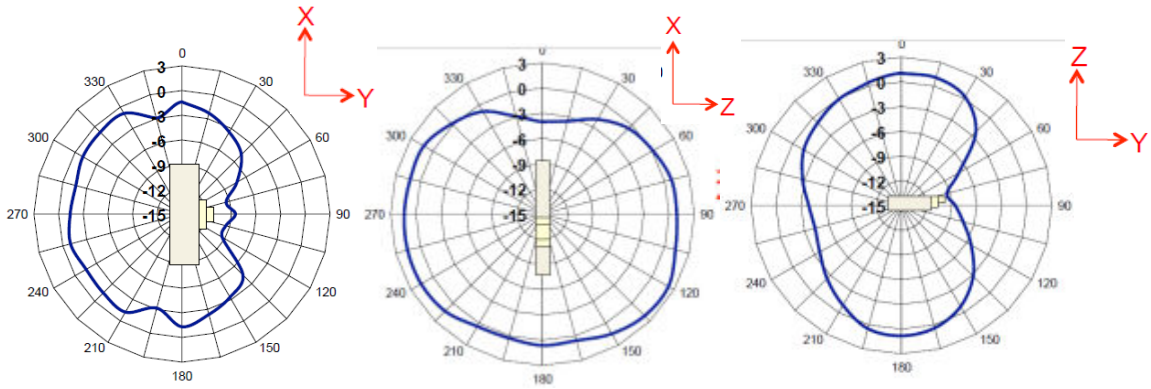

Fig. 2.13 : Radiation pattern of smallest on-ground MID antenna.

In addition to these developments, MID has made footprints in applications such as pressure and flow sensors, aircrafts, computer technology [8][10]. Following sections deal in details the MID technology development in the above mentioned application fields which are already existing in the literature.

2.4. MID: A review of literature

The study of literature on MID technology is presented in this section. This study is classified into MIDs in automobile domain, MIDs in medical domain, MIDs in electronic devices and finally, MIDs in RF circuit designs.

2.4.1. MID for automobile applications

Harting Mitronics has developed a position sensor for adaptive speed control using MID technology [28]. The sensor is developed in ACC (Adaptive Cruise Control) system which allows the driver to select a constant speed while maintaining a safe distance from the vehicle in front. This new MID sensor device features a broad detection angle and high resolution. Other features of this new radar system include: it warns the driver the possibility of rear end collisions, it provides a life saving reduction in the braking distance with foresighted preconditioning of the brakes, detects the pedestrians and objects on the road etc. This sensor can be applied to cars and trucks as well as in industrial arena. Fig. 2.14 shows the MID developed speed control sensor. LPKF LDS technology has been utilized for its development. LCP Vectra E840i LDS is used as the substrate and Ni/Au/Cu (combination of Nickel, gold and copper) is used for the metallization. Several advantages are offered by the use of MID technology in this sensor design; more compact sensor, great precision for the arrangement of components such as hall sensors, photoelectric barriers etc., precise mechanical immobilization of the axle, simplified electrical wiring, etc.

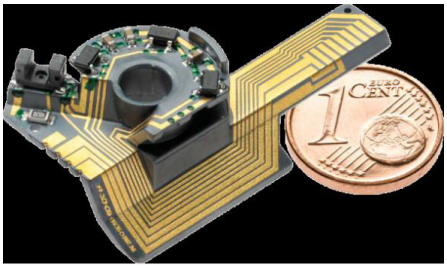

Fig. 2.14 : MID position sensor for adaptive position control.

Another innovative development of Harting Mitronics is a light sensor for climate control [29]. This light sensor supports climate control in car and has been developed based on two shot injection molding. This allows three dimensional arrangement of the optic sensor as a space saving base carrier. The idea of this innovation is to detect the temperature, the intensity and direction of the incident radiation which results in the reduction of overall energy consumption. It also controls the cooling and ventilation in higher solar or heating moments. Fig. 2.15 shows the MID based sun sensor. Two different types of thermoplastic materials such as LCP E820i as a platable and LCP Vectra E130i as non-platable component are used here for two shot molding process and a chemical metallization of Ni/Au/Cu has been utilized. The technology used into this innovative idea provides various advantages such as great miniaturization in connection with increased reliability, number of optic sensors are inbuilt in the component and high level of design freedom.

Fig. 2.15 : MID sun sensor that controls cars interior climate.

Lighting module for vehicle passenger compartment is another innovative development of Harting Mitronics in combination with the technology MID [30]. A compatible vehicle ceiling lighting systems integrating classic interior lighting and the reading light into a single module with compatible interface. It allows in the reduction in number of components, reduction in 35% cost from the previous model and smaller installation height. Fig. 2.16 presents this innovation in light module in vehicle. Based on

LDS fabrication technique, this component has been developed. LCP Vectra E840i is used as the substrate material and Ni/Au/Cu is the metallization.

Fig. 2.16 : MID lighting module for vehicles.

2.4.2. MIDs in medical domain

One of the most innovative development in MID technology for medical application is the design of microphone carrier for a behind the ear hearing aid which is shown in Fig. 2.9 (a). It has multi channel and adaptive directional microphone system with up to three microphone. This features reduction in unwanted ambient noise by directly reacting to noise sources and adjusting noise mode automatically. By using MID technology, a three dimensional hearing aid which eliminates an additional circuit carrier board is possible. LPKF-LDS is used for the injection molding of this compact hearing aid component using LCP Vectra E820i substrate material.

Two innovative circuits for dental care application based on MID technology are shown in Fig. 2.9 (b) and Fig. 2.17 [31]. An MID ring switch implemented on a DIAGNOdent pen from KaVo Dental GmbH (Fig. 2.9 (b)) diagnoses the caries of teeth based on fluorescence. It distinguishes healthy tooth substance from diseased with the help of fluorescence supported by visual and acoustic signals. Using MID technology, the assembling time can be reduced from 330 to 20 seconds with less error rate. Number of components are drastically decreased from eight to three and the cost of manufacturing fall down by 78%. Another innovation in dental care is optics carrier and heating element for diagnosis of caries (see Fig. 2.17). The function of this electronic device is that by irradiating the teeth with 780 nm light, the areas affected by caries can be distinguished from the healthy tooth substances by weaker fluorescence luminosity. The assembly consists of metalized heating elements and loaded optics carrier and a thermoplastic case. MID allows miniaturized as well as highly integration density product development with simplified and reduced number of assembly steps which eventually results in light weight and low cost device. In both the devices, LCP E840i thermoplastic material is used as substrate and LPKF- LDS fabrication method is used for their production.

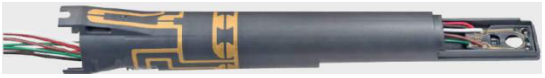

Fig. 2.17 : MID heating element for diagnosis of caries in dental cares.

2.4.3. Electronic MID devices

Few literatures highlight the potential of circuit design using direct write technology in combination with MID technology [32][34]. One example of MID combined with aerosol jet printing is shown in Fig. 2.18 [32]. The silver sensors and circuits are printed on a polyamide 6 (PA6) thermoplastic molded tank. All SMD components are mounted using conductive adhesive. These sensors are used to indicate the water level as it rises to the filling level by lighting the LEDs mounted on it. When the water level reaches its maximum level, the circuit senses the level and reverses the pump direction.

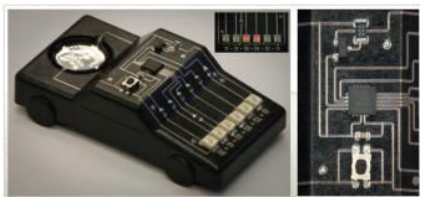

Fig. 2.18 : 3D MID with integrated sensor-Automotive tank level filling sensor.

Another example of aerosol jet printing on MID is shown in Fig. 2.19 [32] where functional thermometer is integrated on a polyamide 10TX (PA 10TX) material.

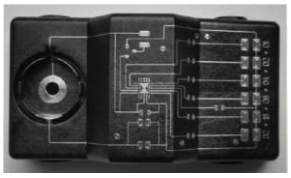

Fig. 2.19 : 3D MID with integrated functional thermometer.

Manufacturing of LED lamps utilizing LDS technology is presented by B. Stumpp in [35]. The smaller, lighter and cheaper features of LED lamps are exploited for the production of these lamps using LDS technology. Here, metal substrates are used as circuit carrier which provides strong mechanical functions, aid in heat dissipation etc. This design enables the cost effective production and design freedom of LDS LED lamps. Fig. 2.20 shows the novel LED lamp using LDS technology. Here, the aluminum body is act as heat sink and LDS powder coating process is applied in an electrostatic process. It is given that LEDs can be directly integrated on to the heat sink. Laser structuring and metallization can be easily implemented in the coated metal substrates as in the same way that thermoplastic parts are.

Fig. 2.20 : LED lamp integrated with LDS technology.

2.4.4. MID in RFID devices

A passive UHF RFID (Radio Frequency IDentification) transponder implemented with MID technology is shown in Fig. 2.21 [36]. A PT 86 (HT) passive UHF transponder is presented here which is suitable in aviation industry under extreme mechanical, chemical and thermal conditions. It allows a frequency range of 860 MHz to 960 MHz. LCP E840i material is used as the material fabricated using LDS technology. MID technology provides various advantages to this RFID transponder development. Some of them are high temperature resistance provided by LCP, low cost of fabrication and higher product quality. Another main advantage is that the RFID chip can be assembled directly on the housing of RFID tag which consequently avoids the requirement of an additional PCB.

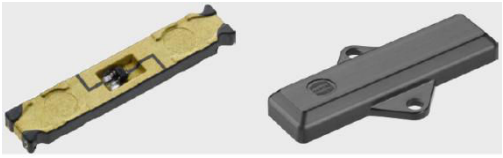

Fig. 2.21 : MID passive UHF transponder.

In electronic payment transactions, strict security should be required for the systems that processes data. The possibility of data theft stored in these systems during the reading and sending it on to the third parties for payment should be reduced. This is achieved by using MID safety caps as shown in Fig. 2.22 which protect electronics [37]. In this safety cap, the bottom side is two long metalized conductor paths. If these conductor paths are interrupted, the electronics will no longer works, which effectively prevents reading and further copying procedures.

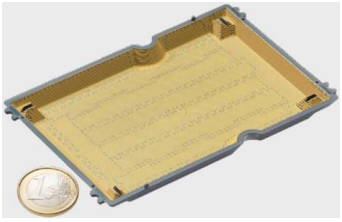

Fig. 2.22 : MID safety cap for electronic payment systems.

MID features simplify assembling steps than conventional security solutions (glued flex- print foils). Also, MID avoids quality problem which occurs in the field in conventional method when adhesive used. Here, LPKF-LDS fabrication method is adopted. The material LCP Vectra E840i is used as substrate.

The use of MID technology in electronic devices has been extended to the design of lighting modules in safety camera systems [37]. A MID lighting module mounted on a PCB used in V200/V300 workstation extended safety camera system from SICK AG is shown in Fig. 2.23. This MID lighting module is realized by LPKF-LDS technology on an LCP E840i substrate offers improved financial advantages compared to conventional methods. More integrating and miniaturized design with a better integration in a single housing, three dimensional arrangements of LEDs, simple assembling steps etc. are the advantages of this MID module.

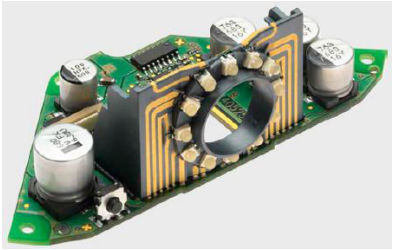

Fig. 2.23 : MID safety camera system from SICK AG.

A charged coupled device (CCD) image sensor built into large format cameras such as AWARE 2 camera implemented using MID technology is shown in Fig. 2.24 [38]. This innovative camera system is supported by PCB which handles sensor power supply and image data transfer to the multi scale camera control module. The camera allows a broadband field of view, larger visual range, greater resolution and multiband imaging capability in any weather and in day and night lighting conditions. Components miniaturization, less weight, simplified assembly are some of this innovative MID device advantages. LPKF LDS with LCP Vectra E840i substrate is used here for its manufacturing.

Fig. 2.24 : 3D MID component for CDD sensor.

Till now, the applications or development of MID technology in medical, automobile and electronics domain were discussed briefly with some examples. As this thesis mainly deals with RF circuit design, literatures on MID RF circuit designs are explained in details in the following section.

2.4.5. RF MID devices

The literatures on MID RF devices mainly show the various design of three dimensional antennas. The design of switched beam 3D-Vivaldi antennas for WLAN (wireless local area network) on an MID substrate, PBT (Pocan Poly- Butylene Terephthalate) is presented in [38]. The work started with the new concept of 3D multi sector antenna with vertical Vivaldi- type antennas combined with a horizontal mother board. The multi sector antennas were introduced in WLAN in order to reduce the interference issue in the wireless network, thereby improving the wireless range and bit rate. 3D vivaldi antennas provide the flexibility in their shape, size etc. Initially, the authors have made study on this concept based on common FR4 laminate. Later, 3D MID technology has been considered on Pocan PBT since MID supports 3D complex circuit design with reduced manufacturing cost. The substrate used here is having ε_r =3.4 and tan δ =0.01 at 6 GHz.

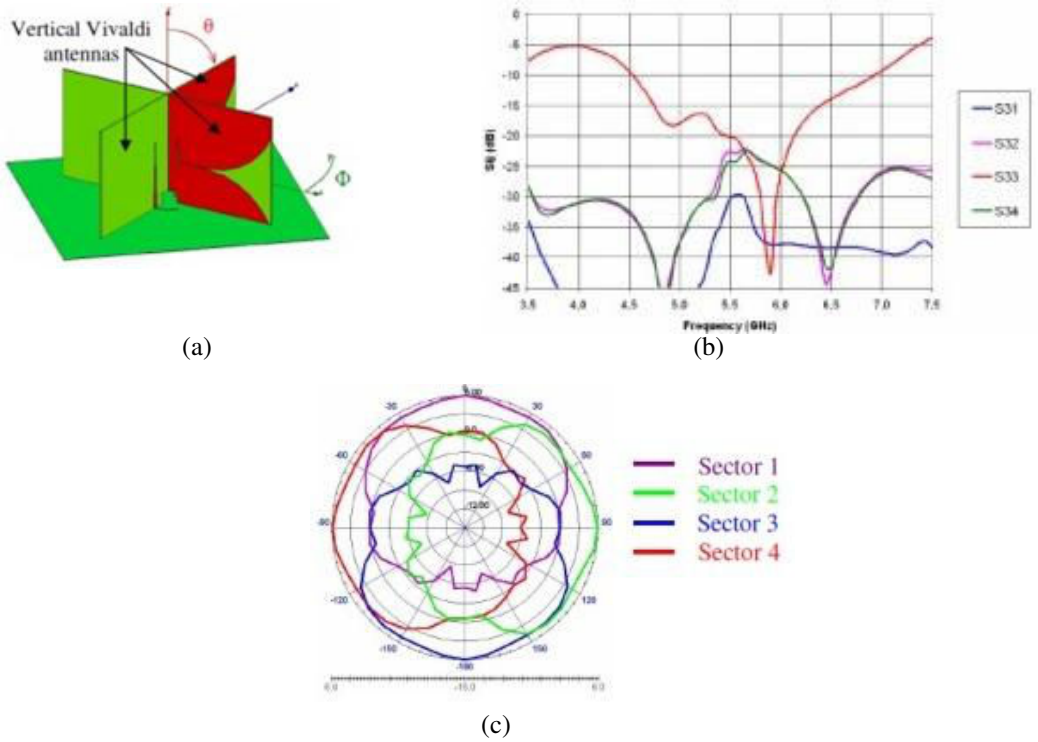

(a) (b)

(c)

Fig. 2.25 : 4 sectors switched beam vivaldi antenna on FR4 substrate, (a) fabricated antenna prototype, (b) its reflection coefficients with all S parameters in dB and (c) its radiation pattern in azimuth plane at 6 GHz.

Fig. 2.25 and Fig. 2.26 show the 4 sector switched beam Vivaldi antenna based on FR4 substrate and Pocan PBT thermoplastic respectively and their simulation response. The plastic antenna allows a mechanical contact with the horizontal FR4 board via metallic pins and holes. The thermoplastic antenna shows a wide frequency band from 4.6 GHz to 7.3 GHz than FR4 antenna with return loss better than -10 dB in the frequency band. As Pocan has lower tangent loss than FR4, Pocan vivaldi antenna provides a maximum gain of 6.4dBi which is higher than that of FR4 which has a maximum gain of 5.8dBi.

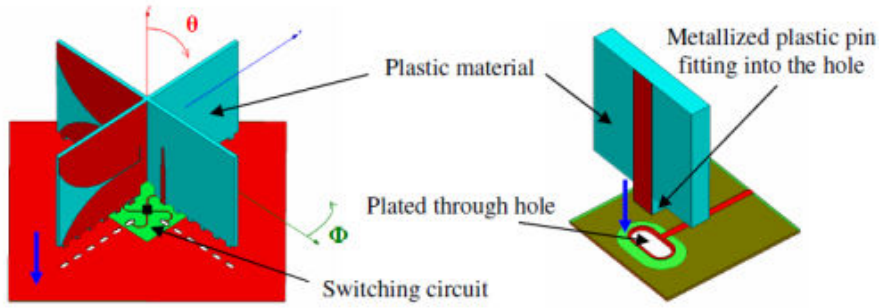

(a)

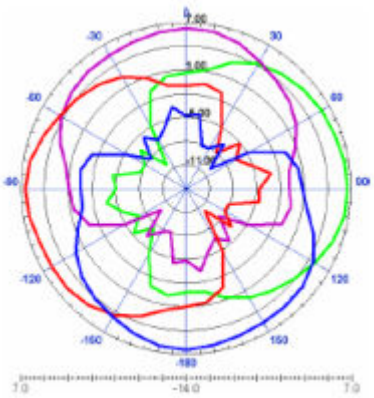

(b)

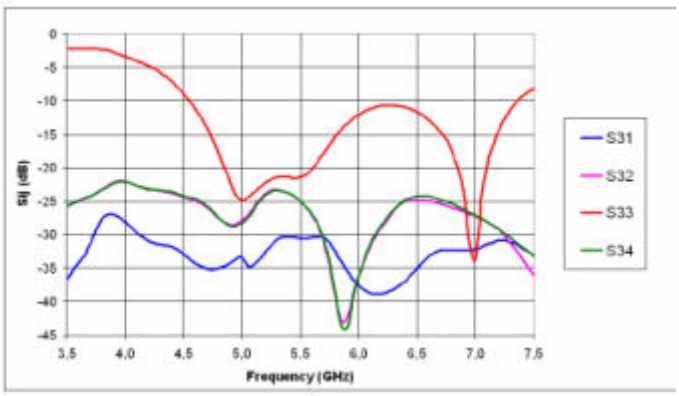

(c)

Fig. 2.26 : 4 sectors switched beam vivaldi antenna system on MID Pocan PBT substrate, (a) fabricated antenna prototype, (b) its radiation pattern in azimuth plane at 6 GHz and (c) its reflection coefficients with all S parameters in dB.

D. Kornek et al. [41] investigated the possibility of 3D antennas on MID substrates in combination with LDS technology. The substrate Pocan DP T7140 LDS having ε_r =3.95 and tan δ=0.0091 was chosen for the antenna design. In this work, the effect of bending simple planar patch antenna structures in 30^0 and 60^0 bend angles have been reported. Fig. 2.27 (a) shows the fabricated bent patch antenna. The experiments show that by increasing the bend angles, the resonance frequency shifts from the planar case (0^0) to higher frequencies which

are clearly depicted in Fig. 2.27 (b). Simulation results show good agreement with the measurement results which proves the potential of LDS technique.

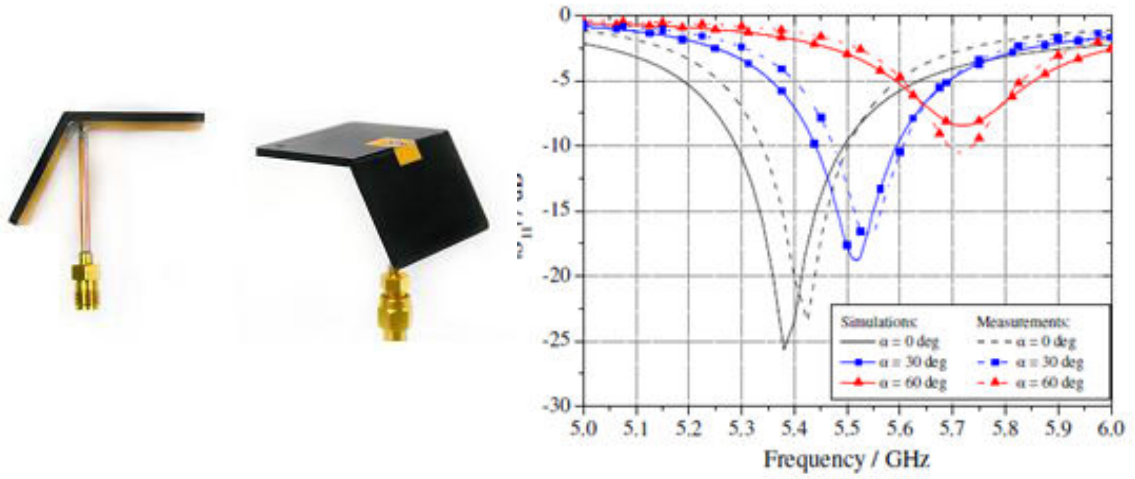

(a) (b)

Fig. 2.27 : MID bent patch antenna, (a) fabricated antenna prototype, and (b) its reflection coefficients in 3 bend angles.

The same idea of integrating 3D antennas on MID substrates was implemented by C. Orlob et al in [42], where a dual- polarized log.- periodic antenna was integrated on a conical MID substrate. The authors have initially investigated the effect of different cone angles of a conical log.- periodic antenna in free space on the input impedance and the radiation characteristics. Studies show that at cone angle of 90^0 the antenna exhibits frequency independent FBR (front to back ratio) and hence fixed for the further design. Subsequently, the antenna was designed and analyzed on a conical MID substrate. A UWB design prototype was introduced for the realization in this work. The substrate chosen for this design was Pocan TP 710-003 LDS. Fig. 2.28 (a) depicted the antenna realized on MID substrate with cone angle of 90^0. The FBR has reduced to 6 dB. This LDS MID fabrication also shows a better compatibility for the 3D RF design. Fig. 2.28 (b) shows a good agreement between the measured and simulated input reflection coefficient indicating a -8dB input matching over the frequency band 3 GHz- 9 GHz.

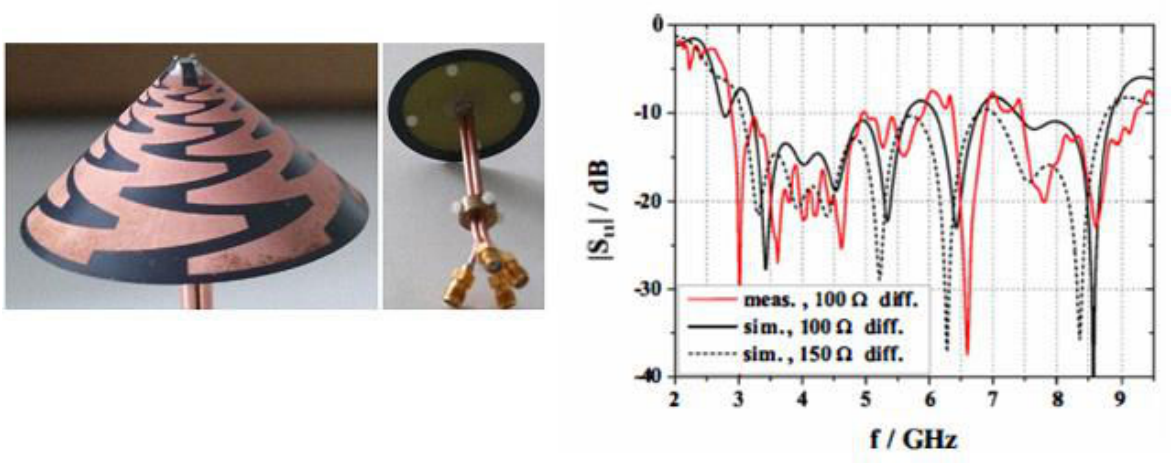

(a) (b)

Fig. 2.28 : MID conical log.- periodic antenna, (a) fabricated antenna prototype, and (b) its measured and simulated reflection coefficients.

Researchers have investigated the possibility of integrating the LDS technology in 4G antenna applications [43][44]. Innovative 4G antennas operating in the frequency band 698-960 MHz have been realized. Therefore, the case of a typical smart phone with 3.5" screen is considered. The size of the used PCB is 114 x 59 x 0.8 mm^3. The available antenna space in this configuration is 57 x 18.5 x 5mm^3. In order to integrate the antenna in the given space within the required frequency band, the authors integrated the antenna on plastic part with the support of LDS process. Two radiating elements were implemented in order to cover this 262 MHz band. The two radiating elements are Inverted-F antennas having resonances at 770 MHz and 910 MHz. In order to recombine these radiating antennas into a single feed, in [43], a power divider/ combiner is utilized whereas in [44] a diplexer is inserted to achieve a wide band. Fig. 2.29 (a) shows the fabricated antenna prototype. In both cases, antenna covers the entire frequency band 698-960 MHz with a return loss better than -6 dB (Fig. 2.29 (b) and (c)). Measured LDS antennas bandwidth is higher than that of commercial phones. Both LDS antenna prototypes provide a total efficiency of above 25% in the entire frequency band. Thus, this design confirms another success of LDS technology.

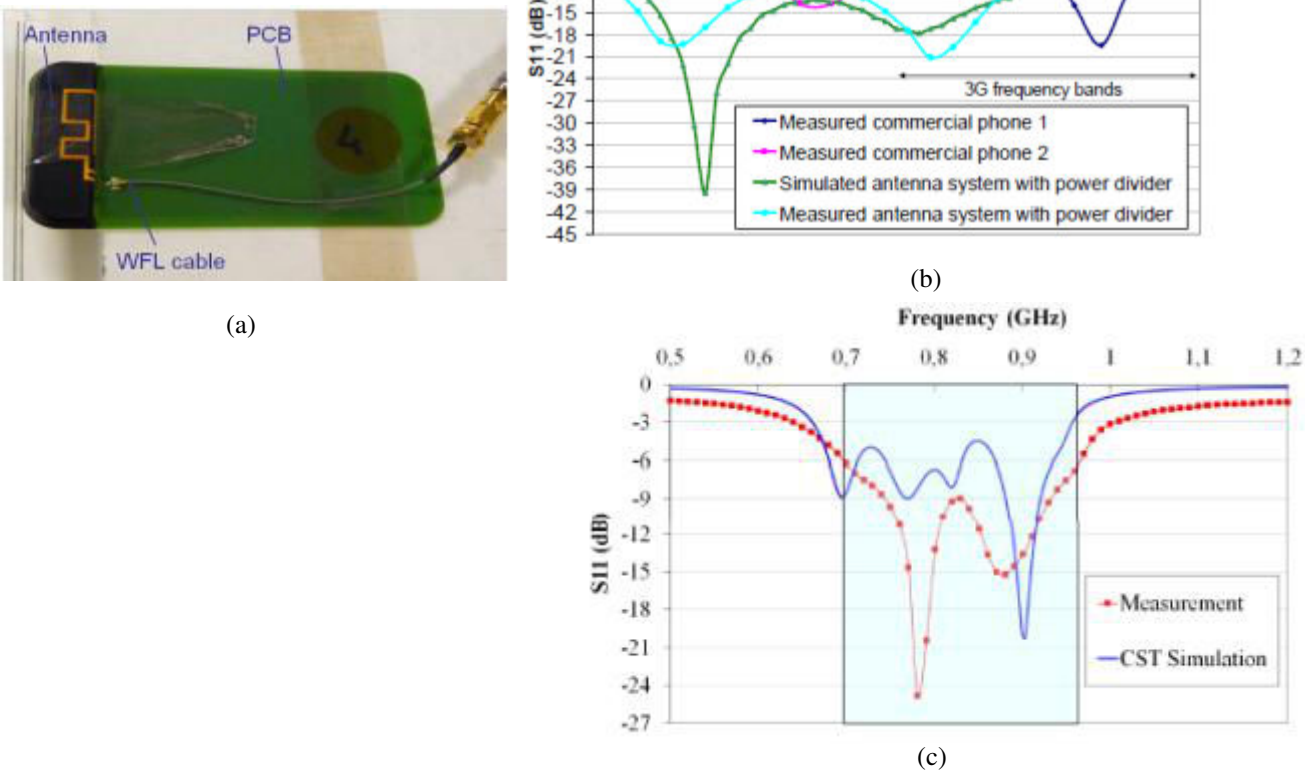

(a)

(b)

(c)

Fig. 2.29 : 4G LDS antenna, (a) fabricated antenna prototype, and (b) reflection coefficient of antenna system having power divider/combiner and (c) reflection coefficient of antenna system having diplexer.

Another study of MID antenna based on LDS-LPKF fabrication process is given in [45] in which the design of internal antennas on typical mobile phones is presented. The performance of the proposed antenna based on their mechanical and electrical performances and their environmental characteristics were studied in this work. If we consider the electrical performance of this antenna, the research work shows that the MID antenna provides the similar 3D radiation patterns and return loss as in commercial metal antennas and thus prove the possibility of LDS-LPKF technology for fabricating functional internal antennas.

An LTE (Long Term Evolution) antenna and its integration with an automotive roof top antenna on a three dimensional mounting surface using MID technology is presented in [46]. Typically, the on board equipment in vehicles consists of automotive on-board antennas like integrated on-glass antenna, rod antenna and integrated roof top antenna in order to achieve the entire number of communication standards. The roof top antenna which provides different broadcasting and telecommunication functionalities, usually enclosed by a dielectric

housing in order to protect it from environmental influence. Mutual coupling between the antenna elements inside the compartment leads to degraded performances in communication services. In order to improve the service delivery and robustness, 4G LTE with multiple antennas technology is required in the automotive industry. In order to increase the space utilization of the roof-top antenna, the direct integration of the antenna functions onto the dielectric loading is implemented in this work. This antenna module is designed on LCP Vectra E840i using LDS technology. The substrate provides a permittivity of 4.2 and tangent loss of 0.0027 at 2.69 GHz. Fig. 2.30 shows the two element LTE antenna with its feeding structure. For the measurement, a stripline is routed from the feeding port straight under the housing and an SMA connector is mounted on the inside edge.

Fig. 2.30 : Realized two antennas system (LTE and automotive roof top antenna) with feeding structure on MID.

This integrated LTE antenna provides an input matching and isolation better than 10 dB in the entire LTE band (Fig. 2.31). Also, the radiation properties of both front and back antennas are shown in Fig. 2.32 for 800 MHz, 1800 MHz and 2600 MHz.

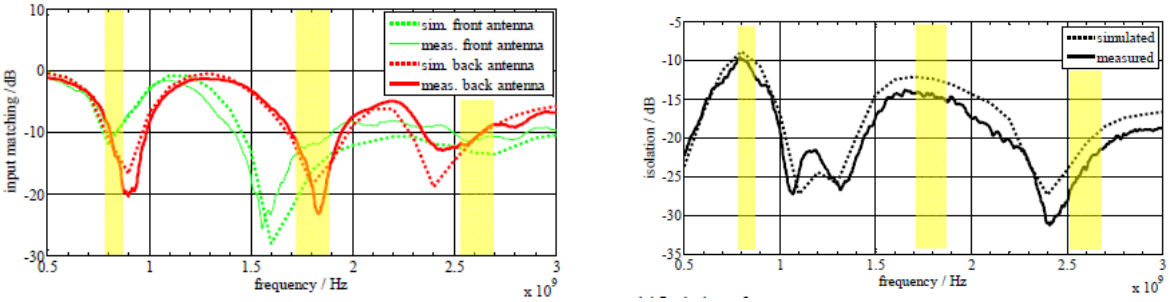

(a) (b)

Fig. 2.31 : (a) Reflection coefficient and (b) isolation of realized two antenna system (LTE and automotive roof top antenna) on MID.

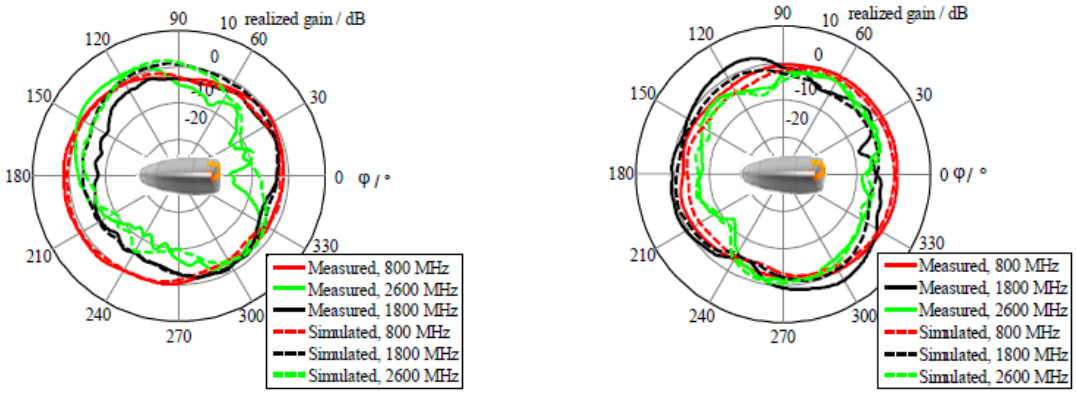

(a) (b)

Fig. 2.32 : (a) Radiation pattern at LTE frequencies of (a) front antenna and (b) back antenna.

Other than these MID antennas, the project organization 'MIDASS (Molded Interconnect Devices Applied to Smart Systems)' has briefly presented an AM/ FM antennas on PC/ABS xantar LDS 3710 [47]. Here, an AM/FM fractal antenna from the rear view mirror has implemented directly on the plastic piece as shown in Fig. 2.33.

Fig. 2.33 : AM/FM fractal antenna on MID.

Transmission lines are the fundamental components of any RF system and its compatibility in MID technology is an important study to be carried out. The design of an LDS Coplanar Waveguide (CPW) transmission line on an MID material Pocan DP T7140 is described in [50]. The objective of the study was to extract the substrate complex permittivity based on CPW S parameter (scattering parameters) measurement over a broad band of frequency from 0.8 GHz to 12 GHz. Other than the complex permittivity extraction of substrate based on line's S parameters measurement, MID transmission lines performance based on their losses or quality factor are hardly found in literature and this motivates the authors to drive attention of this thesis work.

For any RF circuit design, RF characterizations on molded thermoplastic substrates is really a matter of concern and hence a literature on the study on molded thermoplastic substrates has also been carried out. Section below explains them in detail.

2.4.6. Thermoplastic dielectric properties

While designing any RF circuit on MID, the choice of substrate is critical. There are approximately 61900 thermoplastic materials available in market [48]. The number of these commercially available thermoplastics is enormously increasing as the survey on January 2008 was 7000 [49].

The selection criteria of MID substrate are based on the application and fabrication method. Some of them are [49]:

- Thermal stability
- Processing capability for moulding and metallization
- Improved mechanical strength and good chemical resistance
- Reasonable cost and availability of material
- Stable dielectric properties over wide frequency, temperature and humidity range of values
- LDS requires special family of materials having good thermal stability, mechanical characteristics, solderability etc.

Many MID materials have been reported in literature. We can cite: various LCP (Liquid Crystal Polymer) materials, combination of ABS (Acrylonitrile Butadien Styrene) and PC (Polycarbonate), PSF (Polysulfone), PES (Polyethersulfone), PEI (polyetherimide), PPA (polyphthalamide), SPS (syndiotactic polystyrene), etc. [50]. The choice of MID material required for this thesis work is explained in detail in chapter 3. For any RF circuit design, the electromagnetic properties of the substrate used should be known with a good accuracy. Therefore, literature review on MID substrate EM properties was carried out and few information have been found out. Literatures provide EM characterization of MID substrate Pocan DP T7140 LDS based on four different measurement techniques within a frequency range of 0.1 GHz to 12 GHz [51]. Measurement results shows a relative permittivity (ε_r) of 3.9 – 4 and tangent loss (tan δ) of the order of 10^{-02} throughout the measured frequency band. In [42], C. Orlob et al has provided the electrical properties of Pocan TP 710-003 LDS as ε_r =3.26 and tan δ ~0.01. Another kind of Pocan thermoplastic family is Pocan PBT and its dielectric properties ε_r =3.4 and tan δ =0.01 at 6 GHz are given in [38]. The thermoplastic LCP E840i has ε_r =4.2 and tan δ =0.0027 at 2.67 GHz as given in [46]. The electromagnetic properties' characterization of other MID substrates is hardly found in the literature and hence this thesis work starts with the characterization of various MID samples (in chapter 3).

Thus, all the above mentioned MID RF circuits reveal the potential of MID especially for antenna applications. But still, a huge scope of research works on studying the potential and the limitations of MID fabrication techniques are there in the RF domain. Indeed, thermoplastics dielectric properties are still not well known in the literature. Classical RF components such as transmission lines, filters, couplers realized on MID have been studied neither. Thus, this thesis work has focus on the above mentioned areas.

2.5. Conclusion

This chapter introduces the thesis work and its outline to the readers. This chapter presents the overview of MID, its history and various existing fabrication methods. The advantages of using MID technology in comparison to the classical PCB board are presented. It also briefly described the recent development of MID technology in the automobile, medical and electronic circuits applications. Telecommunication domain is one of the main application fields of MID especially in the RF domain. Recently developed RF MID devices such as antennas, transmission lines are studied. The lack of knowledge in the RF domain has motivated the present thesis work. The following chapters discusses the dielectric properties of various molded thermoplastics and present the RF performance of several MID circuits such as transmission lines, filters, couplers, antennas etc. based on LDS, inkjet printing and LSS fabrication processes.

References

[1]. C. Orlob, D. Kornek, S. Preihs and I. Rolfes, "Characterization of Electromagnetic Properties of Molded Interconnect Devices Materials," German Microwave Conference, 2009.

[2]. W. Xu, "Research on Key Technology on MID," Second Pacific Asia Conference on Circuits, Communications and System (PACCS), 2010.

[3]. K. Feldmann, YP Shi, Y. Zhuo, "Three-Dimensional Automatic Routing in Design of Molded Interconnect Devices (MID)," Production Engineering, pp. 65-68, 2003.

[4]. J.A. Grande, "MIDs make a comeback", June 2005. Available online at: http://www.ptonline.com/articles/mids-make-a-comeback.

[5]. P. Mapleston, " 3D Interconnects offer sizeable market oppurtunity," Plasticope, pp. 42-44, March 1999.

[6]. LPKF Laser and Electronics, www.lpkf.com.

[7]. N. Heininger, W. John, and H. J. Bobler, "Manufacturing of Molded Interconnect Devices from Prototyping to Mass Production with Laser direct structuring,".

[8]. K. Feldmann and F. Pohlau, "MID in the automative Industry- Potentials, Benefits and Applications," IEEE CPMT Berlin International Manufacturing Technology Symposium, pp. 76-81, 1998.

[9]. D. Moser, J. Krause, "Multi functional package sensors in Automotive Applications", in the book of Advanced Microsystems for Automotive applications, 2006.

[10]. D. Reynaerts and H. Van Brussel, "Design of an Advanced Computer Writing Tool", Sixth International Symposium on Micro Machines and Human Science, IEEE, pp. 229-234, 1995.

[11]. "Molded Interconnect Devices Reshape electromechanical Design," Sept. 2000, Available online at http://electronicdesign.com/boards/molded-interconnect-devices-reshape-electromechanical-design.

[12]. A. Housden and J. Gould, "Molded Interconnect Devices," Prime Faraday Technology Watch, pp. 1-3, February 2002.

[13]. P. Glendenning, I. Annergren, T. J. Lett, and W. Xincai, "Molded Interconnect Device Technology Development," SIMTech Technical Report (PT/01/031/APP), 2001.

[14]. Three-Dimensional Circuits, LPKF LDS: Laser Direct Structuring for 3D Molded Interconnect Devices. Online available at: http://www.lpkf.fr/_mediafiles/1797-lpkf-lds-process.pdf.

[15]. R. Schlueter, B. Roesener, J. Kickelhain, and G. Naundorf, "Completely additive laser-based process for the production of 3D MIDs, The LPKF LDS process," in 5th International Congress Molded Interconnect Devices, Erlangen, Germany, 2002.

[16]. LPKF Laser and Electronics- Approved LDS materials, Online available at: http://www.lpkf.com/_mediafiles/2074-approved-plastics-lpkf-lds.pdf.

[17]. P. Khuntontong, "Fabrication of Polymer Micro Devices by Ultrasonic Hot Embossing," Doctor of Engineering Science Dissertation, Sukhothai, Thailand, October 2008.

[18]. LPKF Laser & Electronics - Wertpapier Forum, October 6, 2010.

[19]. B. V Thales Nederlands, R. Legtenberg, and H. Adelaar, "A method for plating a copper interconnection circuit on the surface of a plastic device".

[20]. W. Hunziker, "Chip Assembly on MID (Molded Interconnect Device)- A Path to Chip Modules with increased Functionality," Harting tec. News, January 2005.

[21]. K.Gilleo, D. Jones, and G.P.V. Diep, "Thermoplastic Injection Molding: New Packages and 3D Circuits," ECWC conference 10 at IPC Printed Circuits Expo, 2005.

[22]. A. Islam, H. N. Hansen, P.T. Tang, and J. Sun, "Process Chain for the Manufacturing of Molded Interconnect devices," International Journal Adv. Manufacturing Technology, pp.831-841, 2009.

[23]. Y. Zhuo, J. Peng, and Y. Wu, "Design an simulation of molded interconnect devices with two shot molding," Advanced Materials Research, Vol. 295-297, N0. 6, pp. 1651-1655, July. 2011.

[24]. H. J. V. Osch, J. Perelaer, A. W. M. Laat and U. S. Schubert, " Inkjet Printing of Narrow Conductive Tracks on Untreated Polymer Substrates," Advanced Materials, vol. 20, pp. 343-345, 2008.

[25]. H. L. Kao, C. L. Cho, L. C. Chang, C. S. Yeh, B. W. Wang and S. C. Chiu, " Inkjet printing RF bandpass filters on liquid crystal polymer substrates, " Thin Solid Films, pp. 1-5, 2013.

[26]. MID LED- Diodes by 2E Mechatronic GmbH & Co. KG, Germany, Feb. 2013. Available online at: http://news.directindustry.com/press/2e-mechatronic-gmbh-co-kg/mid-led-diodes-2e-71712-384429.html.

[27]. http://www.mouser.com/ds/2/276/987650-5702-1748.pdf.

[28]. C. Goth and M. Romer, "Position Sensor for Adaptive Speed Control," HArting Mitronics. Online available at: http://www.harting-mitronics.ch/fileadmin/hartingmitronics /case_studies/Position_sensor_for_adaptive_speed_control.pdf.

[29]. C. Goth and M. Romer, "Light Sensor Regulating Air Conditioning systems," Harting Mitronics. Online available at: http://www.harting-mitronics.ch/fileadmin/hartingmitronics/case_studies/Sun_sensor_for_climate_control.pdf.

[30]. C. Goth and M. Romer, "Lighting Module for Vehicle Passenger Compartment," Harting Mitronics. Online available at: http://www.harting-mitronics.ch/fileadmin/hartingmitronics /case_studies/Lighting_module_for_vehicle_interior.pdf.

[31]. C. Goth and M. Romer, "Optics Carrier and Heating Element for the Diagnosis of Caries," Harting Mitronics. Online available at: http://www.harting-mitronics.ch/fileadmin/hartingmitronics/case_studies/Optics_carrier_and_heating_element_for_the_diagnosis_of_caries.pdf.

[32]. M. Hedges, "3 D Printed Electronics via Aerosol Jet Printing," March 2013. Available online at: http://webcache.googleusercontent.com/search?q=cache:6hwWoJG0S1gJ:www.zve-kurse.de/Berichte.html%3Ffile%3Dtl_files/pdf/GFE_Forum/07%2B3D%2BPrinted%2BElectronics%2Bvia%2BAerosol%2BJet%2BPrinting.pdf+&cd=12&hl=en&ct=clnk&gl=fr&client=firefox-a.

[33]. J. Hoerber, J. Glasschroeder, M. Pfeffer, J. Schilp, M. Zaeh and J. Franke , "Approaches for Additive Manufacturing of 3D Electronic Applications," Proceedings of the 47th CIRP Conference on Manufacturing Systems, vol. 17, pp.806-811, July 2014.

[34]. K. Schuetz, J. Hoerber and J. Franke , "Selective Light Sintering of Aerosol- Jet Printed Silver Nanoparticle Inks on Polymer Substrates, " Proceedings of the 29th International Conference of the Polymer Processing Society (PPS-29), pp.732-735, May 2014.

[35]. B. Stumpp, "LED-Lampen als Molded Interconnect Devices günstig fertigen", Online available at http://www.all-electronics.de/texte/anzeigen/53057/LED-Lampen-als-Molded-Interconnect-Devices-guenstig-fertigen.

[36]. C. Goth and M. Romer, "PT 86 (HT) passive UHF Transponder, " Harting Mitronics. Online available at: http://www.harting-mitronics.ch/fileadmin/hartingmitronics/case_studies/PT_86__HT__passive_UHF_transponder.pdf.

[37]. C. Goth and M. Romer, "Safety Caps for Payment Terminals," Harting Mitronics. Online available at: http://www.harting-mitronics.ch/fileadmin/hartingmitronics/case_studies/Safety_ caps_for_payment_terminals.pdf.

[38]. C. Goth and M. Romer, “Light Module for a Safety System,” Harting Mitronics. Online available at: http://www.harting-mitronics.ch/fileadmin/ hartingmitronics/case_studies/Lighting_ modules_for_a_safety_system.pdf.

[39]. C. Goth and M. Romer, "Sensor Platform for a Large Format Camera," HArting Mitronics. Online available at: http://www.harting-mitronics.ch/fileadmin/hartingmitronics/ case_studies/Sensor_platform_for_a_large-format_camera.pdf.

[40]. J. Thevenard, D. L. H. Tong, A. Louzir, C. Nicolas, C. Person, J. P. Coupez, “Switched Beam 3D- Vivaldi Antennas for WLAN Applications,” International Symposium on Antennas and Propagation (ISAP), August 2007.

[41]. D. Kornek, E. Slottke, C. Orlob and I. Rolfes, “Experimental Investigation of Bent Patch Antennas on MID Substrate,” European Conference on Antennas and Propagation 2010, April 2010.

[42]. C. Orlob, Q. H. Dao and D. Kornek, “Dual- Polarized Log.- Periodic Antenna on a Conical MID Substrate, ” Proceedings of the 5th European Conference on Antennas and Propagation (EUCAP), 2011.

[43]. F. Sonnerat, R. Pillard, A.Cihangir, F. Ferrero, F. Le Pennec, C. Person, and C. Luxey, “Wideband LDS Antenna using two Radiating Elements,” Loughborough Antennas and Propagation Conference, November 2012.

[44]. F. Sonnerat, R. Pillard, F. Gianesello, F. Le Pennec, C. Person, and D. Gloria, “Innovative LDS Antenna for 4G Applications,” 7th European Conference on Antennas and Propagation (EUCAP), 2013.

[45]. N. Heininger, P. Mansikkamaki, M. Kivikoski, Y. H. Lee, Advanced antennas for mobile phones, Available online at: http://www.lpkf.com/_mediafiles/1633-antennas-formobile-phones.pdf.

[46]. A. Friedrich, B. Geck, O. Klemp, and H. Kellermann, “On the Design of a 3D LTE Antenna for Automotive Applications Based on MID Technology,” 43rd European Microwave Conference (EuMA), 2013, pp.640-643.

[47]. “Molded Interconnect Devices Applied to Smart Systems (MIDASS),” Plastronics Technologies or how Plastics allow Electronics to access the third dimension, December 2010, PEP, France. Online available at :
http://www.innovdays-plasturgie.com/innovdays/Illustrations/Documents/InnovDays/2010 /20101209_plastronique/03_MIDASS.pdf.

[48]. Material property data website, www.matweb.com, Last access: 17-09-2014.

[49]. A. Islam, "Two Component Micro Injection Moulding for Molded Interconnect Devices," PhD Dissertation, Dept. of Mechannical Engineering, Technical University of Denmark, February 2008.

[50]. Electronic design, Moulded Interconnect Devices Reshape Electromechanical Design, available online at http://electronicdesign.com/boards/molded-interconnect-devices-reshape-electromechanical-design.

[51]. C. Orlob, D. Kornek, S. Preihs, I. Rolfes, "Characterization of electromagnetic properties of molded interconnect device materials" German Microwave Conference 2009 (GeMic 2009), Munich, 16- 18 March 2009.

Chapter-3

Electrical Properties of MID Materials

In order to use MID (Molded Interconnect Device) technology for RF (Radio Frequency) applications, the precise knowledge of electromagnetic properties of MID materials is required. Since these parameters are not well quantified in the literature yet, both MID thermoplastic substrates and metallic traces have been characterized. This chapter deals with the thermal and dielectric characterization of MID thermoplastic substrates and electrical measurements of metals used for defining circuit traces. First of all, the thermal properties of various MID substrates based on TGA (Thermal Gravimetric Analysis) method[1] are presented in this work. Later on, this chapter deals with the dielectric characterization of MID thermoplastic substrates based on a resonant cavity method which provides a high accuracy of measurements. Several molded thermoplastics such as LCP (Liquid Crystal Polymer) Vectra E820i, LCP E130i, ABS PC (Acrylonitrile Butadiene Styrene Poly Carbonate) Cycoloy C1200HF, ABS PC Xantar LDS (Laser Direct Structuring) 3710, PC LDS Xantar 3730, PBT (PolyButylene Terephthalate) Pocan 7102 LDS, PBT Ultradur B4520, PPA (PolyPhthalAmide) LDS RTP 4099* 117359D and PA (polyamide) 66 Ultramid A3K have been characterized in terms of their dielectric properties. The tested substrates were selected for their interesting mechanical and thermal properties. These measurement results were used to qualify the substrates for RF applications. Thereafter, four points probe measurement method is used for electrical resistivity measurement of metals[2]. Two different metallization were studied in this thesis work based on the fabrication process of circuit: a metallization based on Ni/Au/Cu (a combination of nickel, gold and copper) used in LDS and laser ablation fabrication method and silver ink metallization in inkjet printing fabrication method. The obtained characterized results were used for the further design of RF circuits presented in the following chapters.

---

[1]Measurements are done by research lab Ecam

[2]Measurements are done by industrial project partner MIND and CMP,EMSE

3.1. Introduction

The electrical performance and reliability of RF components depend strongly on the substrate properties, in particular its permittivity, permeability and the conductivity of metallic traces. In most cases, substrates have no magnetic properties and therefore their permeability is considered similar to that of vacuum. Consequently, the most important parameter to consider for MID substrate characterization is its complex dielectric permittivity. Indeed, it is necessary to know the dielectric properties of the media that interacts with electromagnetic waves. As a rule of thumb, for telecommunication and radar devices, knowing the variation of complex dielectric permittivity over a wide frequency range is important and necessary for performance optimization [1].

In addition, if we want to precisely determine the intrinsic impedance value of a medium (η), which is the ratio of electrical field strength E and magnetic field strength H, the accurate measurement of dielectric constant would be one of the most significant requirements. For a given medium having permittivity and permeability given respectively as ε ($=\varepsilon_0\varepsilon_r$) and μ ($=\mu_0\mu_r$) and conductivity σ associated with it, the intrinsic impedance can be derived from the Maxwell's equations [2] as:

$$\eta = \sqrt{\frac{j\omega\mu}{\sigma + j\omega\varepsilon}} \quad . \tag{3.1}$$

As most of the dielectric materials such as paper, plastic, etc. have no magnetic properties, one can safely assume that μ_r is 1. To this end, many techniques have been developed for the measurement of dielectric material complex permittivity in the RF domain [3][11].

Thermoplastics used in MIDs vary depending on the manufacturer or supplier. The selection of the MID substrate material is often a complex choice, giving the required balance between electrical, thermal and mechanical properties and consideration of ease of manufacture and cost. For RF circuit design in MID technology, thermoplastics with good physical properties and high thermal stability are considered. The selection of thermoplastic depends on the application domain and manufacturing process. Fig. 3.1 illustrates the thermal stability of common LPKF-LDS (Laser Direct Structuring) graded thermoplastic materials [12]. LCP (Liquid Crystal Polymer) grabs the high temperature stability among the other thermoplastics.

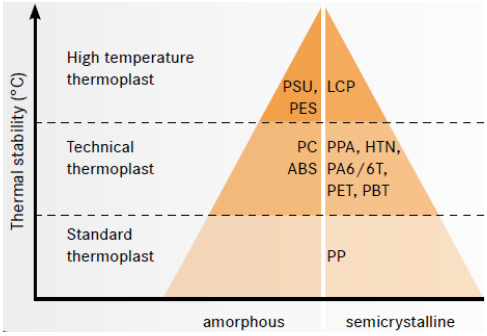

Fig. 3.1 : Thermal stability of LDS thermoplastics [12].

Some advantages of these thermoplastics that attract electronic industries are:

1. Improved mechanical properties: these thermoplastics show high level of rigidity, strength and resistance to faintness.
2. Withstand the environmental condition: thermoplastics resist the exposure of chemicals, solvents, radiation and heat and do not deform its original shape upon exposure.
3. Recyclable: MID thermoplastics are easily recyclable and hence can be remold to any shape several times. The thermoplastic still shows the same dimensional integrity and strength as before.

Several thermoplastics were characterized in this thesis work: LCP Vectra E820i, LCP E130i, ABS PC (Acrylonitrile Butadiene Styrene Poly Carbonate) Cycoloy C1200HF, ABS PC Xantar LDS 3710, PC LDS Xantar 3730, PBT (PolyButylene Terephthalate) Pocan 7102 LDS, PBT Ultradur B4520, PPA (PolyPhthalAmide) LDS RTP 4099* 117359D and PA (polyamide) 66 Ultramid A3K. The fabrication process will be explained in detail in chapter 4. The study of the thermal properties of these thermoplastics have been carried out based on TGA (Thermal Gravimetric Analysis) and are presented in section 3.2. Measurement of dielectric properties of these substrates were performed by using resonant cavity method providing a high accuracy of measurements with an error less than 0.1%. Section 3.3.2.2 presents the measurement results of the above mentioned MID substrates.

In addition to the characterization of dielectric substrates, electrical properties of the metallic traces are essential to define the RF circuit characteristics and particularly losses. The effect of metallization on RF losses is mainly based on the conductivity and the thickness of the metal trace. An alternative current travelling along a conductor experiences losses with the square root of frequency due to the skin effect. The skin effect occurs when the skin depth

is smaller than the thickness of the conductor. The skin depth δ for the conductor having σ as conductivity is given by [13]:

$$\delta = \frac{1}{\sqrt{\pi \mu \sigma f}} \tag{3.2}$$

Where, f is the frequency in hertz. Based on the above equation, the skin depth varies as an inverse square root of frequency. Good conductors have reduced skin depth and overall resistance on current flow. In order to predict any circuit conductive losses, conductivity of metallization should be first determined. In this chapter, the conductivity measurement is achieved based on sheet resistivity and thickness using four points probe measurement method. Metallization properties for LDS, LSS and inkjet printing fabrication method are considered in this thesis work in section 3.4.

3.2. Thermal properties of MID substrates

This section describes the thermal analysis of certain molded MID substrates done by Ecam (Ecole Catholique d'Arts et Métiers), Lyon, France. This section describes the thermal analysis of certain molded MID substrates. The analysis is done based on TGA method. Fig. 3.2 shows the test bench for thermal analysis.

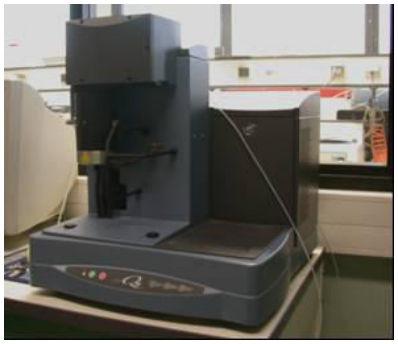

Fig. 3.2 : Photograph of the equipment of TGA.

The study is performed under a working inert atmosphere (N_2) or air flow from 25°C to 1000°C. Sample under test can be in the form of powder, grains or even liquid form. Here, the thermoplastic samples are used for thermal analysis and are provided by Radiall Centr'alp, France. The mass of the sample required is 10 mg. The thermoplastic samples used for analysis are ABS PC Cycoloy, PC Xantar 3730, ABS PC Xantar 3710, PPA RTP 4099 x 117359, PBT Ultradur, PBT Pocan 7102, PA 66 Ultra MID A3K, PPARTP and LCP Vectra E820i. Fig. 3.3 shows the thermal properties of MID LDS samples with respect to their mass. It can be seen that LCP Vectra E820i holds high thermal stability

among the tested samples. Its temperature of degradation is at 511^{0}C whereas all other samples degrade at temperatures below 450^{0}C. PBT Pocan 7102 degrades easily at 348^{0}C. Also, LCP Vectra has less percentage of degradation of mass in comparison to other samples. It holds 60% of mass after degradation till 1000^{0}C, whereas PA66 Ultramid A3K holds only 1% of its mass after degradation till 1000^{0}C. Table 3.1 summarizes the thermal analysis of each MID sample.

Table 3.1: Thermal analysis of MID thermoplastics based on TGA method.

Thermal properties analyzed MID Samples	**Temperature of degradation (°C)**	**Residue of sample (weight %)**
LCP Vectra E820i	511	60
PC Xantar3730	449	30
ABS PC Cycoloy	407	17
PPA RTP	407	17
ABS PC Xantar 3710	400	14
PPA RTP4099 X 117359	365	19
PA 66 Ultra MID A3K	361	1
PBT Ultradur	348	6
PBT Pocan 7102	348	31

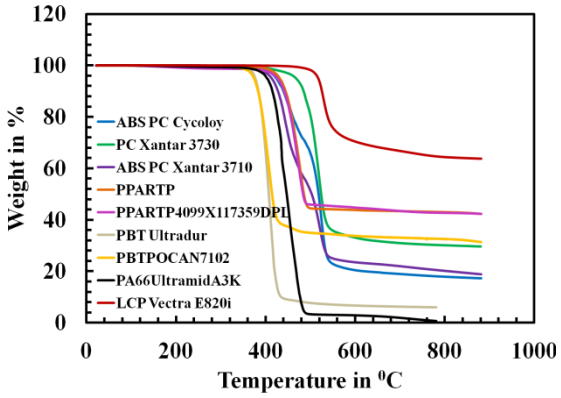

Fig. 3.3 : Thermal analysis of LDS MID thermoplastics based on TGA method under N_2, at 10 ° C / min.

Further dielectric properties characterization of MID substrate materials are presented in the following section.

3.3. Dielectric characterization

Permittivity is a quantity used to describe dielectric properties that influence reflection and transmission of electromagnetic waves at interfaces as well as the wave energy propagation in the materials. In frequency domain, the complex permittivity ε of a material can be expressed in the following form [14]:

$$\varepsilon = \varepsilon_r \, \varepsilon_0 = (\varepsilon_r' - j\varepsilon_r'') \, \varepsilon_0 \tag{3.3}$$

where ε_0 is the permittivity in the vacuum and ε_r is the material relative complex permittivity.

The real part ε_r' refers to the dielectric constant which represents stored energy when the material is exposed to an electric field, while the dielectric loss factor ε_r'' which is the imaginary part, influences energy absorption and propagation attenuation. The frequently used parameter in EM theory is the tangent of loss angle or the loss tangent and the loss tangent of a dielectric medium is defined as [15]:

$$\tan(\delta) = \frac{\varepsilon''}{\varepsilon'} . \tag{3.4}$$

Precise measurement of material's dielectric properties is important to predict the system performance and optimize it in the RF domain. Many methods have been developed for measuring materials' complex permittivity and are discussed in details in the following section.

3.3.1. An overview of dielectric characterization methods

A review on various measurement methods for dielectric characterization of materials has been done. Widely used types of measurement methods at microwave frequencies are:

- coaxial probe method
- free space method
- parallel plate method
- transmission line method
- resonant cavity method

A measurement method for material characterization is selected based on certain criteria; its measurement accuracy, frequency of interest such as narrow band or broad band

frequency, characteristics of material under test (MUT) such as high or low dielectric loss, thin or bulk material, destructive or non destructive MUT preparation etc. [16]. Measurement methods can be further categorized based on discrete frequency measurement or continuous frequency measurement. In discrete frequency measurement, the characterized values are provided at certain resonant EM modes whereas in continuous frequency measurement method, the EM waves pass through the material such that it sweeps a stimulus frequency continuously over the desired frequency band. Description of each measurement method is given below.

3.3.1.1. Coaxial probe method: This is a commonly used convenient method for lossy material characterization at higher frequencies. In this method, an open-ended coaxial probe along with network analyser is used for the measurement of dielectric properties of MUT [22]-[24]. This method is usually used for the dielectric characterization of liquids, semi-solids, biological specimens etc. In this method, the metallic probe is immersed into the liquid or pressed to the flat face of the semi-solid MUT. The probe senses the reflected signal from the MUT. The permittivity is measured based on the reflection coefficient of the probe measured with the network analyser. Fig. 3.4 presents the illustration for a coaxial probe for dielectric characterization. This method provides a broadband frequency range of measurement from 0.5 GHz to 110 GHz [20]. One of the disadvantages of this method is that the measurement shows some deflection for the low permittivity materials [20].

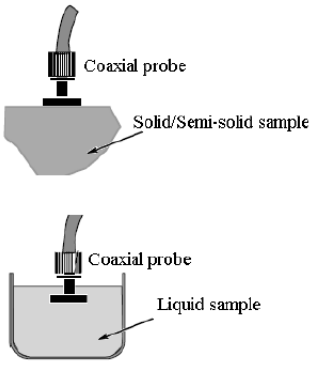

Fig. 3.4 : Coaxial probe method of characterization [19][12].

3.3.1.2. Free space method: This method provides a broadband frequency measurement of permittivity and permeability of MUT. The measurement set up consists of the MUT placed in parallel between two identical horn antennas operating in certain frequency range and connected to network analyzer. The antenna is used to pass microwave energy through the MUT. Fig. 3.5 shows the measurement set up of free space method. It is

based on the measurement of transmission and reflection coefficient of MUT for different polarization states, angle of incidence, MUT thickness and frequencies. MUT can be dielectric or magnetic solids, liquids or gases with large, flat and homogeneous characteristics [21].

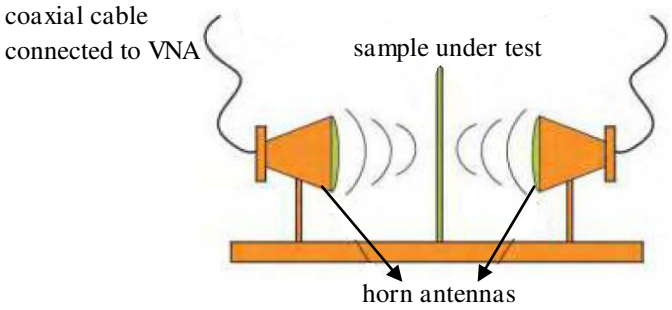

Fig. 3.5 : Free space method of characterization [21][12].

This method is non contacting and is useful to characterize samples to be tested at high temperatures and hostile environment. The sample can be heated inside a furnace that has microwave transparent windows. As the samples are not touched or contacted, the high temperature measurement can be performed.

3.3.1.3. Parallel plate Method: Here, measurements are performed based on the principle of parallel plate capacitor. Thin sheet dielectric MUT is sandwiched between two electrodes to form a capacitor (see Fig. 3.6). Measurements are taken using impedance analyzer or LCR meter and a dielectric fixture. Calculation of dielectric values are based on the dimension of the MUT and capacitance and dissipation factor measured. This measurement provides an accuracy of ±1% for ε_r' and ±5% for ε_r''. This method is usually used for low frequencies measurement, <1 GHz [19].

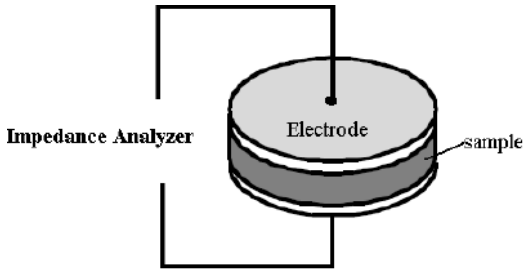

Fig. 3.6 : Parallel plate method of characterization [19][12].

3.3.1.4. Transmission line method: Various transmission line methods can be found in literature for characterizing dielectric samples [22]-[26]. The main advantage of transmission line technique is the broadband continuous frequency measurement of

dielectric properties. The transmission or reflection of signals is measured to characterize the material. Transmission line techniques are further divided into two categories as:

1) **Distribution transmission method**, in which S parameters (scattering parameters) S_{11} and S_{21} are measured for the calculation of dielectric properties. A transverse dielectric sample is loaded in a waveguide and transmission signal (S_{21}) and reflection signal (S_{11}) is measured. Here, the limitation of measurement is mainly based on the thickness of the sample. The thickness should be less than half wavelength to avoid resonance. The loss tangent measurement is a limitation in this method and the loss tangent of greater than 10^{-2} is valid. For samples having loss tangent less than 10^{-2}, the signal deterioration is too small to be precisely detected by the measurement device. Fig. 3.7 illustrates the distribution transmission method.

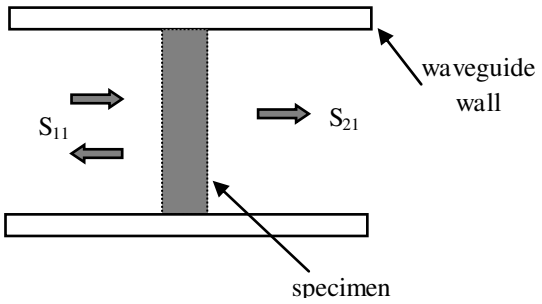

Fig. 3.7 : Distribution transmission method illustration.

2) **Two transmission lines method**: Another accurate method of dielectric characterization in broad band frequency is two transmission line method. In this method, the S parameters of two transmission lines designed on the MUT are used for dielectric characterization. The fundamental concept of this method is to de-embed the parasitic contribution of interconnects needed to access the device under test using S parameter measurements of two transmission lines of different lengths. Dielectric permittivity extractions are based on ABCD matrix, easily extracted from the S parameters [26].

The method of extraction can be explained with the illustration given in Fig. 3.8. Two symmetrical transmission lines test structures of length l_1 and l_2 ($l_2>l_1$) are used for characterization. The transmission matrix of each test structure is composed of the two pads, the intrinsic device and the associated pad line discontinuities. For calculation simplicity, the pad line discontinuities are associated with the two pads. Here, the ABCD matrix of transmission lines l_1 and l_2 are represented by M^t_{l1} and M^t_{l2} respectively.

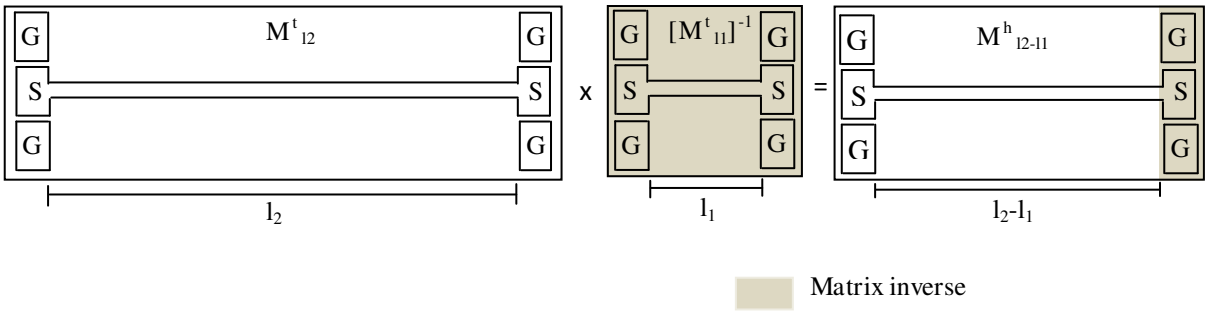

Fig. 3.8 : Two transmission lines method illustration.

The calculation starts by deriving an equation for the intrinsic transmission line ($M^h_{l2\text{-}l1}$) by multiplying M^t_{l2} and inverse of M^t_{l1}.

$$M^h_{l2-l1} = M^t_{l2} * \left[M^t_{l1}\right]^{-1} \tag{3.5}$$

$$M^h_{l2-l1} = M_{p1} M_{l2} M_{l1}^{-1} M_{p1}^{-1} \tag{3.6}$$

$$M^h_{l2-l1} = M_{p1} M_{l2-l1} M_{p1}^{-1} \tag{3.7}$$

Where M_{p1} represents the left pad and $M_{l2\text{-}l1}$ is the intrinsic line segment of the structure. Assuming that the left pad can be modeled by a lumped admittance, Y_L, equation 3.7 becomes:

$$M^h_{l2-l1} = \begin{bmatrix} 1 & 0 \\ Y_L & 1 \end{bmatrix} M_{l2-l1} \begin{bmatrix} 1 & 0 \\ -Y_L & 1 \end{bmatrix} \tag{3.8}$$

Equation 2.8 is referred to as the lumped pad assumption. Under this assumption, $M^h_{l2\text{-}l1}$ can be expressed in terms of Y parameters, as a parallel combination of intrinsic transmission line and parasitic lumped pads. Hence equation 3.8 becomes

$$Y^h_{l2-l1} = Y_{l2-l1} + \begin{bmatrix} Y_L & 0 \\ 0 & -Y_L \end{bmatrix} \tag{3.9}$$

The effect of left pad in the equation can be cancelled by isolating $Y_{l2\text{-}l1}$ by connecting $Y^h_{l2\text{-}l1}$ in parallel with a port swapped version of itself as shown in equation 2.10:

$$Y_{l2-l1} = \frac{Y^h_{l2-l1} + \text{swap}(Y)^h_{l2-l1}}{2} \tag{3.10}$$

For this intrinsic transmission line of physical length l_2-l_1, a complex propagation constant γ and a characteristic impedance Z_c can be derived from the ABCD matrix given as:

$$M_{12-11}=\begin{bmatrix} A & B \\ C & D \end{bmatrix}=\begin{bmatrix} \cosh\gamma(l_2-l_1) & Z_c\sinh\gamma(l_2-l_1) \\ Z_c^{-1}\sinh\gamma(l_2-l_1) & \cosh\gamma(l_2-l_1) \end{bmatrix} \tag{3.11}$$

The effective dielectric constant and loss tangent can be calculated as [14]:

$$\varepsilon_{reff}=\left(\frac{c\beta}{\omega}\right)^2 \tag{3.12}$$

$$\tan(\delta)=\left(\frac{G}{C\omega}\right) \tag{3.13}$$

Where c defines the velocity of light in m/s, β is the phase constant represented as the imaginary part of γ, and ω is the angular frequency. G and C are transmission line parameters respectively as conductance in S/m and capacitance in F/m which can be calculated from Z_c and γ. Equation 3.14 is a first approximation of low losses.

$$G=\mathrm{Re}\left(\frac{\gamma}{Z_c}\right) \tag{3.14}$$

$$C=\frac{\mathrm{Im\,ag}\left(\frac{\gamma}{Z_c}\right)}{\omega} \tag{3.15}$$

Where,

$$\gamma=\frac{a\cosh(A)}{l_2-l_1} \tag{3.16}$$

$$Z_c=\sqrt{\frac{B}{C}} \tag{3.17}$$

3.3.1.5. Resonant cavity method: Resonant cavities are high quality structures with specific resonant frequencies. The resonant cavity method based on the perturbation cavity principle allows the determination of the permittivity with a high accuracy. The dielectric sample is placed at the position of maximum electric field. The required size of the dielectric sample should be small enough so that the electric distribution of the empty cavity changes slightly when the cavity is loaded. Therefore, a shift in resonance frequency and quality factor of the cavity occurs when the sample is inserted.

From measurements of empty and partially loaded cavity, the complex permittivity of the material can be calculated at different resonance frequency points [7]-[9][11][37]. A typical measurement system consists of a network analyzer, a resonant cavity fixture and software to make the calculations. A schematic diagram of an experimental setup of the cavity resonant technique is shown in Fig. 3.9. a, b and c denote respectively width, height and length of the cavity.

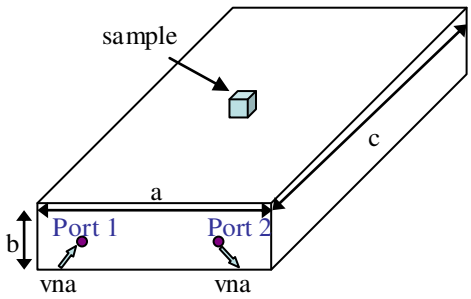

Fig. 3.9 : Schematic diagram of a resonant cavity.

The cavity perturbation method is not a swept frequency measurement. Indeed, the cavity shape as well as the dimensions of the sample determines resonance frequencies. Hence, it can be used only for discrete frequency measurements.

First of all, the resonant frequency and quality factor of the empty cavity are determined for different cavity modes. Then, the sample is inserted and positioned at the E-field antinodes. If the sample is purely dielectric, the maximum electric field can be easily determined. The mode will shift to low frequency side and retraces from there as presented in Fig. 3.10. The sample is kept at the retracing position, where the electric field is maximum.

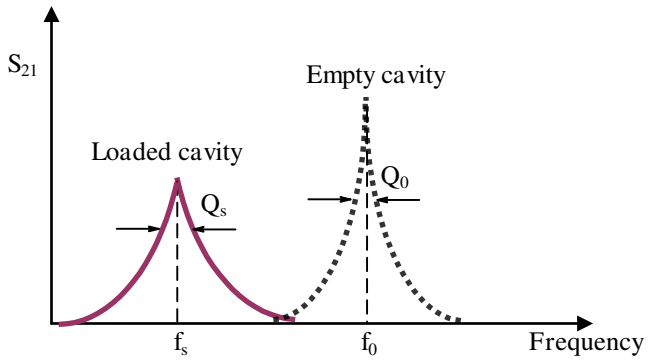

Fig. 3.10 : Frequency responses for empty and loaded cavities.

According to perturbation technique, dielectric permittivity and losses of a sample under study are determined as follows:

$$\varepsilon_r' = 1 + k' \frac{V_c}{V_s} \frac{f_0 - f_s}{f_s} \tag{3.18}$$

$$\varepsilon_r'' = k'' \frac{V_c}{V_s} \left(\frac{1}{Q_s} - \frac{1}{Q_0} \right) \tag{3.19}$$

Where, f_0 is the resonant frequency of the empty cavity, f_s is the resonant frequency of the cavity with sample, V_c is the volume of the cavity and V_s is the volume of the sample, Q_0 is the quality factor of the empty cavity and Q_s is the quality factor of the cavity with sample. *k'* and *k''* parameters are generally assumed to be constant, which depend on the geometry and the location of the sample and resonant mode of the cavity, but approximately independent of the permittivity of samples.

It is very complicated to calculate *k'* and *k''* using classical EM analytical methods. Thus, these parameters are usually obtained by a calibration method using a known permittivity sample. It should be pointed out that the standard sample should be as small as possible and should have a similar geometry with the samples to be measured, so as to improve the measurement accuracy.

The calculations of dielectric properties of the sample are simple based on the resonance frequency and quality factor of partially loaded and empty cavity. However, the main disadvantage of the cavity method is that the measured results are applicable only over a narrow frequency band. The loss tangent measurement of less than 10^{-03} is not recommended with resonant cavity method [38].

In this thesis work, transmission line and resonant cavity methods have been used for MID material characterization. The main difference in the two techniques is that the transmission line technique does a continuous frequency measurement whereas resonance technique does a discrete frequency measurement. Besides, the resonant cavity provides a highest accuracy for permittivity measurement than transmission line technique. This chapter presents the MID dielectric properties obtained from resonant cavity method. In the following chapters, MID characterization based on transmission lines method is achieved.

3.3.2. MID substrate characterization

All MID thermoplastic substrates used for dielectric characterization in this research work have been molded in plates of dimensions of 10 x 10 x 0.2 cm^3 by PEP [27], thanks to the partnership project PLASTRONICS [28]. The LDS molded thermoplastics are low cost compared to classical substrates. LCP holds a cost of nearly 45€/kg, cost of PA is nearly

25€/kg, 15€/kg is the cost of PBT and ABS/PC has 10€/kg. LDS materials are more expensive than classical thermoplastics. Various MID based thermoplastics that are characterized are shown in Fig. 3.11.

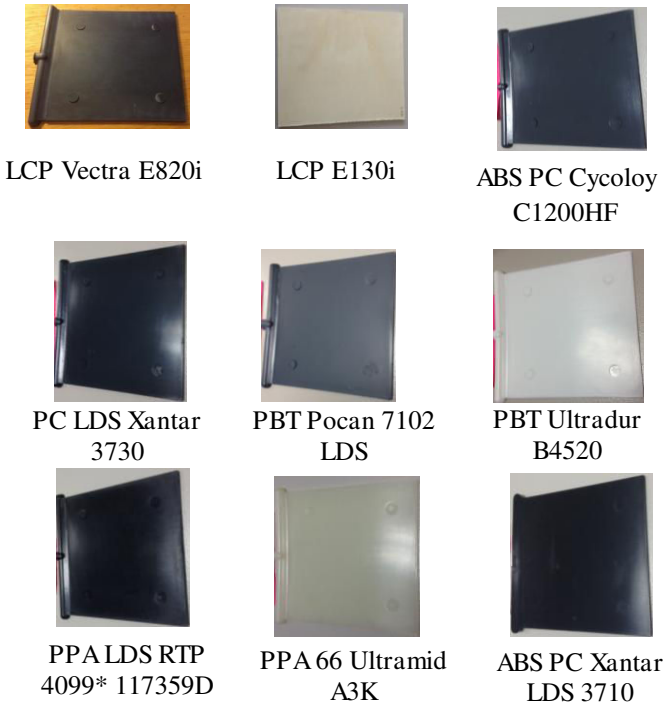

Fig. 3.11 : MID substrates used for characterization.

The measurement set up and its characterization results are given below.

3.3.2.1. Measurement set up

The Damaskos Thin Sheet Tester cavity [29] used for dielectric characterization is presented in Fig. 3.12. The cross sectional dimensions of this cavity are 20 cm in width, 43 cm in length and 3.8 cm in height. It is ideal for thin dielectric sheets measurements ranging in thickness from about 0.05 mm to the order of 3 mm. This cavity offers very good repeatability that can be less than 0.1%. The electric coupling is provided with two symmetrical VNA probes. Two cables should be connected between the SMA connectors on the cavity and ports 1 and 2 on the network analyzer.

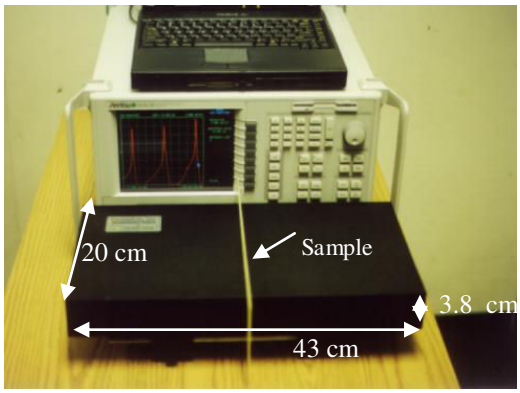

Fig. 3.12 : Damaskos cavity photograph.

Damaskos cavity is furnished with a Cavity™ software pre-installed allowing the direct extraction of the complex permittivity of the sample under test. For some combination of thickness, dielectric constant, and loss tangent, fewer or more resonance frequency points can be measured. The first seven odd TE_{10n} modes of the cavity applied in this work resonate at 0.808 GHz, 1.265 GHz, 1.870 GHz, 2.519 GHz, 3.184 GHz, 3.862 GHz and 4.538 GHz, respectively.

As mentioned before, for a good characterization of dielectric values, a reference material must be measured before moving on to the measurement of the unknown sample. If the known reference sample is not measured, the measurement is not calibrated and the dielectric constant accuracy will be better than 1.5% for 1mm thick samples [29]. Thicker samples exhibit lower accuracy. Also, the reference material for calibration should have thickness and dielectric constant near to the sample under test. For MID substrates characterization, a reference material having dielectric constant 4.2 - 4.3 and thickness 1.958 mm is used (Fig. 3.13). All the MID samples used here for characterization do not cover the entire section of the resonant cavity which results in errors at higher modes of extraction. This error appears in the dielectric extraction results above 4 GHz.

Fig. 3.13 : Reference material used for Damaskos cavity calibration.

3.3.2.2. Dielectric characterization results

The MID materials which are assumed to be isotropic and homogeneous, and are characterized for the first seven resonant frequencies. To study the repeatability in dielectric properties of MID substrates, each sample have been measured two times. Samples can be categorized as LDS and non LDS materials. Thermoplastics LDS LCP Vectra E820i, LDS

ABS PC Xantar 3710, LDS PBT Pocan 7102, LDS PPA RTP 4099 x 117359D and LDS PC Xantar 3730 come under LDS materials and all other characterized thermoplastic come under non LDS materials.

1) LDS LCP Vectra E820i is an LDS material which is highly crystalline, and thermotropic material delivering exceptionally precise and stable dimensions, high temperature performance and chemical resistance. As mentioned before, LCP holds a cost of 45€/kg. Fig. 3.14 depicts the dielectric properties of LCP vectra E820i in terms of its relative permittivity and tangent loss. Two repetitive measurements on characterizations show good agreement between each other in its relative permittivity with a value of 4.2-4.4 and tangent loss of 0.0035 to 0.0048 at 0.80-4.53 GHz. Decrease in permittivity occurs at and above 4 GHz is mainly due to the limited size of sample used for extraction.

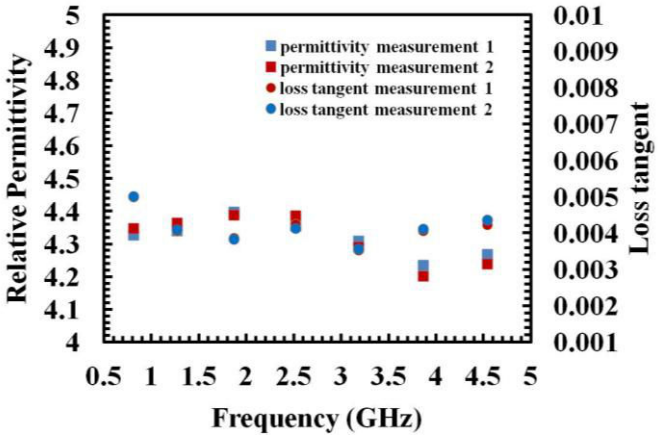

Fig. 3.14 : Dielectric properties of LDS LCP Vectra E820i.

2) LCP E130i, a thermoplastic polymer which is a suitable candidate for electronic applications. Common affordable plastics such as PET (Poly Ethylene Terephthalate) and PA which are used as substrates in printed electronics present a low glass transition temperature which limits the electrical properties of printed patterns. Contrary to that, LCP whose high temperature resistance enables to consider this plastic for the fabrication of electronic printed devices. Also LCP is known for its compatibility with high frequency applications such as RFID (Radio Frequency Identification) technology due to it permittivity and it loss tangent. One disadvantage of this polymer is its surface roughness which is a problem for achieving good conductivities in printed electronics. Also, this thermoplastic is incompatible for LDS fabrication.

The substrate shows a good repeatability in extraction of dielectric properties as shown in Fig. 3.15. It has permittivity value of 3.64-3.72 and tangent loss of nearly 0.0055 -0.0065 in the 0.80-4.53 GHz frequency band.

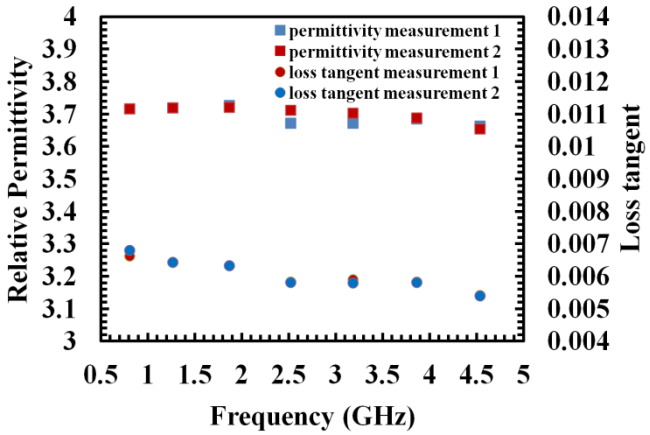

Fig. 3.15 : Measured dielectric properties of LCP E130i.

3) ABS-PC Xantar LDS 3710 is a low-cost thermoplastic resin (10€/kg) commonly used in injection molding applications. The impact strength and heat resistance of PC as well as the flexibility of ABS make this substrate a good candidate for MID applications. Good mechanical and surface properties make ABS PC a consistent quality substrate for electronic devices. Fig. 3.16 presents the measured real part of the permittivity and tangent loss measured with respect to frequency. The measurement results show that the relative dielectric permittivity near to 2.81-2.83 in the 0.80-4.53 GHz frequency band. The measured tangent loss does not exceed 0.007 in the measured frequency band. The dielectric properties have good repeatability with two measurements in the entire frequency band.

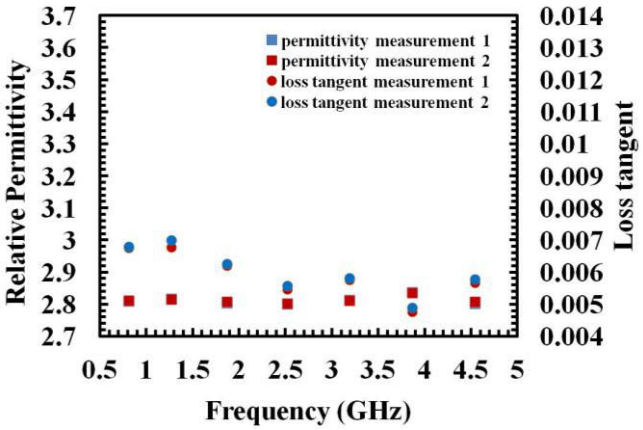

Fig. 3.16 : Dielectric properties of ABS PC Xantar LDS 3710.

4) LDS PBT Pocan 7102 is a high heat grade polymer which makes the blend of PBT and PET polymer and is suitable for reflow and vapour phase welding with lead-free solder. The substrate has high thermal dimensional stability with heat distortion temperature (HDT) of 250^0C [39], less heat expansion and suitable for lead free reflow soldering [30]. This molded substrate is specifically used for LDS fabrication. It provides a low permittivity and medium loss. The measurement results presented in Fig. 3.17 give a permittivity value of 3.32-3.46 with dielectric loss of 0.0085-0.0095.

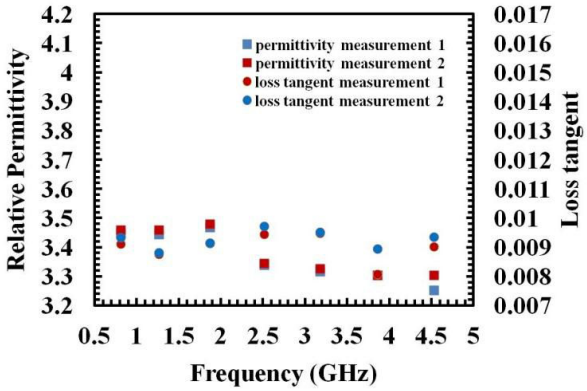

Fig. 3.17 : Measured dielectric properties of LDS PBT Pocan 7102.

5) LDS PPA RTP 4099 x 117359D is a thermoplastic resin used for high temperature electronic and automotive applications. Properties of PPA include high heat and chemical resistance and high dimensional stability. Another great advantage of this thermoplastic is that the material is highly recyclable. PPA shows a dielectric permittivity of 3.7-3.9 and tangent loss of 0.0065- 0.0135 from resonance cavity method in the complete frequency band of 0.80 GHz to 4.53 GHz (Fig. 3.18). The two measurements show good repeatability in their dielectric properties and has a variation of 3% at higher resonant frequency, at and above 4.53GHz.

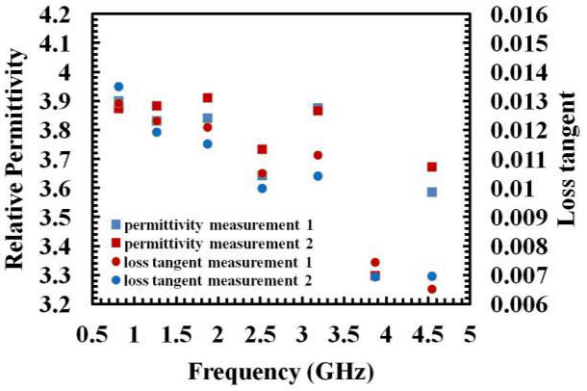

Fig. 3.18 : Measured dielectric properties of LDS PPA RTP4099*117359D.

6) PBT Ultradur B4520 is a medium viscosity, rapidly freezing injection molding grade. This material can be processed over a moulding temperature of 40-80^{0}C. It is a low loss thermoplastic providing a loss tangent of 0.0055-0.0085 and permittivity of 2.85-3.85 and has good repeatability in their dielectric values (Fig. 3.19).

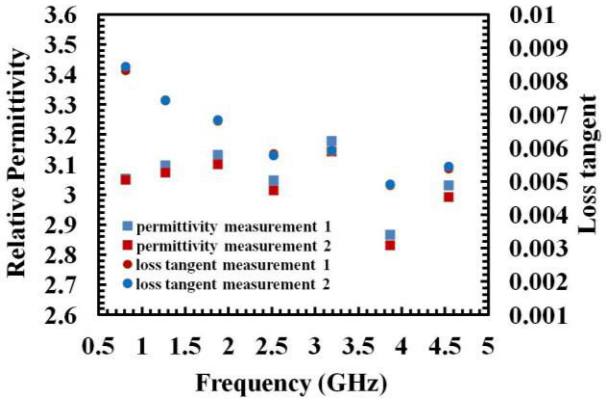

Fig. 3.19 : Measured dielectric properties of PBT Ultradur B4520.

7) PC LDS Xantar 3730 is another low loss thermoplastic resin whose dielectric properties are shown in Fig. 3.20. The LDS molded thermoplastic provides a dielectric permittivity of 2.85 to 3.1 and loss tangent of less than 0.008 at the entire frequency band of 0.80-4.53 GHz.

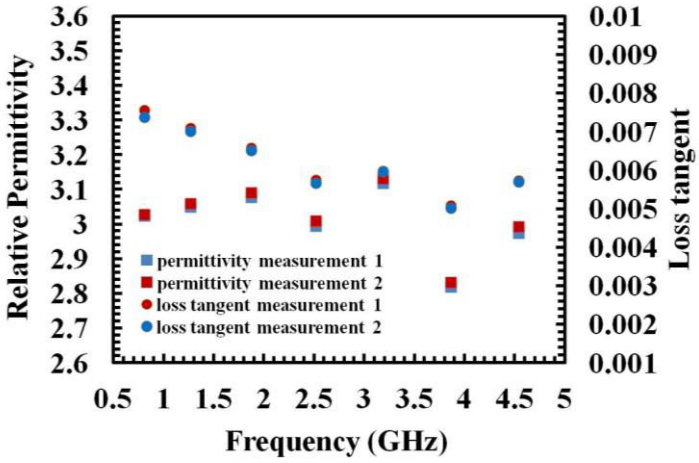

Fig. 3.20 : Measured dielectric properties of LDS PC Xantar 3730.

8) ABS PC Cycoloy C1200HF is a thermoplastic resin blend with polycarbonate and acrylonitrile butadiene styrene. It provides a balanced impact, high heat resistance properties and low temperature ductility for thin sheet substrate molding. It is an excellent commercial thermoplastic polymer well suited for applications requiring durable automotive, appliance

and electrical components. Fig. 3.21 shows the dielectric properties of ABS PC Cycoloy C1200HF polymer. The polymer has a dielectric constant of 2.85-3.1. The polymer's loss tangent varies from 0.005 to 0.026 in the measured frequency band.

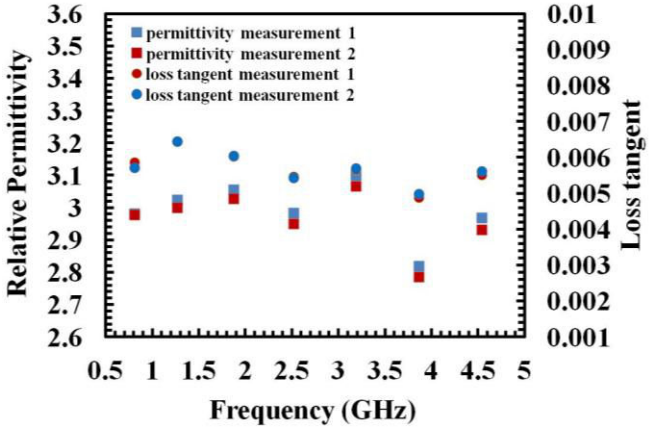

Fig. 3.21 : Measured dielectric properties of ABS PC Cycoloy C1200HF.

9) PA66 Ultramid A3K, is an easy flowing, injection molding grade. It can be processed over a wide range of mold temperatures, however, for applications where aesthetics are critical, a mold surface temperature of 40-80°C. Typical applications include fast processing high stress technical parts or electrically insulating parts. Fig. 3.22 shows the permittivity of the thermoplastic as 2.9-3.1 and tangent loss less than 0.017 for 0.80-4.53 GHz obtained from dielectric characterization measurement.

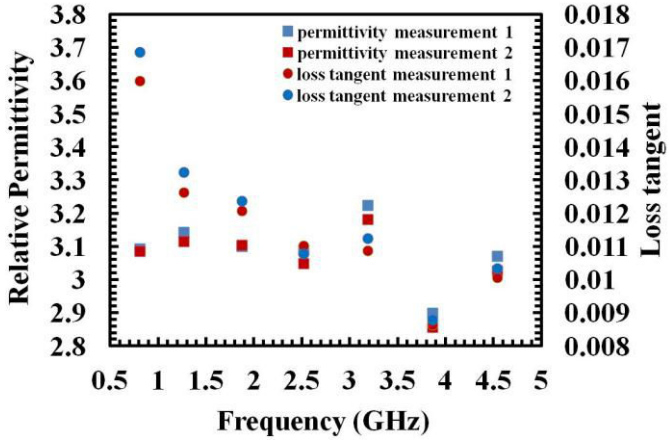

Fig. 3.22 : Measured dielectric properties of PA66 Ultramid A3K.

Thus, Table 3.2 summarizes the dielectric properties of LDS and non LDS thermoplastics characterized using resonant cavity method. The dielectric values at first resonant frequency at 0.808 GHz of all the substrates are summarized in the table. The

dielectric values of all the substrates show good precision of extraction till 4 GHz. Higher frequency extractions show error in the results as explained before due to the smaller size of the sample compared to the cavity width. From all the characterized results, it can be concluded that the MID thermoplastic LCP E820i exhibits the lowest tangent loss of nearly 0.004 with the highest permittivity near to 4.3. As LCP E820i presents higher permittivity, lower losses and higher thermal properties, it presents a good potential for RF applications. Till now, permittivity has been measured at ambient temperature. Future work can be focused on studying permittivity variation versus temperature.

Table 3.2: Summary of LDS Materials dielectric properties at near to 1GHz.

Characterized MID substrates	***Relative Permittivity,*** ε_r	***Loss tangent, tan δ***
LCP Vectra E820i	4.35	0.0048
LCP E130i	3.72	0.0064
ABS PC Xantar 3710	2.81	0.0066
LDS PBT Pocan 7102	3.46	0.009
LDS PPA RTP 4099 x 117359D	3.9	0.0135
PBT Ultradur B4520	3.06	0.0085
PC LDS Xantar 3730	3.03	0.0075
ABS PC Cycoloy C1200HF	2.98	0.0056
PA66 Ultramid A3K	3.09	0.017

The final section of this chapter deals with the conductivity measurements of two types of metallization used for the design of all RF circuits in this thesis work. Following section discusses them in detail.

3.4. Resistivity characterization

The metal resistivity measurement is essential in determining the conductive losses of the device under test. The four point probe measurement method has already proven to be an accurate method of resistivity measurement [31][32]. Fig. 3.23 shows the principle of the four point probes measurement method.

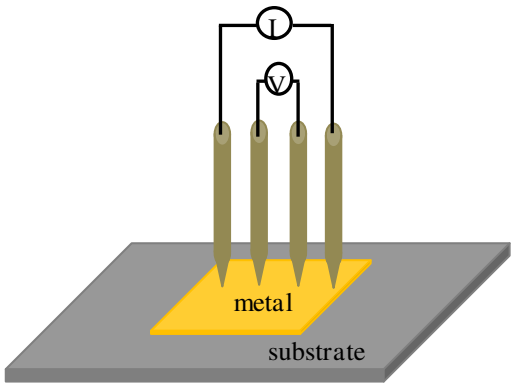

Fig. 3.23 : Principle of four point probe measurement method.

The measurement set up consists of four sharp probes placed on the surface of the metal to be measured. By passing the current through two outer probes and measuring the voltage through the inner probes, the sheet resistivity of the metal can be measured. In order to calculate the electrical resistivity, the thickness of the metallic trace should be measured using a profilometer. The DC intrinsic electrical resistivity is defined as [32]

$$\rho = R_s.t \tag{3.20}$$

Where

$$R_S = \frac{\pi}{\ln(2)}\frac{V}{I} \tag{3.21}$$

Rs is the sheet resistance and t is the thickness of the metallic trace. Detailed resistivity measurements of silver nano ink and a multilayer of nickel gold and copper (Ni/Au/Cu) are given in the following section.

3.4.1. Electrical DC characterization of silver ink

As mentioned before, the silver nano ink is used in inkjet printing of MID RF circuits. Electrical characterization of silver ink was carried out in CMP (Centre of Microelectronics in Provence), a part of EMSE (École nationale supérieure des mines de Saint-Étienne). A hand applied probe system from Jandel has been used for the electrical characterization of silver printed lines. Basically, metal ink is formed by nano particles and solvents vehicles. Thus, a thermal treatment is required to achieve high conductivity through the solid-state sintering of those nano-particles [34]. When printing silver ink is performed on temperature sensitive substrate like PET, PC, etc., a selective sintering process is needed. Printing and further sintering of metal ink is still challenging. In fact, various selective sintering methods

are developed. The sintering step can be achieved essentially by exposing printed metallic patterns to microwave radiation, local joule heating, laser, or by intense light flash using Xenon lamps [30][35][36]. Thus, the final geometrical, mechanical and electrical properties of printed metal are process dependent and characterization needs to be performed according to the target application. In this work, printed square pattern is used in order to characterize the electrical resistivity of silver according to the sintering condition. Sintering of printed structures is performed in conventional oven at 130°C for different process time, and by using flash photonic equipment from Novacentrix (PulseForge®3200). Detailed presentation of sintering will be given in chapter 5. After sintering, optical profilometer using white light interferometry (from Veeco) is used to measure the thickness of printed silver film.

A hand Applied Probe system for four point probe measurement method from Jandel (RM3-AR Test Unit) is used for electrical characterization is shown in Fig. 3.24.

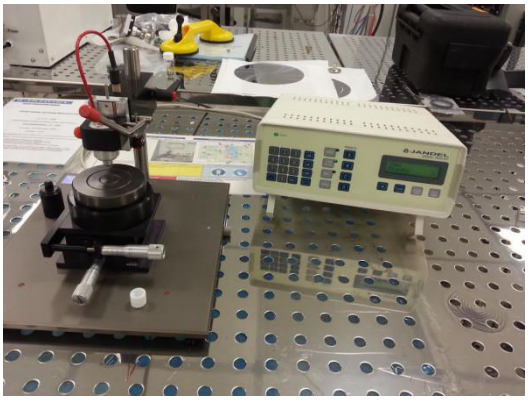

Fig. 3.24 : Four point measurement set up for electrical characterization of silver printed lines.

Table 3.3 shows the conductivity of the silver printed lines calculated for different layers of printed lines. Here, the sintering temperature is fixed at 130°C for 30 minutes process time. Fig. 3.25 is the graphical representation of the variation in sheet resistance with respect to the number of silver printed lines. It is clear from the graph that the sheet resistance decreases when number printed layers increases. Also, the conductivity is ten times smaller than copper. If we consider two frequencies at 1 GHz and 2.45 GHz, the skin depth will be 7.1 µm and 4.5 µm respectively. These values are greater than the thickness of metallization, which in turns provide high conductive losses.

Table 3.3: Conductivity of silver printed lines with respect to number of silver printed layers.

No. of Layers	*Thickness (µm)*	*Sheet resistance (Ω/□)*	*Resistivity (µΩ.m)*	Conductivity (10^6 S/m)
1	0.7	150	105	0.95
2	1.4	98	137	0.72
3	2.1	45	94.5	1.05

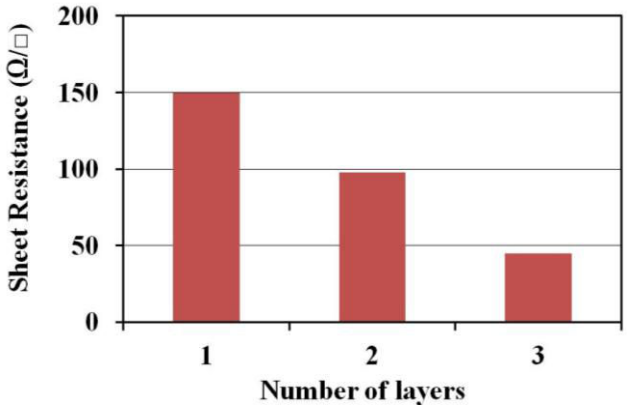

Fig. 3.25 : Variation of sheet resistance with number of printed silver layers.

3.4.2. Electrical DC Characterization of the Combination of Ni/Au/Cu

To define the electrical circuit foot print on LDS technology and laser ablation technology, successive layers of copper, nickel and gold finish are raised on a 2mm thick molded thermoplastic with a defined thickness. The electro chemical deposition is done by Radiall.

The measurement of conductivity of this combination of metallization based on four point probe measurement system is given in Table 3.4. Optimal sheet resistance and electrical conductivity of the metallization is around 25mΩ/□ and 5.10^6 S/m, respectively. If we consider frequencies of 1 GHz and 2.45 GHz, the skin depth is 7.1 µm and 4.5 µm respectively. Here, the skin depth is lower than the metal thickness leading to lower conductive losses in the signal transmission.

Table 3.4: Conductivity of metal with combination of nickel, copper and gold with respect to its thickness.

Metal thickness (µm)	*Sheet resistance (mΩ/□)*	*Resistivity (µΩ.cm)*	Conductivity (10^6 S/m)
8	22.8	18	5.48
10	17	17	5.88

3.5. Conclusion

This chapter presented the thermal and dielectric characterization of MID thermoplastics such as LCP Vectra E820i, LCP E130i, ABS PC Cycoloy C1200HF, ABS PC Xantar LDS 3710, PC LDS Xantar 3730, PBT Pocan 7102 LDS, PBT Ultradur B4520, PPA LDS RTP 4099* 117359D and PA 66 Ultramid A3K. Thermal properties of these thermoplastics have also been studied in this chapter based on TGA method. Thermal analysis of LDS molded thermoplastics shows that LCP holds high temperature stability of 511 ^{0}C among the tested thermoplastics. Cavity resonant method was adopted here for the dielectric characterization due to its accuracy in low loss measurement. It has been found that the substrate LCP vectra E820i presents the lowest tangent losses (0.004) and the highest permitivitty (≈4.3) among the substrates characterized. In addition, all MID characterized substrates show permittivity less than 5.

Furthermore, the resistivity characterizations of silver nano ink and a multilayer of nickel, copper and gold have been carried out. Four point probe measurement system is used for resistivity measurement. Resistivity of silver nano ink is measured at different curing time in sintering process. Silver nano ink exhibits conductivity of the order of 10^6 S/m after 240 min of curing time. In addition, the variation in sheet resistance of silver ink with respect to different layers of printed silver ink is studied. The sheet resistance decreases by increasing the printed silver layers. In similar, the conductivity of the combination of nickel, copper and gold is also measured. Sheet resistance measurement was carried out for different metal thickness. A conductivity of 5.88 x10^6 S/m is obtained for a metal thickness of 10μm.

Based on these characterized measurements of thermal properties, dielectric properties and resistivity properties, the MID RF circuits were designed and fabricated based on LDS, inkjet printing and laser ablation techniques. Following chapters deal with the detailed explanation and results of those MID RF circuits.

References

[1] A. R. Von Hippel, Dielectric Materials and Applications, New-York: J. Wiley & Sons, 1954.

[2] Edward. C. Jordan and Keith. G. Balmain, Electromagnetic Waves and Radiating Systems, 2nd edition, Prentice- Hall, Inc, Englewood Cliffs, New Jersey, 1950.

[3] C. Akyel and R. G. Bosisio, "New developments on automated-active circuits for permittivity measurements at microwave frequencies," IEEE Trans. Instrum. Meas., vol. 28, no. 2, pp. 496-504, April 1989.

[4] D. K. Ghodgaonkar, V. V. Varadan and V. K. Varadan, "A Free-Space Method for Measurement of Dielectric Constants and Loss Tangents at Microwave Frequencies," IEEE Trans. Instrument. Meas., vol. 38, pp. 789-793, 1989.

[5] G. L. Friedsam and E. M. Biebl, "A Broadband Free-Space Dielectric Properties Measurement System at Millimeter Wavelengths," IEEE Trans. Instrument. Meas., vol. 46, n° 2, pp. 515-518, April 1997.

[6] L. F. Chen, C. K. Ong, C. P. Neo and V.V. Varadan, Microwave Electronics: Measurement and Materials, New-York: J. Wiley & Sons, 2004.

[7] R. A. Waldron, "Perturbation theory of resonant cavities," Proc. ht. Elect. Eng.," vol. 107C, pp. 272-214, Sept. 1960.

[8] J. Sheen, "Measurements of microwave dielectric properties by an amended cavity perturbation technique," Measurement, vol. 42, pp. 57-61, 2009.

[9] J. Sheen, "Dielectric Characterization of Low-Loss Materials A Comparison of Techniques," IEEE Trans on Diele and Electrical Insulation, vol. 5, No.4, pp. 571-577, 1998.

[10] J. Sheen, "Microwave Measurements of Dielectric properties Using a Closed Cylindrical Cavity Dielectric Resonator," IEEE Transactions on Dielectrics and Electrical Insulation, vol. 14, No.5, pp. 1139-1144, 2007.

[11] Y. Ye, T. Liu, X. Zeng, J. He and C. Akyel, "Accurate Permittivity Measurement Using the Cavity Perturbation Technique at ISM 5.8 GHz Radio Band," ICMMT'07, pp.1-4, April 2007.

[12] N. Heininger, "3D LDS Components for New Production Opportunities", Microwaves Journal, pp. 46-50, February 2012.

[13] J. C. Rautio, "An Investigation of Microstrip Conductor Loss", Microwave Mag., pp. 60-67, Dec. 2000.

[14] D. Pozar, Microwave Engineering, New York: J. Wiley & Sons, pp.298-299, 2005.

[15] R. E. Collins, Foundations for Microwave Eng., 2nd ed., New York: J. Wiley & Sons.

[16] J. B. Jarvis, M. D. Janezic and D. C. DeGroot, "High-Frequency Dielectric Measurements," IEEE Instrumentation & Measurement Magazine, vol. 13, no. 2, pp. 24-31, April 2010.

[17] T. P. Marsland and S. Evans, "Dielectric Measurements with an open-ended Coaxial Probe," Proc. IEE, vol. 134, pp. 341-349, Aug. 1987.

[18] D. V. Blackham, and R. D. Pollard, "An Improved Technique for Permittivity Measurements Using a Coaxial Probe," IEEE Transactions on Instrumentation and Measurement, vol. 46, No.5, pp. 1093-1098, Oct. 1997.

[19] M. T. Jilani, M. Z. Rehman, A.M. Khan, M. T. Khan and S. M. Ali, "A Brief Review of Measuring Techniques for Characterization of Dielectric Materials ," International Journal of Information Technology and Electrical Engineering, vol. 1, No.1, pp. 1-5, Dec. 2012.

[20] S. N. Jha, K. Narasaiah, A. L. Basediya, R. Sharma, P. Jaiswal, R. Kumar and R. Bharadwaj, "Measurement Techniques and Application of Electrical Properties for Non Destructive Quality Evaluation of Foods- A Review, " Journal of Food Science and Technology, vol. 48, No. 4, pp. 387-411, Aug. 2011.

[21] G. L. Fiedsam, and E. M. Biebl, "A Broadband Free-Space Dielectric Properties Measurement System at Millimeter Wavelengths," IEEE Transactions on Instrumentation and Measurement, vol. 46, No.2, pp. 515-518, April 1997.

[22] Y. M. Hayashi, K. Gen; Hirayama, and Y. Hayashi, "Simultaneous measurement of permittivity and permeability of lossy sheet using flanged rectangular waveguide," Electronics and Communications in Japan, Part II: Electronics, vol.86, No.7, pp. 32-41, 2003.

[23] M. N. Afsar, Y. Wang, and A. N. Andreucci, "Accurate measurement of complex permittivity of liquids using the in-waveguide technique," CPEM Digest (Conference on Precision Electromagnetic Measurements), pp. 6-7, 2002.

[24] J. M. Catala-Civera, A. J. Canos, F. L. Penaranda-Foix, and E. De Los Reyes Davo, "Accurate determination of the complex permittivity of materials with transmission reflection measurements in partially filled rectangular waveguides," IEEE Transactions on Microwave Theory and Techniques, vol. 51, No.1, pp. 16-24, 2003.

[25] M. N. Afsar, N. Suwanvisan, and Y. Wang, " Permittivity measurement of low and high loss liquids in the frequency range of 8 to 40 GHz using waveguide transmission line technique," Microwave and Optical Technology Letters, vol. 48, No.2, pp.275-281, 2006.

[26] A. M. Mangan, S. P. Voinigescu, M. T. Yang and M. Tazlauanu, "De-Embedding Transmission Line Measurements for Accurate Modeling of IC Designs," IEEE Transactions on Electron Devices, vol. 53, pp. 235-241, February 2006.

[27] PEP, Centre technique de la Plasturgie et des Composites. Online available at: http://www.poleplasturgie.net/

[28] PLASTRONICS national Project, Online at: http://www.poleplasturgie.net/plastronics-456.html

[29] Damaskos, Material Measurement Solutions, [online] available at: http://www.damaskosinc.com/.

[30] A. Radeck, "THERMOPLASTIC POLYESTERS FOR LASER DIRECT STRUCTURING," PMI 2005.

[31] L. Valdes, "Resistivity Measurements on Germanium for Transistors, " I. R. E Proceedings., vol. 42, pp. 420-427, 1954.

[32] F. M. Smits, "Measurement of Sheet Resistivities with the Four Point Probe," The Bell System Technical Journal, pp. 711-718, May 1958.

[33] T. Falat, B. Platek, J. Felba, Sintering Process of Silver Nanoparticles in Ink-Jet Printed Conductive Microstructures - Molecular Dynamics Approach,13th International Conference on Thermal, Mechanical and Multi-Physics Simulation and Experiments in Microelectronics and Microsystems, EuroSimE 2012.

[34] R. Cauchois, et al., Impact of variable frequency microwave and rapid thermal sintering on microstructure of inkjet-printed silver nanoparticles, J. Mat. Sci. 2012.

[35] AT. Alastalo, and al., Rapid Electrical Sintering of Nanoparticle Stuctures, MRS Proc. Vol. 1113, 2008.

[36] A. Chiolerio, and al., Inkjet printing and low power laser annealing of silver nanoparticle traces for the realization of low resistivity lines for flexible electronics.MICROELECTRONIC ENG., vol. 88 n. 8, pp. 2481-2483.

[37] D. C. Dube, L. T. Lanagan, J. H. Kim, S. J. Jang, "Dielectric measurements on substrates materials at microwave frequencies using cavity perturbation technique," J. Appl. Phys., vol. 63, pp. 2466-2468, 1988.

[38] J. Sheen, "Study of microwave dielectric properties measurements by various resonance techniques," Measurement, vol. 37, no. 2, pp. 123-130, 2005.

[39] Lanxess Energizing chemistry, Three-dimensional circuit carriers made of plastic: Great application potential in automotive engineering. Online available at: http://lanxess.fr/en/news-france/global-news/great-application-potential-in-automotive-engineering/45/.

Chapter-4

MID RF Circuits Made by Laser Direct Structuring (LDS)

In this chapter, various RF circuits designed on LCP (Liquid Crystal Polymer) Vectra E820i with LDS (Laser Direct Structuring) fabrication technique are presented. LCP Vectra E820i is chosen for its lower dielectric losses and high thermal stability among all the characterized MID substrates for the design of LDS transmission lines, antennas and RF filters. First of all, microstrip, CPW(Coplanar Waveguide) and stripline transmission lines have been designed and measured. From S parameters measurements, the effective and the relative dielectric constant are extracted based on two transmission lines method. Extracted dielectric constant values are in continuous frequency domain and are compared to that obtained from resonant cavity method. LDS transmission lines properties in particular their quality factor and RF losses are studied. The extracted RF losses and quality factor of lines based on three different technologies are compared with the simulation results. The extracted results show a quality factor of 31, 75, and 101 for respectively CPW, microstrip and stripline transmission lines at 1 GHz. LDS LCP Vectra E820i provides the advantage of through hole metallization and hence a microstrip via model is designed on this substrate. Thereafter, planar RF circuits such as filters and antennas are designed and validated thus the potential of LCP Vectra E820i with LDS fabrication for RF applications. Finally, a three dimensional PIFA antenna is implemented and verified with its reflection coefficient and radiation pattern.

4.1. Introduction

Traditional methods of manufacturing such as electrolysis processes, engravings, lithography etc. are not only much time consuming but also produce large quantities of waste. By the definition of MID, injection molded thermoplastic substrates and conductive traces are integrated on the same surface such that both electrical and mechanical functionalities can be achieved on a single device. As discussed in chapter one, one of the widely used and most common method of MID fabrication is LDS (Laser Direct Structuring). Due to its immense fabrication advantages (as explained in chapter two), LDS has been chosen as one of the fabrication techniques studied in this thesis. Thus, this chapter focuses on the study of the performance of MID RF circuits fabricated by LDS technology.

LDS technology enables an injection molded component to be selectively plated with discrete circuit pathways providing thus a good flexibility for RF circuits [1]-[3]. This makes the possibility of fabricating 3D (three dimensional) structures allowing higher level of product integration with reduced number of components and cost and short production lead time [4]. The realization of the MID by LDS is done in 3 steps [3] (Fig. 4.1).

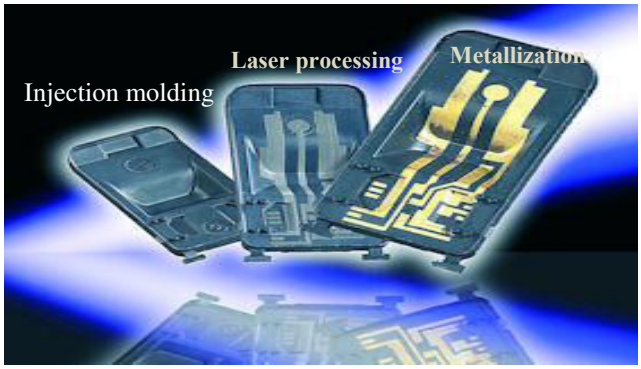

Fig. 4.1: LDS fabrication process.

The first step consists of injection molding of a special thermoplastic doped with metal-plastic additives compatible with LDS technology. Dried and preheated thermoplastic granulates are injected under high pressure into the desired mold. After cooling, the thermoplastic substrate to be metalized is formed with the exact shape of the mold. The substrate is then activated by the laser beam for 5 minutes on a portion of the surface by chemical reaction. The laser beam creates a rough surface on which the metal clings during metallization (see Fig. 4.2). The third step is the metallization by chemical means. It starts with the cleaning step followed by an electroless copper baths. Successively layers of copper (1-10 µm), nickel (1-10 µm) and gold finish (0.8 µm) are then raised with the desired

thickness. Fig. 4.3 shows some LDS fabricated RF circuits on a molded plate of LCP Vectra E820i having dimensions of 10 x 10 x 0.2 cm^3. Approximately 3 hours of fabrication process is needed for LDS fabrication of devices presented in this chapter. The minimal width and gap seperation of metallization is 150 μm.

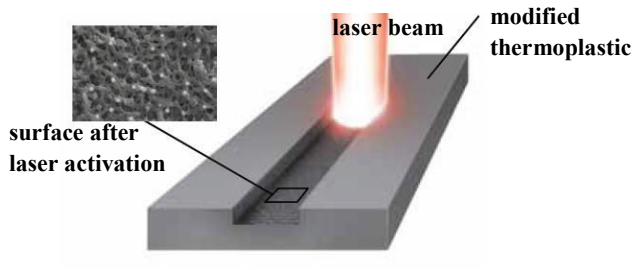

Fig. 4.2: Activated polymer surface by laser ablation.

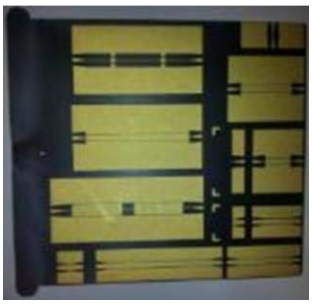

Fig. 4.3: LDS fabricated circuits on a molded LCP Vectra E820i.

The selection of polymers for LDS technology is based on the material characteristics such as thermal, mechanical, electrical properties, solder ability etc [5]. From the thermal properties of various molded thermoplastics presented in Fig. 3.1 and Fig. 3.3 in chapter 3, it is clear that LCP grabs the high temperature stability among the other characterized thermoplastics. Due to the high temperature resistance of LCP, RF circuits designed on this substrate can be easily soldered. The low dielectric loss (tan δ=0.004) of LCP Vectra E820i also makes this substrate a good candidate for RF circuits design.

Several LDS antennas can be found in literature [6][11]. To the author's knowledge, other than antennas applications, LDS technology has not yet been employed for other RF applications. Thus the focus of this chapter is mainly on the study of RF properties of LDS transmission lines, in particular their losses and quality factor. Indeed, RF properties of LDS lines are studied based on CPW (coplanar waveguide), microstrip and stripline technologies and extracted measurement data from different configurations on LDS will be compared. Later, microstrip and CPW configurations are selected for the design and fabrication of RF

circuits due to its easiness of fabrication in comparison with stripline. In addition, the study of microstrip via model on LDS is also carried out.

4.2. Planar transmission lines

A number of different configurations of transmission lines are generally used for the design of RF circuits [12]. Microstrip and CPW have been the most popular and widely used transmission lines in microwave circuit applications. Stripline has also been widely used to deliver excellent high frequency performance, good noise immunity and high isolation between adjacent circuit traces [13]. The basic principles of planar CPW, microstrip and stripline transmission lines will be reviewed in this section.

4.2.1. CPW lines

A classical CPW line consists of a center conductor with ground planes on either side, all on the top of a dielectric substrate as shown in Fig. 4.4 (a). The gap in CPW supports electric field concentration on the substrate. CPW exhibits low dispersion even in the absence of fringing field in free space. Frequency dispersion mainly depends on the center strip dimensions: narrow lines provide less frequency dispersion than wide lines. The thickness of the substrate should be thick enough so that the EM fields die out without radiating out the substrate. The two lateral ground planes must be symmetrical in order to avoid unwanted propagation modes. Unsymmetrical ground planes provide a higher field in one gap than in the other. This configuration supports quasi-TEM mode of propagation, but at higher frequencies, the field becomes less TEM and more TE in nature. Fig. 4.4 (b) shows the electric and magnetic field distribution of CPW line. Magnetic field is elliptical in nature.

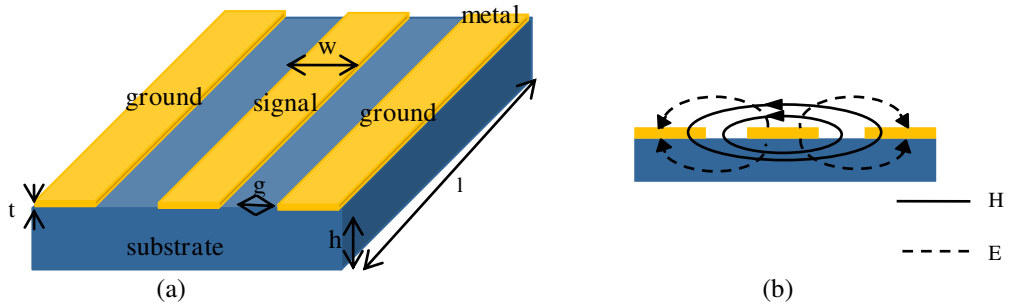

Fig. 4.4: CPW transmission line structure (a) 3 D view with dimensions and (b) its EM field distribution.

The dimensions of the center strip (w, l and t), the gap between the ground plane and the center conductor (g), thickness and permittivity of the substrate (h and ε_r respectively)

determine the effective dielectric constant (ε_{reff}), characteristic impedance (Z_c) and the attenuation of the line (α). The transmission characteristics of CPW such as Z_c and ε_{reff} can be expressed as follows [14]:

$$\varepsilon_{reff} = 1 + \frac{\varepsilon_r - 1}{2} \frac{K(k_2)}{K'(k_2)} \frac{K'(k1)}{K(k_1)} \tag{4.1}$$

$$Z_c = \frac{30\pi}{\sqrt{\varepsilon_{reff}}} \frac{K'(k_1)}{K(k_1)} \text{ in } \Omega \tag{4.2}$$

where $K(k_1)$, $K(k_2)$ and $K'(k_1)$, $K'(k_2)$ are respectively the elliptic integrals of first kind and its complement and can be defined as:

$$k_1 = \frac{0.5 \times w}{0.5 \times w + g} \tag{4.3}$$

$$k_2 = \frac{\sinh\left(\frac{pi \times 0.5 \times w}{2 \times h}\right)}{\sinh\left(\frac{pi \times 0.5 \times w + g}{2 \times h}\right)} \tag{4.4}$$

Where w, a and h represent the dimensions of CPW line (see Fig. 4.4 (a)). The attenuation of CPW line, α can be expressed as the sum of conductive loss, α_c and dielectric loss, α_d, assuming that radiation losses are negligible. Thus the losses can be expressed as:

$$\alpha_d = \frac{27.3 \times \varepsilon_r}{(\varepsilon_r - 1) \times (\varepsilon_{reff} - 1)} \times \frac{\tan(\delta)}{\sqrt{\varepsilon_{reff}}} \frac{1}{\lambda_0} \quad \text{in dB/m} \tag{4.5}$$

$$\alpha_c = \frac{8.68 \times R_s \times \sqrt{\varepsilon_{reff}}}{480 \times \pi \times K(k_1) \times K'(k_1) \times \left(1 - k_1^2\right)} \times A + B \quad \text{in dB/m} \tag{4.6}$$

where,

$$A = \frac{\pi + \log\left(\frac{(8\pi \times 0.5 \times w(1 - k_1))}{t \times (1 + k_1)}\right)}{0.5w} \tag{4.7}$$

$$B = \frac{\pi + \log\left(\frac{(8\pi \times (0.5 \times w + g)(1 - k_1))}{t \times (1 + k_1)}\right)}{0.5w + g}. \tag{4.8}$$

The phase constant β of a line which determines the sinusoidal phase of the signal propagating along a transmission line. It can also be determined from the effective permittivity of the substrate and angular frequency ω as:

$$\beta = \frac{\omega \times \sqrt{\varepsilon_{reff}}}{c} \tag{4.9}$$

Thus, we can understand from the above analytical equations that the electrical characteristics of CPW line depend on the geometrical parameters of the line and the substrate dielectric properties. These equations are followed for determining the electrical properties of MID LDS CPW lines presented in sections 4.3 and 4.4.

4.2.2. Microstrip lines

Fig. 4.5 shows a microstrip structure and its quasi-TEM field configuration. A conductive narrow strip is printed over a ground plane. The spacing between the strip and the ground plane is the substrate. The height of the substrate determines the radiation of the strip and substrate height of less than or equal to the wavelength minimizes radiation. The fields in the microstrip extend within two media- air above and dielectric below- so that the structure is inhomogeneous. For small strip width to substrate height ratio, dispersion becomes prominent and can be avoided with wider strip conductor. For higher frequencies, ε_{reff} increases towards ε_r and thus the phase velocity gradually decreases.

Fig. 4.5: Structure of a microstrip transmission line with its EM configuration.

The calculation of microstrip transmission characteristics such as Z_c and ε_{reff} involves in the determination of w/h ratio. Two different calculations are involved based on the ratio of w/h and can be expressed as follows [15].

When w/h≤1:

$$\varepsilon_{reff} = \frac{\varepsilon_r + 1}{2} + \frac{\varepsilon_r - 1}{2}\left\{\left(1 + 12\frac{h}{w}\right)^{-0.5} + 0.04\left(1 - \frac{w}{h}\right)^2\right\} \tag{4.10}$$

$$Z_c = \frac{\eta}{2\pi\sqrt{\varepsilon_{reff}}} \ln\left(\frac{8h}{w} + 0.25\frac{w}{h}\right) \tag{4.11}$$

where η=120π Ω in wave impedance in free space.

When w/h≥1:

$$\varepsilon_{reff} = \frac{\varepsilon_r + 1}{2} + \frac{\varepsilon_r - 1}{2}\left\{\left(1 + 12\frac{h}{w}\right)^{-0.5}\right\} \tag{4.12}$$

$$Z_c = \frac{\eta}{\sqrt{\varepsilon_{reff}}}\left\{\frac{w}{h} + 1.393 + 0.677\ln\left(\frac{h}{w} + 1.444\right)\right\}^{-1} \tag{4.13}$$

The above calculations evolve without considering the finite thickness (t) of the microstrip. Consideration of t makes the calculation a bit more challenging by replacing w in the above equations 4.12 and 4.13 with effective width w_e:

$$w_e = w + \frac{t}{\pi}\left[1 + \ln\left(\frac{2h}{t}\right)\right] \quad \text{for} \quad \frac{w}{h} \geq \left[\frac{1}{2\pi}\right] \tag{4.14}$$

$$w_e = w + \frac{t}{\pi}\left[1 + \ln\left(\frac{4\pi w}{t}\right)\right] \quad \text{for} \quad \frac{w}{h} \leq \left[\frac{1}{2\pi}\right] \tag{4.15}$$

where these corrections are further applicable under the conditions that $t \leq h$ and $t \leq \frac{w}{2}$.

In similar to the transmission line characteristics discussed above, losses in microstrip are important to be determined and considered in RF circuit design. As considered in CPW line section, two main losses of microstrip lines are considered; dielectric losses and conductive losses with the assumption that radiation losses are negligible. Dielectric losses of the microstrip line can be calculated based on equation 4.5. Conductive losses can be calculated as [15]:

$$\alpha_c = \frac{1.38 \times C}{h \times Z_c} \times D \times R_s \text{ in dB/m} \tag{4.16}$$

where, $C = \frac{32 - (w_e/h)^2}{32 + (w_e/h)^2}$ and $D = 1 + \frac{h}{w_e(1 + 1.25/\pi * \log(2 * E/t))}$ (4.17)

$$E=2\pi a \quad \text{if} \quad \frac{w}{h} \le \frac{1}{2\pi} \quad \text{else } E=h.$$

$$\text{if} \quad \frac{w}{h} \le \frac{1}{2\pi}, \qquad w_e = w + \frac{1.25*t}{\pi(1+\log(4\pi w/t)} \tag{4.18}$$

$$\text{else} \qquad w_e = w + \frac{1.25*t}{\pi(1+\log(2h/t)} \tag{4.19}$$

These equations have been used to calculate microstrip MID transmission line properties given in section 4.4.

4.2.3. Stripline

Strip line configuration has three conductors, where the inner conductor is called the signal and the two outer conductors are called the ground planes. The signal conductor is implanted in a homogeneous and isotropic dielectric. Stripline supports TEM mode of propagation. The phase velocity and characteristic impedance of TEM mode does not vary with frequency. It provides natural shielding against radiation and incoming spurious signals even at higher frequencies. Fig. 4.6 shows the strip line structure and its field configuration.

Fig. 4.6: Structure of a stripline transmission line and its EM field configuration.

In order to have an exact analysis and design of stripline circuit, accurate characteristic impedance is strongly required. Numerical calculations of Z_c exist for zero and finite metal thickness. The analytical expression for zero thickness was given in [16] where the stripline is considered as an ideal transmission line. In practical, the center width has a finite thickness and conductivity. The calculations are approximated in this case in [12][17] based on the ratio of w and B, where w is the width of the central signal line and B is the sum of thickness of metallization and twice the height h of substrate. The expressions given below can be used for calculating characteristic impedance of stripline which is valid in the case the strip thickness (t), i.e., t is not negligible.

$$\text{if} \quad \frac{w}{B} \geq 0.35, \qquad Z_c \approx \frac{1}{\sqrt{\varepsilon_r}} \frac{94.15}{\left[(\frac{w}{B}) / (1 - \frac{t}{B}) \right] + Z_k / \pi} \tag{4.20}$$

$$\text{where,} \quad Z_k = \frac{2}{1-(t/B)} \ln\left(\frac{1}{1-(t/B)} + 1 \right) - \left(\frac{1}{1-(t/B)} - 1 \right) \ln\left(\frac{1}{1-(t/B)^2} - 1 \right) \tag{4.21}$$

$$\text{and if} \quad \frac{w}{B} \leq 0.35, \quad Z_c \approx \frac{60}{\sqrt{\varepsilon_r}} \ln(\frac{4B}{\pi Z_k}) \tag{4.22}$$

$$\text{where,} \quad \frac{w_{eff}}{B} = \frac{w}{B} - \left(0.35 - \frac{w}{B} \right)^2 \tag{4.23}$$

$$\text{and} \quad Z_k = \frac{w_{eff}}{2} \left[1 + \frac{t}{\pi w_{eff}} \left\{ 1 + \ln \frac{4\pi w_{eff}}{t} + 0.51\pi \left(\frac{t}{w_{eff}} \right)^2 \right\} \right]. \tag{4.24}$$

The effective dielectric constant ε_{reff} of stripline is equal to the relative dielectric constant ε_r as the wave propagation occurs only in the substrate. Thus, stripline holds higher ε_{reff} than microstrip and CPW configurations which in turns reduces the speed of wave propagation by the equation,

$$v_p = \frac{c_0}{\sqrt{\varepsilon_{reff}}}. \tag{4.25}$$

RF Losses in the stripline can be of dielectric and conductive losses calculated as given below in dB/m:

$$\alpha_d = \frac{2.318 * f * \tan(\delta) \sqrt{\varepsilon_r}}{8.68 * 0.0254} \tag{4.26}$$

$$\alpha_c = \frac{(2.02e^{-3} * \varepsilon_r * Z_c \sqrt{f} * 6.2e^{-5} / B) * (k + x + y * z)}{8.68 * 0.0254} \tag{4.27}$$

where,

$$k = \frac{1}{1 - t/B}, \; x = \frac{2w/B}{(1 - t/B)^2}, \; y = \frac{(1/\pi) * (1 + (t/B))}{(1 - t/B)^2}, \text{ and } z = \log(\frac{(k+1)}{(k-1)}) \tag{4.28}$$

These expressions of stripline transmission characteristics are used for calculating and studying RF properties of MID LDS stripline transmission lines in the section 4.4.

4.2.4. Electrical properties extraction from S parameters

A linear two ports network is shown in Fig. 4.7 [18], where the network is determined by its transfer matrix. Z_1 and Z_2 represent the image input impedances at port 1 and port 2 respectively.

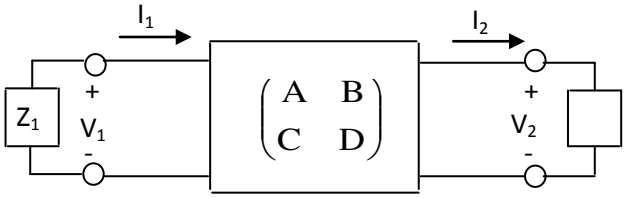

Fig. 4.7: A two port linear network.

For a two ports network, the transfer matrix, also known as the ABCD matrix, can be easily extracted from the S parameters. The transfer matrix represents the relationship between the voltage and the current at the input (port 1) and the output (port 2) ports as:

$$\begin{pmatrix} V_1 \\ I_1 \end{pmatrix} = \begin{pmatrix} A & B \\ C & D \end{pmatrix} \begin{pmatrix} V_2 \\ I_2 \end{pmatrix} \tag{4.29}$$

where V_1 and I_1 represents the voltage and the current at port 1 and V_2 and I_2 those at port 2 respectively.

For a transmission line of physical length l, a complex propagation constant γ and a characteristic impedance Z_c, the ABCD matrix can be written as:

$$\begin{pmatrix} A & B \\ C & D \end{pmatrix} = \begin{pmatrix} \cosh(\gamma l) & jZ_c \sinh(\gamma l) \\ \dfrac{j \sinh(\gamma l)}{Z_c} & \cosh(\gamma l) \end{pmatrix} \tag{4.30}$$

Consequently, the complex propagation constant γ and the characteristic impedance Z_c can be deduced from the ABCD matrix:

$$\gamma = \frac{\text{Arc}\cosh(A)}{l} \tag{4.31}$$

$$Z_c = \sqrt{\frac{B}{C}} \tag{4.32}$$

Numerous methods have been developed for the transmission lines quality factor calculation [18]-[21] based on S parameters measurement of transmission lines. This parameter can be derived from the propagation constant, $\gamma=\alpha+j\beta$ where α is total attenuation constant and β the phase constant [18]. Knowing α and β, the quality factor can be deduced using equation (4.33).

$$Q = \frac{\beta}{2\alpha} \quad . \tag{4.33}$$

This definition takes into account the average energy stored, including the magnetic and the electric energies.

However, the transmission line losses are the sum of the conductor losses (α_c) and the dielectric losses (α_d). In order to separate the losses origin, a low losses approximation is used, and both the losses are given by the following expressions:

$$\alpha_c \approx \frac{R}{2Z_c} \tag{4.34}$$

$$\alpha_d \approx \frac{G * Z_c}{2} \tag{4.35}$$

where R and G are respectively the unit series resistance of the signal line and the unit leakage conductance from signal line to ground. R and G parameters are directly related to the complex propagation constant γ and the characteristic impedance Z_c [18] as given in (4.36) and (4.37).

$$R = Re(Z_c * \gamma) \tag{4.36}$$

$$G = Re(\frac{\gamma}{Z_c}) \tag{4.37}$$

Thus, the following section deals in detail the design and RF performance of MID transmission lines in CPW, microstrip and stripline technology based on LDS fabrication method.

4.3. LDS transmission lines

Transmission lines are fundamental components of RF systems. In order to study MIDs potential for RF applications, transmission lines are designed and fabricated on a 2mm thick LCP LDS Vectra E820i. CPW, microstrip and stripline technologies are considered. A thickness of 10 µm of metallization is deposited with a conductivity of $5.8*10^{6}$ S/m (see Table 3.4).

4.3.1. MID CPW line

Fig. 4.8 shows two CPW transmission lines of length (l) 1 cm and 5 cm on LCP Vectra E820i realized by LDS. Geometrical dimensions (w=2.2 mm, s=0.25 mm) were chosen in order to get a characteristic impedance near to 50 Ω. Tapered access of l'= 5 mm and w'= 1.5 mm is introduced on either side of the transmission line for connecting lines.

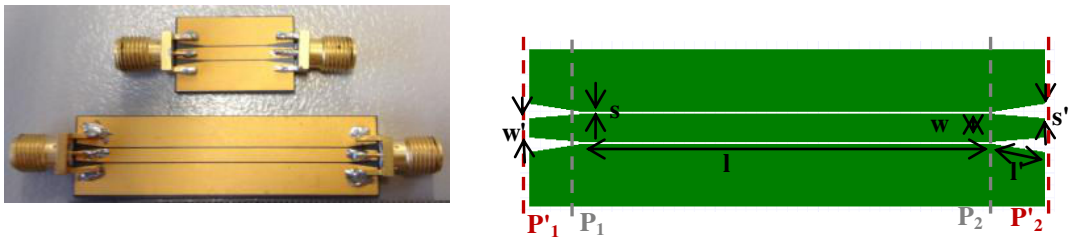

Fig. 4.8: CPW transmission lines on LCP Vectra E820i.

Two types of measurements have been carried out; one in P'_1-P'_2 planes (using Ecal measurement) and second one is in P_1-P_2 planes (using TRL measurement).

4.3.1.1. Ecal Measurements

Transmission lines have been measured till 10 GHz, using N5222A Agilent PNA [22]. Ecal calibration (electronic calibration) has been done for calibrating PNA for measurement. P'_1-P'_2 planes are considered as measurement planes in Ecal calibration, which includes the actual transmission line and the tapered access on either side of the lines (see the geometry in Fig. 4.8). Ansys HFSS [23] and Ansoft designer have been respectively used for the EM and electric simulations. In HFSS simulations of both lines, the effects of connectors on either side were also taken into account. The simulated structures on both HFSS and Ansoft designer are presented in Fig. 4.9.

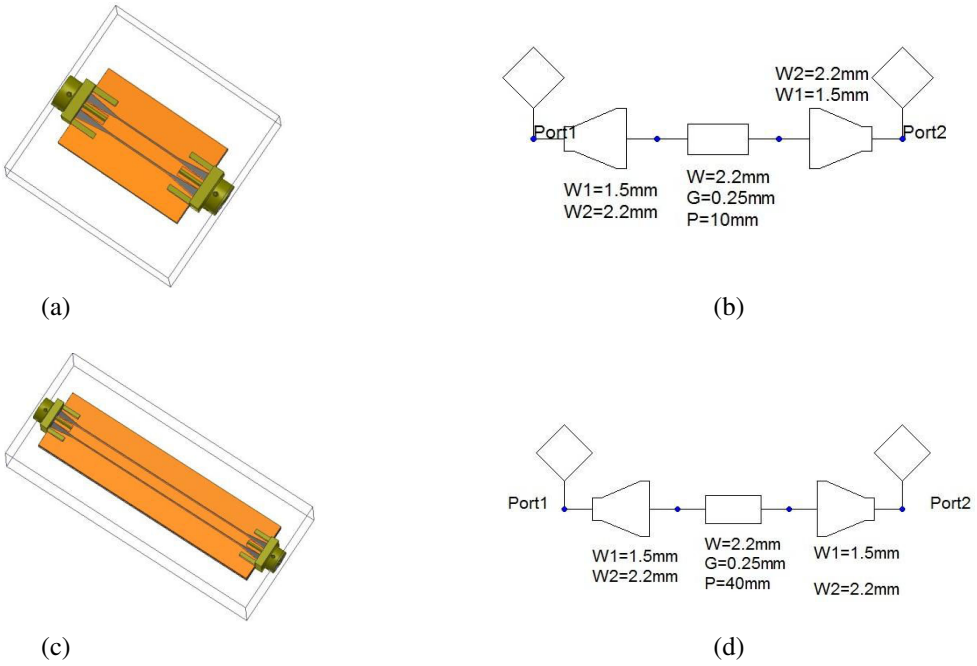

Fig. 4.9: Simulated structures of CPW lines of 1 cm and 4 cm on LCP Vectra E820i in P'_1-P'_2 planes, (a) and (c) 1 cm and 4 cm in Ansoft HFSS and (b) and (d) of 1 cm and 4 cm in Ansoft designer electric simulation.

Fig. 4.10 and Fig. 4.11 respectively show the comparison between simulation (EM and electric) and measurement of S parameters of 1 cm line and 4 cm CPW lines in the P'_1-P'_2 planes. For 1 cm line, a good agreement is obtained between measurements and simulation results till 3.5 GHz (Fig. 4.10 (a) and Fig. 4.10 (b)). As frequency increases, the losses increases and matching decreases and it can be more seen in the measurement results. The differences appear between simulations and measurement results are due to the effect of real SMA connectors, cable access and soldering. Measurements provide a matching better than -15 dB and losses less than 0.5 dB till 3.5 GHz. The EM simulation for the phase provides a better agreement than electric simulation with Ecal measurement since that the effect of SMA connectors is not considered in the electric simulation (Fig. 4.10 (c)).

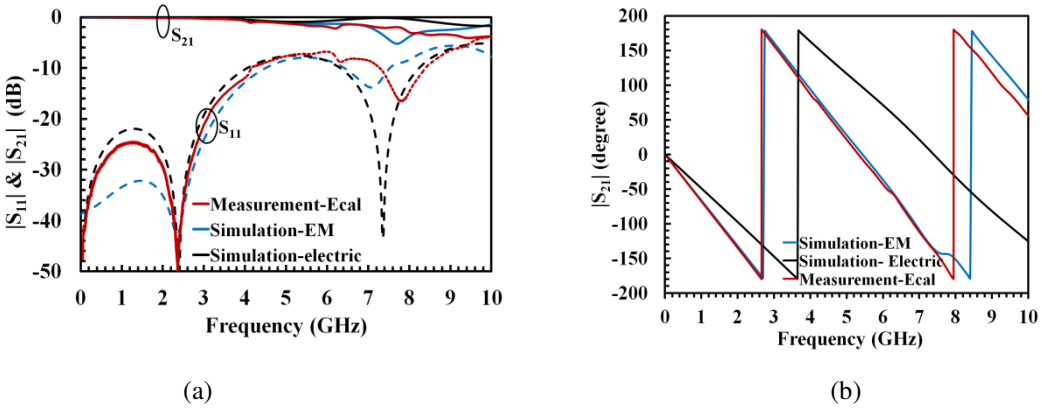

Fig. 4.10 : S parameters of CPW lines of length 1cm on LCP Vectra E820i in the P'_1-P'_2 planes (a) magnitude in dB and (b) phase in degree.

Similarly, Fig. 4.11 (a) and (b) show the S parameters of 4 cm line in dB. Both return and insertion losses obtained from measurement are in agreement with both simulations (EM and electric). However, measured return loss is higher than simulations. Measurement shows a return loss of better than 15 dB and an insertion loss of less than 0.5 dB till 1.5 GHz. As frequency increases, losses increases and matching decreases. Return loss is increasing with frequency due to the presence of the tapered access. Also, measurements show mismatch with simulations especially at higher frequencies which can be explained as the effect of SMA connectors, cable access for measurement and soldering. Though there is a difference occurred in the insertion phase S_{21} between measurement and electric simulation in Fig. 4.11 (c), by considering connector access on either sides of the line in HFSS simulation, the S_{21} phase obtained is in good agreement with the measurement.

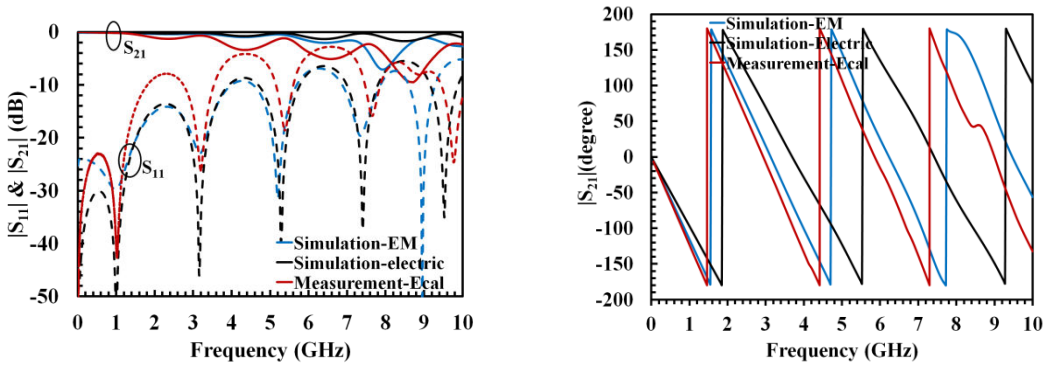

(a) (b)

Fig. 4.11 : S parameters of CPW lines of length 4cm on LCP Vectra E820i in the P'_1-P'_2 planes (a) magnitude in dB and (b) phase in degree.

Measured S parameters obtained with ecal calibration are considered after deembedding using two transmission lines method [25] in order to study CPW transmission line losses and permittivity extraction of LCP Vectra E820i in a continuous frequency band. These results will be discussed in section 4.4.

4.3.1.2. TRL Measurements

In order to avoid the effect of tapered lines added on either side of the lines and SMA connectors (to get P_1-P_2 planes), TRL (THRU-REFLECT-LINE) calibration is done and transmission lines measurements are carried out. TRL calibration is a full two port calibration method that measures two transmission lines standards (THRU and LINE) and one reflection standard (REFLECT). This calibration technique is often used to remove the effect of tapered

access and connectors. The TRL calibration relies on the transmission line impedance used for calibration (LINE) and hence it minimizes signal reflection and significant mismatch ripples [24]. The standard THRU should have the form and the length of the access to remove. The electrical length of the LINE gives the limitation frequency of the TRL calibration. In order to obtain a broad band frequency measurement, multiple LINE standards have to be considered for calibration.

Fig. 4.12 shows the TRL calibration kit designed on LCP Vectra E820i for the de embedding of MID CPW lines. The calibration kit consists of a zero length THRU which provides zero loss and reflection, a REFLECT, and a LINE with a physical length equal to 1 cm and impedance of 50 Ω. This line length provides a TRL calibration valid till 3.5 GHz. The measurement can be extended to higher frequencies by the use of multiLINE for TRL calibration.

(a) (b) (c)

Fig. 4.12 : CPW TRL calibration kit on LCP Vectra E820i, (a) THRU, (b) REFLECT and (c) LINE.

Based on this TRL calibration, transmission line measurements and simulations were carried out. Fig. 4.13 (a) and (b) show the simulated structures of two transmission lines in the P_1-P_2 planes designed for EM simulation in HFSS and electric simulation in Ansoft designer. Here in simulations, we consider a reference of 50 Ω by normalising port impedance.

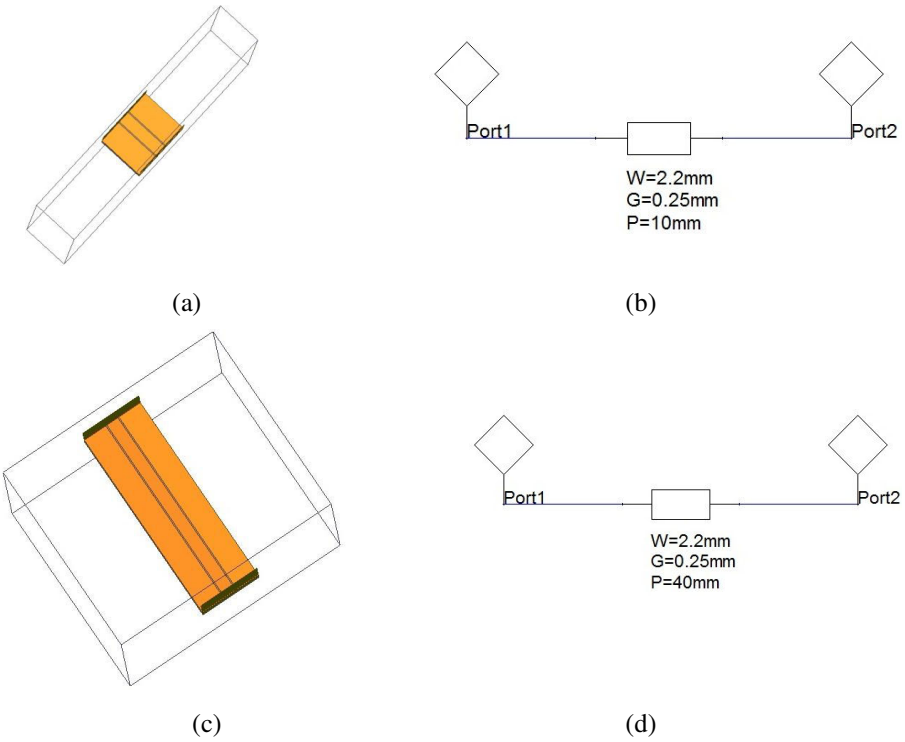

Fig. 4.13 : Simulated structures of CPW lines of length 1 cm and 4 cm on LCP Vectra E820i in P_1-P_2 planes (a), (c) in Ansoft HFSS of 1cm and 4 cm and (b), (d) in Ansoft designer electric simulation of 1 cm and 4 cm.

Fig. 4.14 and Fig. 4.15 respectively show the S parameters of 1 cm and 4 cm CPW lines in P_1-P_2 planes. One can easily find out the good return loss provided by the TRL calibration by comparing the measured return loss with Ecal calibration method in Fig. 4.10 (a) and Fig. 4.14 (a). Indeed, a matched transmission line should exhibit low return loss. Using Ecal calibration, the measured return loss of 1 cm line is 20 dB at 3.5 GHz (Fig. 4.10 (a)). The Ecal return loss increases with frequency due to the presence of the taper to line interface. With TRL calibration, the same line provides a return loss of -39 dB at 3.5 GHz with reduced mismatch ripples (Fig. 4.14 (a)). Similar performances can be observed for 4 cm lines if we compare Fig. 4.11 (a) and Fig. 4.15 (a). The TRL calibration is valid till 3.5 GHz. For comparison study of the Insertion loss, the frequency of 1 GHz is considered. An insertion loss of -0.03 dB is obtained at 1 GHz for 1 cm line and -0.16 dB (3 dB/ μm) for 4cm line. As frequency increases the losses increases and average losses of less than -0.4 dB (4 dB/μm) is obtained for both lines at 3.5 GHz. (Fig. 4.14 (b) and Fig. 4.15 (b)). TRL measurements on the phase of two lines show good agreement with the electric and EM simulations (Fig. 4.14 (c) and Fig. 4.15 (c)).

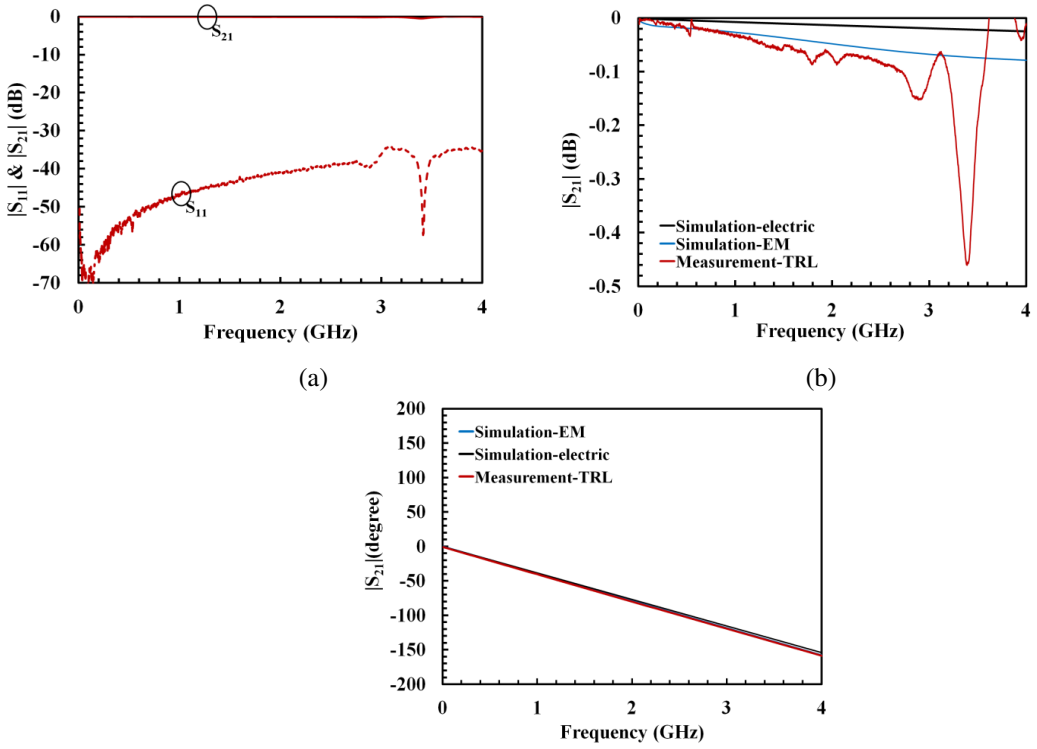

Fig. 4.14 : S parameters of MID CPW lines of length 1 cm on LCP Vectra E820i in P_1-P_2 planes, (a) magnitude measured in dB, (b) Zoomed S_{21} magnitude in dB and (c) S_{21} phase in degree.

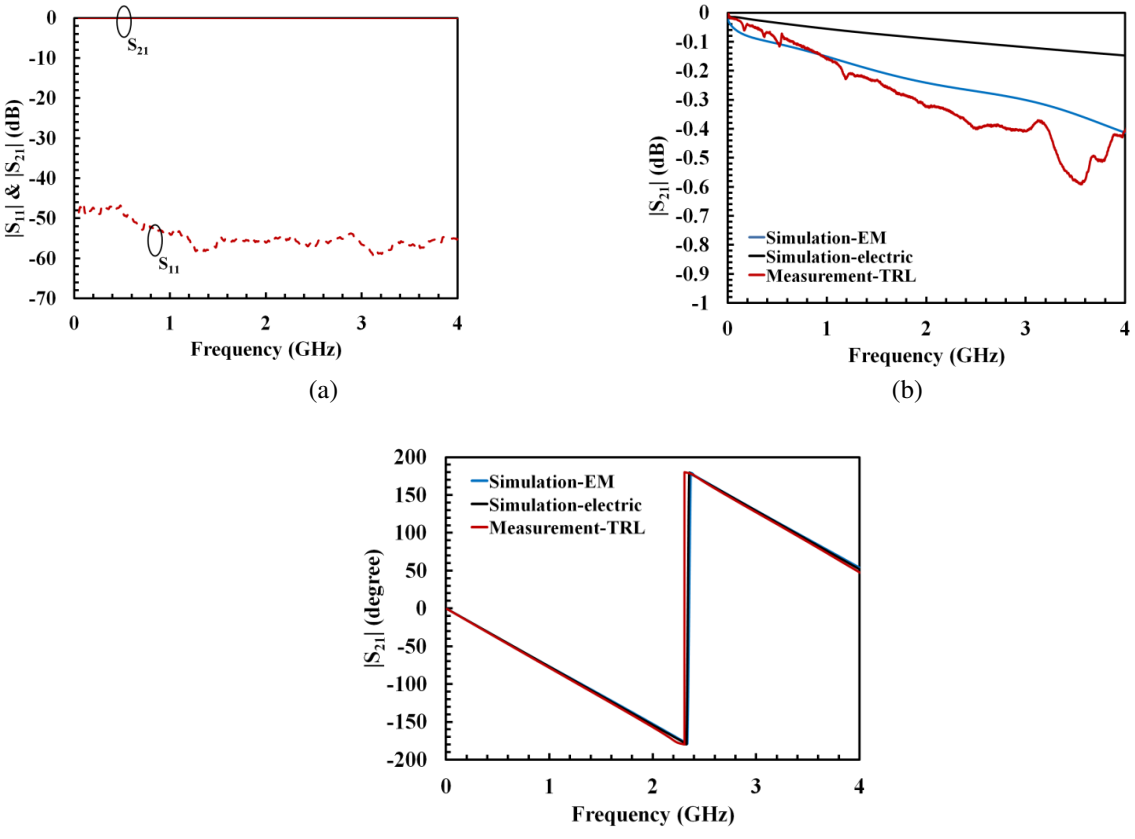

Fig. 4.15 : S parameters of MID CPW lines of length 4 cm on LCP Vectra E820i in P_1-P_2 planes, (a) magnitude measured in dB, (b) Zoomed S_{21} magnitude in dB and (c) S_{21} phase in degree.

4.3.2. MID Microstrip line

Fig. 4.16 shows the microstrip transmission lines fabricated by LDS on LCP Vectra E820i. Two transmission lines of length l=4 cm and 1cm and width w=3.8 mm are fabricated by LDS method. In similar to CPW lines, two taper accesses were introduced on either side of the transmission lines having length 5mm and edge width of 1.5mm. Two soldering pads of 4 mm length (l_t) and 1.5 mm width (w_t) were also added to get good connector mechanical soldering stability.

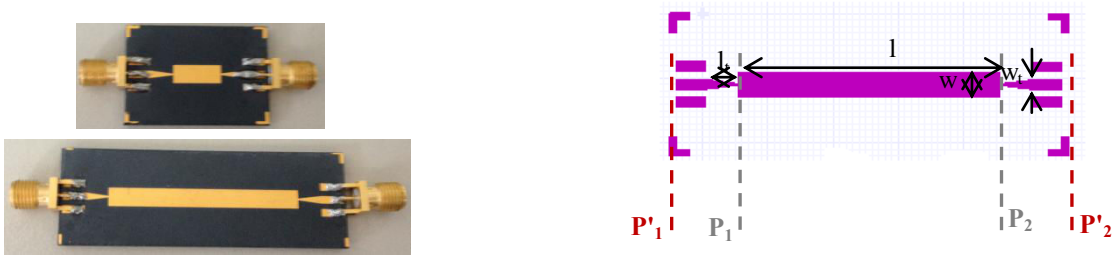

Fig. 4.16 : MID microstrip transmission lines on LCP Vectra E820i and its geometry.

Similar to CPW transmission line, two measurement planes were considered in this microstrip line structures; P'_1-P'_2 planes and P_1-P_2 planes (see Fig. 4.16). S parameters in P'_1-P'_2 planes are obtained by using Ecal calibration. Here, the presence of tapered access and soldering pads on either side of transmission lines are included in the measurements. EM and electric simulations using respectively Ansys HFSS and Ansoft designer are carried out. Fig. 4.17 (a) and Fig. 4.17 (b) respectively show the simulated structures of 1cm line and 4 cm line in the above mentioned simulation softwares. HFSS simulations consider the effect of SMA connectors.

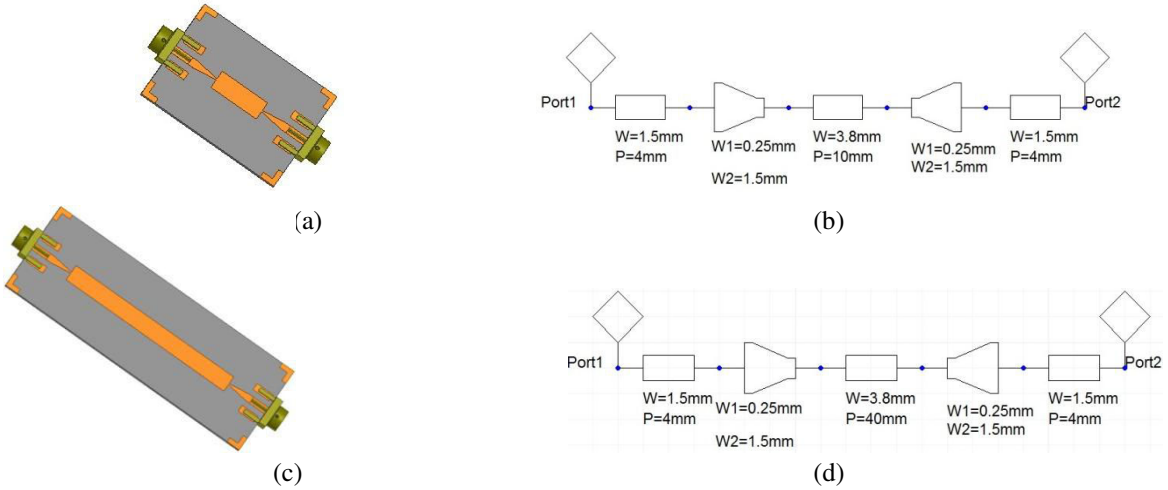

Fig. 4.17 : Simulated structures of MID microstrip lines of length 1 cm and 4 cm on LCP Vectra E820i in P'_1-P'_2 planes, (a) and (c) 1 cm and 4 cm in Ansys HFSS and (b) and (d) of 1 cm and 4 cm in Ansoft designer electric simulation.

4.3.2.1. Ecal Measurements

Fig. 4.18 and Fig. 4.19 respectively present the S parameters obtained with Ecal calibration of 4 cm and 1 cm MID microstrip transmission lines on LCP vectra E820i. All measurements have been taken till 10 GHz using N5222A Agilent PNA. A good agreement is obtained between measurements and simulations for S parameters till 5 GHz. HFSS simulations taking into account connectors provide a better agreement with measurements than Ansoft designer. The measurements of 1 cm and 4cm MID microstrip lines respectively provide a good matching of 15 dB till 2.5 GHz and 1.5 GHz (Fig. 4.18 (a) and Fig. 4.19 (a)). Matching decreases as frequency increases due to presence of the taper acces.

Measured insertion phase (S_{21} in degrees) of two MID lines are given in Fig. 4.18 (c) and Fig. 4.19 (c). The 1 cm line has 180^0 insertion phase at 1.97 GHz and 4 cm line has 180^0 insertion phase at 1.1 GHz and both measurements provide good agreement with EM simulation results till 5 GHz.

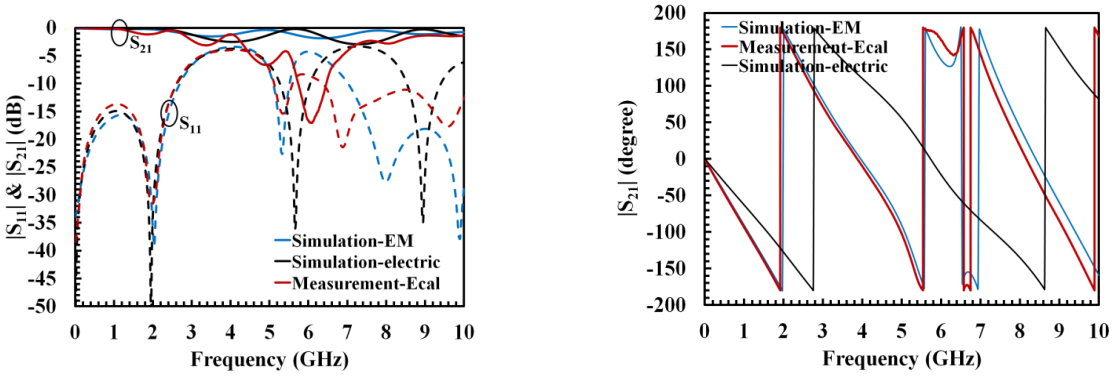

(a) (b)

Fig. 4.18 : S parameters of MID microstrip line of length 1 cm on LCP Vectra E820i in the P'_1-P'_2 planes, (a) magnitude in dB and (b) S_{21} phase in degree.

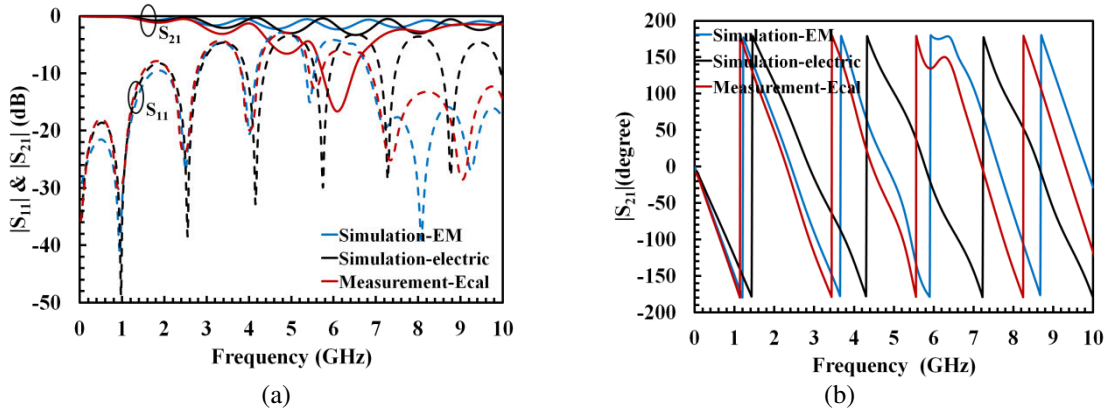

(a) (b)

Fig. 4.19 : S parameters of MID microstrip line of length 4 cm on LCP Vectra E820i in the P'_1-P'_2 planes, (a) magnitude in dB and (b) S_{21} phase in degree.

4.3.2.2. TRL Measurements

In order to get the exact transmission line characteristics, i.e., in P_1-P_2 planes, TRL calibration is performed in the PNA and measurements are carried out. The TRL kit used for calibration is shown in Fig. 4.20. The kit includes a THRU with zero length, a REFLECT and a LINE of 1 cm length and 50 Ω impedance. With 1 cm Line length, the TRL calibration can be achieved till 3 GHz .

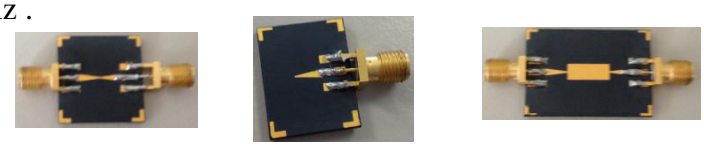

(a) (b) (c)

Fig. 4.20 : Microstrip TRL calibration kit on LCP Vectra E820i, (a)THRU, (b) REFLECT and (c) LINE.

Fig. 4.21 shows the TRL simulated structures of 1 cm and 4 cm lines considered in HFSS and Ansoft designer. Considering these structures in simulations, their S parameters are compared with those obtained from TRL measurements of both lines.

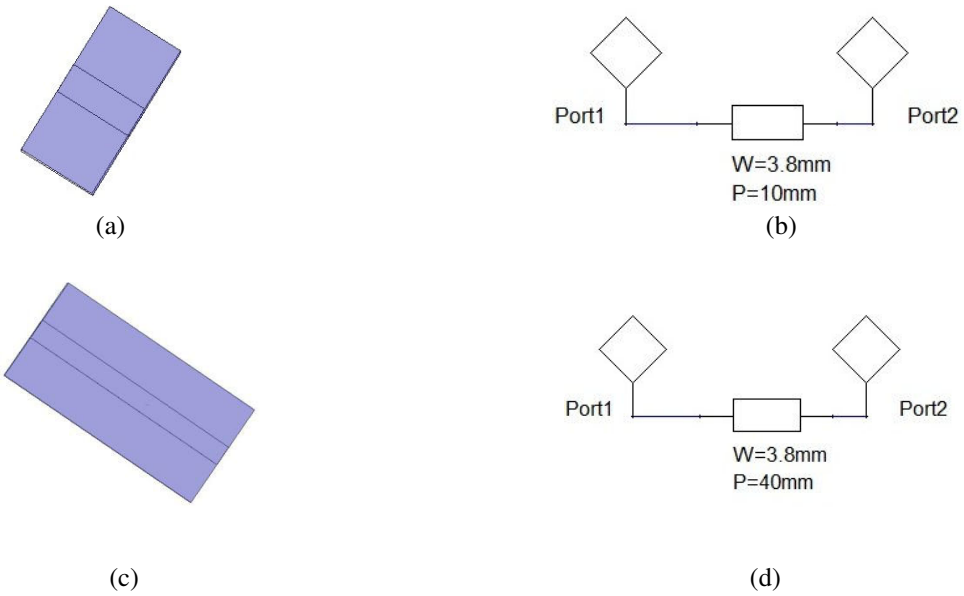

(a) (b)

(c) (d)

Fig. 4.21 : Simulated structures of CPW lines of length 1 cm and 4 cm on LCP Vectra E820i in P_1-P_2 planes (a), (c) in Ansoft HFSS of 1cm and 4 cm and (b), (d) in Ansoft designer electric simulation of 1 cm and 4 cm.

TRL measurements provides a good matching of transmission lines as the Line impedance is considered as a reference. From Fig. 4.22 and Fig. 4.23 the lines of 1 cm and 4 cm respectively provides a low loss signal transmission of and 0.01 dB (1 dB/ μm) and

0.05 dB (5 dB/ μm) till 1 GHz. In addition, the losses are less than 0.35 dB in the entire frequency band till 3 GHz.

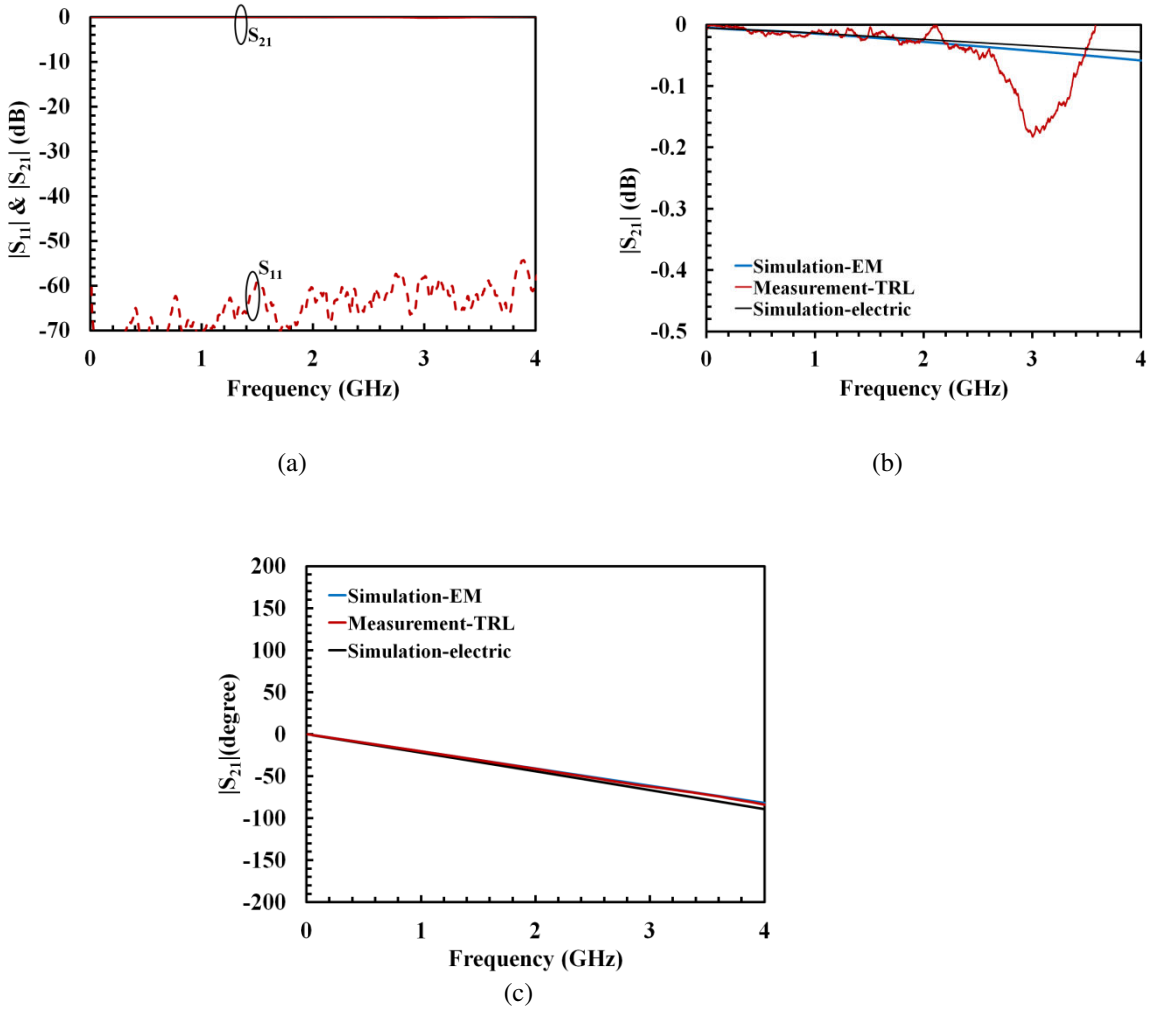

Fig. 4.22 : S parameters of MID microstrip lines of length 1 cm on LCP Vectra E820i in the P'_1-P'_2 plane, (a) magnitude measured in dB, (b) Zoomed S_{21} magnitude in dB and (c) S_{21} phase in degree.

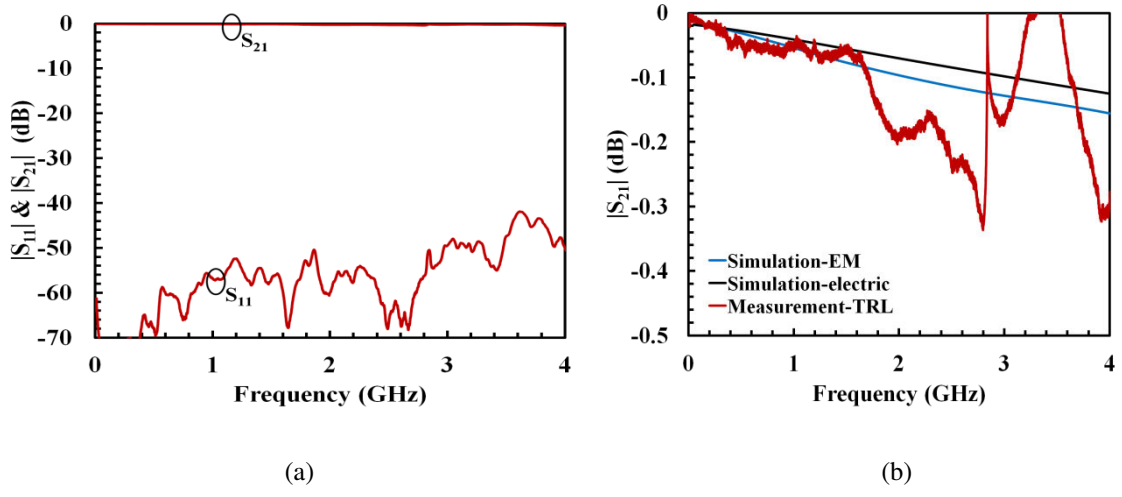

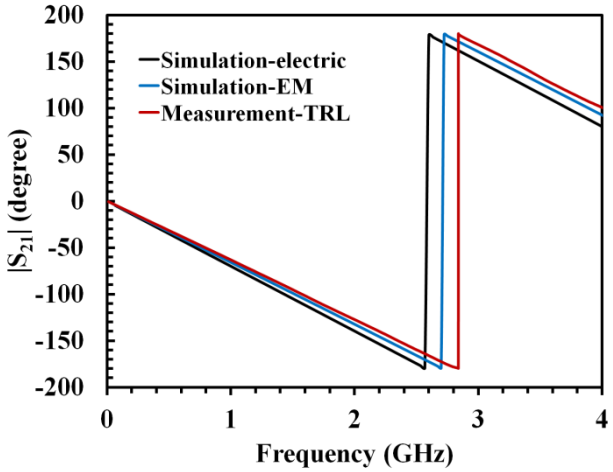

(c)

Fig. 4.23 : S parameters of MID microstrip lines of length 4 cm on LCP Vectra E820i in the P'_1-P'_2 planes, (a) magnitude measured in dB, (b) Zoomed S_{21} magnitude in dB and (c) S_{21} phase in degree.

Both measurements using Ecal and TRL calibrations provide a good agreement with that obtained from EM simulation results. Hence, these measurement results are taken in order to study the losses and quality factor of MID microstrip lines and to extract the substrate effective permittivity in continuous frequency band. These studies will be presented in section 4.4.

4.3.3. MID Stripline

Fig. 4.24 (a) and (b) respectively present the photographs of two MID stripline transmission lines of length 2 cm and 4 cm fabricated on LCP Vectra E820i using LDS method of fabrication. Microstrip line of width 1.45 mm has been covered by a one-face metalized LCP Vectra E820i in both striplines. Similar to CPW lines and microstrip lines, both EM and electric simulations are also acheived for this stripline transmission line study. Ansys HFSS and Ansoft designer are used for EM and electric simulations. In HFSS simulation, an air gap of 0.13mm (it is the thickness of center conductor of the SMA connectors used) is considered in between two substrates. Fig. 4.25 shows the simulated structures of 2 cm line and 4 cm line in two simulation platforms.

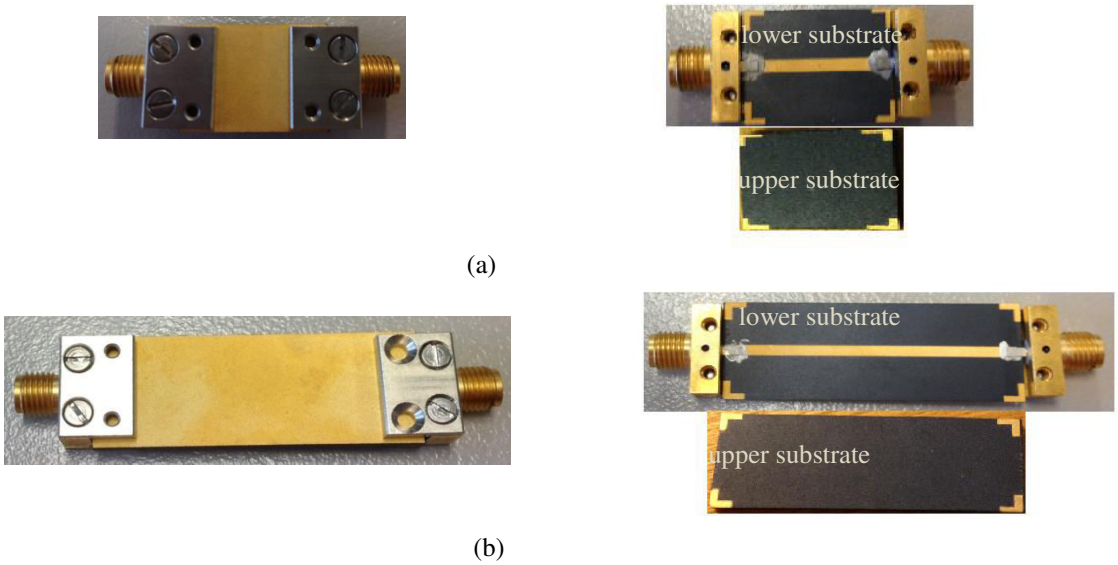

Fig. 4.24 : Striplines on LCP Vectra E820i, (a) of length=2cm, and (b) of length=4 cm.

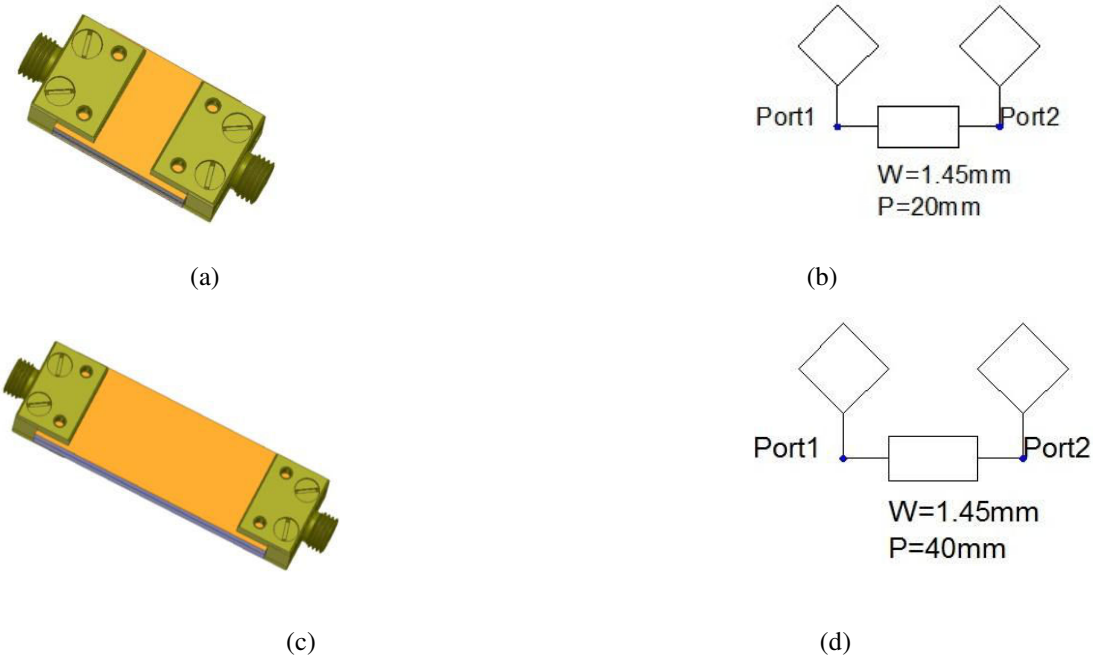

Fig. 4.25 : Simulated structures of MID striplines of length 2 cm and 4 cm on LCP Vectra E820i , (a) and (c) in Ansys HFSS and (b) and (d) in Ansoft designer electric simulation.

Here, S parameters measurements using Ecal calibration are carried out till 10 GHz. Comparisons between S parameters of 2 cm and 4 cm stripline transmission lines obtained from measurements and simulations are shown in Fig. 4.26 and Fig. 4.27. The 2 cm MID stripline exhibits good electrical performances on the moulded LCP Vectra E820i in very good agreement with EM simulations. Due to the absence of SMA connectors on either side of the line in the electric simulated structure, a difference between measurements and electrical simulations is observed. The 2 cm line exhibits a matching better than -13 dB in the

entire frequency range of measurement till 10 GHz. It shows an insertion loss of less than -0.5 dB till 6 GHz and it increases to 1 dB at 10 GHz leading to insertion losses of 0.068dB/mm at 6 GHz.

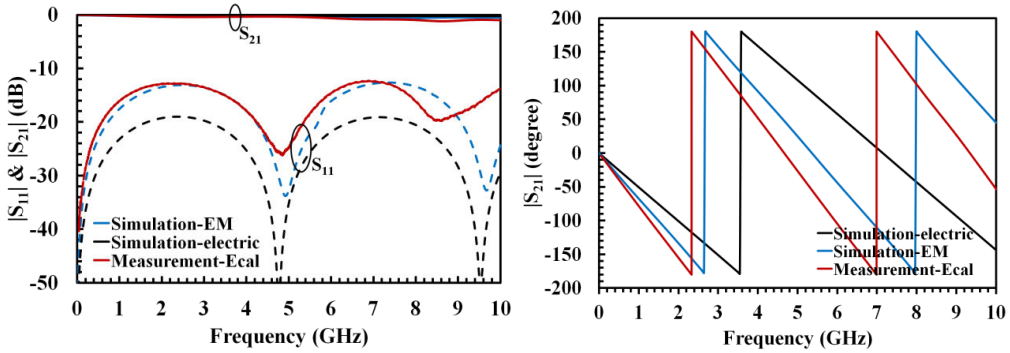

(a) (b)

Fig. 4.26 : S parameters of MID stripline of length 2 cm on LCP Vectra E820i, (a) magnitude in dB, and (b) S_{21} phase in degree.

For the stripline of length 4 cm, a measured return loss of better than -15 dB is obtained throughout the frequency range from 1 MHz to 10 GHz (Fig. 4.27 (a)). Fig. 4.27 (b) and (c) respectively show the magnitude and phase of S_{21} obtained from measurements and simulations. Magnitude of S_{21} which represents losses of the line increases with frequency. The line shows a loss of less than 0.5 dB till 5 GHz. The phase of S_{21} obtained from measurement coincides with that obtained from simulations, especially with EM simulation.

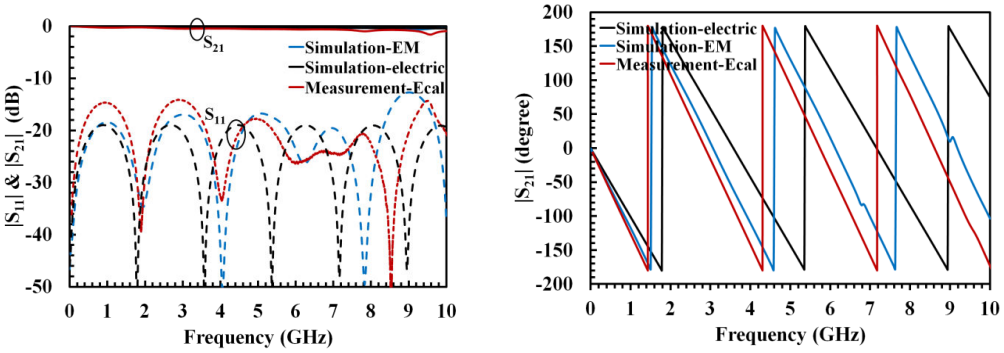

(a) (b)

Fig. 4.27 : S parameters of MID stripline of length 4 cm on LCP Vectra E820i, (a) return loss and insertion loss in dB, and (b) phase in degree.

In this section, MID transmission lines in three different technologies: CPW, microstrip and stripline are designed, fabricated and measured. Measurements and simulations of S parameters are presented. A good agreement is obtained between measurements and simulation. These first results confirm the compatibility LDS fabrication method for RF transmission lines. More analysis is yet to be studied based on transmission lines electrical properties such as propagation constant, losses, quality factor, etc. The following section will be focusing on the transmission lines electrical properties.

4.4. Electrical properties of LDS transmission lines on LCP Vectra E820i

4.4.1. Theoretical electrical properties

This section deals with the calculation of the electrical properties of molded transmission lines on LCP Vectra E820i such as losses and quality factor. Equations presented in section 4.2 giving theoretical values of losses and quality factors for CPW, microstrip and striplines technologies on LCP Vectra E820i based on transmission line dimensions and substrate properties are considered for a line characteristic impedance of 50 Ω. Fig. 4.28 and Fig. 4.29 show the theoretical values of losses and quality factor of these MID lines on LCP Vectra E820i with respect to frequency till 10 GHz. The CPW lines show more conductive losses (α_c) of 0.3 Np/m at 1 GHz and stripline shows more dielectric losses (α_d) of 0.1 Np/m at 1 GHz among the transmission lines. Indeed, the stripline holds more dielectric losses due to the presence of dielectric on either sides of the signal line and CPW exhibits more conductive losses due to the larger conductor strip required to achieve the 50 Ω characteristic impedance.

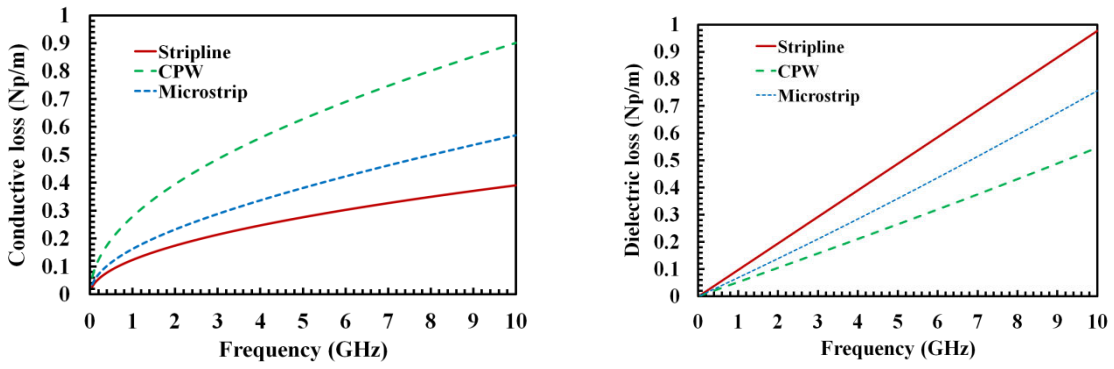

(a) (b)

Fig. 4.28 : Theoretical losses in transmission lines on LCP Vectra E820i, (a) conductive loss in Np/m, and (b) dielectric loss in Np/m.

The theoretical values of total attenuation constant (α) and the phase constant (β) of 50 Ω MID lines are shown in Fig. 4.29. As radiation losses are neglected, the total attenuation is the sum of dielectric and conductive losses. CPW exhibits higher losses as conductive losses predominates dielectric losses in all the three transmission lines (Fig. 4.29 (a)). Phase constant is based on the phase velocity of the signal along the transmission line. As for stripline line, the EM field is only in the dielectric; phase velocity is slower leading to a higher constant phase in Fig. 4.29 (b). Based on these calculations, quality factors of transmission lines are calculated using equation 3.28. From Fig. 4.30, theoretical quality factors of CPW, microstrip and stripline are 45, 80 and 110 respectively at 1 GHz.

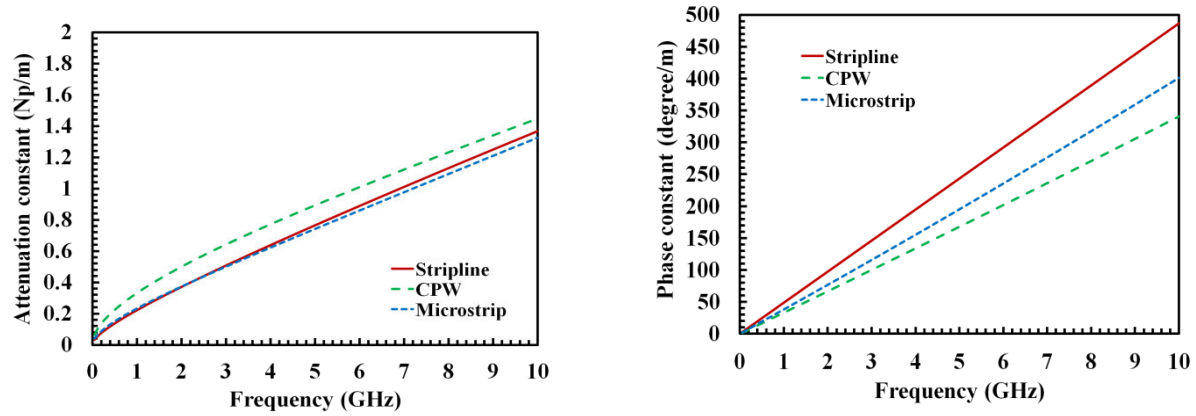

(a) (b)

Fig. 4.29 : Theoritical calculations of propagation constant of transmission lines on LCP Vectra E820i, (a) attenuation constant (α) in Np/m, and (b) phase constant (β) in degree/m.

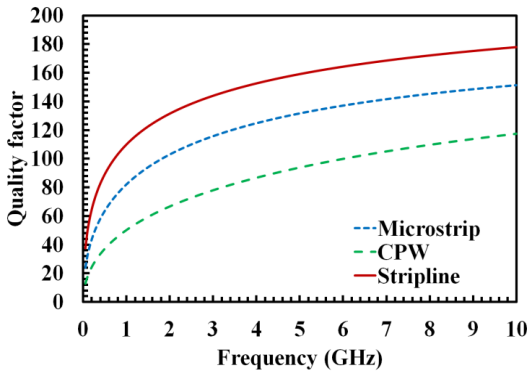

Fig. 4.30 : Theoritical calculations of quality factor of transmission lines on LCP Vectra E820i.

These theoretical calculations are made as references for the study and comparison of the electrical properties extracted from measurements of fabricated MID transmission lines. Following section presents those extracted electrical properties of MID transmission lines in three different technologies based on their S parameters measurements. The results are compared with the Ansys HFSS simulations.

4.4.2. Measured electrical performances

For accurate extraction of transmission lines electrical properties, two transmission lines method [25] is adopted. The fundamental concept of this method is to de-embed the parasitic contribution of interconnects needed to access the device under test using S parameters measurements of two transmission lines of different lengths. The detailed mathematical calculations of this method can be found in section 3.3.1 in chapter 3. Transmission lines in CPW, microstrip and stripline technologies resepectively present their resonances at 3.4 GHz, 3.1 GHz and 2.2 GHz. The extracted results thus presented till 4 GHz, because above this frequency the extraction could not be exploited.

4.4.2.1. Characteristic impedance

The study begins by extracting the characteristic impedance of the measured lines. Fig. 4.31 (a) shows the real part of impedance extracted from the simulated and measured S parameters of MID lines on CPW, microstrip and stripline configurations. Extracted characteristic impedances from measurement are respectively 52.66 Ω, 57.6 Ω and 56.7 Ω for CPW, microstrip and stripline transmission lines. If we compare these values to the characteristic impedance of 50 Ω, variations of 5.32%, 14.2% and 12.6% are observed for lines in CPW, microstrip and stripline technolgies. Near to the resonance frequency, the value of the characteristic impedance cannot be exploited (see Fig. 4.31 (b)).

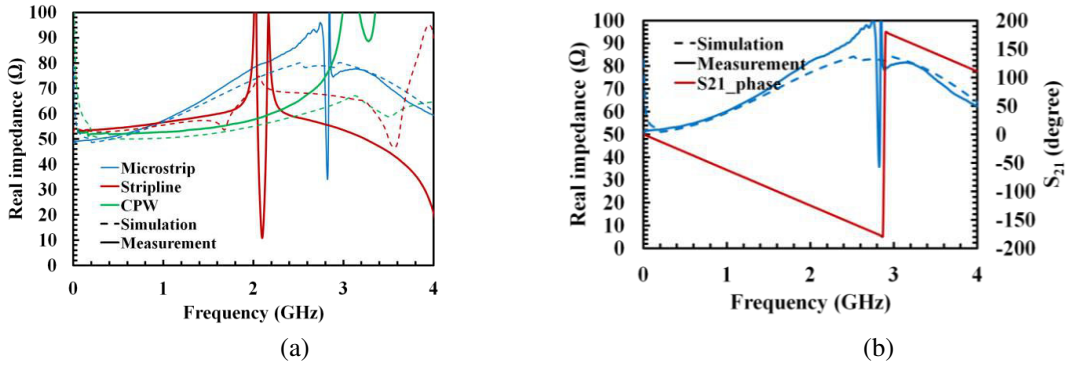

Fig. 4.31 : (a) Real part of impedance extracted from measurements and simulations of MID transmission lines on LCP Vectra E820i and (b) resonance study.

4.4.2.2. Effective permittivity

Later on, the effective dielectric constant of LCP Vectra E820i can be calculated using the equation:

$$\varepsilon_{reff} = \left(\frac{\beta c}{\omega}\right)^2 \tag{4.38}$$

where c is the velocity of light in meter per second, β *(=ϴ/l)* is the phase constant in radians per meter, l is the length of the line in meter and ω is the angular frequency in hertz. The effective dielectric constants of the substrate obtained from CPW, microstrip and stripline transmission lines are given in Fig. 4.32. The plot presents a good comparison between measurement and simulation results with a difference less than 1.16%, 1% and 2.6% respectively shown for CPW, microstrip and stripline at 1 GHz. ε_{reff} are in the order of 2.56, 3.26 and 4.5 respectively obtained from the measured phase of CPW, microstrip and stripline transmission lines at 1 GHz.

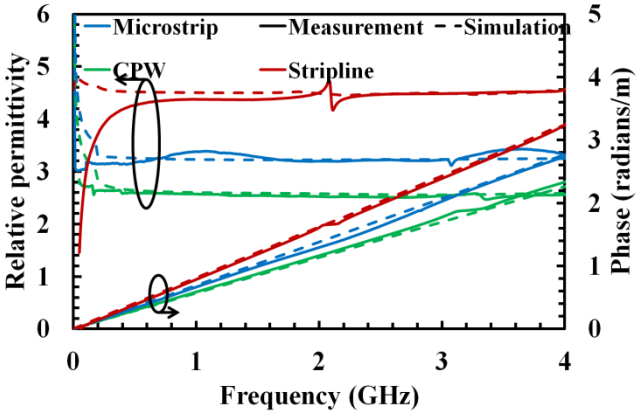

Fig. 4.32 : Effective relative permittivity and phase of LCP Vectra E820i extracted from MID transmission lines measurement and simulations.

4.4.2.3. Relative permittivity

Further extraction of relative permittivity ε_r can be done based on effective permittivity. Other than stripline transmission lines whose ε_r is equal to ε_{reff}, Fig. 4.33 shows the extracted ε_r of CPW and microstrip transmission lines from measurement and simulation. The graph also compares the relative permittivity value obtained from the resonant cavity method (from Fig. 3.14 in chapter 3).

A good agreement is obtained between the cavity method and the transmission lines method for relative permittivity characterization. A relative permittivity of 4.28 and 4.34 were extracted from the measurements of CPW and microstrip configurations at 1 GHz. If we compare the measurement results with those obtained from resonance cavity method, for example at 1.26 GHz (the second resonance in resonance cavity method), a difference of 1.26% can be seen with CPW lines and 0.92% in microstrip lines.

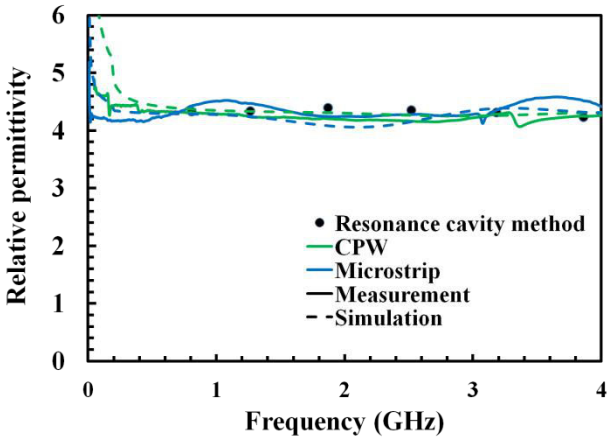

Fig. 4.33 : Relative permittivity of LCP Vectra E820i extracted from MID transmission lines measurement, simulations and resonance cavity method.

4.4.2.4. Losses

In order to investigate the losses origin of LDS lines, the transmission line parameters or RLGC parameters (resistance, inductance, conductance and capacitance respectively for R, L, G and C) of CPW, microstrip and stripline are extracted based on the impedance of the line.

The obtained RLGC values at 1 GHz are presented in Table 4.1. Based on these RLGC parameters, both conductive and dielectric losses are extracted. Fig. 4.34 presents the extracted losses of LDS transmission line measurements up to 5 GHz. It shows a comparison between the losses in three transmission line technologies. A good agreement is obtained

between measurements and simulations. Table 4.1 summarizes both conductive and dielectric losses at 1 GHz for the three technologies. It is clear that for CPW topology, conductive losses are higher than dielectric losses which is not the case for both microstrip and stripline topologies.

Table 4.1. Measured electrical properties of LDS MID transmission lines at 1 GHz.

Technology	Z_{real} (Ω)	R (Ω/m)	L (nH/m)	G (S/m)	C (pF/m)	α_d (Np/m)	α_c (Np/m)	α_T (Np/m)	β (radians/m)	Q factor
CPW	52	27.5	301	2.6	98	0.04	0.26	0.48	0.58	31.34
Microstrip	59	15.5	589	2.5	108	0.034	0.11	0.35	0.66	75.15
Stripline	57	12	429	1.5	113	0.07	0.05	0.31	0.78	101

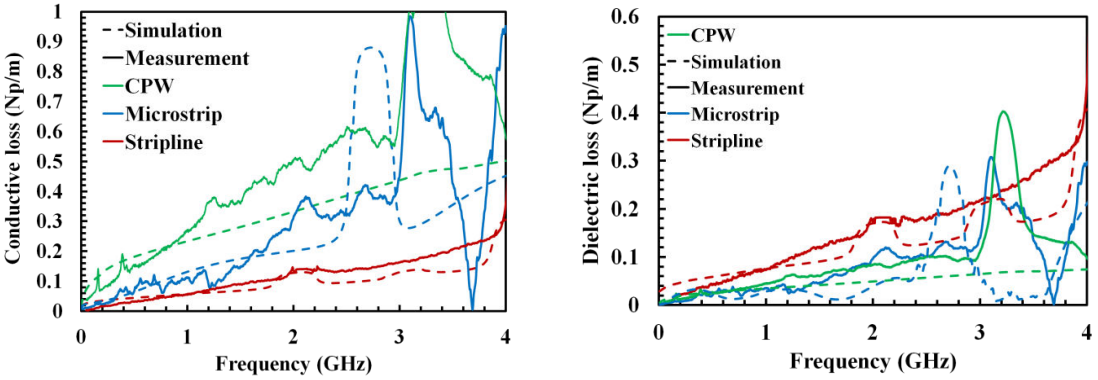

(a) (b)

Fig. 4.34 : Losses of LDS transmission lines, (a) conductive loss in Np/m and (b) dielectric loss in Np/m.

Indeed, total losses for the all LDS transmission lines are lower than 0.5 Np/m at 1 GHz (Fig. 4.35(a)). The LDS transmission lines present thus acceptable losses and can be used for RF applications. As the quality factor describes the power loss for a given phase, the MID transmission lines realized by LDS on LCP Vectra E820i presents quality factor as 31, 75 and 101 respectively at CPW, microstrip and stripline respectively (see Fig. 4.35(a)).

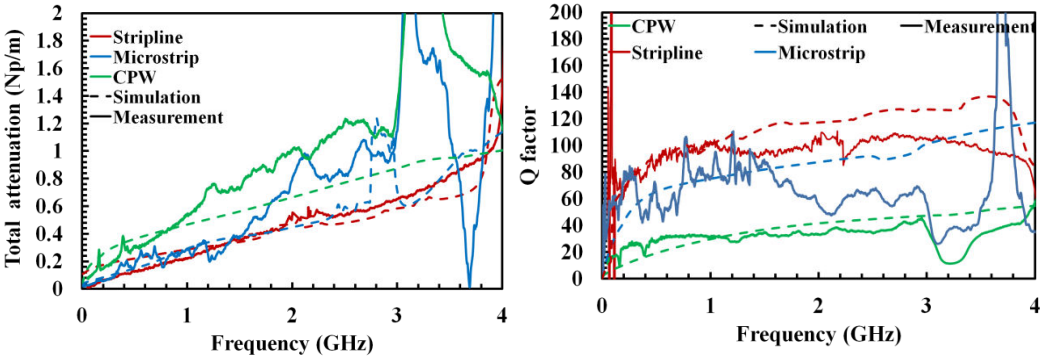

(a) (b)

Fig. 4.35 : (a) Attenuation constant in Np/m and (b) Q factor of LDS transmission lines.

In order to study the LDS MID lines performance, the microstrip configuration is selected and the quality factor of LDS microstrip lines is compared with that of the transmission lines fabricated on good quality classical Rogers RO4003 and a low cost FR4 substrates using photolithography fabrication method. Fig. 4.36 shows the comparison of quality factor between MID lines and the classical lines. At 1 GHz, quality factors for FR4 and RO4003 are 39 and 137. LCP Vectra compared to FR4 presents a good compromise between cost and quality factor.

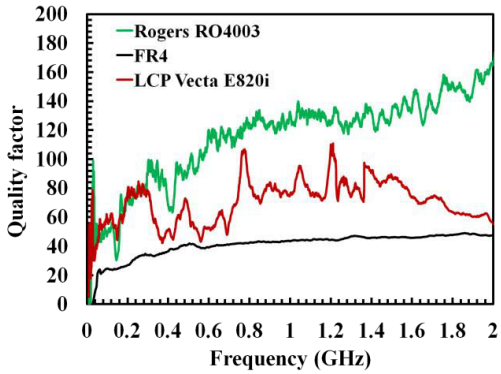

Fig. 4.36 : Comparison of Q factors of classical substrates Fr4, Rogers RO4003 and LDS LCP Vectra E820i transmission lines.

From all the above results, the LDS technology using LCP Vectra E820i presents a good potential for RF devices. Hence the research now focuses on the design and analysis of RF circuits on LDS LCP Vectra E820i substrate such as filters and antenans. Before moving onto these sections, a grounded via hole which is key element in microstrip technology is considered in order to study its model in LDS technology. Following section thus presents MID LDS microstrip via model in details.

4.5. LDS via hole model

Reliable via hole plating can be produced with LDS technology. This expands the possibilities for MID RF circuits. A via hole is a key element in multilayer RF circuits to route the signal flow in different layers. Grounding microstrip circuits with via holes is frequently used. A via hole consists of a metalized cylindrical hole drilled out through the substrate towards the ground plane. A rectangular or circular conducting pad is placed above the cylindrical via to provide contacts with the transmission lines. The performance of the via structure can significantly affect the device response especially at higher frequencies. Hence, the equivalent circuit of LDS via holes is required to study its impact on the frequency response of the MID RF circuit.

In this work, study on microstrip LDS via plated hole on LCP Vectra E820i substrate is performed. The effect of via on signal transmission is studied on a short microstrip line. An electrical model of via fitting with Ecal calibration measurements is extracted. The TRL calibration standard THRU is taken into account for the study of via model in LDS microstrip (see Fig. 4.37). It can be called as the device under test (DUT).

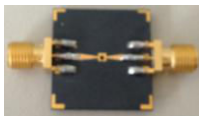

Fig. 4.37 : Microstrip via THRU from TRL calibration kit.

4.5.1. Modelling and analysis of LDS via

In order to study the model of LDS via, a short microstrip line with a grounded via hole in the center is considered (Fig. 4.38). In addition to the microstrip via plane, tapered access and soldering pads were also considered on either side of transmission line for better connector access.

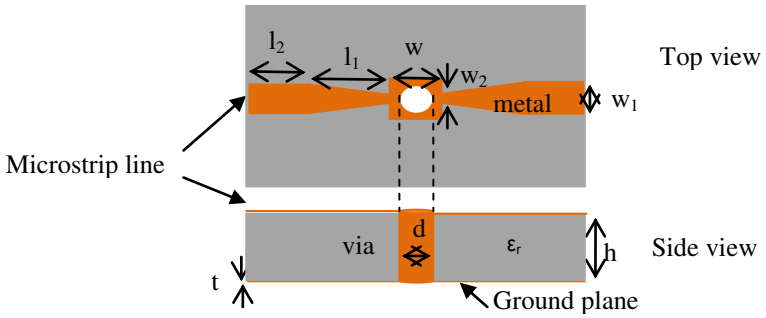

Fig. 4.38 : Top and side views of LDS via model in microstrip, w=1.6mm, w_1= 1.5mm, w_2=0.25mm, d=0.7mm, l_1=l_2=5mm, h=2mm, t=10 μm, and ε_r=4.3.

A via grounded hole can be modeled by an inductance in series with a resistance. The parasitic inductance effect increases with increase in frequencies. It mainly depends on the diameter and length of the mirostrip via hole [26]. Several methods of analyzing the equivalent circuit of via can be found in literature [27][30].

In this work, the via hole model in microstrip presented in [29] is considered. The equivalent inductance of a microstrip cylindrical via is given by:

$$L_{via} = \frac{\mu_0}{2\pi}\left[h.\ln\left(\frac{h+\sqrt{r^2+h^2}}{r}\right) + \frac{3}{2}\left(r-\sqrt{r^2+h^2}\right)\right] \quad (4.39)$$

where r is the radius of the via, h is the height of substrate, μ_0 is the permeability in vacuum which is 4π x 10^{-07} A.m . In this model, the effect of the via pad is not considered. According to the author in [29], the dependency of the via pad is small resulting in a variation of less than 4% from the above calculation. The effect of resistance of the via hole is negligible and is mainly depend on the fabrication process and thickness of metallization. Via resistance can be calculated as:

$$R_{via} = R_{dc}\sqrt{1+\frac{f}{f_\delta}}. \quad (4.40)$$

where,

$$f_\delta = \frac{1}{\pi\mu_0\sigma t^2} \quad (4.41)$$

$$R_{dc} = \frac{1}{\sigma\omega t} \quad (4.42)$$

Based on the above equations, the electrical model parameters are calculated. Fig. 4.39 shows the via resistance with respect to frequency. The effect of resistance is in between 0.1 -5.2 Ω from DC to 10 GHz. The LDS via inductance of 0.5 nH was calculated based on the equation (4.39).

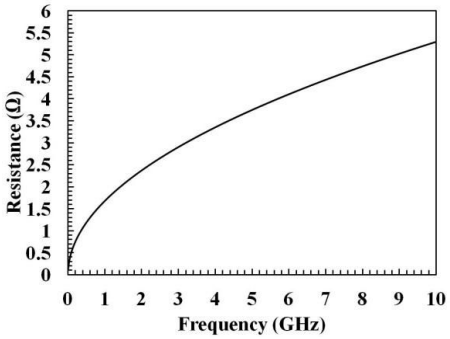

Fig. 4.39 : The resistance of LDS microstrip via hole as a function of frequency.

Fig. 4.40 shows the electrical model of via modeled for a TRL calibration standard THRU. The THRU standard is at zero length, which is more accurate with no loss and reflection.

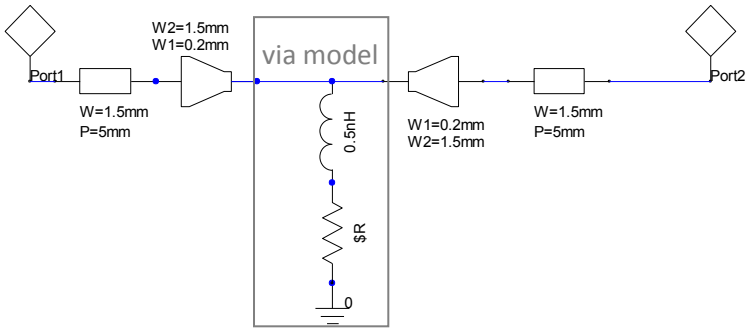

Fig. 4.40 : Electrical model of LDS microstrip via.

The graph in Fig. 4.41 shows the frequency response of the electrical model of the device keeping the value of Rvia =2.5 Ω. As expected, the device acts as a short circuit with a reflection near to -5 dB and a poor transmission of -20 dB till 5 GHz. As frequency increases, the response of the device degrades.

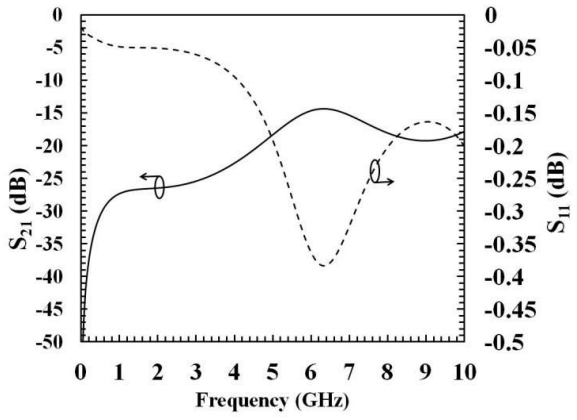

Fig. 4.41 : Simulated frequency response of S_{21} and S_{11} of LDS microstrip model.

A parametric study of the variation of inductance is shown in Fig. 4.42. Three inductance values 0.4 nH, 0.5 nH and 0.6 nH are used for the study.

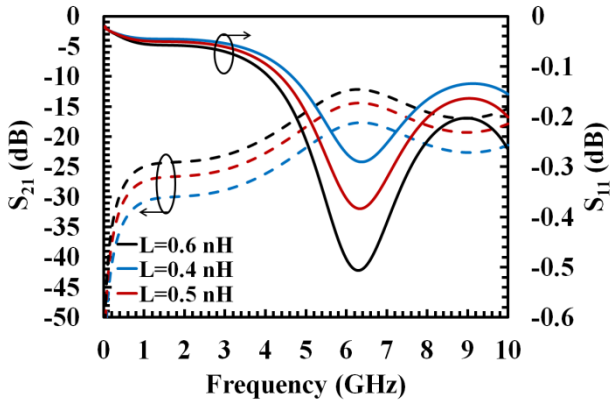

Fig. 4.42 : Variation of inductance value on S_{21} and S_{11} of LDS microstrip model.

Fig. 4.43 shows the S parameter response of the device and its simulation in Ansys HFSS. Measurements have been done considering the effect of via pad and soldering pads using Ecal calibration and simulations have been done considering SMA connectors on either sides of the device. The graph also compares the response of fabricated microstrip via on LDS LCP Vectra with that obtained from electrical via model shown in Fig. 4.41. The graph shows fair agreement with the via model.

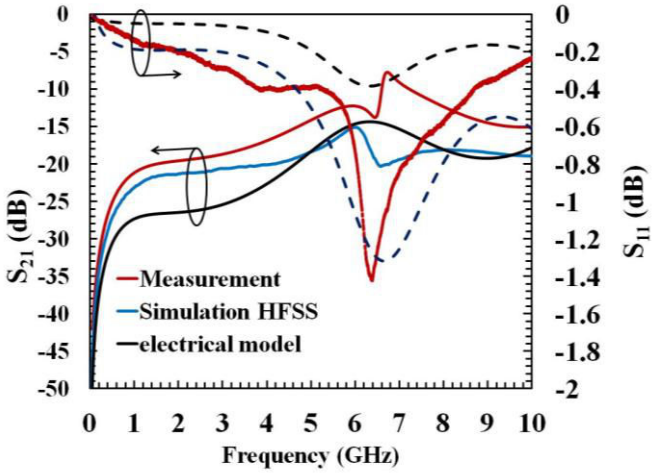

Fig. 4.43 : Frequency response of fabricated THRU with grounded via hole.

A difference between electrical model response and that of HFSS simulation and measurements can be observed in the plots. The response of via model can be improved by adding two capacitors on either side of the via model. These capacitances occurs due to the

presence of the discontinuity between the taper and the via pad. Fig. 4.44 shows the comparison of LDS via with improved via model response.

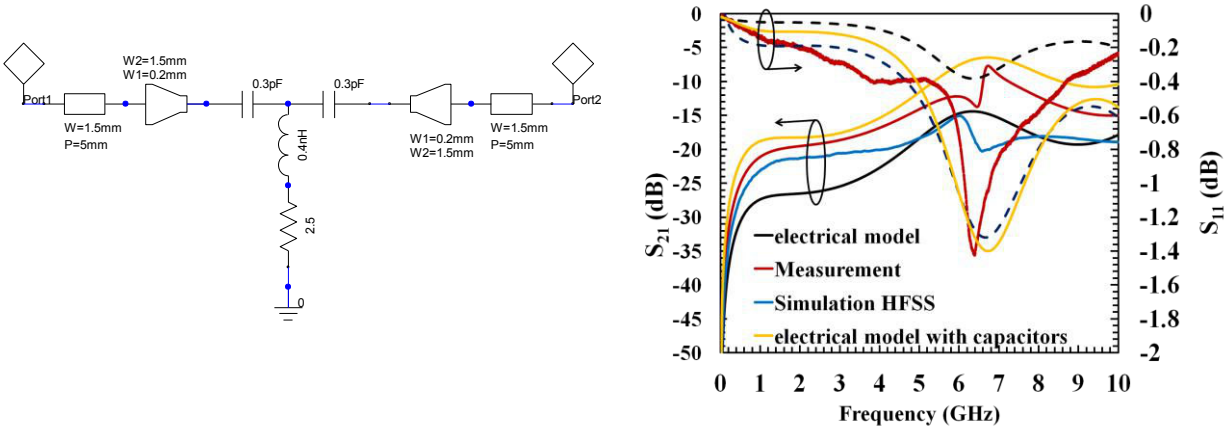

(a) (b)

Fig. 4.44 : LDS microstrip via model with two capacitors.

Simulation and measurement results of MID microstrip via model proof that LDS provides a good quality and reliable via hole fabrication. The good performances of LDS LCP substrate combined to MID technology has extended for the study of MID filters and are discussed below.

4.6. Low pass Filters

To validate the potential of MIDs for RF applications in filter design and fabrication, distributed and hybrid low pass filters in both CPW and microstrip technologies are fabricated are designed, realized and measured on LCP Vectra E820i. Distributed low pass filter (DLPF) is based on a classical stepped impedance topology alternating high impedance and low impedance transmission lines [18][34]. In hybrid low pass filter (HLPF), the high impedance section is replaced with Surface MounTed capacitors (SMT) allowing the size miniaturization of the device [35]. Fig. 4.45 (a) and (b) respectively present the schematic diagrams of DLPF and HLPF. Z_l and Z_h are the values of low and high impedance and C is the equivalent capacitance needed to replace the low impedance section in HLPF.

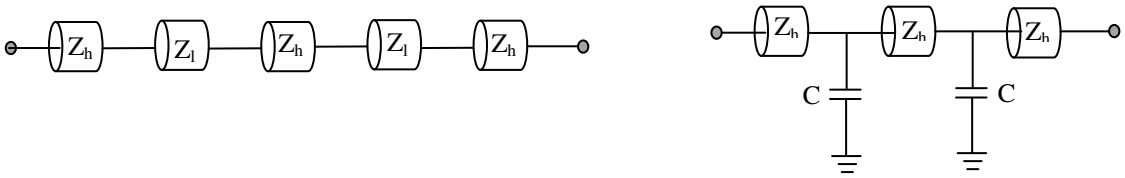

(a) (b)

Fig. 4.45 : Schematic diagram of low pass filters, (a) distributive low pass filter and (b) hybrid low pass filter.

4.6.1. CPW technology

Fig. 4.46 shows the DLPF ($F_{cut\ off}$ = 2.2 GHz) and HLPF with a cut off frequency at ($F_{cut\ off}$ = 1.1 GHz) designed in CPW technology. The size of stepped impedance low pass filter given in Fig. 4.46 (a) has been miniaturized by replacing the low impedance section with two capacitors of value 2.4 pF in Fig. 4.46 (b). Similar to previously mentioned transmission line structures, in low pass filters, tapered sections of length 4mm and end width of 1.5 mm were introduced on each side to have ease in connector access. Thus, P'_1-P'_2 planes represent the low pass filters with two tapered access and P_1-P_2 planes are the actual low pass filter plane. Table 4.2 depicts the dimensions of the CPW low pass filters.

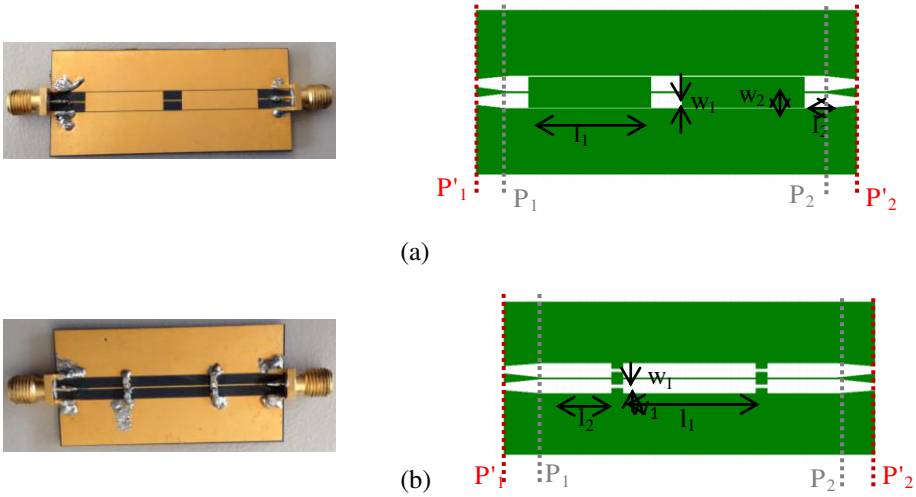

Fig. 4.46 :Photograph of a CPW transmission low pass filter made by LDS on LCP vectra E820i (a) distributed low pass filter, (b) hybrid low pass filter.

Table 4.2: CPW LPF dimensions

Parameters (mm)	DLPF	HLPF
w_1	0.2	0.2
w_2	4.6	-
l_1	19.2	17.5
l_2	4.8	9.3

Fig. 4.47 (a) shows a good agreement between the simulated and measured S parameters for the distributed low pass filter in the P'_1-P'_2 plane. The measurement of DLPF gives a -3 dB cut-off frequency at 2.24 GHz. The return loss is always better than -9 dB, with attenuation remaining near to 0.6 dB in the pass band. It shows a -3 dB cut off at 2.3 GHz. The return loss can be improved if we consider the plane of measurement as P_1-P_2. TRL measurements using calibration kit given in Fig. 4.12 have been taken into account here in order to get the exact filter plane at P_1-P_2 planes. In Fig. 4.47 (a), the plots in green color represent the TRL measurements of the DLPF. The plot shows ripples in pass band and an improvement in the filter performance with a return loss always better than -15 dB in the passband. Spurious frequencies with a level of -20 dB are occuring at 4.7 GHz times the filter cut off frequency.

Fig. 4.47 (b) shows the performance of HLPF P'_1-P'_2 planes. Measurements are in good agreement with EM and electric simulations. The return loss is always better than -12dB, with attenuation remaining near to 0.3 dB in the pass band. The filter shows a -3 dB cut-off frequency at at 1.1 GHz. Filter measurements can be improved by eliminating the effect of taper access on the filter using TRL calibration. Graphs in green color in Fig. 4.47 (b) shows TRL measurement results of HLPF. The filter always shows return loss is always better than 17dB, with attenuation remaining near to 0.3 dB in the pass band. Spurious frequency bands are rejected at the entire frequency band till 5 GHz.

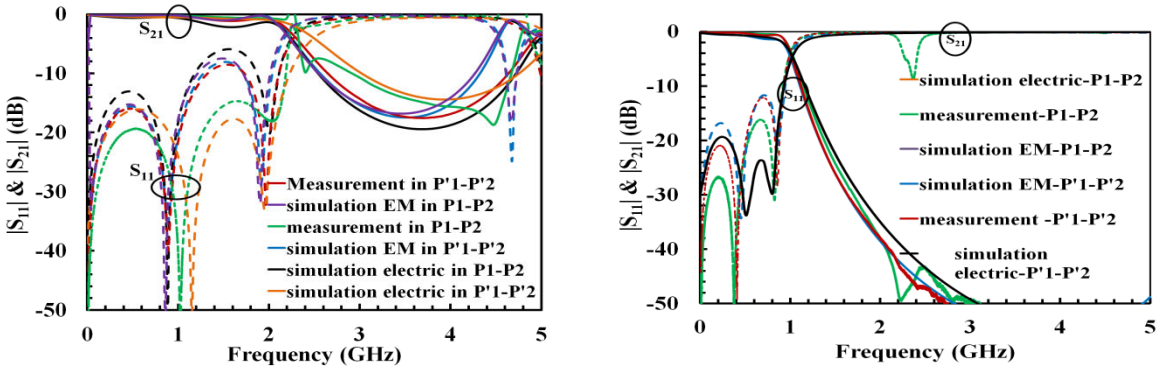

(a) (b)

Fig. 4.47 : S parameters of CPW filters (a) distributed low pass filter, (b) hybrid low pass filter.

4.6.1.1. Study on the effect of losses and capacitance on the performance of HLPF

The electric circuit of a HLPF is shown in Fig. 4.45 (b). The low impedance section of a DLPF is replaced by SMT capacitors. A study on the effect of variation in capacitance has been studied. The two capacitors used here have value of 2.4 pF ± 0.2 pF. A parametric

study of capacitance value from 4.6 pF and 5 pF is done in CPW HLPF structure. Table 4.3 shows the variation of -3dB cut-off frequency with capacitances. For 0.1 pF variation in capacitance, 10 MHz variation in -3dB cut-off frequency is observed. Pass band losses are negligible with variation in capacitance values. Fig. 4.48 is the graphical representation of the variation. We can see that frequency variation is inversly proportional to capacitance variation.

Table 4.3: Capacitance Vs cut off frequency

Capacitance (pF)	**-3dB cut off freq (GHz)**	**Insertion loss (dB)**
4.6	1.06	-0.139
4.7	1.05	-0.141
4.8	1.04	-0.143
4.9	1.03	-0.146
5	1.01	-0.149

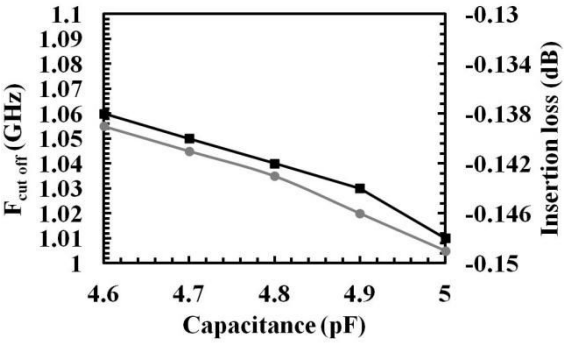

Fig. 4.48 : variation in CPW HLPF cut off frequency with respect to capacitance variation.

At radio frequencies, it is necessary to estimate the losses effect on RF circuit performance for MID substrate. Table 4.4 and Table 4.5 respectively show the effect of conductive losses and dielectric losses on HLPF's pass band losses. From Table 4.4, it can be seen that bandpass losses increase when conductivity decreases. Here, MID holds one tenth of copper conductivity and hence more losses are obtained for the MID filter (0.3 dB instead of 0.07 dB). All conductivity variations have been carried out by setting loss tangent of the substrate equal to zero. Similarly, variation in substrate losses study is presented in Table 4.5. In this study, conductivity of metallization was set to perfect conductivity. Pass band losses increase with increase in loss tangent value. MID holds a loss of 0.004 which is five times less than classical low cost FR4 substrate's loss (=0.02). Dielectric losses due to the LCP E820i substrate are near to 0.002 dB.

Table 4.4: Effect of conductivity

Conductivity (σ)	**Pass band losses (dB)**
PEC	-0.01
Cu	-0.065
Cu/10 **(MID)**	-0.29
Cu/100	-2.35

Table 4.5: Effect of dielectric losses

Dielectric losses *(tan δ)*	**Pass band losses (dB)**
0.04	-0.05
0.004 **(MID)**	-0.034
0.0004	-0.032
0	-0.03

4.6.2. MirostripTechnlogy

In similar to CPW LPF, microstrip technology was also taken into account in LDS MID fabrication. Fig. 4.49 show the microstrip LPF configurations in distributed and hybrid low pass filter. The optimized dimensions of the realized filters are listed in Table 4.6. In HLPF, two capacitors of 4.8 pF are utilized to replace the two low impedance sections in DLPF.

Table 4.6: Microstrip LPF dimensions.

Dimensions (mm)	**DLPF**	**HLPF**
w_1	8	-
w_2	0.2	0.2
l_1	13	17
l_2	3	6

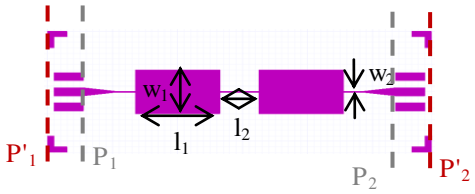

(a)

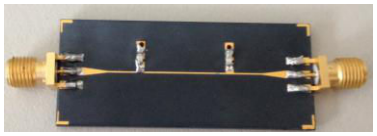

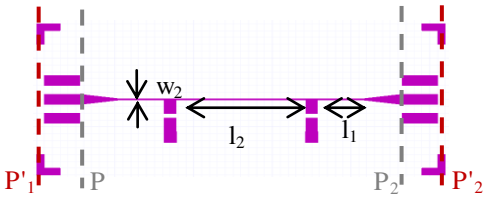

(b)

Fig. 4.49 : Photo of a microstrip low pass filter made by LDS on LCP vectra E820i (a) distributed low pass filter, (b) hybrid low pass filter.

Fig. 4.50 depicts the frequency response of LDS microstrip low pass filters on LCP vectra E820i. All simulations are done with Ansoft designer and Ansys HFSS and

measurement are done with N5222A Agilent PNA with Ecal calibration. Simulations have been done in the P'_1- P'_2 planes which consider the two tapered access mounted on each side of the filters. Simulations are in good agreement with measurements done with ecal calibration. For DLPF in Fig. 4.50 (a), ecal measurement show poor matching of 5 dB and insertion loss of 2 dB. By applying TRL calibration in order to get the real filter plane, i.e., at P_1-P_2 planes, the filter shows 3 dB cut-off frequency at 1.9 GHz. The return loss of 20 dB is obtained throughout the pass band frequency and insertion loss of 0.26 dB is obtained (see green color plots in the graph).

For HLPF, a cut-off frequency at 1 GHz is shown in Fig. 4.50 (b). With Ecal measurements, the measured return loss is better than 15 dB in the entire pass band and insertion loss of 0.62 dB. TRL measurements of HLPF are shown as green color plots in Fig. 4.50 (b). Similar to the previously presented filter, return loss has improved to -25 dB with TRL measurement or in the P_1- P_2 plane. In TRL measurements, spurious frequency bands are rejected to values below 20 dB up to 3.5 GHz which is 3.5 times the cut-off frequency.

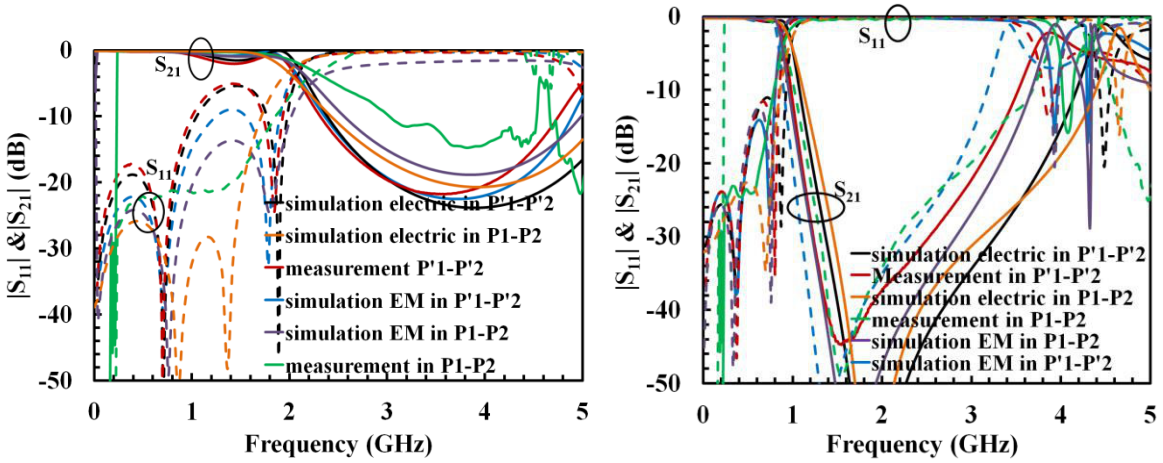

(a) (b)

Fig. 4.50 : Comparison of S parameters between measurement and simulation of microstrip transmission lines (a) distributed low pass filter, (b) hybrid low pass filter.

4.7. Band pass Filters

4.7.1. Narrow bandpass filter using dual behavior resonators

In RF communication systems, narrow band pass filter is an essential component usually used in transmitters and receivers. Severe constraints and requirements are added in RF filter design in telecommunication systems such as RF front end modules [36]. Some of

these contraints include out of band rejection, pass band losses, reduced size and cost of the device, etc. Several researches have already been developed in filter design to meet these constraints which include the use of high permittivity and low loss substrates, addition of lumped components etc. [37]. Dual Behavior Resonator (DBR) filter is an interesting topology for its simplicity and ease of fabrication. The principle of DBR filter is based on the parallel association of two transmission line stubs that can independantly control the transmission zeros in the lower and upper stop bands and the pass band in between them [38]. This DBR was introduced by Rizzi as tapped line bandpass filter. Later, in 2005, C. Quendo et al. has published the design equations of DBR filter [39].

Fig. 4.51 shows the basic structure of a DBR filter. It consists of two different open stubs connected in parallel. Each stub brings its own transmission zeros depends on its band stop conditions. In addition, the combination of these two stubs provides an operating frequency band. The graph shown in Fig. 4.51 shows typical frequency response of a DBR filter.

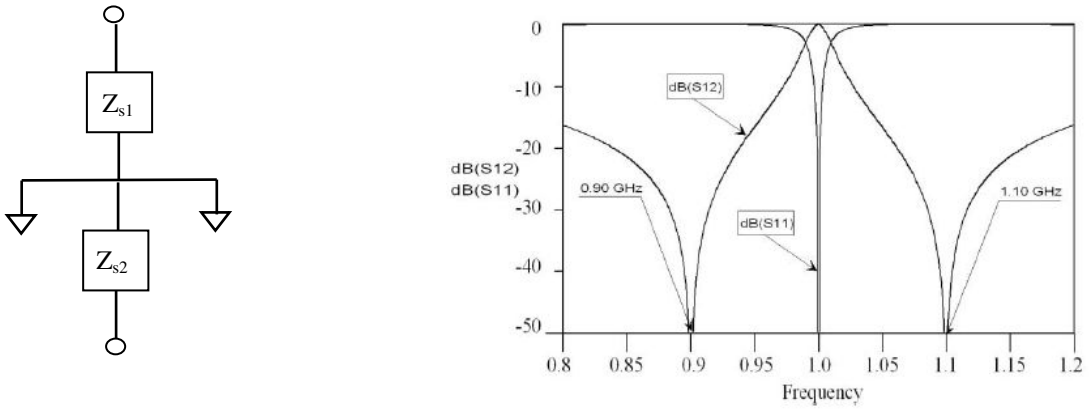

Fig. 4.51 : DBR electrical circuit principle and its typical frequency response [39].

The impedance of the whole DBR filter can be given as

$$Z = \frac{Z_{s1} Z_{s2}}{Z_{s1} + Z_{s2}} \tag{4.43}$$

In order to get a transmission zero to occur (band stop), this impedance should be zero, which in turn require either Zs_1 or Zs_2 equal to zero. In similar, for a band pass behavior, the impedances Zs_1 and Zs_2 should have same modulus with out of phase, which in turn makes Z to infinity (from equation 4.43). In order to modify the transmission zero location, each stub is decomposed into two cascaded transmission lines with different impedances as shown in Fig. 4.52.

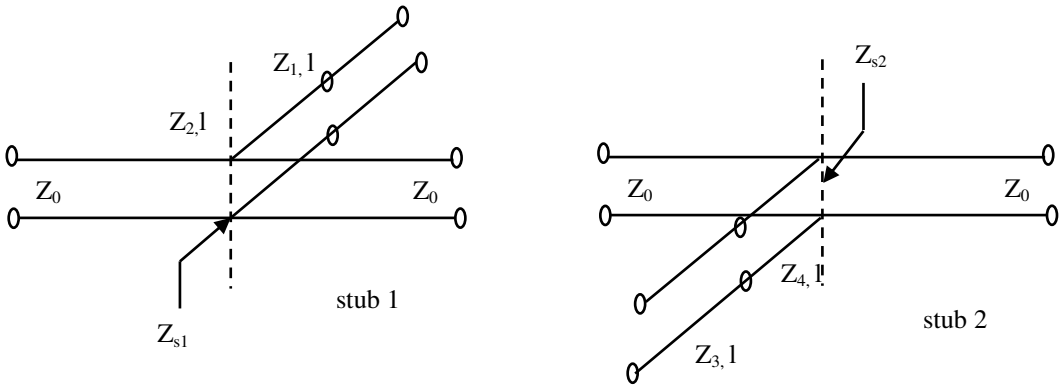

Fig. 4.52 : Equivalent impedance at each stub [39].

where $Z_1=Z_4$ and $Z_2=Z_3$. For the calculations of unknown parameters such as Z_1, Z_2 and l, the following calculations are adopted.

$$\tan^2(\theta_1)=\frac{Z_1}{Z_2} \tag{4.44}$$

$$\tan^2(\theta_2)=\frac{Z_2}{Z_1} \tag{4.45}$$

$$\tan^2(\theta_0)=\frac{2Z_1Z_2}{{Z_2}^2+{Z_1}^2} \tag{4.46}$$

$$l=\frac{c_0}{4F_0(k_1+k_2)} \tag{4.47}$$

where F_0 is the centre frequency, Θ_1 and Θ_2 are respectively the electrical lengths of first and second section of stubs, Θ_0 is the electrical length at F_0, and c_0 is the speed of light in vaccum. For calculation of k_1 and k_2,

$$\delta=k_2-k_1 \tag{4.48}$$

$$\sigma=k_2+k_1 \tag{4.49}$$

One can assume a given value of σ and

$$\delta=\frac{2\sigma}{\pi}\arccos\left(\sqrt{2}\sin\left(\frac{\pi}{2\sigma}\right)\right) \tag{4.50}$$

from here, Z_2 can be calculated as

$$\frac{Z_2}{Z_0}=\frac{\left(\tan^2\theta_1+1\right)\left(\tan^4\theta_1+1\right)\pi}{\tan^2\theta_1\left(1-\tan^2\theta_1\right)^2(k_1+k_2)b} \tag{4.51}$$

where,

$$\theta_2 = \frac{2\pi k_2 F_0}{c_0} l \tag{4.52}$$

$$\theta_1 = \frac{2\pi k_1 F_0}{c_0} l \tag{4.53}$$

Based on these calculations, a DBR filter at 5.2 GHz was designed and fabricated on an LCP E820i substrate. Electric design of this filter was initially carried out using Ansoft designer. Further dimension optimizations were done in the EM simulation structure. The layout and fabricated photo of the MID DBR filter are shown in Fig. 4.53. Dimensions are listed in Table 4.7.

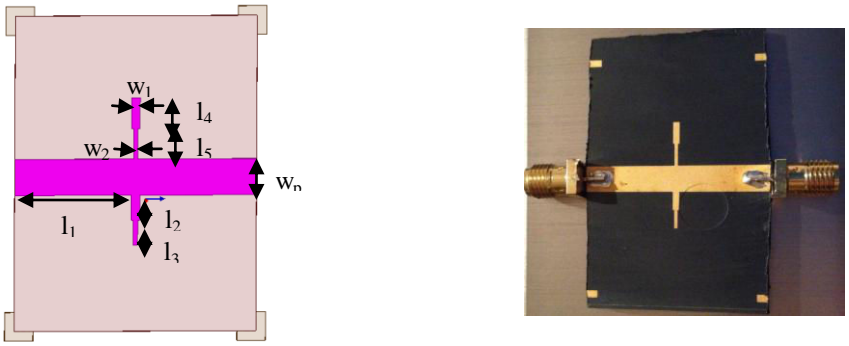

(a) (b)

Fig. 4.53 : DBR filter on LCP Vectra E820i, (a) layout and (b) its fabricated photo.

Table 4.7: Microstrip dual band reonator filter dimensions.

Parameters	Dimensions (mm)
w_p	3.78
l_1	15.9
l_2	3.2
l_3	3.2
l_4	5.32
l_5	5.32
w_1	0.88
w_2	0.45

Simulation and measurement results are shown in Fig. 4.54. A good agreement between simulation and measurement can be observed. A slight variation in the frequency response is observed due to connector effect and fabrication accuracy. The measured insertion loss is at -1.78 dB and return loss is -18 dB in the pass band. Lower transmission zero occurs at 4.68 GHz and upper transmission zero occurs at 7.03 GHz. This results in a lower cut off frequency at 4.78 GHz and upper cut off frequency at 5.86 GHz.

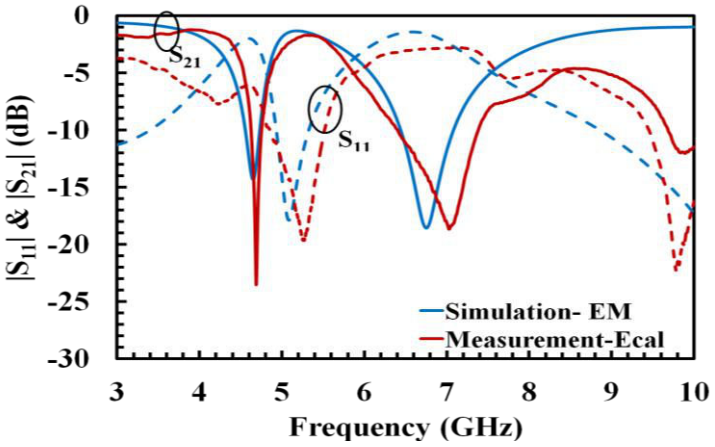

Fig. 4.54 : Simulated and measured DBR filter response on LCP Vectra E820i.

4.7.2. Wide band hair pin bandpass filter

Another topology of band pass filter is hair pin filter. The concept of this filter is same as parallel coupled half wavelength resonators filters. The main advantage of this filter is the optimal space utilization. This is achieved by folding the half wavelength long resonators as shown in Fig. 4.55. By folding the resonator in the form of a hair pin, the voltage occurs at the end of each arm is antiphase which results in a capacitance in between the arms. This added capacitance reduces the resonant frequency of the filter. To avoid this, a slide angle is introduced at the end of each section. Detailed explanation of the design equations is given in [18].

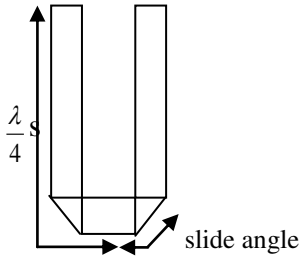

Fig. 4.55 : Schematic of hair pin resonator

The characteristics of this filter depend on the length of the coupled region, space between each arms, and line width. The spacing between each arm has more impact on attenuation while width and length of each arm have more impact on centre frequency, ripples in pass band etc. Higher order filters can be utilized to get more steeped slopes in the cut off region.

A fourth order band pass filter is chosen in this work for the design of a band pass filter at 5.8 GHz. The design of hair pin filter is started using electric simulation tool Ansys

designer. Further dimensional optimization is done in EM simulation in Ansys HFSS. The minimal gap dimension is limited to 250 µm due to the fabrication limitation. The fabricated device and its layout are shown in Fig. 4.56. Optimized dimensions are listed in Table 4.8. Simulation and measured hair pin filter response are shown in Fig. 4.57. The measured filter response has a band pass of 150 MHz in the pass band and the centre frequency is at 5.8 GHz. The insertion loss of -1.93 dB and return loss of -10 dB in the pass band are observed from the measurement. The difference between measurements and simulations is due to the fabrication accuracy and connector effects.

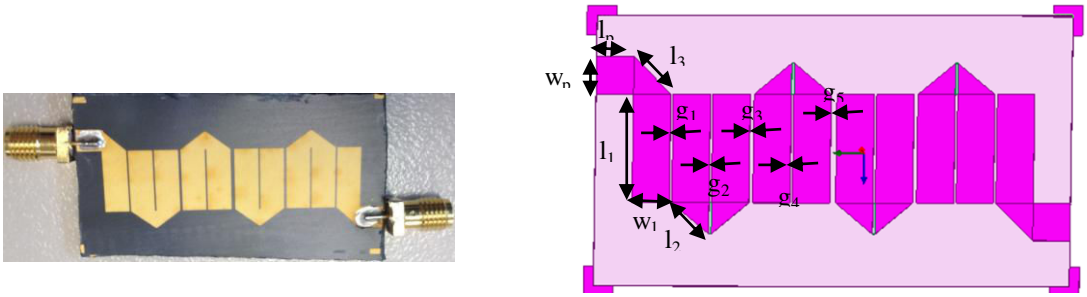

(a) (b)

Fig. 4.56 : Hair pin band pass filter on LCP E820i, (a) fabricated photo and (b) its layout.

Table 4.8: Microstrip hair pin filter dimensions.

Parameters	Dimensions (mm)
w_p	3.78
l_p	3.78
w_1	3.78
l_1	12
l_2	6
l_3	5
g_1	0.257
g_2	0.251
g_3	0.4
g_4	0.251
g_5	0.6

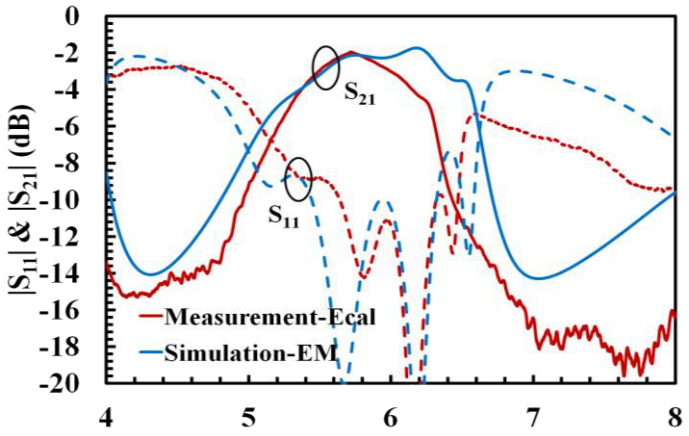

Fig. 4.57 : MID hair pin filter response in measurement and simulation.

The study of MID LDS RF compatibility is now move on to the design and analysis of radiating devices such as antennas.

4.8. Microstrip patch Antennas

Rectangular microstrip patch antennas constitute a widely used configuration in radio frequency domain. As they are easy to design, fabricate and analyze, they are more attractive among other microstrip antennas. Basically, a microstrip patch antenna consists of a metallic patch on one side of the dielectric substrate and a ground plane on the other side. This study has focused on MID planar and bend patch antennas performances on LDS LCP Vectra E820i.

4.8.1. Planar Patch antennas

Two microstrip patch antennas are designed for 2.63 GHz and 5.8 GHz resonant frequencies on a planar plate of LCP LDS E820i (Fig. 4.58). The optimized dimensions for both antennas are given in Table 4.9.

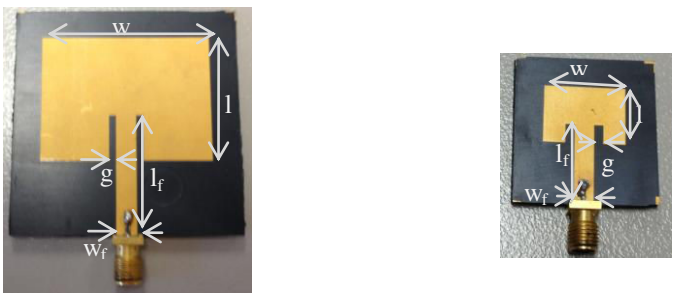

(a) (b)

Fig. 4.58 : LDS MID antenna structures on LCP Vectra E820i: (a) at 2.63 GHz and (b) at 5.8 GHz.

Table 4.9: Microstrip patch antennas dimensions.

Dimensions (in mm)	F_r=2.63 GHz	F_r=5.8 GHz
W	49	16.6
W_F	4.1	4.2
L	27.6	12.25
L_F	26	16.7
g	1	1.91

Simulation and measurement results of patch antennas are compared in terms reflection coefficients and radiation characteristics. All simulations have been done using Ansoft HFSS. Reflection coefficient measurements have been done using N5222A Agilent PNA with Ecal calibration.

In Fig. 4.59, the S parameters comparison for both microstrip patch antennas are depicted. The measurement and simulation results of both antennas show the presence of a resonance frequency at 2.63 GHz and 5.8 GHz respectively. The return loss is always better than -12 dB for both the LDS antennas.

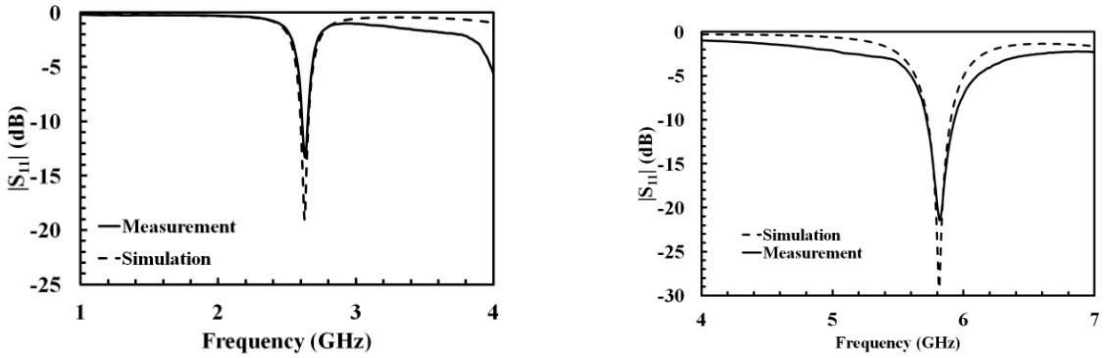

(a) (b)

Fig. 4.59 : Simulated and measured return loss results for the microstrip patch antenna on LCP Vectra E820i (a) F_r=2.63 GHz (b) F_r=5.8 GHz .

In similar, radiation patterns in the E plane using an anechoic chamber are performed. Fig. 4.60 details the radiation behaviour of LDS antennas on LCP Vectra E820i. Measurements are in good agreement with HFSS simulations. LDS antenna resonating at 2.63 GHz provides a maximum gain of 5.1 dB as shown in Fig. 4.60 (a) and antenna with resonance at 5.8 GHz provides a gain of 6 dB (see Fig. 4.60 (b)). Thus LDS antennas behave like conventional microstrip patch antennas and thus prove the potential of MID technology for antennas applications.

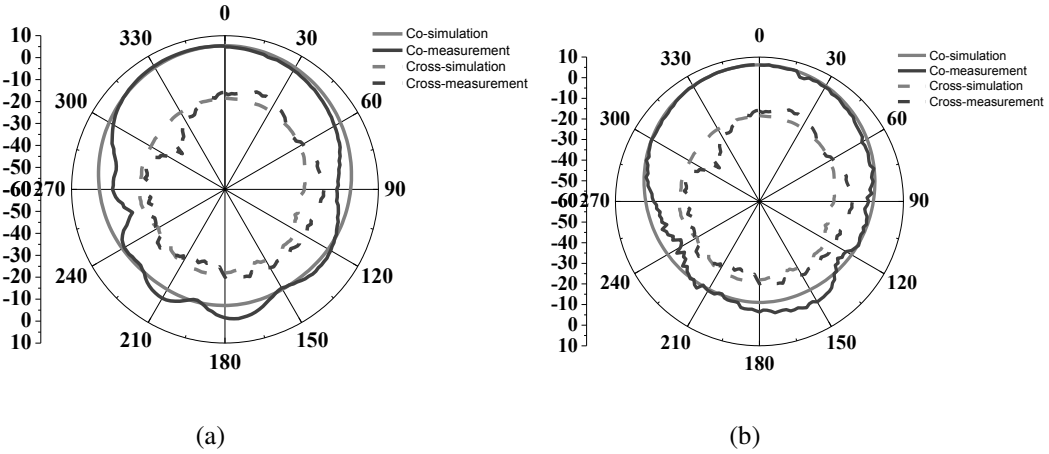

(a) (b)

Fig. 4.60 : Radiation characteristics of microstrip patch antenna on LCP Vectra E820i with (a) F_r=2.63 GHz (b) F_r=5.8 GHz.

As MID technology allows the possibility of three dimensional circuit, the possibility of 3D antennas were considered in this thesis work. Following section presents the microstrip bend patch antennas design and its fabrication method.

4.8.2. Bend patch antennas

Several three dimensional antennas utilizing MID technology are described in [31][33]. In [31], experimental investigation of bend patch antenna with coaxial feed is discussed. Bend patch antenna refers to the study of the effect of change in the antenna properties based on different bend angles. Indeed, increasing bend angles leads to a shift of the resonance to higher frequencies. The reason for the forward shift in resonance frequency is due to the presence of local capacitance at the bend. The local capacitance occurs due to the disturbance of electric field flow between patch and ground. As referred to this concept, the patch antenna at 2.63 GHz was taken into account to study the bend effect at 0^0 and 45^0 bend angles. Fig. 4.61 shows inset fed bend patch antennas at 0^0 bend and 45^0 bend angles. Due to fabrication difficulties and unavailability of mould to creat a three dimensional LCP Vectra substrate, the idea of bend antennas have been implemented by fabricating the planar part and bend part seperately as shown in Fig. 4.61. The two parts were pasted together using copper tape in angles 0^0 and 45^0 and measurements have been taken out. As an air gap occurs while joining two parts together, an air gap of 1mm is considered in HFSS simulations.

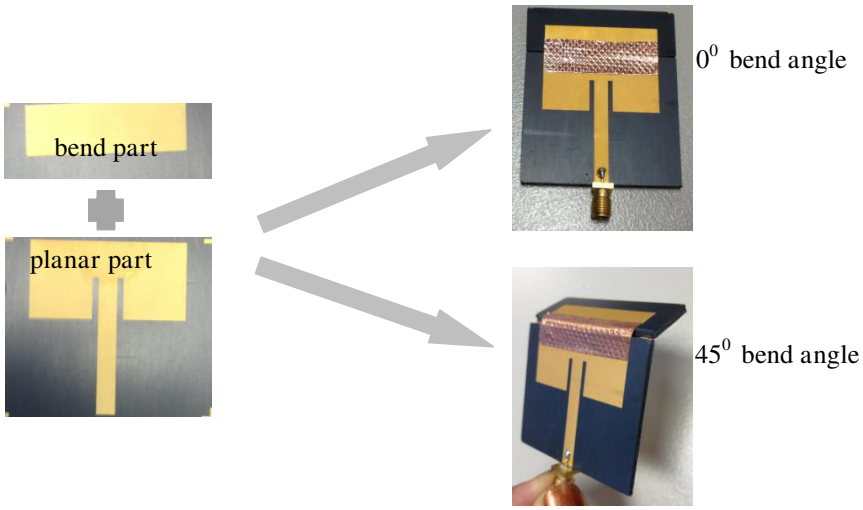

Fig. 4.61 : Microstrip bend patch antennas on LCP Vectra E820i.

Fig. 4.62 shows the response of bend patch antennas in 0^0 and 45^0 bend angles. The reflection coefficient shows good matching between measurement and simulations for both bend angles. If we consider radiation pattern of both antennas, a small variation between simulation and measurements can be found out. For 0^0 bend antenna, the measurement results show a difference of 0.3 dB variation is occured whereas for 45^0 bend antenna, the difference is near to 1 dB. The difference can be explained by the sensistivity of this antenna configuration composed of 2 parts. While rotating, the angle may be slighlty modified.

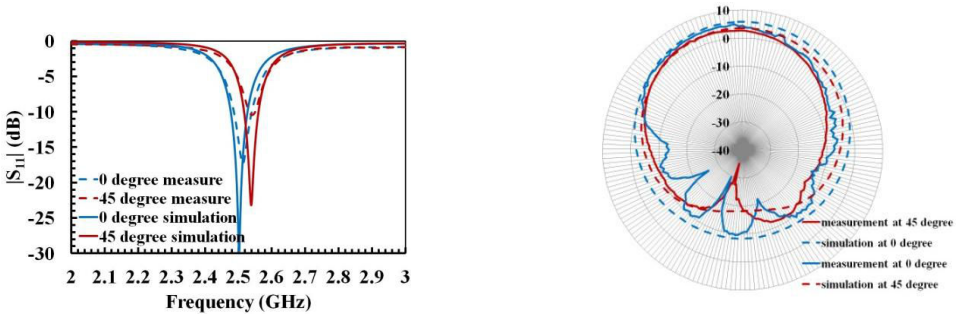

(a) (b)

Fig. 4.62 : Microstrip bend patch antennas response, (a) reflection coefficient in dB and (b) their radiation pattern.

A first impression on three dimensional MID circuit has been investigated through the above bend patch antennas. The antennas would definitely perform well in real three dimensional molded substrates. The capacity of EM simulation tool to perdict 3D antennas behavior is also proved. MID technology is thus validated on RF radiating circuits. The next section will be presenting circuits based on circuits based on guided propagation such as filters.

Thus, based all of the above studies on MID planar devices such as transmission lines, RF filters and patch antennas, it can be easily concluded that the MID technology in combination with the LDS fabrication technique is very well compatible with the RF circuit design. In order to exploit the three dimensional fabrication features of MID technology, a thre dimensional antenna is designed and fabricated. The final section of this chapter deals with the design of a three dimensional antenna on MID technology.

4.9. Three dimensional PIFA antenna

In this section, an original design of 3-D MID antenna based on PIFA (Planar Inverted F Antenna) configuration is presented. The PIFA antenna is placed on the external face of a LCP Vectra E820i thermoplastic case and the ground plane is placed at the internal face of the thermoplastic case as shown in Fig. 4.63.

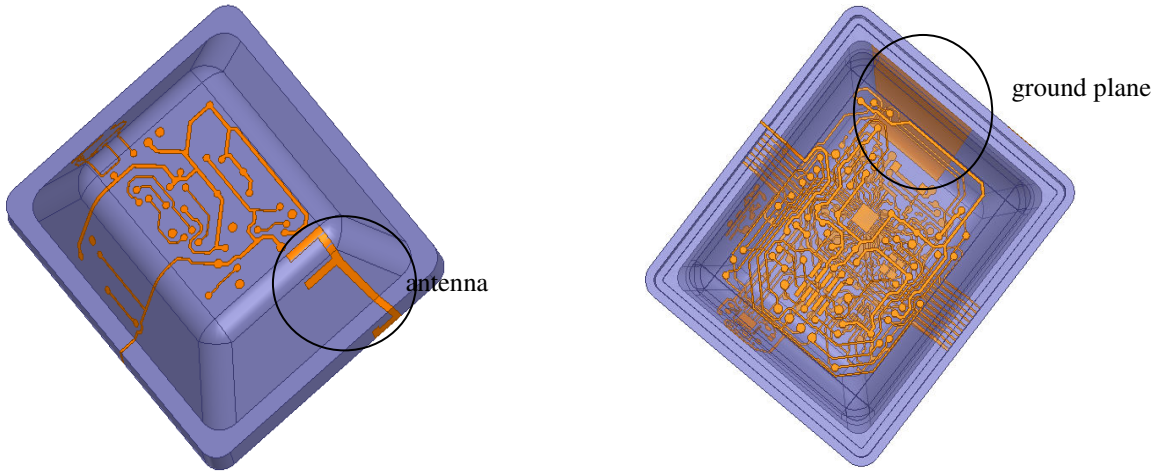

(a)

(b)

Fig. 4.63 : Three dimensional PIFA antenna on LCP Vectra E820i, (a) simulated structure and (b) fabricated photo.

The simulations were carried out using Ansoft HFSS and measurements were done using Ecal calibration. From the fabricated photo, it can be seen that a connector with a coaxial cable wih length 3 cm is used to have signal. This connector affects the resonance frequency of the antenna. As seen in Fig. 4.64, the measured resonance frequency is shifted downwards in comparison to the simulation. The antenna was originally designed for 2.45 GHz and the measurement results show a frequency of response at 2.185 GHz with antenna loss better than 15 dB. This shift in grequency is mainly due to the presence of a dense electric circuit near to the antennas. In simulation, the antenna was only taken into account. This resonance frequency is considered for the measurement of radiation pattern. The fabricated antenna provides a maximum gain of 1.2 dB with an omni directional radiation pattern. The measurement results thus confirm the validation of MID technology in the design of three dimensional antennas.

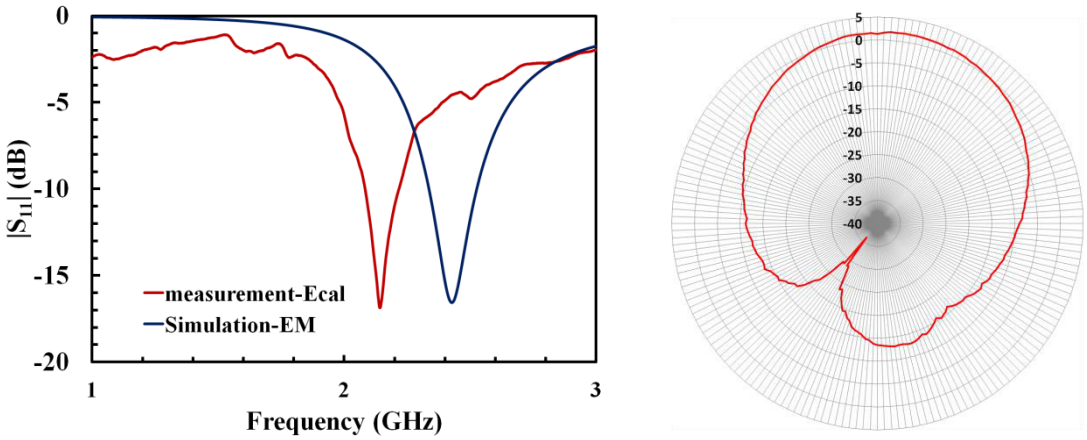

(a) (b)

Fig. 4.64 : Simulated and measured response of 3D PIFA antenna on LCP Vectra E820i by LDS fabrication, (a) reflection coefficient in dB and (b) measured radiation pattern.

4.10. Conclusion

For a microwave design system, MID substrates must be selected based on their dielectric properties. In this work, LCP Vectra E820i has been chosen due to its high temperature stability, high relative permittivity (ε_r=4.3) among all other tested substrates and low dielectric losses (tan δ=0.004).

Matched MID transmission lines are designed and fabricated on CPW, microstrip and stripline technologies. A continuous frequency extraction of relative permittivity of LCP vectra E820i based on two transmission lines method has been done. It has been found that the substrate LCP Vectra E820i presents effective permittivity of 2.56, 3.26 and 4.5 from

CPW, microstrip and striplines respectively. Relative permittivity of 4.28 and 4.34 were respectively obtained from CPW and microstrip lines giving a good agreement between the resonance cavity method. Moreover, the MID transmission lines performances have been studied based on the transmission line losses and quality factors. Measurements show that stripline holds less conductive loss of 0.05 Np/m whereas CPW holds higher conductive loss of 0.26 Np/m at 1 GHz. Dielectric losses are higher for stripline (0.07 Np/m) due to the presence of two plates of dielectrics while CPW and microstrip have nearly 0.04 Np/m at the same frequency. CPW line shows a low quality factor of 31, whereas microstrip has 75 and stripline holds higher value of 101 at 1 GHz. As LCP Vectra E820i supports through hole metallization, a microstrip via model on the substrate has been studied. Measurement results show excellent performance of the microstrip MID via.

Furthermore, microstrip patch antennas and RF filters were designed and fabricated on LCP Vectra E820i. HLPF and DLPF in CPW and microstrip technologies were designed and realized. HLPF filters with -3 dB cut-off frequency near to 1 GHz and DLPF with -3 dB cut-off frequency near to 2.3 GHz have been measured. Good agreement is obtained between measurements and simulations. Effects of capacitance used in place of low impedance section of DLPF were also considered in this work. Further design of band pass filters were also carried out and fabricated. A narrow band pass filter based on DBR was designed at 5.2 GHz. Similarly, a wide band hair pin filter working at 5.8 GHz was also designed. Both the filters show fair agreement between measurement and simulation results.

In addition, two microstrip patch antennas at 2.63 GHz and 5.8 GHz were designed and fabricated on LDS technology. The antennas respectively provided maximum gain of 5.1 dB and 6 dB. As MID technology offers the possibility of three dimensional circuit design this research work has started the study of three dimensional antennas called as bend patch antennas.The antennas at 0^0 and 45^0 bend angles were considered for the study. The measurement results of bend angles show interesting results as that obtained in simulations with slight variation due to the fabrication error.

In total, all realized devices provide good agreement with simulation results and show interesting properties as conventional RF circuits highlighting thus the potential of LDS technology for RF MID applications. These results made the study extended for the design of a 3 D PIFA antenna on a 3 D LCP Vectra E820i thermoplastic shape. The antenna works at 2.185 GHz in the measurement with a return loss of better than 15 dB. The radiation pattern measurement shows a maximum gain of 1.2 dB.

References

[1] C. Orlob, D. Kornek, S. Preihs, and I. Rolfes, "Characterization of Electromagnetic Properties of Molded Interconnect Device Materials," German Microwave Conference, 2009.

[2] W. Xu, "Research on Key Technology of MID," 2010 Second Pacific-Asia Conference on Circuits, Communications and System (PACCS), pp. 133–135.

[3] LPKF, circuits imprimes, stencils pour les CMS, MID, prototypage rapide de circuits imprimes-LPKF Laser & Electronics AG, November 2011, available online at. http://www.lpkf.fr/.

[4] N. Heininger, "3D LDS Components for New Production Opportunities", Microwaves Journal, February 2012, pp. 46-50.

[5] S. Geurts, "LDS Technology Explanation, Guide for the LDS Developer," pp. 25, August 2008.

[6] D. Kornek, E. Slottke, C. Orlob and I. Rolfes, "Experimental Investigation of Bent Patch Antennas on MID substrate," European conference on antennas and propagation 2012.

[7] C. Orlob, Q. H. Dao and D. Kornek, "Dual Polarized Log Periodic Antenna on a Conical MID Substrate, " Proceedings of the 5th European conference on Antennas and Propagation(EUCAP).

[8] F. Sonnerat, "Wideband LDS Antenna using two radiating elements, Antennas and propagation conference (APC), " Nov. 2012.

[9] F. Sonnerat, R. Pillard, F. Gianesello, F. Le. Pennec, C. Person, and D. Gloria, "Innovative LDS antenna for 4G applications," European conference on Antennas and Propagation(EUCAP), April 2013.

[10] www.pulseelectronics.com

[11] http://www.molex.com/molex/products/family?key=laser_direct_structuring_lds_technology&channel=products&chanName=family&pageTitle=Introduction.

[12] B. C. Wadell, Transmission Line Design Handbook, Artech House, Inc., 1991.

[13] J. Coonrod, "Comparing Microstrip and CPW Performance," Microwave Journal, vol. 55, no. 7, pp. 74-82, July 2012.

[14] K. C. Gupta, R. Garg, I. Bahl, and P. Bhartia, Microstrip Lines and Slot Lines, 2nd ed. Artech House, Boston, 1996.

[15] J. Hong, and M. Lancaster, "Microstrip Filters for RF/ Microwave Applications," A WILEY- Interscience Publication, ISBNs: 0-471-38877-7 (Hardback); 0-471-22161-9 (Electronic), 2001.

[16] S. B. Cohn, "Characteristic Impedance of a shielded- strip transmission line," IRE Trans., Microwave Theory Tech., no.2, pp. 52-57, July 1954.

[17] R. Orta, "Transmission Line Theory," pp. 31-32, Nov. 2012. Online available at http://personal.delen.polito.it/Renato.Orta/PassOpticalComp/TransmissionLinesLectureNotes Nov2012.pdf.

[18] D. M. Pozar, Microwave Engineering. New York: J. Wiley & Sons, 2005.

[19] Y. H. Chou, M. J. Jeng, Y. H. Lee and Y. G. Jan, "Measurement of RF PCB Dielectric Properties and Losses," Progress in Electromagnetics Research Letters, Vol. 4, pp. 139-148, 2008.

[20] J. Zhang, M. Y. Koledintseva, G. Antonini, J. L. Drewniak, A. Orlandi and K.N. Rozanov, "Planar Transmission Line Method For Characterization of Printed Circuit Board Dielectrics," Progress in Electromagnetics Research Letters, Vol. 102, pp. 267-286, 2010.

[21] J. Carroll, M. Li and K. Chang, "New Technique to Measure Transmission Line Attenuation," IEEE Transactions on Microwave Theory and Techniques, Vol. 43, pp. 219-222, January 1995.

[22] N5222A PNA Microwave Network Analyser Manual, Online available at : http://www.keysight.com/en/pd-2001963-pn-N5222A/pna-microwave-network-analyzer? cc= FR&lc=fre.

[23] Ansys HFSS, online available at http://www.ansys. com/Support/Training +Center/ Courses/Introduction+to+ANSYS+HFSS.

[24] Agilent Technologies, "Agilent Network Analysis Applying the 8510 TRL Calibration For Non-Coaxial Measurements", Product Note 8510-8A.

[25] A. M. Mangan, S. P. Voinigescu, M. T. Yang and M. Tazlauanu, "De-Embedding Transmission Line Measurements for Accurate Modeling of IC Designs," IEEE Transactions on Electron Devices, vol. 53, pp. 235-241, February 2006.

[26] R. Faraji-Dana and Y. L. Chow, "Edge condition of the field and AC resistance of a rectangular strip conductor," IEE Proceedings, vol. 137, no. 2, pp. 133-140, Apr. 1990.

[27] H. Johnson and M. Graham, High-speed Digital Design, A Handbook of Black Magic, Prentice Hall, 1993.

[28] E. B. Joffe and K. S. Lock M. Graham, Grounds for Grounding: A Circuit to System Handbook, Wiley, 2011.

[29] M. E. Goldfarb and R.A. Pucel, "Modelling Via Holes Ground in Microstrips," IEEE Microwave and Guided Wave Letters, vol.1, no.6, June 1991.

[30] M. E. Goldfarb and R.A. Pucel, "Simulation and Analysis of Via Effects on High Speed Signal Transmission on PCB," Proceedings on Radio Science Conference, pp.283-286, Aug. 2004.

[31] D. Kornek, E. Slottke, C. Orlob and I. Rolfes “Experimental investigation of bend patch antennas on MID substrate, ” European conference on antennas and propagation 2010.

[32] C. Orlob, Q. H. Dao and D. Kornek, “Dual polarized log periodic antenna on a conical MID substrate,” Proceedings of the 5th European conference on Antennas and propagation (EUCAP).

[33] J. Thevenard, D. Lo Hine Tong, A. Louzir, C. Nicolas, Ch. Person, J.Ph.Coupez, “Switched beam 3 D vivaldi antennas for WLAN applications, ” Proceedings of ISAP2007, pp. 708–711.

[34] G. L. Matthaei, L. Young and E. M. T. Jones, Microwave Filters, Impedance Matching Networks, and Coupling Structures. , New Jersy, Artech house, 1980.

[35] D. Kaddour, E. Pistono, J. M. Duchamp, J. D. Arnould, H. Eusebe, P. Ferrari, and R. G. Harrison, “A compact and selective low-pass filter with reduced spurious responses, based on CPW tapered periodic structures”, IEEE Transactions on Microwave Theory and Techniques, vol. 54, no. 6, pp. 2367-2375, June 2006.

[36] I. Hunter, Theory and Design of Microwave Filters, London: IEE Press, 2000, pp. 3-6.

[37] H. Issa, J. M. Duchamp, and P. Ferrari, “Miniaturized DBR Filter: Formulation and Performances Improvement”, IEEE Microwave and Techniques Theory Symposium (MTT-S) Transactions on Microwave Theory and Techniques, pp. 671-674, June 2008.

[38] P. Rizzi, Microwave Engineering Passive Circuits, Prentice Hall, 1988.

[39] C. Quendo, E. Rius, and C. Person, “Narrow Bandpass Filters Using Dual- Behavior Resonators”, IEEE Transactions on Microwave Techniques and Theory, vol. 51, no.3, pp. 734-743, March 2003.

Chapter-5

Inkjet Printed RF Circuits on MID

This chapter focuses on the study of RF performances of inkjet printed circuits on MID. In this work, two different thermoplastics have been considered: ABS PC (Acrylonitrile Butadiene Styrene Poly Carbonate) and LCP (Liquid Crystal Polymer) E130i. The first part of this chapter *is concentrated to the ABS PC substrate. Firstly, two 50* Ω transmission lines inkjet printed with silver nano particles are designed, realized and measured on a 2 mm thick ABS PC in both CPW and microstrip technologies. S parameters measurements allow the extraction of both permittivity and RF losses. Results show a nearly constant relative permittivity of 2.8 for both transmission line technologies which is in good agreement with that obtained from resonant cavity method. Conductive losses are predominant in total transmission line losses in both CPW and microstrip configurations due to the low thickness metallization leading to skin effect. Further, a coplanar UWB (Ultra Wide Band) antenna based on a half circular disc monopole and a rectangular patch with two steps is designed and realized by inkjet printing on ABS PC. This printed antenna provides a good impedance matching over the entire bandwidth of 3 GHz - 13 GHz with omni directional radiation pattern in the H planes till 5 GHz. Radiation patterns are deformed at higher frequencies due to the higher order modes. The second part of this chapter demonstrates the LCP compatibility for printed electronics. LCP E130i presents usually a significant surface roughness that makes it not suitable for electronic inkjet printing applications. In order to smooth the LCP surface, a planarization technique is studied. It consists of printing a primer UV(ultraviolet) curing layer via an inkjet printer. A UV/Ozone treatment is used to adjust the LCP surface energy in order to make it compatible with the dielectric ink. Performances of silver printed lines on planarized substrates are studied in this work. The electrical resistivity of the printed structures is compared with and without planarization and results show the high potential of this new method. Transmission lines and low pass filters are designed on this planarized substrate and their RF properties are characterized showing a good agreement with simulations.

5.1. Introduction

The demand for inkjet printing technology has been widely enhanced in RF circuit fabrication due to its direct write technology which enables to print the circuit pattern directly on the substrate. Unlike traditional subtractive methods such as photolithography, there is no need of any mask thus reducing the manufacturing cost. Indeed, inkjet printing method uses nozzles to jet ink droplets in the desired position and thus the ink consumption can be saved [1]. In addition, inkjet printing is environmentally friendly based on the fact that the chemicals necessary for traditional etching process can be eliminated [2][3]. Thus, great interest has been recently given to additive technologies especially to inkjet printing since it allows fast prototyping and patterns customization at reduced cost and without waste. This has open new perspectives for RF circuit implementation by inkjet printing on different substrates like plastic or paper [4][5].

The choice of substrate is critical in inkjet printed RF circuit design. Good thermal, mechanical, and dielectric properties are required to achieve circuits with high electrical performances. For RF applications, low loss tangent and low surface roughness are needed in order to decrease circuit losses and to ensure good metallization contact. As stated in chapter 2, ABS PC (Acrylonitrile Butadiene Styrene Poly Carbonate) is a low cost thermoplastic resin commonly used in injection molding applications. The impact strength and heat resistance of PC as well as the flexibility of ABS make this substrate a good candidate for MID applications. In this chapter, transmission lines on ABS PC are designed, realized and measured. Dielectric permittivity and RF losses are extracted from the S parameters measurements. Extracted results are used for the design of an UWB (Ultra Wide Band) monopole antenna. The literature review shows a number of different techniques for UWB monopole antennas design on classical substrates [6]-[12]. However, in this work, the potential of MID technology in combination with inkjet printing technique has been exploited for the realization of UWB antenna. Measurement results show good agreement with simulation results. In addition, the ink jet printing fabrication process of these circuits are also presented.

The second part of this chapter deals with the RF performance study on molded LCP (Liquid Crystal Polymer) E130i. LCP is known for its compatibility with high frequency applications such as RFID technology [13]-[15] due to its permittivity (3.65) and loss tangent (0.006). The challenge of this work starts with the difficulties to print metal by inkjet process on LCP. One disadvantage of this polymer is its surface roughness, which is a problem for

achieving good quality conductors in printed electronics. Very few studies on inkjet printing process on LCP substrates can be found in literature [16]-[17]. The main target of this work is to use LCP substrate which presents originally high surface roughness (up to 8-9µm) for high quality printed lines resolution. To achieve good results, it is necessary to smooth the substrate surface. In this work, the substrate is planarized by printing a primer layer. Besides, this substrate has to present great surface wetting properties to be printed. Because of hydrophobic properties of this polymer, it has been exposed to a UV (ultra violet)/O_3 (ozone) treatment to match the UV ink with the substrate. Then, the sample has been sintered in a traditional oven at different curing conditions, for different durations of time. Several microstrip transmission lines are fabricated on planarized LCP and their RF properties have been studied in terms of losses and quality factor. To demonstrate the potential of planarized printed LCP, a distributed stepped-impedance low pass filter has also been designed and measured. Good agreement between measurements and simulations is obtained.

5.2. Inkjet printed MID RF circuits on ABS PC

Before moving on to the discussion of MID RF performances on molded ABS PC substrate, the inkjet printing fabrication will be discussed. All circuits have been fabricated in collaboration with our project partner CMP (Centre of Microelectronics in Provence), a part of EMSE (École nationale supérieure des mines de Saint-Étienne). The fabrication process of inkjet printed MID RF circuits on ABS PC will be discussed in detail in the following sections.

5.2.1. Inkjet printing and sintering set up

Printing metal patterns are performed on a 2 mm thick ABS PC, using drop on demand inkjet printer from Ceradrop (Ceraprinter X-series). 30 pL print heads containing 128 nozzles are used to print silver ink. This ink from Sun Chemical (Ref 5714) [18] is a colloidal suspension with 40% wt metal content with particles mean diameter of about 30 nm. After cleaning with Isopropanol, the surface energy of ABS PC is modified using UV/O_3 treatment for 1 minute. This treatment increases the ABS PC surface energy from 41 mN/m to 54 mN/m, allowing thus the printing of silver ink. The surface energy measurement is performed using a goniometer from Apollo instruments.

Sintering of printed structures is performed using two techniques: conventional oven at 130°C for different curing time, and flash photonic equipment from Novacentrix (PulseForge®3200). As expected, the electrical conductivity for conventional sintering

process increases with the curing time (Fig. 5.1). Measurements of sheet resistance are done using four probe measurement method from Jandel (RM3-AR Test Unit) (see Fig. 3.25) and ink thickness is measured with a profilometer. Fig. 5.1 shows that the electrical conductivity increases with the curing time. The higher electrical conductivity is reached at 5.5 x 10^{06} S/m for a curing time of 240 minutes.

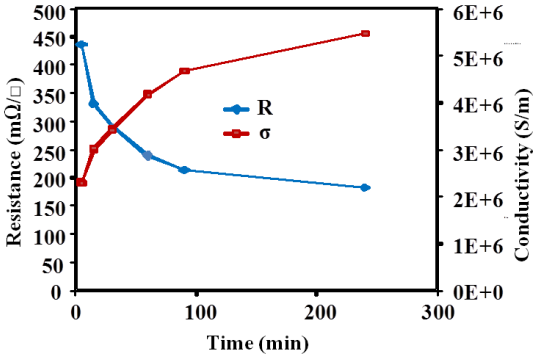

Fig. 5.1: Variation of sheet resistance and electrical conductivity of printed silver film on ABS PC with time (sintered in oven@ 130°C, thickness of 1µm).

When temperature exceeds 130°C, an irreversible thermo-mechanical deformation of ABS PC occurs (Fig. 5.2). And hence the maximum sintering temperature is fixed at 130°C. If we compare the thermal properties of ABS PC with respect to their mass, the material degrades at 400^{0}C (see Fig 3.3). The conventionally sintered silver film exhibits a conductivity of about 5.5 x 10^{6} S/m after 240 min of curing time. This conductivity is lower by a factor of ten in comparison to the bulk silver material (6.5 x 10^{7} S/m).

Fig. 5.2: The sintering effect on ABS PC and silver films above 130°C.

For flash photonic sintering, optimization was conducted by varying parameters like pulse duration, energy, and frequency. It was found out that an efficient process for sintering silver on ABS PC is obtained with the following parameters such as pulse number (300), pulse duration (200-500 µs), voltage (190V+/-20V) and frequency (10-20 Hz). Optimal sheet resistance and electrical conductivity is around 250 mΩ/□ and 4.10^{6} S/m, respectively. The thickness of flash sintered silver film is about 1 µm.

In this work, inkjet printing silver nano ink metallization with three passes is needed to increase metallization thickness in order to achieve better electrical performances. The initial layer is firstly printed and then an initial curing step is performed in standard oven at 130°C for 10 minutes. Later on, alignment step is achieved and two additional layers are printed successfully using wet to wet approach. The final sintering step is performed at 130°C for 30 minutes and the final metal film on ABS PC exhibits an electrical conductivity of 5 x 10^6 S/m for a total thickness of 4.5 µm. Optical profilometer using white light interferometry (from Veeco) is used to measure the thickness printed silver film.

Fig. 5.3 shows the AFM (Atomic Force Microscope) scan for ABS PC surface using Veeco mark. In the perpendicular direction to the injection, the measured peak to valley roughness (R_{pv}) is 500 nm with root mean square (RMS) of 65 nm. In the direction parallel to the injection, R_{pv} of 1640 and RMS of 270 nm are obtained. Therefore, it is better to print the silver layer by following the perpendicular direction to the injection.

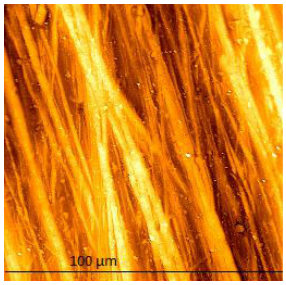

Fig. 5.3: ABS PC surface AFM.

Transmission lines are designed, fabricated and measured on ABS PC substrate. The RF performances of transmission lines on this ABS PC are studied in detail in the following section.

5.2.2. RF characterization

In order to study the electrical properties of inkjet printed MID on ABS PC, it is important to measure the characteristics of various planar transmission lines in the microwave region. Traditional microstrip and CPW technologies are adopted. The minimal gap seperation is 50-60 µm and minimum width is 50-90 µm for inkjet printed devices presented here. Two lines method of de-embedding [19] is chosen for electrical parameters' extraction. Measurements of all transmission lines were done with Ecal calibration (electronic calibration) using N5222A Agilent PNA. The dimensions of the fabricated lines are described

below. The initial design of the lines presented in this section were carried out by considering the dielectric properties of ABS PC obtained from resonance cavity method (Fig. 3.16).

5.2.3. CPW lines on ABS PC

This section describes the design of CPW lines on ABS PC, their simulation and measured permittivity, impedance, losses and quality factor extractions are given.

1) Design

In this work, two CPW transmission lines with lengths of l_1= 2 cm and l_2= 4 cm are designed on a 2 mm thick ABS PC substrate. The inkjet printed silver layer thickness is 4.5µm. The CPW lines dimensions are w=3.7mm and g=0.2mm in order to reach 50 Ω characteristic impedance. Additional taper lines are added at each end of the transmission lines to have good access with the connectors. Two simulation tools such as Ansys HFSS and Ansoft designer have been respectively used for the EM and electric simulations of the lines. Fig. 5.4 (a) shows the photographs of fabricated transmission lines. Fig. 5.4 (b) and (c) show the simulated structures of two transmission lines in Ansys HFSS (EM simulation) and Ansoft designer (electric simulations).

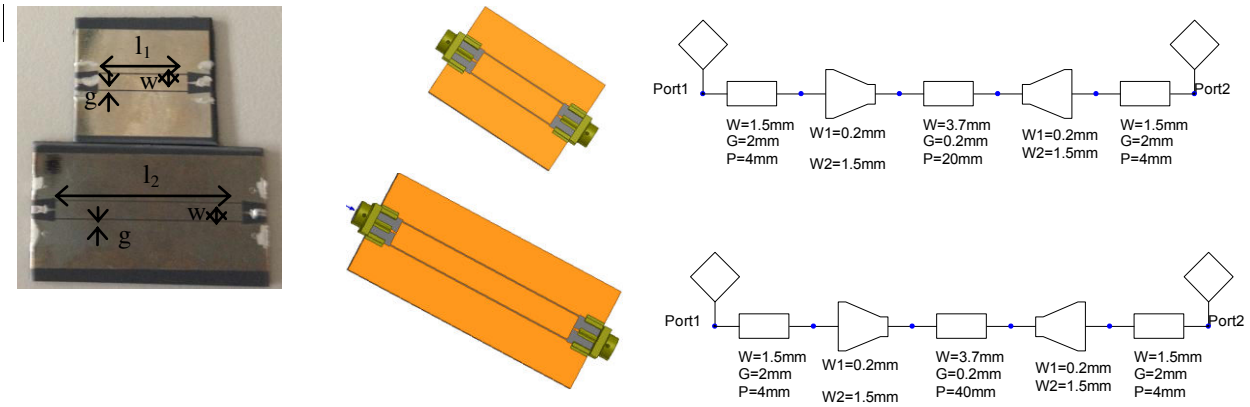

(a) (b)

Fig. 5.4: CPW transmission lines on ABS PC (a) fabricate
(c) electric simulated structur

2) S parameters

Fig. 5.5 compares the S parameters of these transmission lines obtained from measurements and simulations. Measurement results of all transmission lines show good agreement with simulation results. Transmission lines of lengths 2 cm and 4 cm respectively show a matching of better than 15 dB till 3.5 GHz and 4 GHz. Lower mismatching level occurs at higher frequencies and is mainly due to the tapered access presented at the end of each lines. If a frequency at 2 GHz is considered, 2 cm length transmission line provides a measured insertion loss of 1.3 dB (0.04dB/mm) whereas 4 cm line provide insertion loss of 2 dB (0.061 dB/mm). These losses are due to conductive losses of the silver layer, dielectric losses of ABS PC and losses due to connectors.

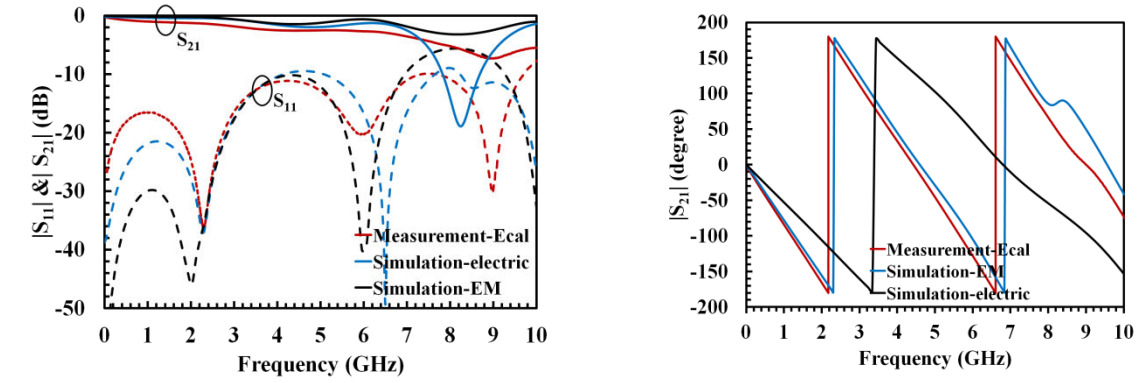

(a)

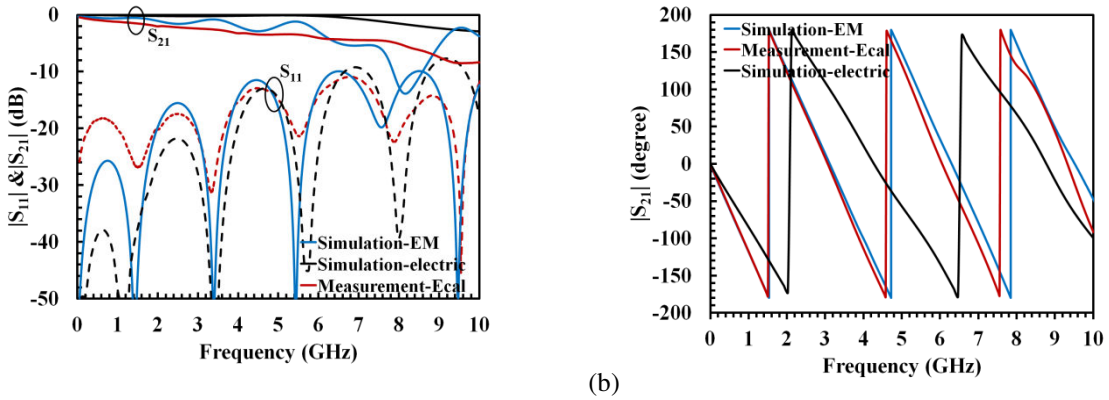

(b)

Fig. 5.5: S parameters magnitude in dB and phase in degree of inkjet printed CPW transmission lines on ABS PC (a) 2 cm line and (b) 4 cm line.

3) Permittivity extraction

The measured S parameters presented in the previous section were taken into account in order to extract the relative permittivity of the substrate in continuous frequency domain using two transmission line method [19]. The relative permittivity of ABS PC within a

frequency range of 1 GHz -10 GHz is plotted in Fig. 5.6. The cavity measurement extraction is limited at frequencies higher than 6.5 GHz and error occurs at and above 4.53 GHz. A comparison between the permittivity value obtained from the measurement of two transmission lines inkjet printed and the results obtained from the resonant cavity characterization of bare ABS PC is given in the plot. It demonstrates a good agreement between both methods leading to the same mean permittivity value of 2.8 with a variation of 3% on the frequency range 1 GHz to 6.5 GHz.

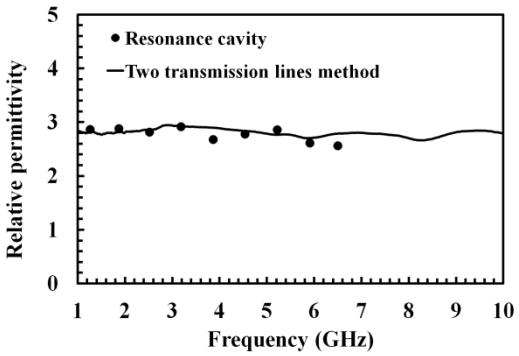

Fig. 5.6: Measured dielectric permittivity of ABS PC obtained from resonance cavity method and two transmission lines method.

4) Characteristic Impedance

From the S parameters, the characteristic impedance of the measured lines can be extracted using the two lines method (see Fig. 5.7). It can be seen that the measurement is in good agreement with the HFSS simulation with 8.2% variation over the entire frequency band. The impedance value varies from 50 Ω to 60 Ω in the entire frequency band.

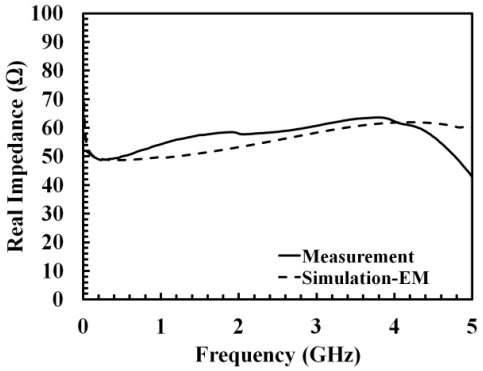

Fig. 5.7: Real part of impedance of inkjet printed CPW lines extracted from their measurement and simulations.

5) Losses and Q factor extractions

CPW transmission lines measurements are also used for continuous losses characterization with respect to frequency. The method of calculation of losses and quality factor used here is similar to that discussed in chapter 4 (see section 4.21 and 4.24). Based on the analytical model of transmission line given in [20], both conductive (α_c) and dielectric (α_d) losses can be calculated using the expressions in equations (4.33) and (4.35). The extracted losses are shown in Fig. 5.8. Measured R, L, C and G parameters per unit length are given in Table 5.1 for frequency points at 1 and 2 GHz. From Fig. 5.8 (a), it can be seen that conductive losses are predominant in the total losses of this transmission line, confirming thus the benefits of using ABS PC as low dielectric loss substrate for RF applications. At 1 GHz, the unit resistance is 90.2 Ω/m, while the unit conductance is 4.4 mS/m. This high value of resistance is due to the low thickness compared to the skin effect and is responsible of the high conductive losses. Dielectric losses increase proportionally with frequency and a value of 0.28 Np/m is obtained at 2 GHz, while conductive losses of 2 Np/m are obtained at 2 GHz. Conductive losses in inkjet printed CPW transmission lines losses are higher to that in LDS transmission lines (0.49 Np/m at 2 GHz). The conductive losses can be decreased by increasing the metal thickness (see Fig 5.8 (b)).

Table 5.1: RLGC parameters of inkjet printed CPW lines on ABS PC

Frequency (GHz)	*Resistance (Ω/m)*	Inductance (nH/m)	Conductance (mS/m)	Capacitance (pF/m)
1	90.2	255	4.5	54.3
2	196	271	8.6	50.8

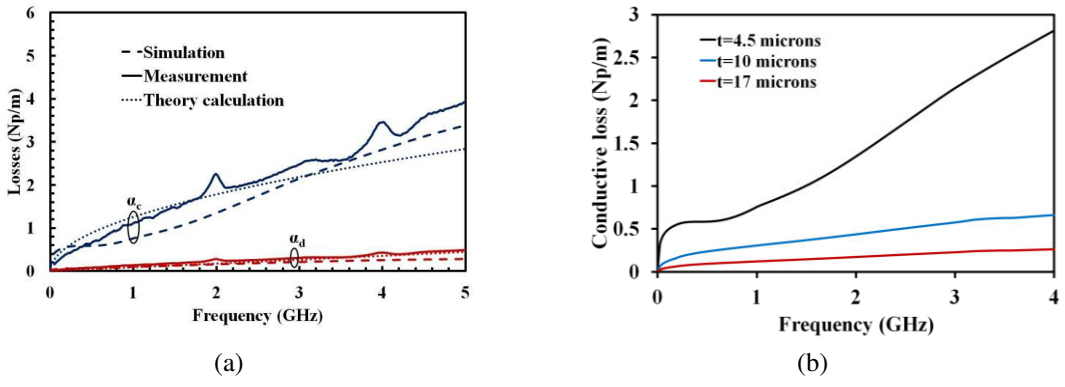

(a) (b)

Fig. 5.8: (a) Losses extracted from measurement and simulations of inkjet printed CPW lines and (b) conductive losses and thickness study.

The higher conductor losses also significantly depend on the ratio of metal thickness to the skin depth at the frequency of interest [21]. It was given in [22][23] that conductive

losses can be minimized if the metal thickness is about three times the skin depth. As a matter of interest, calculation of skin depth based on equation (5.1) was done and its variation with respect to frequency is plotted in Fig. 5.9. A skin depth of 7 µm is calculated at 1 GHz. At this frequency, the skin depth is higher than the metal thickness (4.5 µm) which explain the high conductive losses of the inkjet printed line. Transmission line losses can be reduced by increasing the metal thickness by using higher conductivity inks.

$$\delta = \sqrt{\frac{2}{\omega\mu\sigma}} \tag{5.1}$$

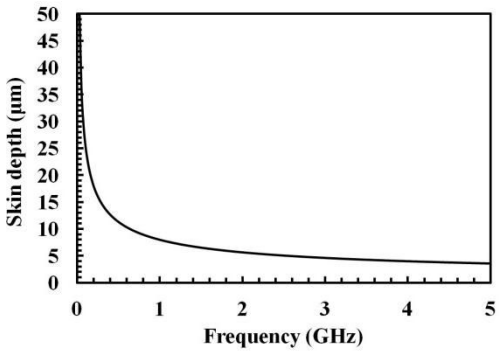

Fig. 5.9: Skin depth calculated for inkjet printed lines on ABS PC.

Fig. 5.10 (a) illustrates the total losses of the inkjet printed transmission line. Inkjet printed losses are mainly conductive and are higher than those of the LDS MID line presented in chapter 3 (see Fig. 4.34 (a)). Indeed, losses for the inkjet printed transmission line are 2.81 Np/m at 2 GHz whereas that obtained from LDS CPW lines is 1 Np/m at 2 GHz. The variation of the propagation constant is plotted on Fig. 5.10 (b). As the dielectric permittivity of the ABS PC is lower than that of the LDS LCP Vectra, the corresponding propagation constant is also lower. Quality factor describes the power loss for a given phase of the transmission line. The MID transmission line realized by inkjet printing shows a poor quality factor in comparison with LDS line. Fig. 5.10 (c) shows that the quality factor increases with frequency and a poor quality factor of 10.5 is obtained at 2 GHz which defines much power loss per given phase in comparison with the LDS lines since LDS LCP CPW line has a quality factor of 37 at 2 GHz.

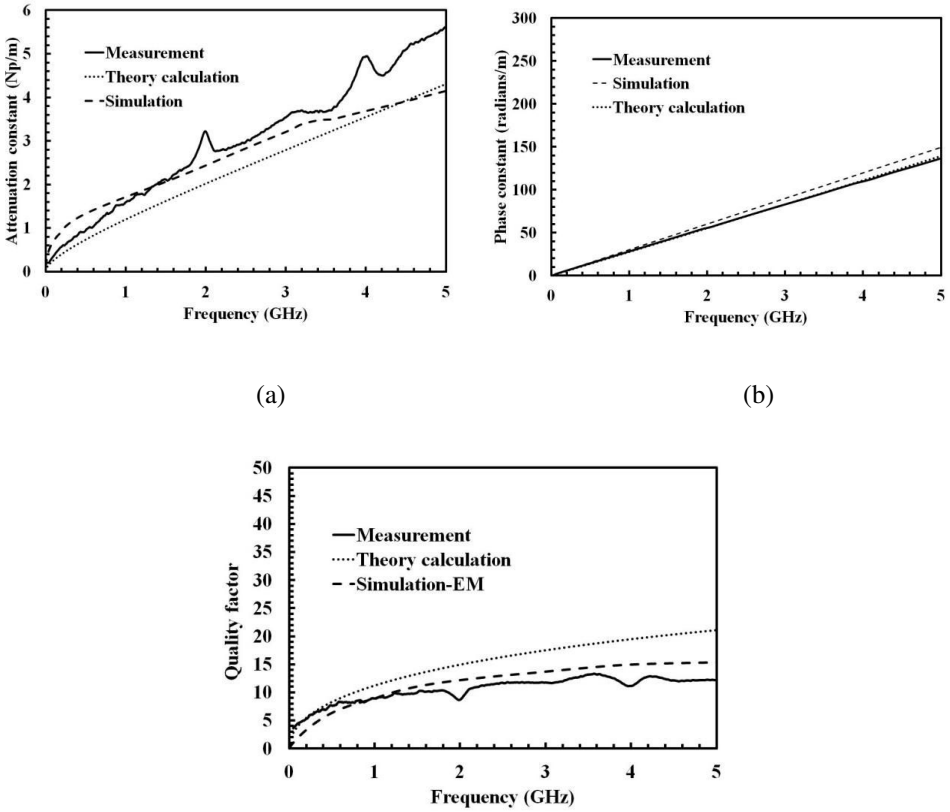

Fig. 5.10 : Propagation constant, γ and Q factor of CPW lines on ABS PC, (a) attenuation constant, (b) phase constant and (c) quality factor.

In similar to the study of electrical properties of CPW transmission lines on molded ABS PC, microstrip lines on ABS PC are also studied. Following section deals with inkjet printed microstrip transmission lines on ABS PC.

5.2.4. Microstrip lines on ABS PC

In similar to the RF characterization of CPW lines on ABS PC, S parameters of microstrip lines are considered to extract the characteristic impedance (Zc), propagation constant (γ), losses (α), effective dielectric constant (ε_{reff}) and further dielectric permittivity (ε_r). These characteristics are discussed below.

5.2.5. 1) Transmission lines design

Two microstrip transmission lines of length l_1=2cm and l_2=4cm are realized on ABS PC as shown in Fig. 5.11 (a). In order to reach 50 Ω characteristic impedance, a conductor width of w =0.51 cm is selected. Tapered lines and soldering pads are added at either side of

transmission lines with a length of 4 mm and width of 1.5 mm. Simulated structures of transmission lines in Ansys HFSS and Ansys electric circuit designer are shown in Fig. 5.11(b) and (c).

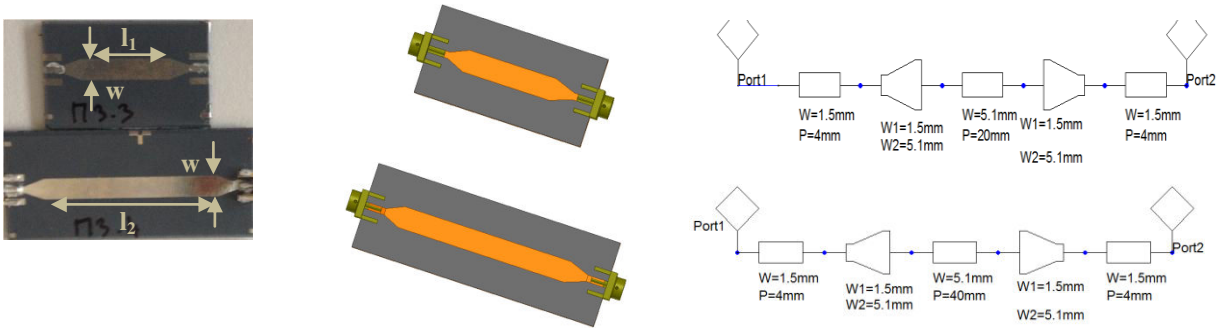

(a) (b) (c)

Fig. 5.11 : Structure of a 50 Ω microstrip transmission lines realized by inkjet printing on ABS PC, (a) fabricated devices, (b) EM simulated structure in HFSS and (c) electric simulated structure in Ansoft designer.

2) S parameters

Fig. 5.12 (a) and (b) respectively show the S parameters magnitude in dB and phase in degree of two transmission lines of length 2 cm and 4 cm obtained from measurements and simulations. Measurement results are in good agreement with simulation results. EM simulation results fits more with the measurement results and can be more seen in the phase of the lines. Phase shift occurs in electric simulation compared to the measured phase. It is due to the absence of the end connectors in electric simulation. For the 2 cm line, the return loss of better than 13 dB and insertion loss of less than 1 dB are obtained till 3 GHz. For 4 cm line, a return loss of 13 dB and an insertion loss of less than 1 dB are obtained till 2.5 GHz.

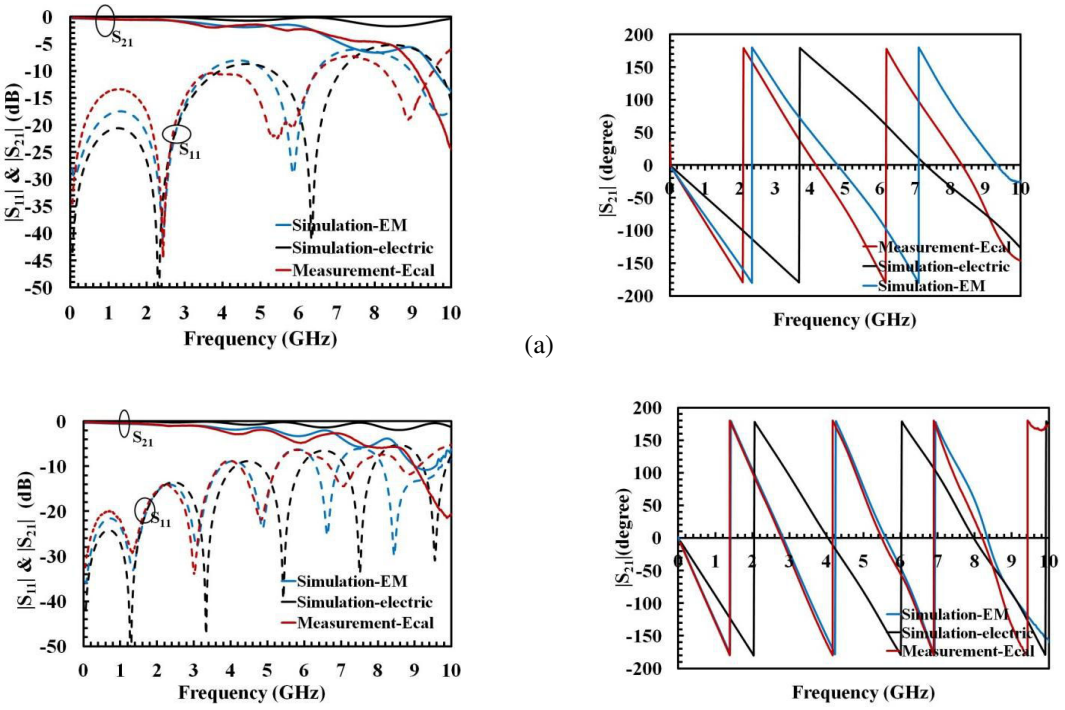

(a)

(b)

Fig. 5.12 : S parameters: magnitude in dB and phase in degree of inkjet printed microstrip transmission lines on ABS PC (a) 2 cm line, and (b) 4 cm line.

3) Permittivity

All extractions are shown in till 5 GHz. Higher frequencies show poor extraction of electrical properties. Fig. 5.13 dictates the effective and relative permittivities of ABS PC till 5 GHz. Calculations are done based on two transmission line method [19]. An ε_{reff} of nearly 2.25 and ε_r of nearly 2.8 are obtained from the S parameters extraction. If we compare the ε_r obtained from resonance cavity method given in Fig. 2.10, we can conclude that the extracted ε_r is in good agreement with that obtained from the resonance cavity method. Thus, both permittivity extraction methods (resonance cavity method and two transmission line method) give the same permittivity value of 2.8 with a variation of 2.8% at higher frequencies. The results thus demonstrate a good reproducibility in relative permittivity of ABS PC.

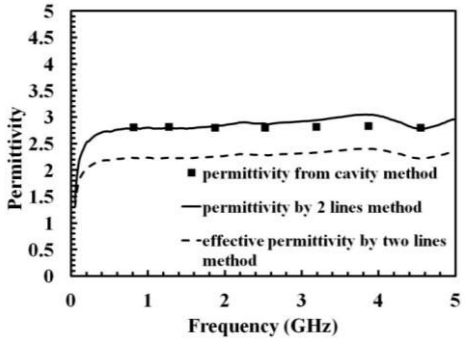

Fig. 5.13 : Measured dielectric permittivity of ABS PC obtained from resonance cavity method and two transmission lines method.

4) Impedance

Based on the impedance extracted from the S parameters of the lines, transmission line parameters and losses of these lines are extracted. Fig. 5.14 compares both simulated and measured real part of impedance. An impedance in the range from 50 Ω to 60 Ω can be observed till the resonance frequency (2.5 GHz). Poor extraction of impedance at the resonance point can be observed from the plot.

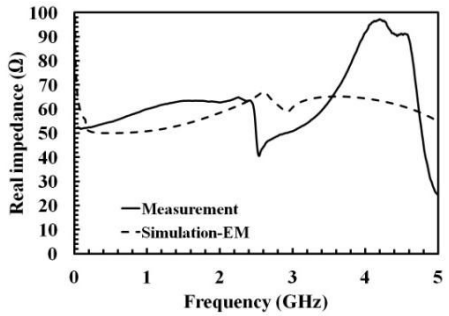

Fig. 5.14 : Measured and simulated real part of impedance of inkjet printed microstrip transmission lines on ABS-PC.

5) Losses and Q factor extractions

Table 5.2 shows typical values of RLGC parameters per unit length as a function of frequency. The principal characteristics of the line are closely related to that of CPW lines. In comparison with CPW, the microstrip line exhibits a lower value of the series unit resistance R which explains the lower conductive losses than CPW (R =196 Ω). The unit resistance is smaller in microstrip technology due to the larger conductor width.

Table 5.2: RLGC parameters of inkjet printed microstrip lines on ABS PC

Frequency (GHz)	*Resistance (Ω/m)*	Inductance (nH/m)	Conductance (mS/m)	Capacitance (pF/m)
1	52.6	241	4.0	68
2	71.5	265	4.8	67

Fig. 5.15 depicts losses in inkjet microstrip transmission lines on ABS PC. Neglecting radiation losses, the microstrip losses are separated into conductive and dielectric losses as given in Fig. 5.15 (a). Difference between measurement and simulations may due to the connection between connectors and lines with silver ink that can give a poor connection quality. In similar to inkjet printed CPW lines on ABS PC, conductive losses are more significant than dielectric losses due to the low thickness and skin effect and can seen from the total losses in Fig. 5.15 (b). Conductive losses of 0.7 Np/m and dielectric losses of 0.2 Np/m are obtained at 2 GHz. Additional layers of silver ink can reduce conductive losses and thus improve signal transmission. At the frequency of resonance point, i.e., at 3.8 GHz, there is drastic change in losses extraction can be found out. This effect can be seen in all extracted values.

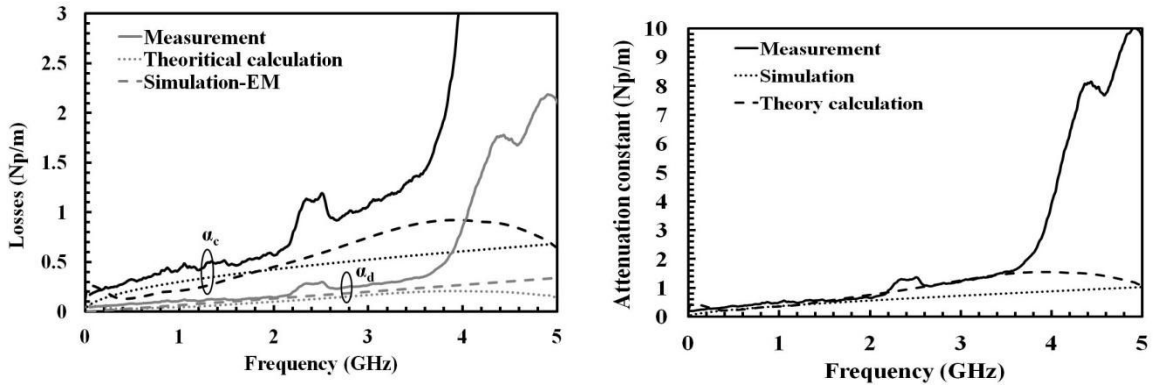

(a) (b)

Fig. 5.15 : Losses in inkjet printed MID microstrip transmission line on ABS PC, (a) conductive and dielectric losses in Np/m, and (b) total attenuation in Np/m.

From the propagation constant,($\gamma=\alpha+j\beta$) given in Fig. 5.15 (b) and Fig. 5.16 (a), the quality factor of inkjet printed MID microstrip line on ABS PC is calculated. The variation of quality factor versus frequency is presented in Fig. 5.16 (b). A quality factor of 32 is obtained at 2 GHz for this microstrip lines which is three times higher than inkjet printed CPW lines on ABS PC (see Fig. 5.10 (c)) but two times less than that of microstrip lines on LDS LCP Vectra (Q=65 at 2 GHz).

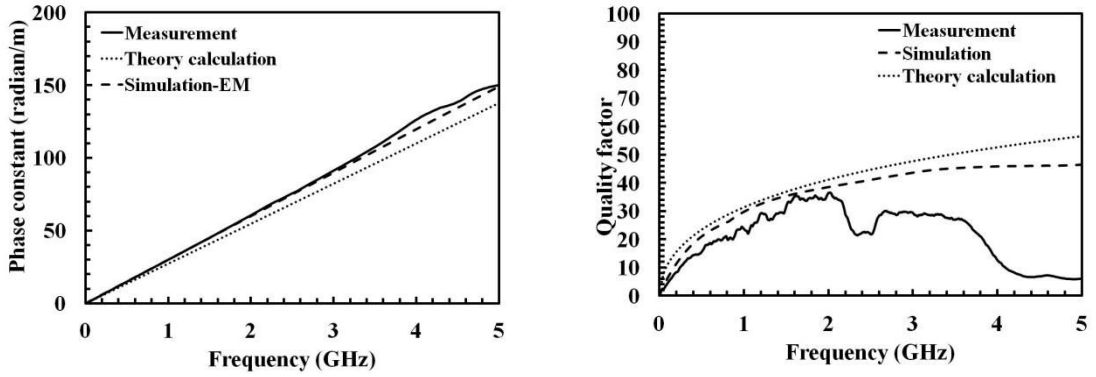

(a) (b)

Fig. 5.16 : (a) phase constant and (b) quality factor of inkjet printed MID microstrip transmission line on ABS PC.

Thus, the electrical properties of MID transmission lines on ABS PC in both CPW and microstrip technologies have been studied. Further steps of inkjet printed MID antenna designs are carried out and discussed in the following sections.

5.2.6. Inkjet printed MID Antennas on ABS PC

Inkjet printed MID antennas are presented in this section. A simple microstrip patch antenna and a CPW fed UWB antennas on ABS PC are chosen for the study. The fabrication process and the metallization are same as that used in the transmission lines discussed above.

5.2.3.1 Microstrip patch antenna

Microstrip patch antennas have gained much attention as popular radiators due to their compact shape, less design complexity, low fabrication cost and ease of integration with microwave circuitry [24]. For this reason, we started the analysis of MID technology in antenna by designing a rectangular microstrip patch antenna. Fig. 5.17 (a) shows a rectangular microstrip patch antenna with a resonance frequency of 2.63 GHz, designed on a 2 mm thick ABS PC substrate. The antenna is made up of a 4.15 cm x 3.25 cm radiating element. A single layer of silver ink metallization which provides a thickness of 700 nm.

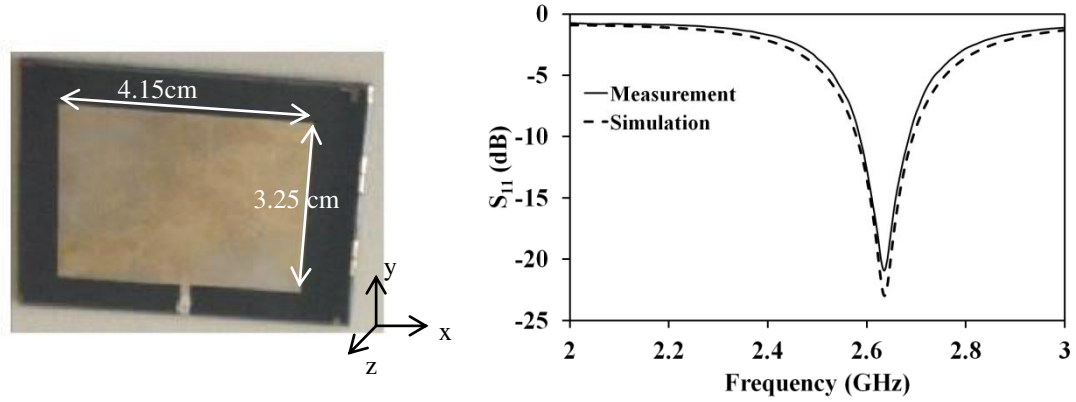

(a) (b)

Fig. 5.17 : Microstrip patch antenna on ABS PC (a) photograph and (b) reflection coefficient.

In Fig. 5.17 (b), the comparison between Ansys HFSS simulation and Ecal measurement of the microstrip patch antenna reflection coefficient is depicted. Measurement and simulation results show the presence of a resonance frequency at 2.63 GHz and the return loss is always better than -20 dB. The antenna provides a 10 dB bandwidth of about 41.8 MHz.

Fig. 5.18 (a) and (b) represent the measured and simulated H (xz plane) and E planes (yz plane) far-field radiation pattern. All simulations have been done with Ansys HFSS and the radiation pattern measurements were carried out in anechoic chamber. A very good agreement between measurement and simulation results can be seen in both planes of radiation. MID antenna has good directional radiation pattern as conventional microstrip patch antenna in the E and H planes. A maximum gain of 3 dB is achieved from the measurement result. In the main beam direction, the cross polar components are suppressed by -35 dB in the H plane and -30 dB in the E plane.

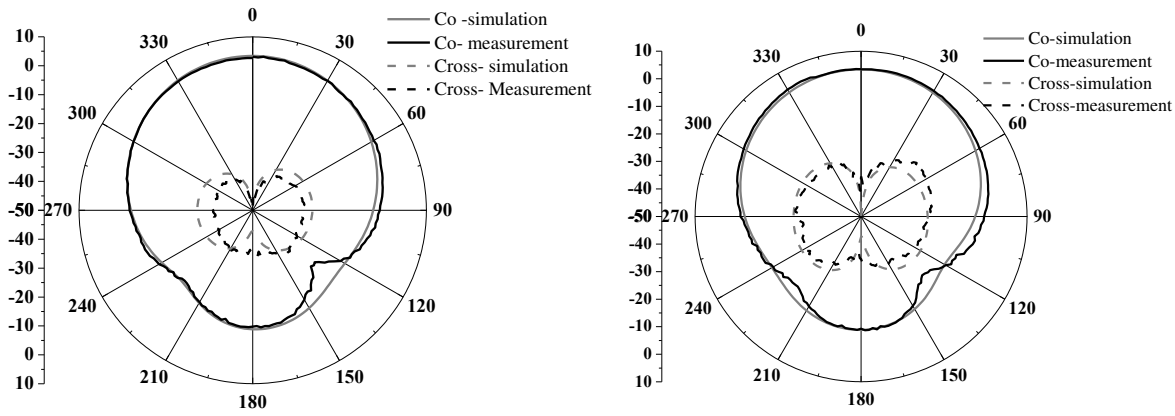

(a) (b)

Fig. 5.18 : Measured and simulated radiation pattern of MID microstrip patch antenna on ABS PC (a) the H plane and (b) the E plane.

5.2.3.2 MID UWB Antenna on ABS PC

The UWB communication systems have become popular since Federal Communications Commission (FCC) allowed an unlicensed frequency spectrum of 3.1 GHz to 10.6 GHz for commercial applications [25]. To validate the potential of inkjet-printing in MID technology and for UWB applications, a planar monopole antenna is designed and realized. Here, a circular disc monopole antenna configuration is adopted due to its simple structure, wide band features, and omni-directional radiation characteristics. A CPW signal feeding is used so that both radiating element and ground plane can be printed on the same side of the substrate.

The geometry and photograph of the proposed MID UWB monopole antenna designed on a 2 mm thick ABS PC is shown in Fig. 5.19. The black shaded part of the geometry defines the conductive plane where 4.5 µm of silver ink is deposited. The antenna is made up of a half circular disc of radius r_1 and a rectangular patch with two steps. The cuttings steps are used to achieve a good impedance matching throughout the entire UWB bandwidth. Along with the antenna topology, the feed line gap also influences much on achieving -10 dB return loss in the entire frequency band. The optimized values of the proposed antenna parameters are given in Table 5.3.

Table 5.3: MID UWB antenna geometric parameters

Parameters	**L**	**L_1**	**L_2**	**L_3**	**L_4**	**L_5**	**r_1**	**r_2**
Dimension (mm)	42	10.4	4.7	2	6	2	10	20
Parameters	**w**	**w_1**	**w_2**	**w_3**	**w_4**	**w_5**	**w_6**	**g**
Dimension (mm)	48	4	3	6	4.5	6	19	0.25

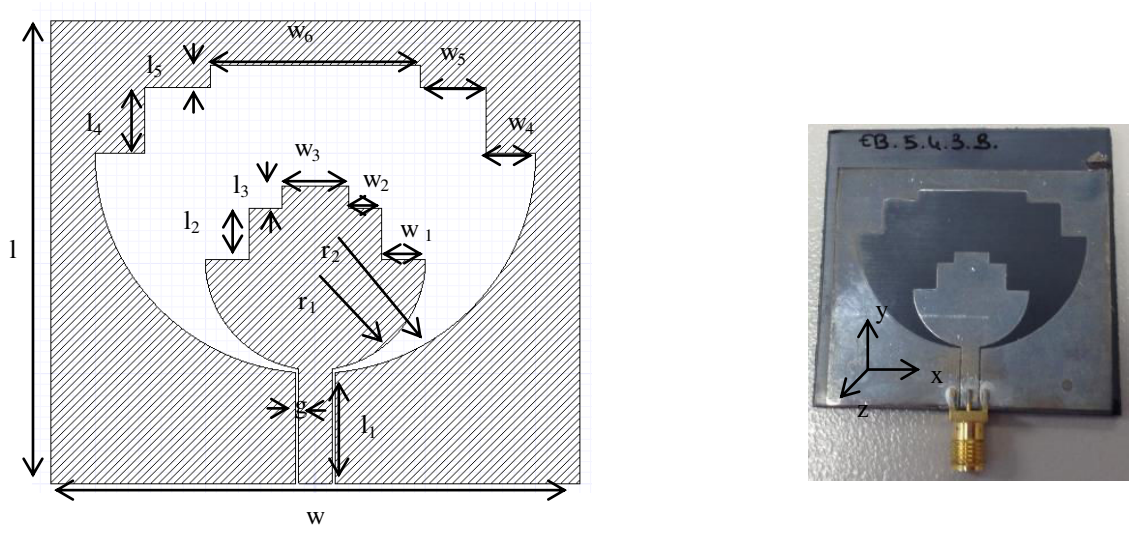

Fig. 5.19 : Geometry and photograph of MID UWB antenna on ABS-PC.

Reflection coefficient measurements are performed from 2 GHz to 13 GHz with N5222A Agilent PNA using Ecal calibration procedure and results are shown in Fig. 5.20. Good agreement between measurement and simulation results is obtained. A measured reflection coefficient better than -10 dB is achieved from 3 GHz to 13 GHz covering thus the entire UWB frequency band. A small difference can be observed in the measurement and simulation results which is due to the effect of connector.

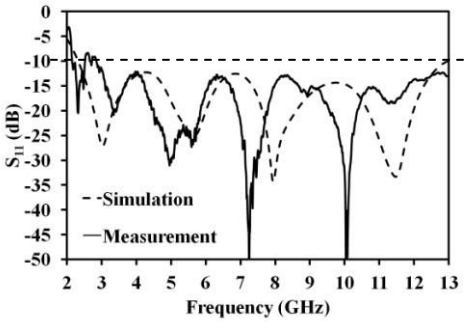

Fig. 5.20 : Measured and simulated reflection coefficient of MID UWB antenna on ABS-PC.

Four resonances are observed in the frequency response shown in Fig. 5.20. The origin of these resonances is explained by the antenna current distribution at each resonance as given in Fig. 5.21. From the figure, it is clear that the current distribution is maximal at the edge of each step. In addition, the first resonance is produced by a quarter wavelength variation in current distribution and the number of quarter wavelengths increases as resonant frequencies go higher.

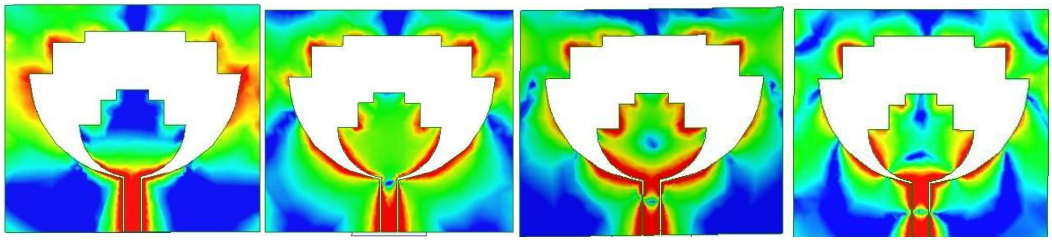

(a) (b) (c) (d)

Fig. 5.21 : Current distribution of the antenna at (a) 3.03GHz, (b) 5.4 GHz, (c)7.9 GHz and (d) 11.8 GHz.

Measured and simulated radiation patterns having co and cross polarization in the H plane (xz plane) and E plane (yz plane) at 3 GHz, 5 GHz, and 7 GHz are given respectively in Fig. 5.23 (a), (b) and (c). Measurements are in good agreement with simulations. The antenna shows omni-directional radiation patterns in the H plane and it presents a null in the E plane due to the feed line till 5 GHz. As frequency increases, higher order modes are excited which results in a deformation in radiation pattern, which appears mostly as cross polarization in H plane and a tilt in the main beam of E plane. For all frequencies, the cross polar components of E plane are less than -20 dB. The gain variation is 1 dB from 3 GHz to 7 GHz with a maximum gain of 4.2 dB (Fig. 5.22).

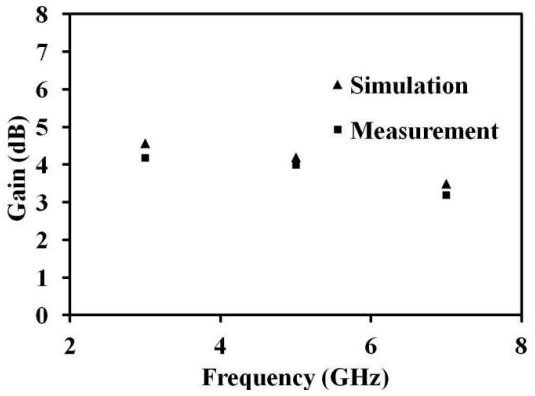

Fig. 5.22 : Measured and simulated gain of MID UWB antenna on ABS PC versus frequency.

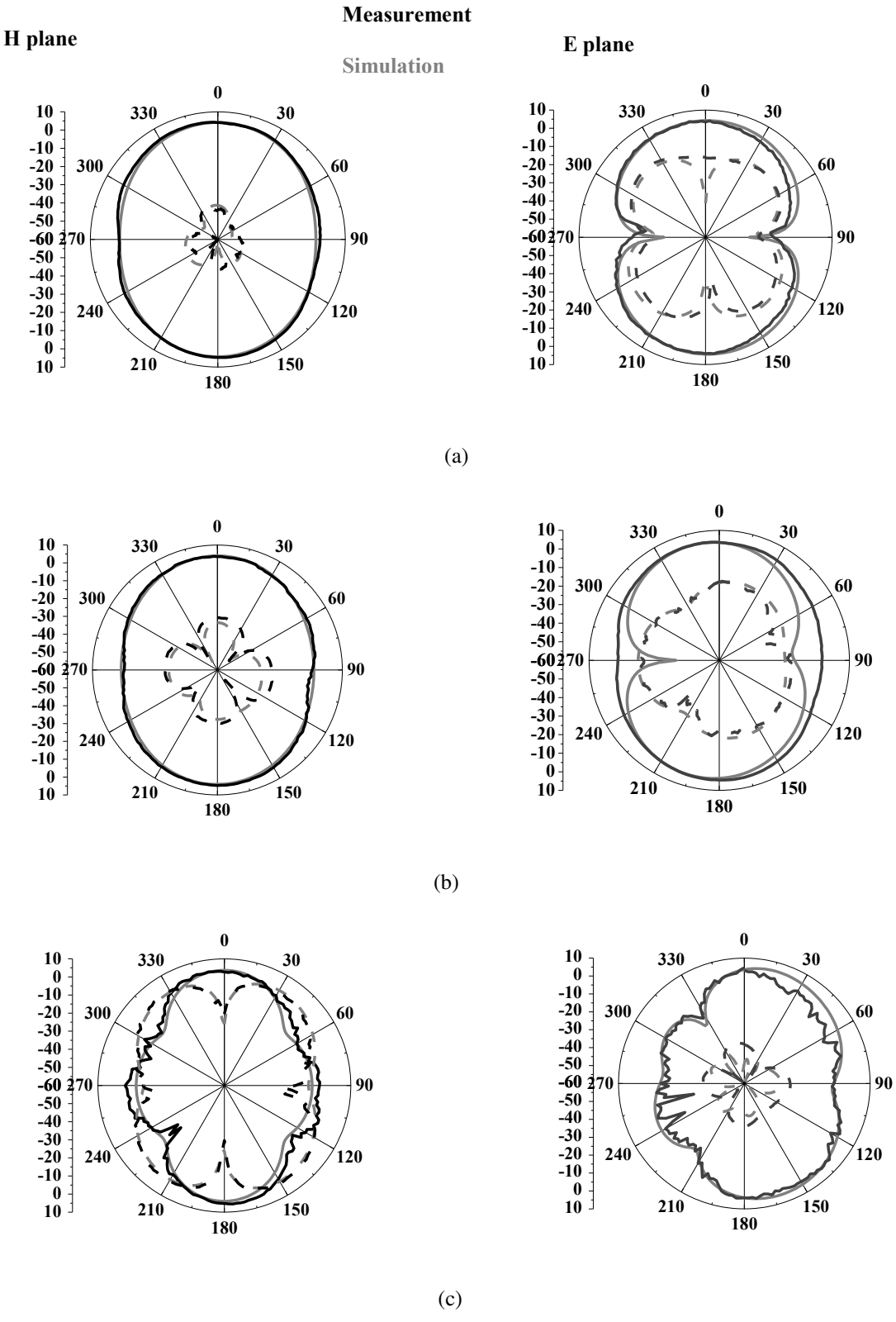

Fig. 5.23 : Measured and simulated radiation patterns of MID UWB antenna on ABS-PC (a) 3 GHz, (b) 5 GHz, and (c) 7 GHz (solid lines represents co polarization and dotted lines represents cross polarization).

These results prove that inkjet printed MID technology offers a great potential for UWB antennas.

5.3. Inkjet printed MID RF circuits on LCP E130i

Following sections are dedicated to inkjet printing technology on molded LCP E130i. LCP is a low cost high thermal stability substrate. LCP presents usually a significant surface roughness (up to 8-9µm) that makes it not suitable with electronic applications requiring high printing resolution.

Fig. 5.24 (a) shows an inkjet printed transmission line designed on LCP E130i. Fig. 5.24 (b) shows the measurement of the line. It clearly explains the incompatibility of inkjet printed lines on LCP E130i substrate. The measurement of this transmission line shows a high insertion losses of 2 dB and return loss of less than 8 dB at 1 GHz. Thus, planarization of LCP E130i substrate is required. To smooth the surface of LCP, printing a primer UV curing layer via an inkjet printer has been considered. The following sections deal the details of LCP planarization technique and electrical characterization of MID lines on LCP.

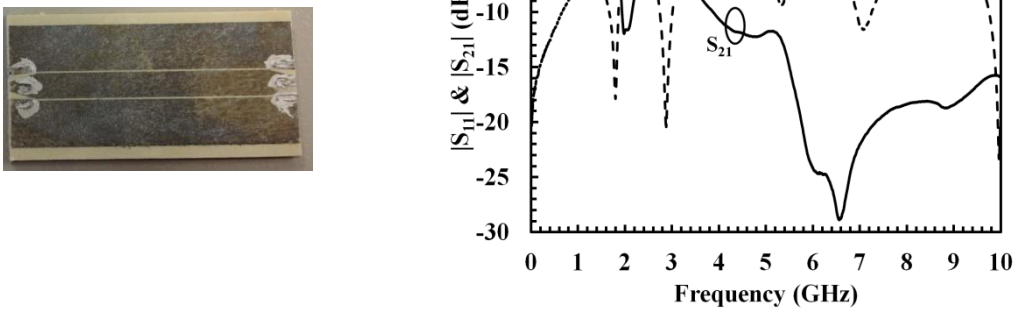

(a) (b)

Fig. 5.24 : MID microstrip transmission lines on a non planarized LCP E130i substrate, (a) fabricated photo and (b) its S parameters response.

5.3.1. Experimental details of substrate planarization

Various steps of planarization have been done such as surface treatment, characterization of the substrate to measure the surface roughness and then the planarization to reduce the surface roughness. Finally, dielectric characterization of the planarized substrate has been carried out to know its complex permittivity. Inkjet printing process followed here for the circuit fabrication is same as the method explained in section 5.2.1. All the

planarization method is done is CMP (Centre of Microelectronics in Provence), a part of EMSE (École nationale supérieure des mines de Saint-Étienne).

5.3.1.1 Surface treatment

A 2 mm thick LCP E130i is used for surface treatment after cleaning it with isopropanol. To remove the possible impurities in LCP substrate and to adapt the LCP surface energy, samples have been irradiated with UV light using a system from Nanonex Corporation which contains a mercury UV lamp that generates ozone. The cleaning effect and "hydrophilic treatment" after an UV/O_3 exposure have been demonstrated here via contact angle measurements. A goniometer from Appolo Instruments is used to determine the surface energy using three standards liquids: demonized water, ethylene glycol solution and diiodomethane. The calculated results are based on Owens Wendt method. No roughness corrections were applied for the calculations. The LCP surface energy is around 37.3 mN/m which is too low to match with the selected UV inks. Indeed the polar component of the surface energy calculated using the Owens Wendt method is increased after UV/O_3 treatment, which rises the number of surface polar groups. Also the UV/ O_3 combination allow removing organic impurities [26] such as contaminants adsorbed by the substrates exposed to the air, human skin oil. Fig. 5.25 indicates that the contact angle of liquids was modified by changing the surface treatment time. Measured angle is decreased by increasing the time of surface treatment. It allows to evaluate the results of cleaning treatment and to determine the accurate treatment duration in order to make the substrate printable.

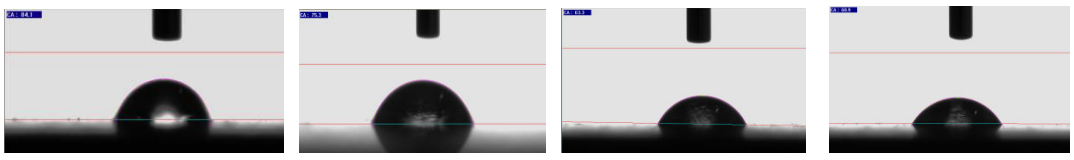

(a) (b) (c) (d)

Fig. 5.25 : Angle contacts after (a) 0s, (b) 60s, (c) 120s, and 180s UV/ozone treatment onto a LCP substrate (using deionized water).

The preferred surface wettability has been chosen around 46mN/m. Table 5.4 shows that a 120 second (s) duration treatment is more accurate to match the surface energy of the UV inks with the surface energy of the substrate. After 120s of treatment, it has been observed that the contact angle has been saturated. Increasing the time of treatment doesn't change the total surface energy but can alter the surface roughness.

Table 5.4: Surface energy (SE) versus UV/O_3 time treatment

Treatments	0s	60s	120s	180s
Surface energy (SE) (mN/m)	37.3	43.1	46.2	46.1
SE polar	4	9.6	14.4	15.2

5.3.1.2 Characterization of substrate

Determining the surface roughness of the substrate is essential in this study to know if LCP is compatible with the inkjet process. The LCP surface roughness parameters are measured using in AFM in non contact mode and are given in Fig. 5.26.

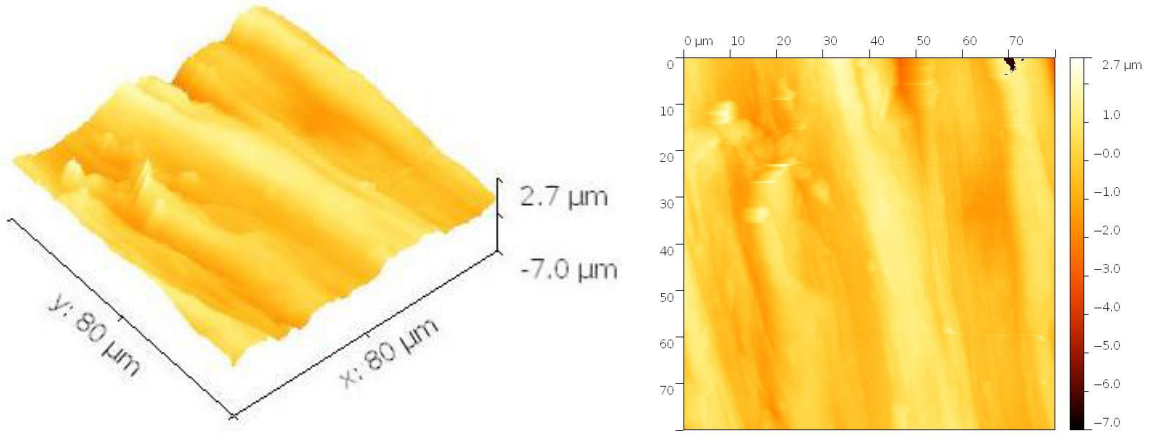

Fig. 5.26 : AFM Images of LCP surface roughness 80 x 80 µm^2.

Table 5.5 detailed the surface roughness of LCP. The measured R_{pv} and R_{RMS} of LCP measured indicates a significant surface roughness up to 9 µm. This roughness value comes from microfibrils which have been reported in [27]. To match with the inkjet printing technology and thin films printing with thickness variation does not exceed few microns, the substrate needs to be smoother and peak to valley roughness should be decreased and hence planarization is required.

Table 5.5: Surface roughness parameters of LCP

Surface (µm)	Frequency (Hz)	R_{p-v} (nm)	R_{RMS} (nm)	Average roughness, Ra (nm)
80 x 80	0.1	9691	752	617

5.3.1.3 Planarization

To decrease the electrical resistivity of printed patterns, and to optimize the spread of silver ink onto the substrate and the resolution, a planarization technique consisting of printing a pre-layer has been investigated in this work. Commercial inks such as SC 1 7103, SC 2 5388 and SC 3 6415 from Sun Chemical have been selected and tested with the Dimatix inkjet printer. These inks are UV curing, inkjet printable insulator coatings which are recommended to be suitable for printed electronics. The tested inks have a surface tension around 23-27 mN/m for SC 1 7103, 27-31 mN/m for SC 2 5388 and 35-37 mN/m for SC 3 6415. Besides the curing dose required, SC3 requires a post thermal curing of 30 min at 150°C (indication given by Sun Chemical company). The printing parameters were: 25 µm for drop spacing, 40°C for inks' jetting temperature, 32V for jetting voltage. Fig. 5.27 shows the thickness of the printed layers for UV inks. Regarding the LCP peak to valley roughness parameter, a single layer is not enough to planarize the substrate. Two layers are recommended to smooth the LCP surface.

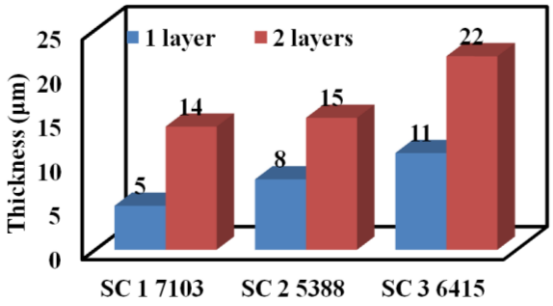

Fig. 5.27 : Thickness of UV layers.

Topographical imaging of the UV layers have been realized with the AFM in non contact mode (Fig. 5.28). The profile has been characterized by R_{pv}, R_{RMS} and the surface area index (R_a). The surface roughness parameters (see Table 5.6) for each ink underlines that the surface roughness has been reduced by a factor of 4 for the SC 1 and SC 3 and by a factor of 2 for SC 2. The peak to valley roughness has also significantly decreased from 9 µm to less than 1µm for SC1 and SC3.

Table 5.6: Surface roughness parameters for printed UV layers determined via the AFM software Proscan.

Inks	**SC 1 7103**			**SC 2 5388**			**SC 3 6415**		
Roughness (nm)	R_{pv}	R_a	R_{RMS}	R_z	R_a	R_q	R_z	R_a	R_q
1 layer	850	135	160	2440	450	530	1020	350	400
2 layers	550	150	175	1200	310	360	900	180	220

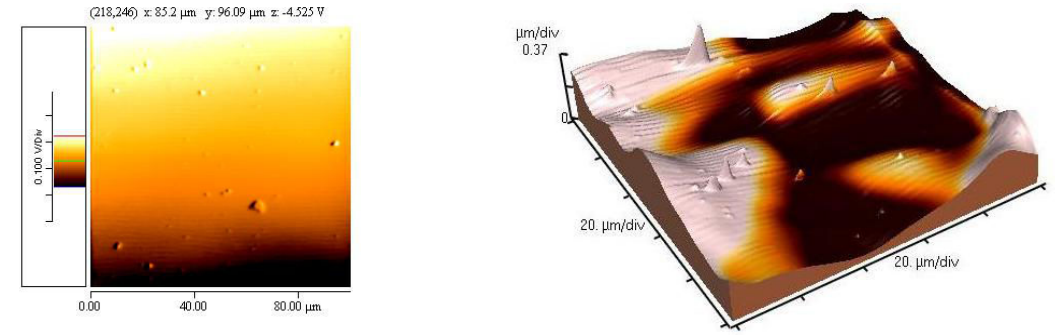

(a)

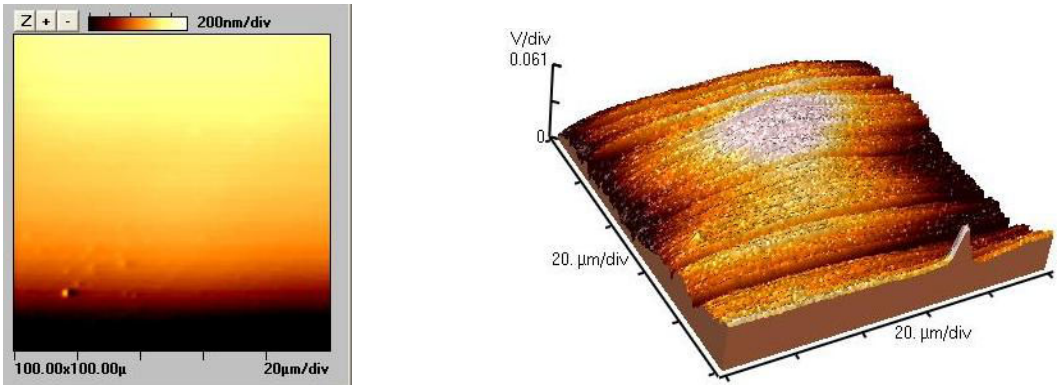

(b)

Fig. 5.28 : AFM images of one (a) and two (b) printed UV layers.

To estimate if the surface tension of the dried dielectric layers is compatible with the surface energy of the silver ink, a series of angles contact measurements have been conducted using a goniometer. Table 5.7 shows the surface energy (SE) of UV printed inks onto LCP. As the surface tension of the silver ink estimated by the supplier is between 27-31 mN/m, no surface treatment is required for SC1 and SC3 but it would be necessary for SC2 in order to print the conductive ink. Regarding the characteristics of UV inks, SC 1 shows deformation

at high temperatures or is sensible to high temperature (up to 150°C) and a color change has been noticed whereas SC2 requires a complementary thermal cure at 150°C for 30 min before printing silver ink which would not appear to be convenient for an industrial process. SC3 is the best candidate to planarize the LCP as it remains stable during thermal curing in oven. Therefore, SC 3 has been selected as a pre-layer for this study.

Table 5.7: Surface energy of UV inks printed onto LCP using the Owens Wendt method.

Ink	SC1	SC2	SC3
Surface energy (mN/m)	43	29	46

5.3.1.4 Dielectric characterization

Based on the resonant cavity method explained in chapter 2, the planarized LCP substrate is characterized for their dielectric properties. Fig. 5.29 shows the real part of permittivity and tangent losses of LCP for the first four cavity resonances. Planarized LCP shows a relative permittivity of nearly 3.72 and tangent loss of nearly 0.0065. Fig. 5.29 also compares the dielectric properties of planarized and non planarized LCP substrates. From the graphs, it can be seen that the planarized substrate presents almost the same permittivity and tangent loss compared to non- planarized LCP substrate. The improvement in the height of the substrate to several μm due to the planarization makes the differences in permittivity and loss.

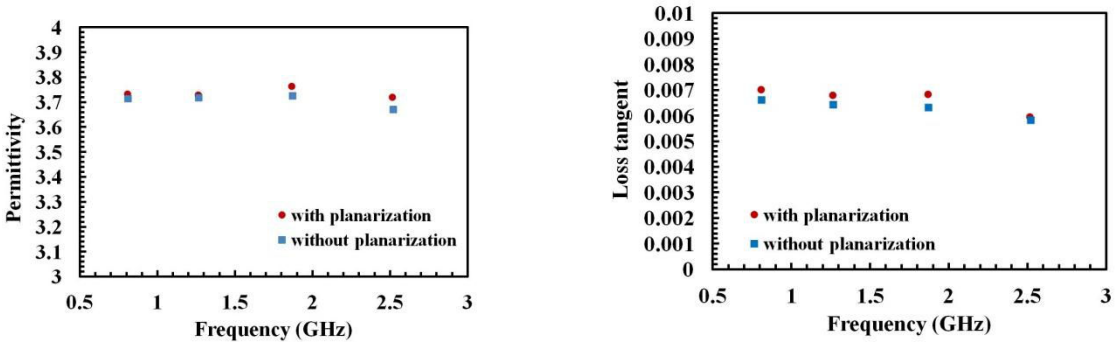

(a) (b)

Fig. 5.29 : Dielectric properties of LCP with and without planarization (a) relative permittivity and (b) tangent loss.

5.3.1.5 Printings: Interpretation

A 20 wt % of silver nanoparticles ink from Sun Chemical has been printed with a Ceradrop ink-jet printer on LCP substrates with and without UV layer (SC3). The geometrical measurements realized by optical microscopy shows a great improvement of the quality of the printed line after planarization. Also planarization avoids discontinuities for the high resolution lines. Fig. 5.30 shows photographs of printed LCP with and without planarization.

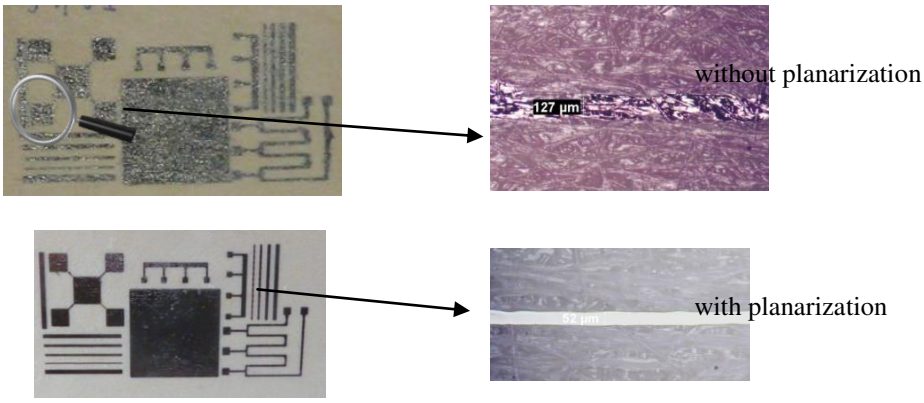

Fig. 5.30 : Photographs of a printed LCP with and without planarization.

The electrical resistivity of printed patterns on both substrates (planarized and non planarized) have been compared to demonstrate the efficiency of this new planarization technique. For the non planarized LCP, the electrical resistivity of printed patterns on LCP varies from 35 µΩ.cm at 150°C to 29.4 µΩ.cm at 200°C for 30 min.

Fig. 5.31 points out the electrical resistivity for the planarized samples at 150°C, 200°C and 230°C varying the duration of sintering in a conventional oven. The optimized results have been found for 30 min of curing. Tests have been conducted at different temperatures and time. It is found that electrical resistivity decreases to 22.4 µΩ.cm at 150°C, 7.3 µΩ.cm at 200°C and 5.6 µΩ.cm at 230°C for 30 min. The best electrical conductivity is obtained at 230°C. However, a visible degradation of UV layer is observed for 30 min and cracks on the silver layer occur leading thus to a poor conductivity (see Fig. 5.32).

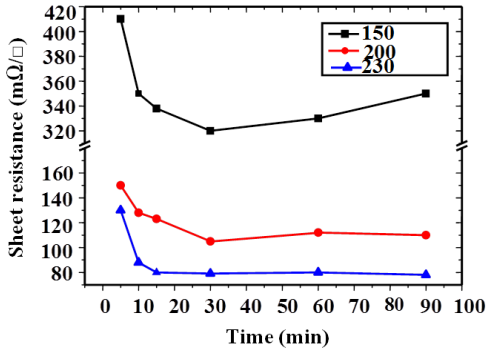

Fig. 5.31 : Sheet resistance of one printed silver layer within different curing temperatures versus time of curing.

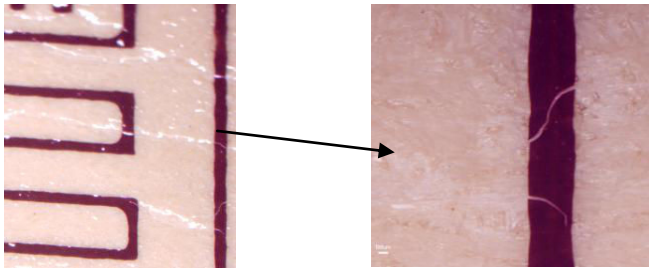

Fig. 5.32 : Cracks observed via microscopy onto a silver layer cured at 230°C.

The measurements using 4 point probe technique with the PA200 semi-automatic probe station allows the measurements of the square resistance. Electrical tests have been conducted varying the length of measured lines. The probes have been placed on different contact pads positions (see Fig. 5.33). Electrical resistivity has been calculated based on the resistance measurements, the lines geometry (width and length) and the thickness measurement. The electrical resistance varies linearly depending on function of the length shown an actual linear behavior (Fig. 5.34).

Fig. 5.33 : Microscope images of printed patterns.

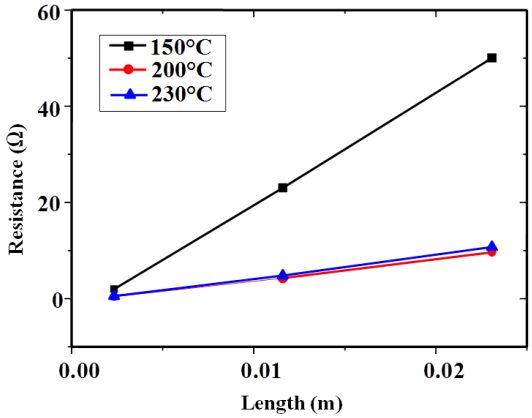

Fig. 5.34 : Resistance of circuits versus length.

This planarized LCP substrate is used for the design of RF circuits. Following sections discusses the electrical characteristics of inkjet printed RF circuits on planaized LCP E130i.

5.3.2. RF devices on planarized LCP E130i

In order to demonstrate that planarized LCP is compatible with inkjet printing technique for RF applications, microstrip transmission lines and distributed low pass filters are fabricated and measured.

5.3.2.1 Transmission lines

1) Design

Fig. 5.35 (a) and (b) show two sets of transmission lines where each set is having two transmission lines of lengths l_1=5cm and l_2=2cm. Each set of transmission lines are differentiate based on the number of metalized layers. Single layer and double layers of silver metallization have been considered with each layer having a thickness of 700nm. The set of transmission lines given in Fig. 5.35 (a) and Fig. 5.35 (b) respectively have single layer and double layers of silver metallization. The width of w=0.38cm was chosen for all transmission lines in order to get a characteristic impedance of 50 Ω. The selected temperature for curing the conductive silver ink was 200°C for 30 min. The effect on the metallization on transmission line losses and signal attenuation is depicted in this section.

.

(a) (b)

Fig. 5.35 : Microstrip transmission lines on planarized LCP E130i with different metallization thickness (a) with 0.7 µm , and (b) with 1.4 µm.

2) S parameters

Fig. 5.37 to Fig. 5.39 deal with insertion and return loss of above mentioned transmission lines. Each transmission line was simulated using Ansys HFSS (EM simulation) considering the effect of SMA connectors and Ansoft designer (electrical simulation). The simulation results are compared with the transmission line measurements using Ecal calibration.

Transmission lines with single layer metallization show good matching better than -15 dB till 4.5 GHz and transmission lines with double layer metallization show good matching better than -15 dB till 5 GHz. To compare losses of both transmission lines, we consider a frequency at 2 GHz. At 2 GHz, transmission lines with single layer metallization show an insertion loss of 1.22 dB and double metallization line show an insertion loss of 0.74 dB. The skin effect explains the high losses of the transmission lines (see Fig. 5.40). Insertion losses measured at high frequencies are slightly higher than HFSS simulation in all cases. The phase shift shown in the electric simulation with that of measurement is due to the absence of RF connectors in the simulation.

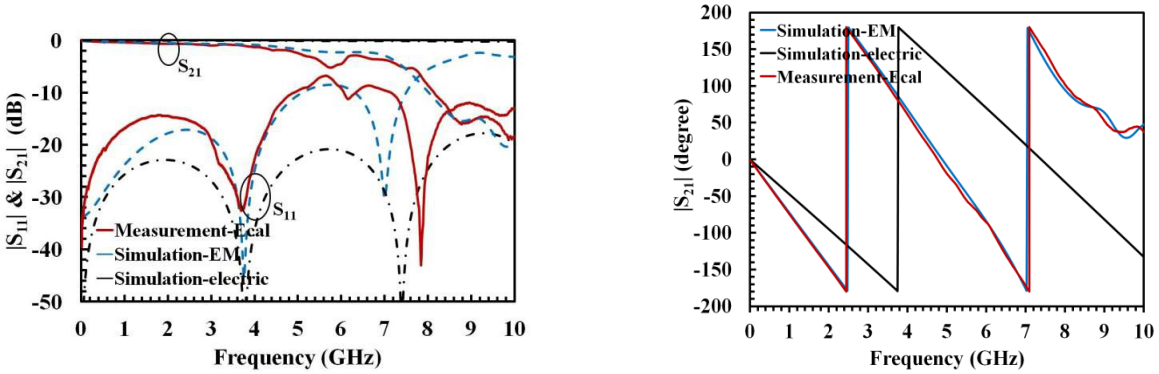

(a) (b)

Fig. 5.36 : Scattering parameters of single layer silver metalized microstrip transmission line with length 2 cm realized by inkjet printing on planarized LCP E130i, (a) in dB and (b) in degree.

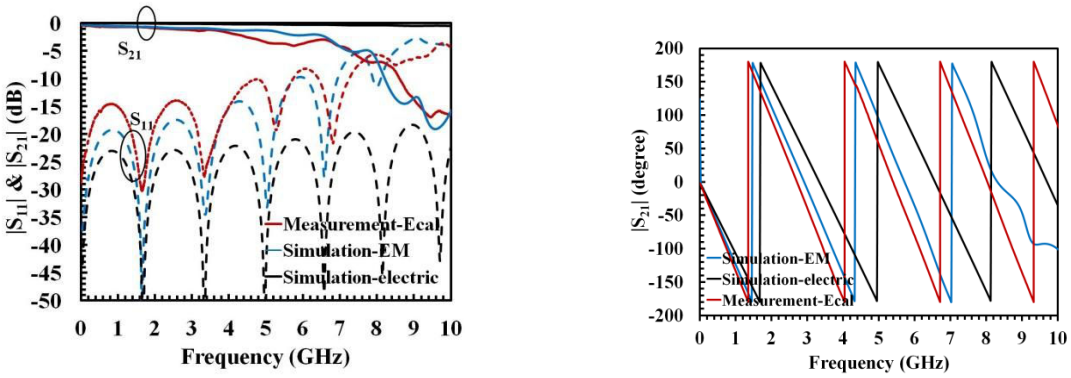

(a) (b)

Fig. 5.37 : Scattering parameters of single layer silver metalized microstrip transmission line with length 4 cm realized by inkjet printing on planarized LCP E130i, (a) in dB and (b) in degree.

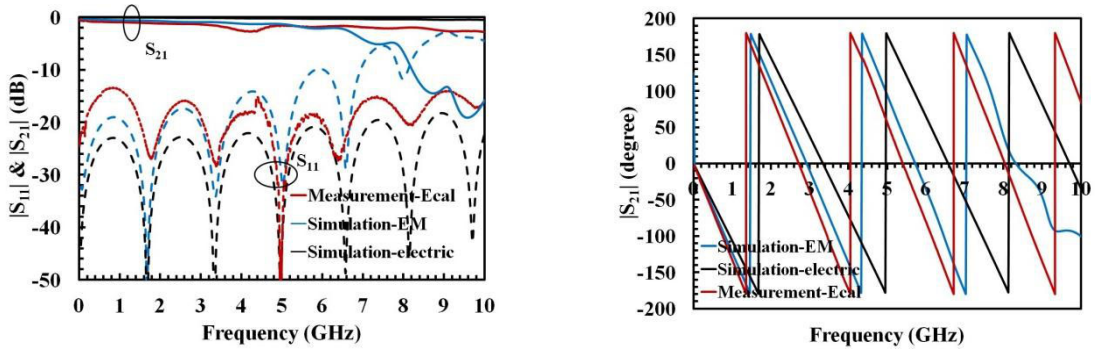

(a) (b)

Fig. 5.38 : Scattering parameters of double layers silver metalized microstrip transmission line with length 4 cm realized by inkjet printing on planarized LCP E130i, (a) in dB and (b) in degree.

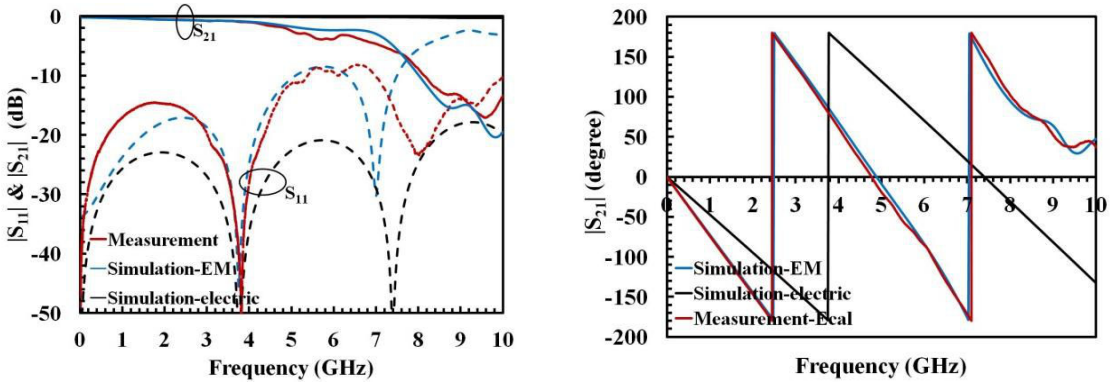

(a) (b)

Fig. 5.39 : Scattering parameters of double layers silver metalized microstrip transmission line with length 2 cm realized by inkjet printing on planarized LCP E130i, (a) in dB and (b) in degree.

Based on the conductivity of the printed lines, the skin depth of the metal is calculated and is given in Fig. 5.40. A skin depth of 5 μm is obtained at 2 GHz.

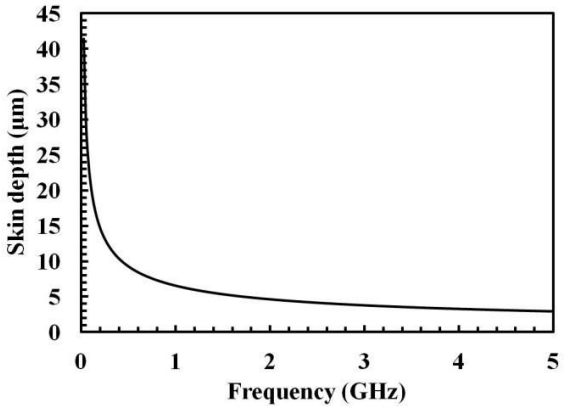

Fig. 5.40 : Skin depth for silver ink with conductivity = 4 10^{06} S/m.

3) Impedance

First of all, the characteristic impedance of the measured transmission lines is extracted using the two lines method [19]. Fig. 5.41 plots the characteristic impedance versus frequency. Extracted characteristic impedances from measurement are respectively 42 Ω and 47 Ω for single and double metallization lines at 1 GHz, which provides a variation of 10.6% between two lines. Near to the resonance frequency, the value of the characteristic impedance cannot be exploited.

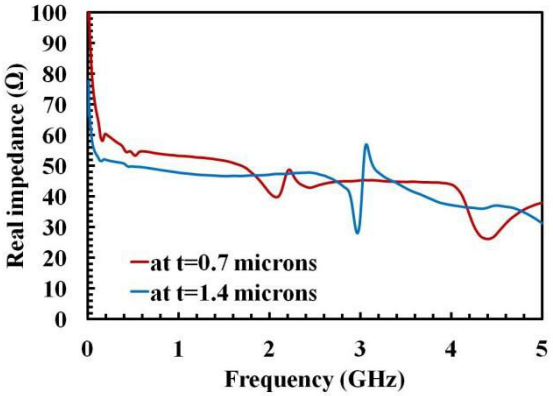

Fig. 5.41 : Real part of impedance of the lines with t=0.7µm and t=1.4 µm .

4) Losses and quality factor extractions

Table 5.8 shows the comparison of RLGC parameters extracted from measurements of transmission lines with different thickness. Transmission lines with single layer metallization show higher unit resistance and higher conductive losses than that of transmission lines with double metallization layers as expected.

Table 5.8: RLGC line parameters of transmission lines with different metallization layers on planarized LCP E130i.

Transmission lines	*R (Ω/m)*		L (nH/m)		G (mS/m)		C (pF/m)	
	1 GHz	2 GHz	1 GHz	2 GHz	1 GHz	2 GHz	1 GHz	2 GHz
Single layer metalization	151	158	331	324	5.14	7.9	98.7	100
Double layers metalization	114	124	331	324	4.5	5	91.1	94

In order to investigate losses origin, dielectric and conductive losses were calculated based on RLGC parameters [20]. It is clear from Fig. 5.42 that dielectric losses are negligible compared to conductive losses and thus conductive losses contribute much on signal attenuation. Indeed, single layer metalized transmission lines exhibit more conductive losses of 1.5 Np/m than that of double layer metalized transmission lines which has conductive loss of 1 Np/m at 2 GHz. Measured losses are higher that losses expected by simulations. This difference may due to the connection between connectors and lines with silver ink that can give a poor connection quality. In addition, both transmission lines show high conductive losses in comparison with those of LDS LCP Vectra E820i microstrip transmission lines (0.25 Np/m at 2 GHz) and ink jet printed transmission lines on ABS PC (0.7 Np/m at 2 GHz).

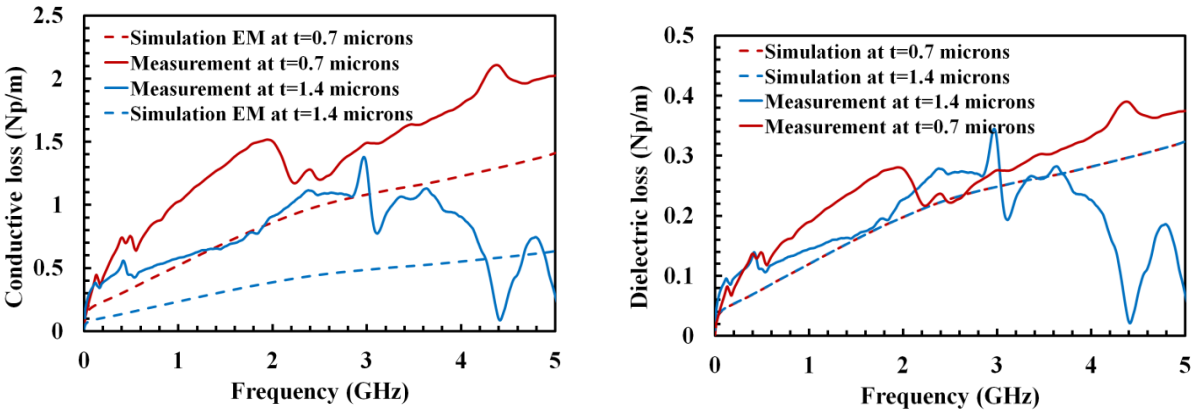

(a) (b)

Fig. 5.42 : Losses of inkjet printed MID microstrip transmission line on planarized LCP E130i with metal thickness of 0.7µm and 1.4 µm, (a) conductive loss and (b) dielectric loss.

5) Quality factor

Fig. 5.44 shows the extracted quality factors of single and double layer metalized transmission lines extracted based on the propagation constant (Fig. 5.43) as $Q=\alpha+j\beta$ [20]. Quality factor increases with increase in frequency and poor values of 17 and 37 are observed at 2 GHz respectively for single and double layer metalized transmission lines. The quality factor can be improved with thicker metalized layers of silver ink. If we compare ABS PC lines by ink jet printing (quality factor=32 at 2 GHz), the double layer metallization lines shows improved quality factor.

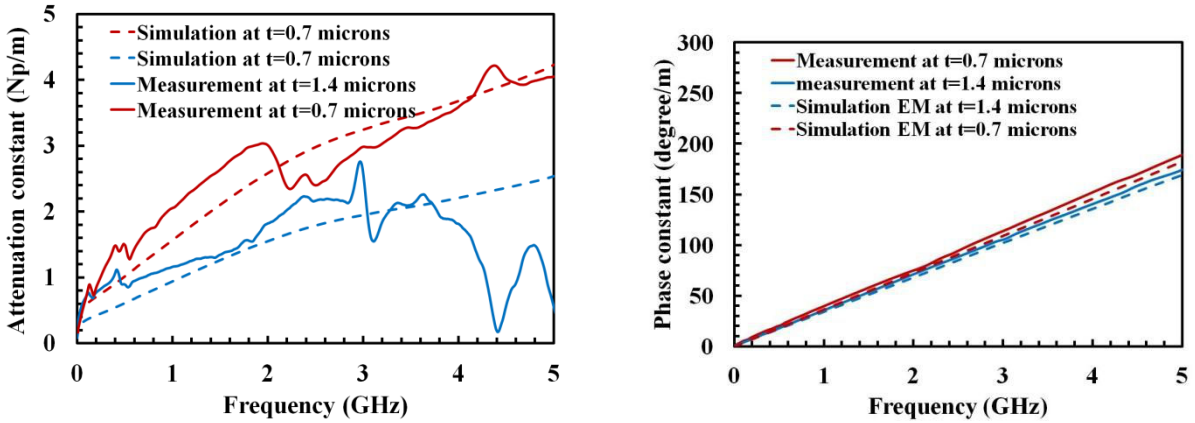

(a) (b)

Fig. 5.43 : Propagation constant of inkjet printed MID microstrip transmission line on planarized LCP E130i with metal thickness of 0.7µm and 1.4 µm, (a) attenuation constant and (b) phase constant.

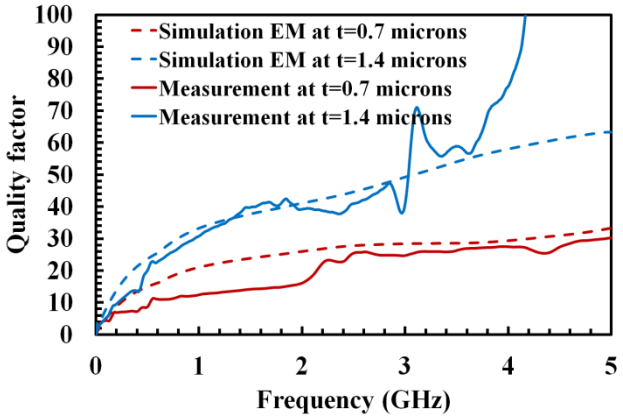

Fig. 5.44 : Quality factor of inkjet printed MID microstrip transmission line on planarized LCP E130i with metal thickness of 0.7µm and .4 µm.

5.3.2.2 Low pass filter

In order to validate the potential of planarized LCP for RF applications, a stepped-impedance low pass filter alternating high and low characteristic impedance transmission lines is designed for -3dB cut-off frequency of 4 GHz. The filter is realized in a CPW technology requiring two layers of conductive patterns. In order to connect the filter to RF connectors, tapering sections have been added to both extremities of the filter. The selected temperature for curing the conductive silver ink was 200°C for 30 min.

Fig. 5.45 shows the layout and photograph of the realized low-pass filter. This device is fabricated on a 38 x 34 mm^2 LCP substrate. The dimensions of the low and high impedance sections are respectively the following : l_1=11.45mm, w_1=4.6mm, l_2=1.25mm and w_2=0.2mm.

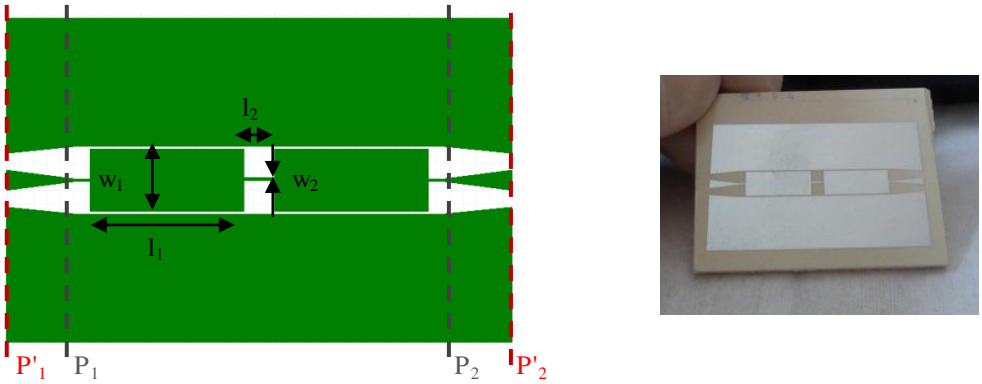

Fig. 5.45 : Geometry and photograph of distributed low pass filter on planarized LCP E130i.

The measurement has been done in $P'_1P'_2$ planes using N5222A Agilent PNA with an Ecal calibration. All simulations were carried out using Ansys HFSS. Measured and simulated S parameters up to 10 GHz are shown in Fig. 5.46. In the figure, measured results (red lines) and simulated results (blue lines) provide a return loss of better than -12dB till 1.7 GHz, with an attenuation near to 0.5 dB in the pass band. Lower matching level occurring for higher frequencies is mainly due to the presence of tapered access for connecting line. By deembedding the tapered access on either side of the filter can provide an improved matched filter response. In Fig. 5.46, the black lines show the simulated results without the tapered access (P_1P_2 planes), which provides a good matching of -17 dB. Unfortunately, a fabrication problem occurred on the TRL calibration kit and the TRL calibration allowing to get results in P_1P_2 planes was not achieved. Still, the measurement results again prove the compatibility of molded planarized LCP substrate in inkjet printing technology.

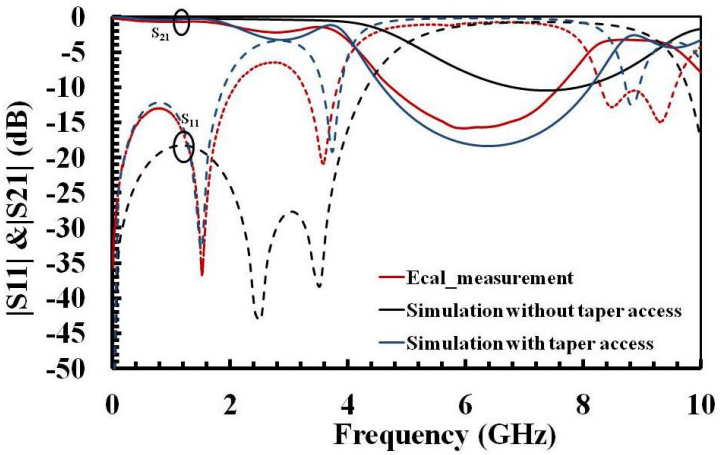

Fig. 5.46 : Comparison between the simulated (blue and black lines) and the measured (red lines) S parameters for the fabricated low pass filter.

5.4. Conclusion

In this study, we demonstrated the potential of an inkjet printed MID devices for RF applications. Two MID substrates (ABS PC and LCP E130i) are considered materials in this work. The study begins with the inkjet printing and sintering process of ABS PC. Metal ink with silver nano particles is inkjet printed and subsequent curing and sintering step are performed to create metal thin-films with electrical conductivity of 5.5 x 10^6 S/m.

RF characterization of transmission lines on ABS PC is done based on CPW and microstrip technologies. ABS PC permittivity is characterized using two transmission lines method and is compared with that measured from resonant cavity method. A relative permittivity of nearly 2.8 was obtained from both methods. In addition, conductive and dielectric losses of inkjet printed transmission lines on ABS PC are extracted. Electrical characterization shows that the conductive losses predominate dielectric losses and thus confirm the high conductive losses for inkjet printing techniques. These high losses result in a poor quality factor of 10.5 from CPW lines and 32 from microstrip lines at 2 GHz. In order to reduce conductive losses, the conductor thickness should be increased. Based on these characterization results, an MID microstrip patch antenna and inkjet printed UWB antenna were designed and realized. Measurements are in good agreement with EM simulations. The microstrip patch antenna provides a gain of 3 dB at the resonance frequency of 2.63 GHz. The UWB antenna exhibits a -10 dB reflection coefficient bandwidth from 3 GHz to 13 GHz with a maximum gain of 4.2 dB. These results prove that inkjet printed technique on MID antennas offers great potential for RF antennas applications.

The second section of this research work deals with the combination of inkjet printing technique and molded LCP E130i substrate. Planarization technique was introduced on to an LCP substrate which originally presents a significant surface roughness of 8-9µm. The substrate has been cleaned and treated via a UV/O_3 treatment which has allowed to match the surface tension of the substrate with surface tension of the UV inks. The planarization has allowed to reduce the electrical resistivity by a factor 4 from 29.4 µΩ.cm to 5.7 µΩ.cm at 200°C.

Transmission lines and stepped impedance low pass filter at 4 GHz cut off were further realized on LCP planarized substrate. Fabricated devices show good agreement between measurement and simulation results, proving thus the potential of the planarized LCP substrate for RF applications. The transmission lines on planarized LCP provides a quality factor of 37 at 2 GHz (for double layer metallization) comparable to quality factor inkjet printed microstrip on ABS PC (32 at 2GHz). These results allow to consider this planarized substrate as a candidate to replace polyimides and PET for printed electronic applications.

References

[1] H. J. V. Osch, J. Perelaer, A. W. M. Laat and U. S. Schubert, "Inkjet Printing of Narrow Conductive Tracks on Untreated Polymer Substrates , " Advanced Materials, vol. 20, pp. 343-345, 2008.

[2] A. Rida, L. Yang, R. Vyas, S. Basat, S. Bhattacharya, and M. M. Tentzeris, "Novel Manufacturing Processes for ultra-Low-Cost Paper-Based RFID Tags with Enhanced Wireless Intelligence," Procs. 57th IEEE-ECTC Symp. Sparks, NV, p. 773, 2007.

[3] S. Seo, S. Park, and J. Joung, "Micro Pattering of Nano Metal Ink for Printed Circuit Board Using Inkjet Printing Technnology,"J. the Korean Soc.Prec. Eng., vol. 24, 89-96,'07.

[4] O. Azucena, J. Kubby, D. Scarbrough and C. Goldsmith, " Inkjet Printing of Passive Microwave Circuitry ," Microwave Symposium Digest, 2008 IEEE MTT-S International, pp. 1075-1078, June 2008.

[5] L. Yang, A. Rida, R. Vyas and M. M. Tentzeris, "RFID Tag and RF structures on a Paper Substrate Using Inkjet- Printing Technology, " IEEE Transactions on Microwave Theory and Techniques.,no.12, vol. 55, pp. 2894-2900, Dec. 2007.

[6] O. Ahmed, A. R. Sebak, "A Printed Monopole Antenna with two steps and a Circular Slot for UWB Applications, " IEEE Antennas and Wireless Propagation Letters.,vol. 7, pp. 411-413, Nov. 2008.

[7] A. K. Gautam, S. Yadav, and B. K. Kanaujia, "A CPW-Fed Compact UWB Microstrip Antenna, " IEEE Ant and Wireless Propag Let.,vol. 12, pp. 151-154, March 2013.

[8] H. K. Lee, J. K. Park, and J. N. Lee "Design of a Planar Half-Circle-shaped UWB Notch Antenna, " Microwave and Optical Tech Letters.,vol. 47, no. 1, pp. 9-11, Oct. 2005.

[9] M. Ding, R. Jin, J. Geng, and Q. Wu "Design of a CPW-Fed Ultrawideband Fractal Antenna, " Microwave and Optical Tech Letters.,vol. 49, no. 1, pp. 173-176, Jan. 2007.

[10] D. T. Nguyen, D. H. Lee, J. Geng, and H. C. Park, " Very Compact Printed Triple Band-Notched UWB Antenna With Quarter-Wavelength, " IEEE Antennas and Wireless Propagation Letters, vol. 11, pp. 411-414, 2012.

[11] D. T. Nguyen, D. H. Lee, J. Geng, and H. C. Park, " Novel Compact Eye-Shaped UWB Antennas, " IEEE Ant and Wireless Propagation Letters, vol. 11, pp. 184-187, 2012.

[12] D. T. Nguyen, D. H. Lee, J. Geng, and H. C. Park, " Inkjet Printing of UWB Antennas on Paper Based Substrates, " IEEE Ant and Wireless Propag Let ,vol. 10,111-114, Jan. 2011.

[13] D. L. Paul, L. Zhang, and L. Zheng, "Flexible Dual-Band LCP Antenna for RFID Applications, " Proc of 2013 URSI Int Symposium on EM Theory , pp. 973-976, May 2013.

[14] S. S. Basat, S. Bhattacharya, L. Yang, A. Rida, M. M. Tentzeris and J. Laskar, "Design of a Novel High- Efficiency UHF RFID Antenna on Flexible LCP Substrate with High Read-Range Capability, " IEEE Antennas and Propagation Society International Symposium 2006 , pp. 973-976, July 2006.

[15] M. A. Aris, E. A. Kadir, M. Y. M. Zain, Z. I. Rizman and N. H. R. Husin, "A Miniature UHF Rectangular Microstrip RFID Tag Antenna for Aluminium Can Application," World Applied Sciences Journal 23 (Enhancing Emerging Market Competitiveness in the Global Economy), pp. 96-102, 2013.

[16] H. L. Kao, C. L. Cho, L. C. Chang, C. S. Yeh, B. W. Wang and H. C. Chiu, "Inkjet printing RF bandpass filters on liquid polymer substrates",Thin Solid film,vol.544,64-68, '13.

[17] G. Shaker, M. Tentzeris, S. N. Safieddin, "Low cost Antennas for mm-Wave Sensing Applications using Inkjet Printing of Silver Nano-particles on Liquid Crystal Polymers ," IEEE Antennas and Propagation Society International Symposium (APSURSI), July 2010.

[18] Data sheet available online at www.sunchemical.com.

[19] A. M. Mangan, S. P. Voinigescu, M. T. Yang and M. Tazlauanu, "De-Embedding Transmission Line Measurements for Accurate Modeling of IC Designs," IEEE Transactions on Electron Devices, vol. 53, pp. 235-241, February 2006.

[20] D. M. Pozar, Microwave Engineering. New York: J. Wiley & Sons, 2005.

[21] E.J. Safieddin, "Losses of Microstrip Lines ," IEEE Transactions on Microwave and Techniques, vol.28, no. 6, June 1980.

[22] J. D. Welch and H. J. Pratt, "Losses in microstrip transmission systems for integrated microwave circuits," NEREM Rec., vol. 8, 1966.

[23] R. Horton, B. Easter, and A. Gopinath, "Variation of microstrip losses with thickness of strip; Electron. Utf., vol. 17, no. 17, pp. 490-491, Aug. 26, 1971.

[24] J. R. James, and P. S. Hall, Handbook of Microstrip Antennas. Peter Peregrinus, London, UK, 1989.

[25] Federal Communication Commission, Washington DC, USA, "Revision of part 15 of the Commission's rule Regarding Ultra-Wideband transmission systems FCC 02-48,", First Report and Order, Feb. 2002.

[26] John R. Vig, "UV/ozone cleaning of surfaces," U.S. Army Electronics and Devices Laboratory, ERADCOM, 1984.

[27] T. Y.Hin, C. Liu and P. P. Conway, "Surface characterization of plasma treated flexible substrates for waveguide –on –flex application," Surface & Coatings technology, vol. 203, no.24, pp.3741-3749, September 2009.

Chapter-6

Laser Direct Structuring (LSS) Microstrip Devices on MID

This chapter presents the design, fabrication and characterization of MID transmission lines and directional couplers fabricated with laser ablation technique. A combination of nickel, gold and copper (Ni/Au/Cu) with 10 μm thickness is considered for defining the circuit traces in LSS technique. The compatibility of two different molded thermoplastic substrates for RF applications is demonstrated in this work. Two substrates are LCP (Liquid Crystal Polymer) E130i and high K material. The compatibility of inkjet printed planarized LCP E130i in RF *circuit design has been already demonstrated in chapter 5. Laser ablated 50 Ω microstrip* transmission lines on bare LCP E130i shows conductive losses of 0.35 Np/m at 2 GHz. Measured conductive losses are lower than that of inkjet printed transmission lines on planarized LCP (=1 Np/m at 2 GHz) and higher than that of LDS lines (=0.27 Np/m at 2 GHz). This leads to a high quality factor of 56 at 2 GHz to be compared with that obtained for ink jet printed lines on planarized LCP E130i, 37 at 2 GHz. Thereafter, a study of permittivity enhancement by adding complex charges such as Al_2O_3 (Aluminium Oxide) is carried out. Other than High K material, this technique was also used to increase the permittivity of thermoplastic materials such as are PS (PolyStyrene) and PE (PolyEthylene). An high increment of the permittivity of the High K material from 3.3 to 8.5 is observed among the other experimented substrates. This high permittivity value makes this substrate suitable for RF circuit miniaturization. Measurements of two transmission lines realized by LSS on the High K material allowed the extraction line's quality factor as 117 at 2 GHz which is higher than LDS lines. These good electrical performances make this substrate a good candidate for RF applications. This high permittivity property is exploited to design single and three sections -10 dB directional coupler at 1 GHz center frequency. Experimental results of the single section directional coupler show return loss and isolation better than -15 dB across the complete frequency band from 0.2 GHz to 2 GHz. The coupling measured at 1 GHz was -10.78 dB. In similar, 3- sections directional coupler show return loss and isolation better than -15 dB across the complete frequency band from 0.2 GHz to 2 GHz. The coupling measured at 1 GHz was -10.85 dB.

6.1. Introduction

Since 1982, the UV (ultraviolet) laser ablation has been utilized in many experimental and theoretical studies of polymers. Literature reviews show a number of studies in the field of LSS (Laser Subtractive Structuring) on polymers, its processing, material removal, surface modification etc. [1]-[6]. LSS has already used in standard PCB (Printed Circuit Board) manufacturing for laser drilling vias. In contrary to the mask based fabrication approach where the mask has to be designed and fabricated first before the metal layer can be patterned, LSS is a non-mask based technology that can be used for fast modeling of circuits [7][8]. Pulsed UV laser ablation became an important fabrication technique since the interaction of laser beams bring less thermal damage to the intended polymer materials [9]. Due to the excellent UV absorption behavior and high thermal stability, LSS can be used for thermoplastic circuits fabrication.

In the last two chapters, RF circuits based on additive technologies such as Laser Direct Structuring (LDS) and inkjet printing were presented. This chapter deals with the LSS technique of MID circuit fabrication where unwanted metallization is removed from the fully metalized substrate surface by means of laser beam to form the desired circuit pattern. This method of fabrication is suitable for high density metal circuits. Fig. 6.1 shows a laser ablated MID circuit board on an LCP E130i substrate.

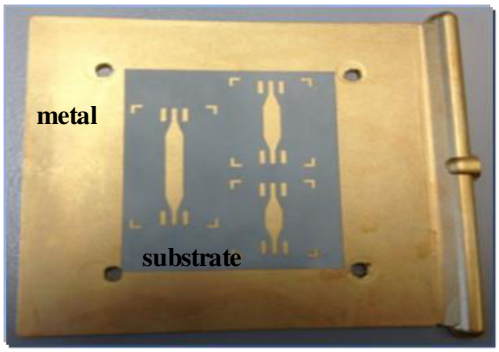

Fig. 6.1: Laser ablation fabrication model.

The thermoplastic material has been molded in plates of 2 mm thickness and put in an electroless copper bath. Successively layers of copper (1-10 μm), nickel(1-10 μm) and gold (8 μm) finish were raised with a thickness of 10 μm and conductivity in the order of 5.48 x 10^6 S/m. Then, the LSS technique was used to define the electrical circuit footprint in a minimal time of 3 hours. Here, minimal gap seperation and minimum width is 160μm.

Among the thermoplastics listed in Fig. 3.11 in chapter 3, which are characterized based on their thermal stability, LCP holds the highest thermally stability. Its better

mechanical and thermal properties and chemical stability of LCP makes LCP an alternative for high performance classical PCBs [10]. In this chapter, the electrical properties of laser ablated MID transmission lines on bare LCP E130i are first presented. The second section of this chapter discusses the development of higher permittivity substrates compliant with LSS technique by using additive charges in order to increase the polymers' permittivity and consequently reduce RF components size and cost. A high K material with permittivity 8.5 provides higher permittivity among the tested polymers and hence used for the design of miniaturized RF circuits. Measurement results of transmission lines and directional couplers realized by laser ablation on this novel material are presented.

6.2. Microstrip transmission line properties on LCP E130i

In order to evaluate the laser ablated MID lines RF properties, two 50 Ω planar microstrip transmission lines on LCP E130i are designed (see Fig. 6.2). The dimensions of these lines are w=0.4cm, l_1=1 cm and l_2=4cm. Two tapered access and soldering pads of edge width 1.5mm and length 5mm are added at the end of each transmission lines to have good and proper connector access. Two simulation tools such as Ansys HFSS and Ansoft designer have been respectively used for the EM and electrical study of the transmission lines behaviors.

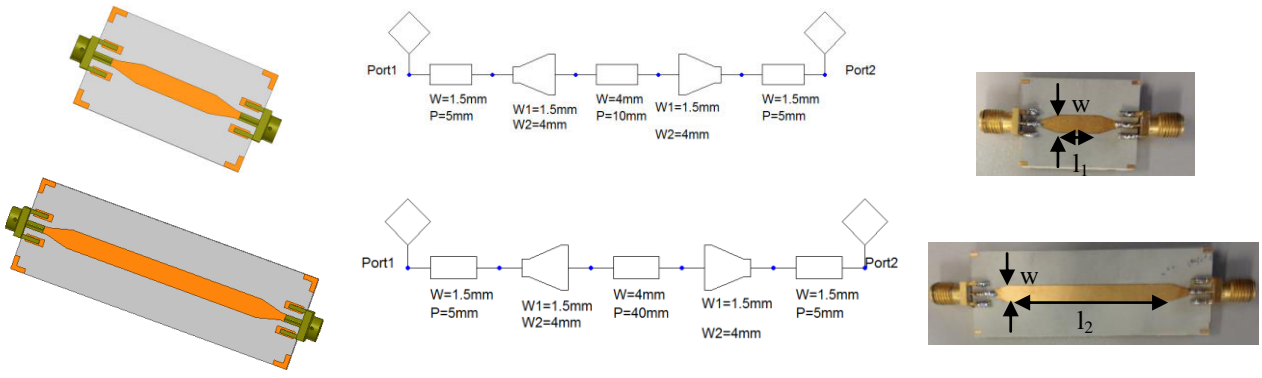

Fig. 6.2: Laser ablation transmission lines of two different lengths on LCP E130i (a) EM simulation structures, (b) electric simulation structures, and (c) fabricated photos of the lines.

The permittivity (ε_r) of 3.65 and loss tangent (tan δ) of 6 x10^{-3} obtained from resonant cavity method (see Fig. 3.15) was used for the initial design in the simulations. All transmission line measurements were done with Ecal measurements using N5222A Agilent PNA. The S parameters of two transmission lines of length 1 cm and 4 cm are given in

Fig. 6.3 and Fig. 6.4 respectively. The results are presented till 10 GHz. The plots compare the S parameters obtained from measurement, EM and electric simulations. EM simulations show better agreement with the measurement results for both transmission lines. Indeed EM simulations take into account the presence of connectors. The presence of tapered access lines causes the degradation of transmission lines matching at higher frequencies.

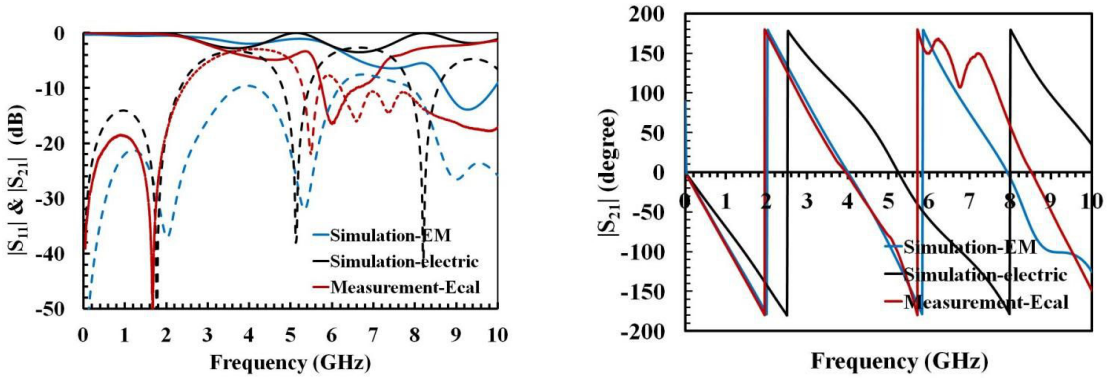

(a) (b)

Fig. 6.3: S parameters of Laser ablation MID transmission lines of 1 cm length (a) in dB and (b) in degree.

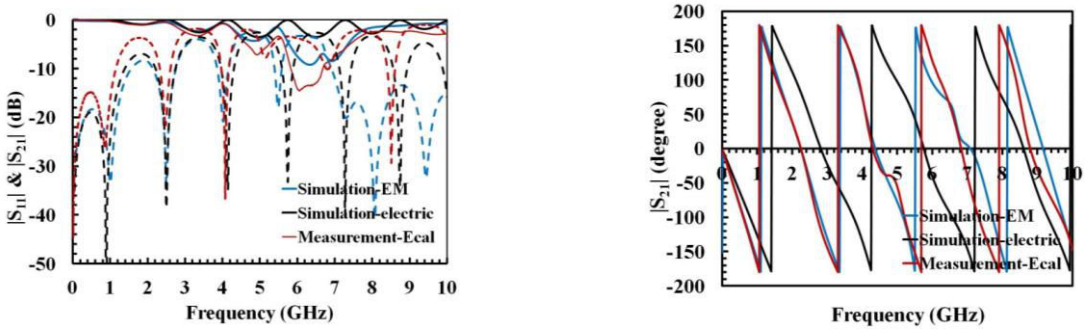

(a) (b)

Fig. 6.4: S parameters of Laser ablation MID transmission lines of 4 cm length (a) in dB and (b) in degree.

Moreover, the effective and relative permittivities of LCP E130i are extracted from these S parameters measurements based on the two transmission lines method [11]. From the phase of the line extracted from two lines method, given in Fig. 6.5, the effective dielectric permittivity of LCP E130i is derived and a value in the order of 2.8 is obtained (Fig. 6.5). The relative dielectric permittivity of the substrate calculated from transmission line analytical model given in [12] is in the order of 3.7 and is comparable with those obtained from resonance cavity in Fig. 2.9. A variation of 5% can be observed at above 3 GHz which can be due to the smaller size of the sample within the cavity.

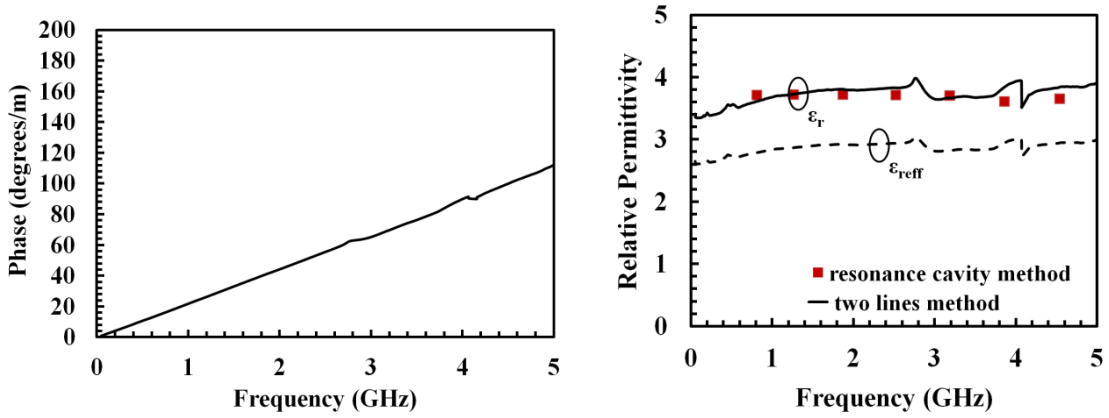

(a) (b)

Fig. 6.5 : Extracted relative and effective permittivity of LCP E130i from simulation and measurements.

Further extraction of losses and quality factor were done and are presented in the section below.

6.2.1. Losses of microstrip line

All the transmission line properties presented in this section are extracted from the characteristic impedance Z_c and propagation constant γ. Fig. 6.6 plots the variation of the characteristic impedance Z_c till 2.5 GHz. The extracted impedance is near to 50 Ω for low frequency. Impedance extractions are no more valid for higher frequencies (> 2.5 GHz) when resonance frequencies is achieved. The transmission line parameters or RLGC parameters per unit length of microstrip transmission lines on LCP E130i extracted from measurements at 1 GHz and 2 GHz are presented in Table 6.1.

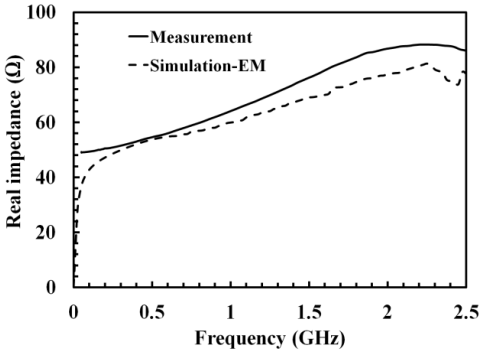

Fig. 6.6: Extracted real part of impedance from transmission lines simulation and measurements.

Based on the extracted RLGC parameters, losses are calculated by following the equations presented in chapter 4 using a MATLAB program. Fig. 6.7 (a) presents the comparison between conductive, dielectric and total losses for both EM simulations and

measurements. Measured conductive losses are higher than dielectric losses and contribute more in the total attenuation of the signal. Extracted dielectric and conductive losses at 2 GHz are respectively are 0.24 Np/m and 0.35 Np/m. Indeed, the attenuation constant increases with increase in frequency and reaches 0.63 Np/m at 2 GHz. Fig. 6.7 (b) shows the extracted quality factor with respect to frequency. A quality factor of 56 is observed at 2 GHz. This quality factor is smaller than the one of the microstrip transmission lines LCP Vectra E820i by LDS technology (see Fig 3.35 where quality factor = 61 at 2 GHz). Indeed, the LCP E130i exhibits higher dielectric losses and a lower permittivity.

Table 6.1: RLGC parameters of inkjet printed microstrip lines on LCP E130i

Frequency (GHz)	***Resistance (Ω/m)***	**Inductance (nH/m)**	**Conductance (mS/m)**	**Capacitance (pF/m)**
1	27.8	203	4.5	59.7
2	54.9	285	4.52	43.6

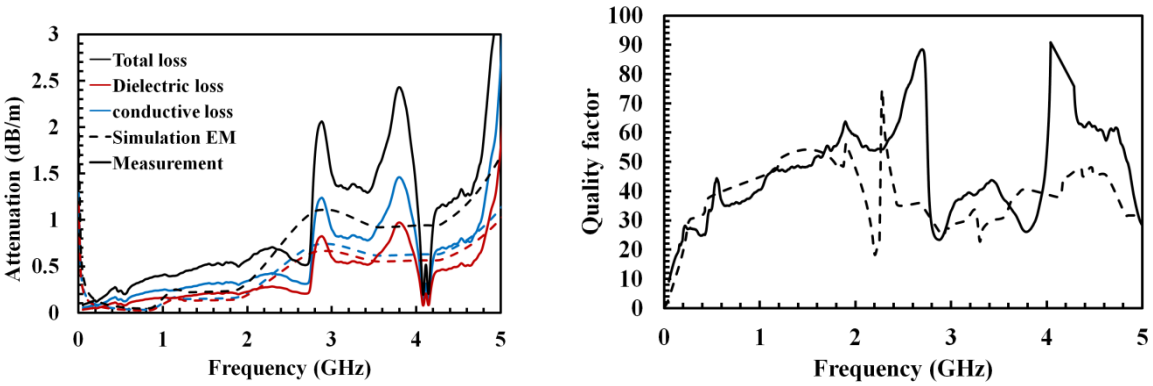

(a) (b)

Fig. 6.7: Electrical properties of laser ablated transmission lines on LCP E130i, (a) losses α including dielectric and conductive losses and (b) quality factor.

6.3. Thermoplastic materials' permittivity improvement study

This section presents the characterization of several classical thermoplastic materials whose permittivity has been improved using additive charges. Three thermoplastic materials are considered for the study. Since the details of the composition of the substrates for permittivity improvement is under patent, the details are not presented in the thesis.

6.3.1. Thermoplastic materials characterization

In order to increase the permittivity of PE and PS, Al_2O_3 (Aluminium oxide) additive charges are used. The dielectric properties of the thermoplastics PS and PE with 15% and 30 % concentrations of Al_2O_3 were measured [15]. Fig. 6.8 shows the samples of PE and PS.

Fig. 6.8: Characterized thermoplastic materials, (a) PE with 15% of Al_2O_3, (b) PE with 30% of Al_2O_3, (c) PS with 15% of Al_2O_3 and (d) PS with 30% of Al_2O_3.

Resonance cavity method has been utilized for the characterization [16]. Characterization results of PE and PS are presented in Fig. 6.9. Characterizations have been done for the first three frequency of resonances: 0.815 GHz, 1.280 GHz and 1.891GHz. It can be seen from measurement results that the premittivity value increases with additive charges Al_2O_3 concentration. For the PE sample , permittivities of 2.31 and 3.12 are respectively obtained at the third frequency resonance for 15% and 30% of Al_2O_3 (Fig. 6.9 (a)). Similarly, for the sample PS, the permittivity of 2.88 and 3.22 are respectively obtained for 15% and 30% of Al_2O_3 (Fig. 6.9(b)). The permittivity enhancement is thus proved, thanks to Al_2O_3 charges addition. Higher permitivities allows the improvement of quality factor and the miniaturisation of RF circuit devices.

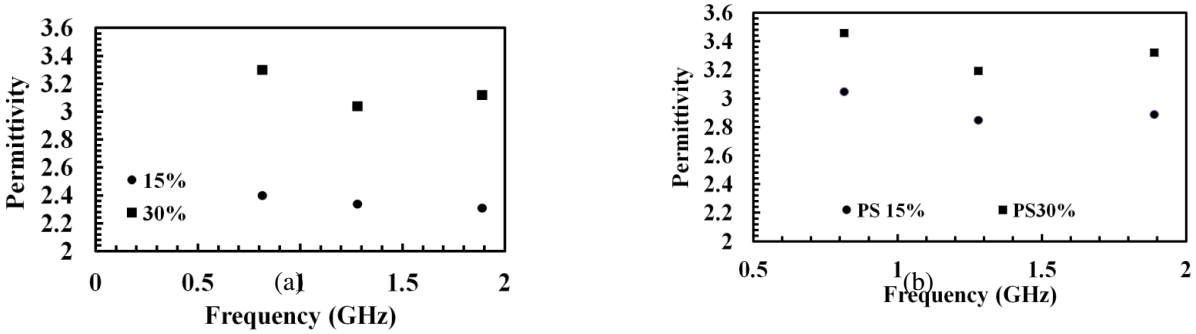

Fig. 6.9: Dielectric permittivities of characterized thermoplastic materials with additive filler Al_2O_3, (a) PE and (b) PS.

Another novel material with additive charges is introduced in this chapter. Indeed, this additive charges increases the polymer permittivity and thus consequently reduce RF

components size and cost [13]. Fig. 6.10 (a) shows the sample molded in 10 x10 x 0.2cm^3 dimension. The real part of the measured permittivity using resonant cavity method is presented in Fig. 6.10 (b). The measurement results show that the relative dielectric permittivity is near to 8.5 in the 0.8-1.89 GHz frequency band. This sample shows a high permittivity value compared to all other thermoplastic substrates presented in this thesis.

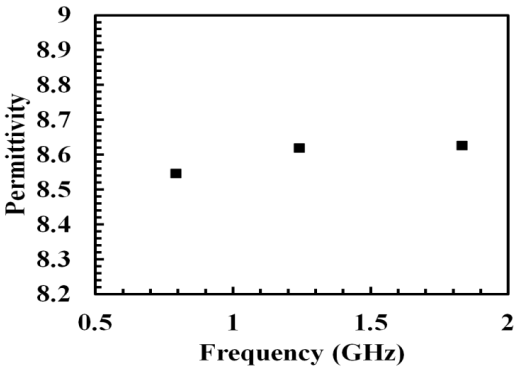

(a) (b)

Fig. 6.10 : The thermoplastic substrate, (a) the characterized plate and (b) real part of relative permittivity.

The measured tangent loss does not exceed 7x10^{-3} in the measured frequency band. These measured dielectric properties make this novel polymer a good candidate for RF applications. These dielectric properties of the sample were exploited and are considered for the design of microstrip transmission lines and miniaturized couplers. Following section details the performances of these devices.

6.3.2. Transmission line properties on PEEK-$BaTiO_3$

Fig. 6.11 shows two MID microstrip transmission lines of length l_1= 2 cm and l_2= 5 cm realized on the novel high permittivity substrate by laser ablation. A line width, w = 2.2 mm was chosen in order to reach a characteristic impedance of 50 Ω.

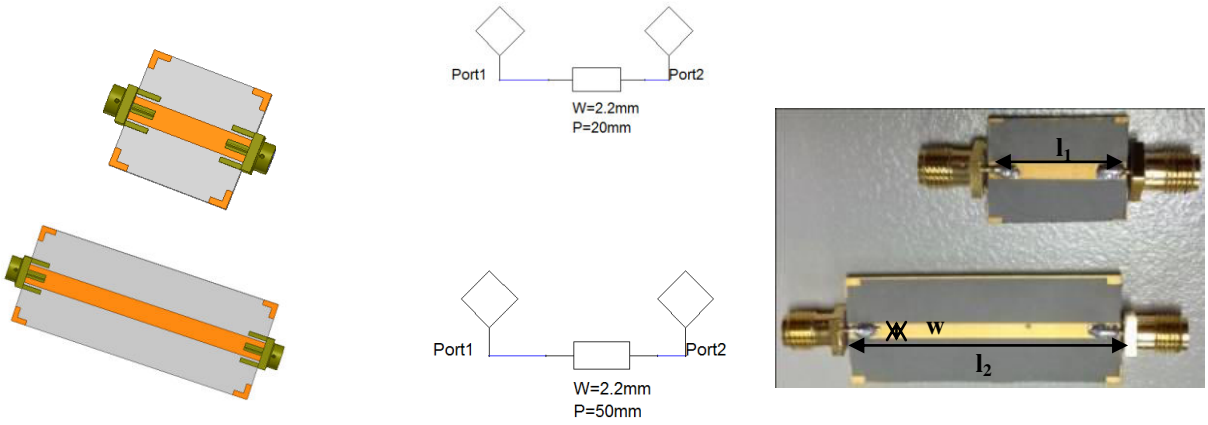

(a) (b) (c)

Fig. 6.11 : Structures of microstrip transmission lines designed on PEEK- $BaTiO_3$, (a) in EM simulation, (b) in electric simulation and (c) fabricated structure.

As in the transmission line studies presented in the previous sections, two simulation softwares such as Ansys HFSS and Ansoft Designer were respectively made use for the simulation studies in EM and electric domain. All measurements were carried out in N5222A Agilent PNA calibrated using electronic calibration. Fig. 6.12 (a) and (b) respectively show the S parameters of these laser ablated transmission lines of 2 cm and 5 cm length till 5 GHz. A good agreement between measurement and simulation results can be seen in both transmission lines response. The 2 cm line provides a 15 dB matching till 2.7 GHz whereas the return loss of -15 dB of 5 cm line limits at 1.2 GHz. These lines provide an insertion loss of less than 1dB till these frequencies.

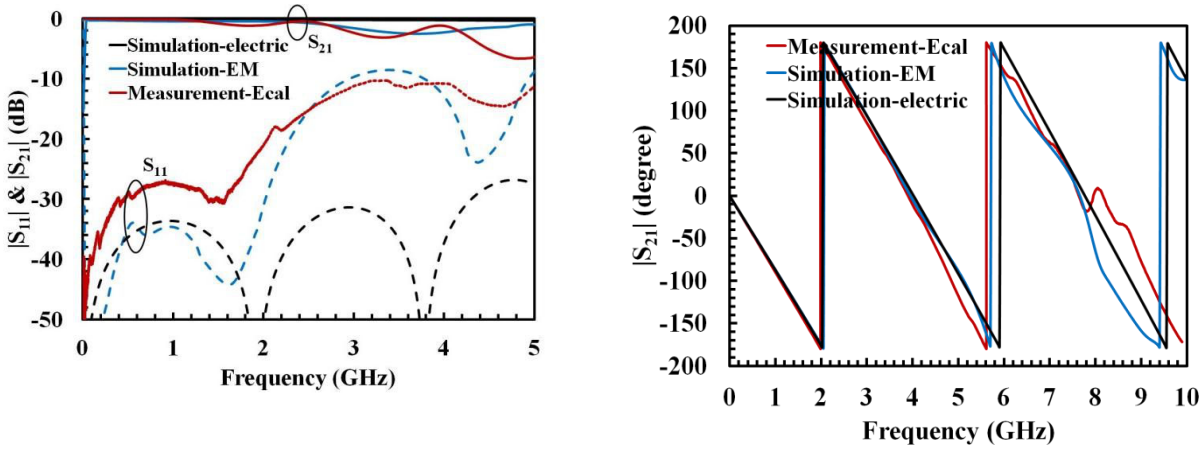

(a)

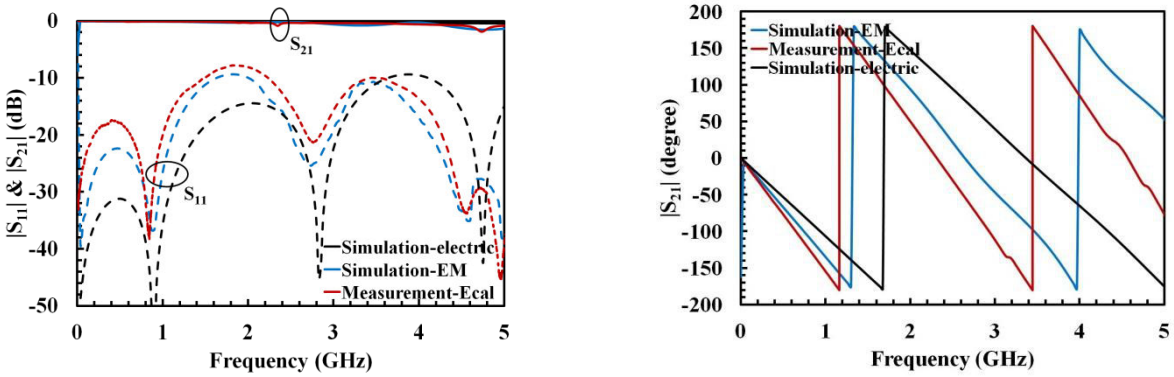

(b)

Fig. 6.12 : S parameters of laser ablated transmission lines in magnitude (dB) and phase (degree), (a) 2 cm line response and (b) 5 cm line response.

Further extraction of permittivity in continuous frequency domain, losses and quality factor were carried out using the above presented transmission line S parameters. Two transmission lines method [11] is used for these parameters' extraction. The effective dielectric permittivity derived from the phase of the line is of the order of 5.5 (see Fig. 6.13). Compared to the conventional MID substrate LDS LCP vectra [4] with ε_{reffe} = 2.48, the miniaturization of 55% can be achieved with this substrate. The relative dielectric permittivity derived from analytical model of microstrip transmission line technology [12] is of the order of 8.6. This result of permittivity extraction is comparable with that obtained from resonant cavity method with a variation of 1.1% (see Fig. 6.10 (b)).

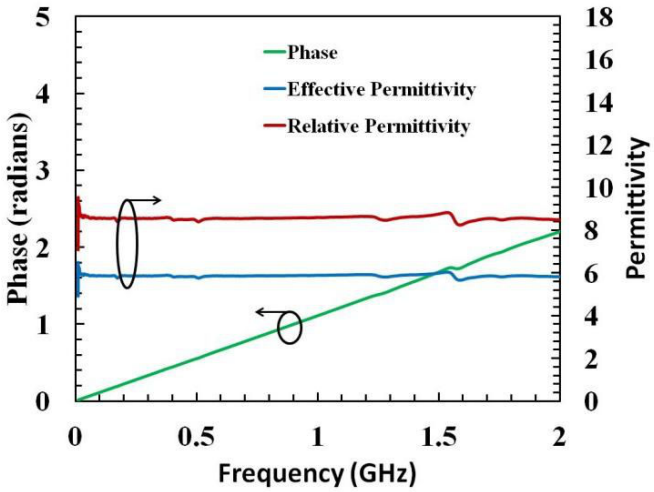

Fig. 6.13 : Permittivity extraction of High K material based on two microstrip transmission lines' measurement.

Fig. 6.14 (a) and (b) show the measured and simulated transmission line losses on High K material. Simulations results are in good agreement with measurements for frequencies lower than 2 GHz. When resonance frequency is achieved, extraction of losses is less accurate. Dielectric losses predominate conductive losses due to the loss tangent of the substrate (see Fig. 6.14 (a)). A conductive loss of 0.33 Np/m and dielectric losses of nearly 0.36 Np/m are extracted from the measurement results at 2 GHz. The quality factor of this laser ablated transmission line on High K material is calculated and extracted. A high quality factor equal to 117 at 2 GHz. Due to the high losses shoot at above 3GHz, the Q factor decreases accordingly.

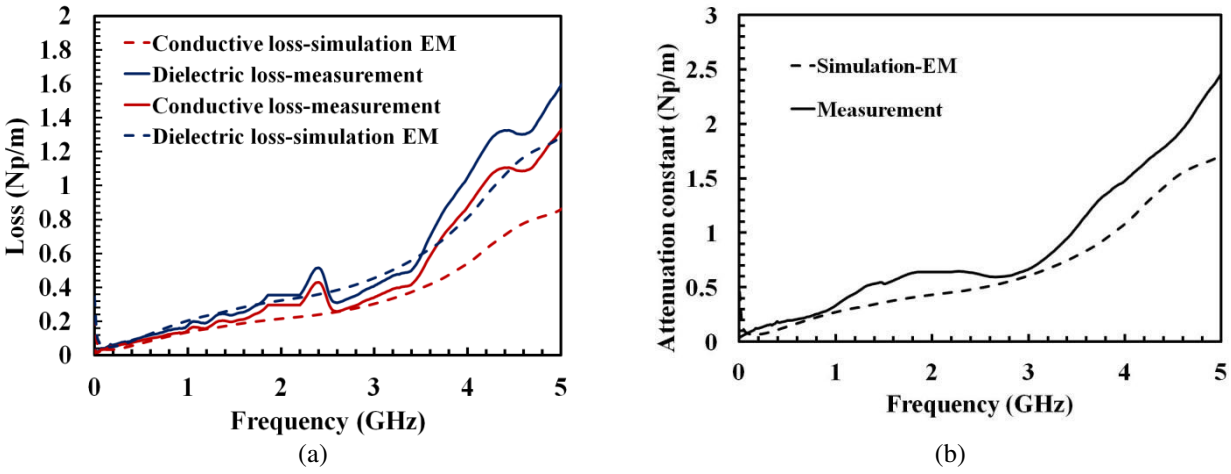

Fig. 6.14 : Losses of microstrip line on High K material, (a) conductive and dielectric losses and (b) total losses.

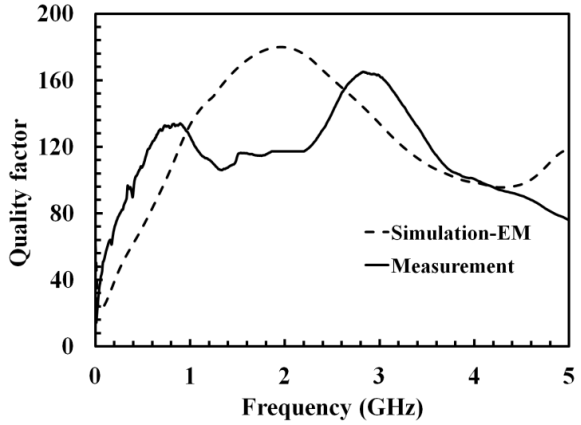

Fig. 6.15 : Quality factor of microstrip line on High K material.

In order to compare MID transmission lines behavior to conventional MID substrates, 50 Ω microstrip transmission lines on LCP Vectra E820i presented in chapter 4 and on LCP E130i presented in section 6.2 are used. Fig. 6.16 (a) and (b) present respectively α and β of microstrip MID line on novel High K material and conventional transmission lines on LCP Vectra E820i and LCP E130i. It can be seen from Fig. 6.16 (a) that the transmission line attenuation increases with frequency and that of MID laser ablated transmission line on High K material reaches at 0.32 Np/m at 1 GHz whereas LDS LCP Vectra E820i and laser ablated LCP E130i respectively show attenuation of 0.28 Np/m and 0.4 Np/m at 1 GHz. This novel MID transmission lines losses remain higher than that of LDS LCP Vectra E820i transmission line with a difference of 0.04 Np/m and smaller than laser ablated LCP E130i. In addition, phase constant mainly dependent on the permittivity value shows high phase constant for MID transmission line compared to classical ones (see Fig. 6.16 (b)). Fig. 6.16 (c) shows the comparison of quality factor of transmission lines till 2 GHz. MID line provides a quality factor of 117 at 1 GHz whereas transmission lines on LDS LCP Vectra E820i and LCP E130i provide quality factor of respectively 61 and 56. Therefore, laser ablation technique combined with these high permittivity substrates offers a good potential for RF circuit design.

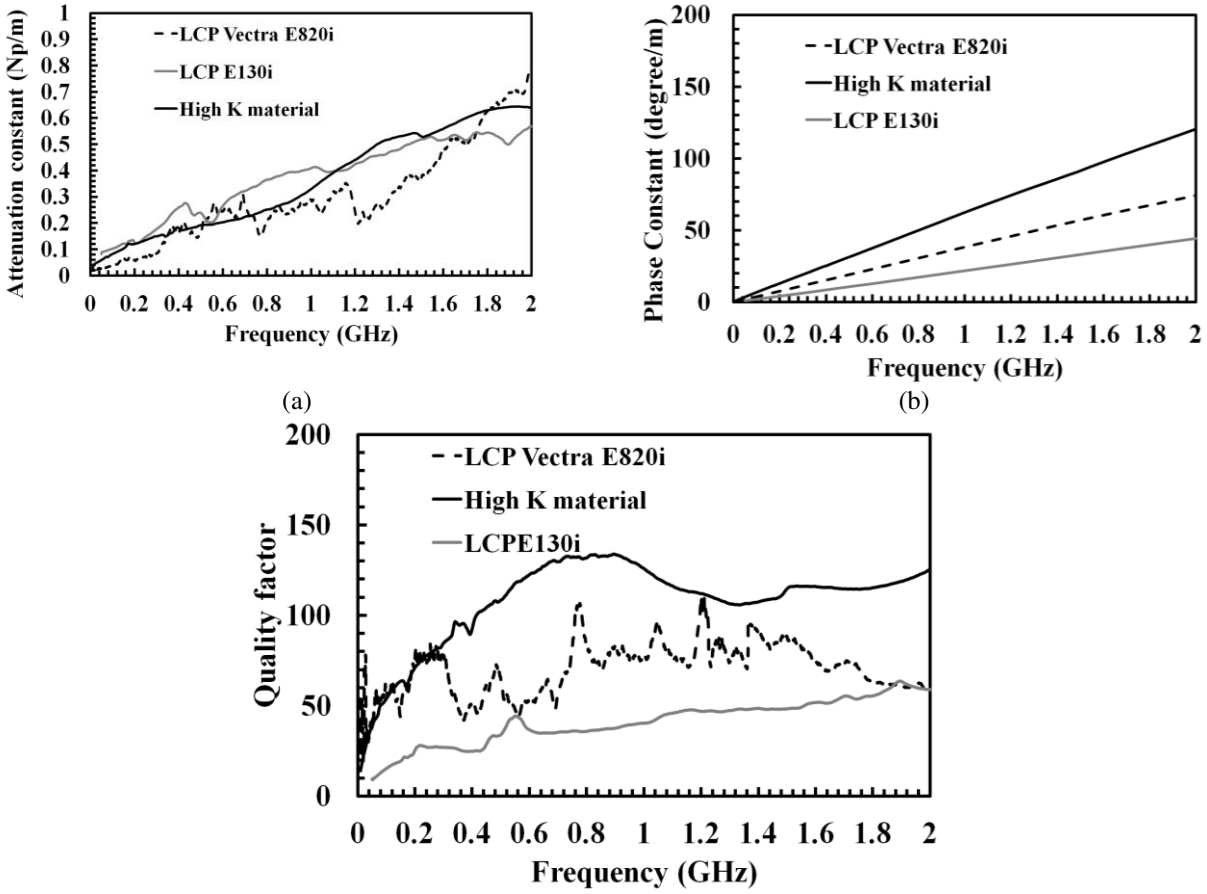

Fig. 6.16 : Comparison between extracted complex propagation constants γ and quality factors of the MID lines on novel High K thermoplastic material and on classical MID substrates LDS LCP Vectra E820i and laser ablated LCPE130i (a) attenuation constant, α and (b) phase constant, β, and (c) quality factor.

In order to exploit this good quality factor, a single section directional coupler and three section direction couplers are designed and realized. Following section discusses them in detail.

6.3.3. MID Single section directional coupler on PEEK-$BaTiO_3$

A -10 dB single section directional coupler with a center frequency of 1 GHz is presented in this section. Microstrip parallel coupled lines topology is selected due to its simple configuration and ease of fabrication. Fig. 6.17 shows the electrical circuit of a single section coupled lines [12].

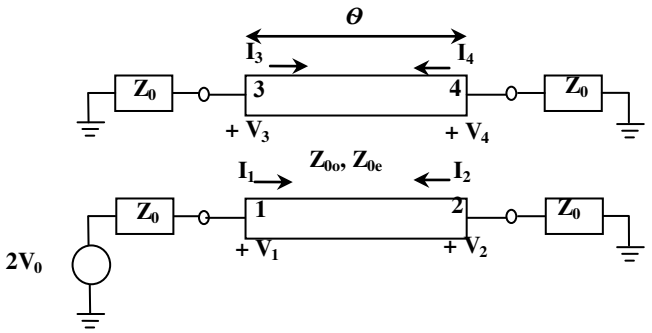

Fig. 6.17 : A single section coupled lines electrical circuit

Parallel coupled lines have even and odd mode characterized by their characteristic impedances and propagation velocities. If the characteristic impedance (Z_0) and the coupling coefficient (C) are determined, even Z_{0e} and odd Z_{0o} characteristic impedances can be calculated using following equations [12]:

$$Z_{0e} = Z_0\sqrt{\frac{1+C}{1-C}} \tag{6.1}$$

$$Z_{0o} = Z_0\sqrt{\frac{1-C}{1+C}} \tag{6.2}$$

Based on the relative position of isolated port to the input port, directional couplers are classified as co-directional, contra-directional and trans-directional [17]. A contra directional coupler design technique is followed in this work. The analysis of two coupled microstrip lines is done using Ansys HFSS simulation software. In order to achieve a coupling of -10 dB for a characteristic impedance of Z_0 =50 Ω, the odd and even mode characteristic impedances are set to Z_{0o} =37 Ω and Z_{0e} =70 Ω respectively. The gap between the two coupled transmission lines of 2 mm width is set to 700 µm.

Fig. 6.18 presents the even and odd mode effective permittivities. Odd mode effective permittivity $\mathcal{E}_{reffo}$ =4.4 and even mode effective permittivity $\mathcal{E}_{reffe}$ =5.6 are depicted from Fig. 6.18. In order to achieve a maximum coupling at coupled port, the transmission lines length is set to one- quarter wavelength at 1 GHz design frequency. The arithmetic mean of the even and odd mode effective permittivities is considered to calculate the optimal length of the coupled lines, 33.7mm.

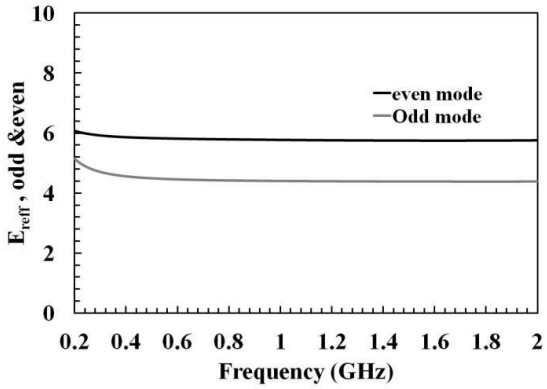

Fig. 6.18 : Even and odd mode effective dielectric constants for coupled lines on High K material.

Bend lines on each port are added in order to facilitate connectors access. The simulated structure of the single section directional coupler and its photograph realized on this high permittivity material by laser ablation fabrication technique is shown in Fig. 6.19.

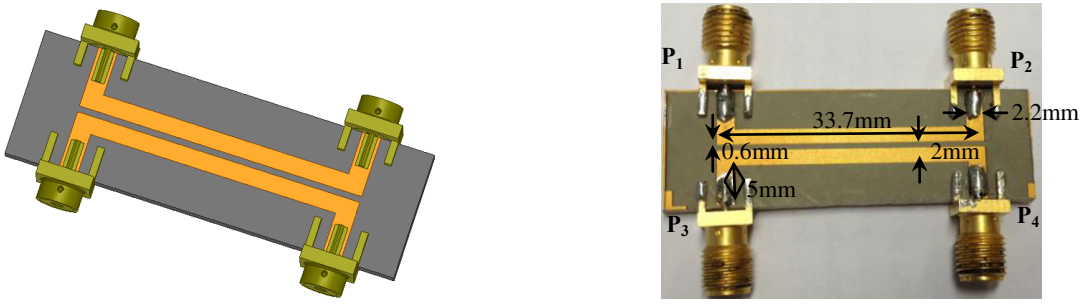

(a) (b)

Fig. 6.19 : Single section directional coupler realized on High K material, (a) the simulated structure (b) the fabricated device.

To validate the coupler design, S parameters measurements were performed on N5222A Agilent PNA using Ecal calibration. Fig. 6.20 (a) and (b) show the simulated and measured S parameters of the proposed single section MID directional coupler. The measurements are in good agreement with Ansys HFSS simulation results. From the measurements, a coupling factor of -10.7 dB is obtained at 1 GHz center frequency with a -1 dB bandwidth of 348 MHz. The -0.7 dB variation observed in the measurement result on coupling factor is due to the coupling gap precision of less than 100 µm in fabrication. The coupler exhibits a good impedance matching with S_{11} better than -20dB. In addition, insertion losses do not exceed 0.7 dB at 1 GHz. Insertion losses are mainly due to dielectric losses. A measured isolation better than -20 dB is shown across the complete frequency band from 0.2 GHz to 2 GHz.

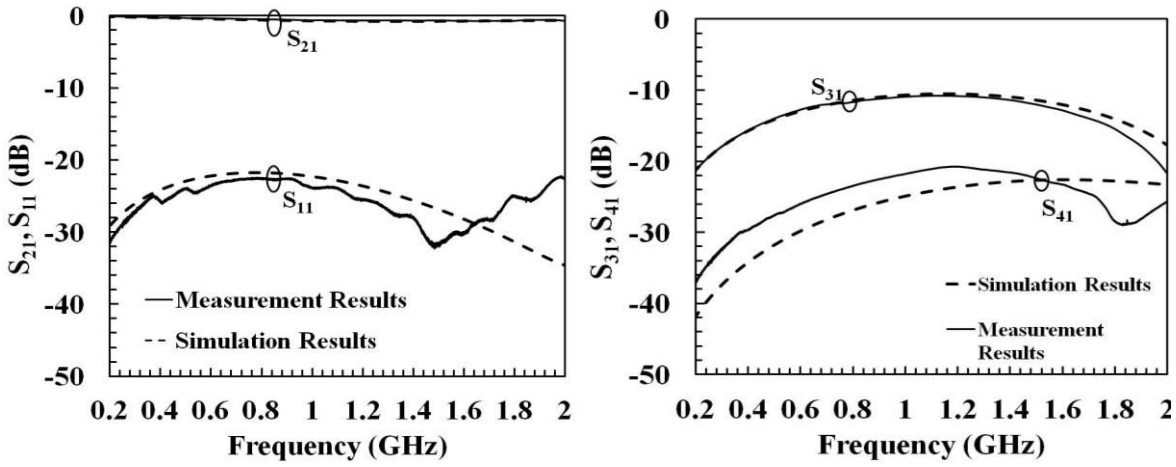

(a) (b)

Fig. 6.20 : Simulated and measured S parameters of single section directional coupler on High K thermoplastic material, (a) return loss and insertion loss and (b) isolation and coupling.

If we compare the dimension of a single section coupler with coupling of 10 dB deigned on LCP Vectra E820i, a miniaturization of 21% in length and 43 % in width can be achievable with this novel High K thermoplastic substrate .

6.3.4. Three sections directional couplers on MID

Multiple sections directional couplers are considered when the coupling due to single section coupler is limited in bandwidth due to the quarter wavelength requirement. Bandwidths can be improved using multiple sections directional couplers [12]. Therefore, a three sections directional coupler with coupling at 10 dB in 1 GHz is also considered in this thesis for the analysis of the newly developed High K substrate in combination with laser ablation technology. The contra directional coupler design is followed in this work.

For a characteristic impedance of Z_0 =50 Ω and a coupling at -10 dB, the odd and even mode characteristic impedances of the outer sections of the coupler are set to Z0o =45 Ω and Z0e =51 Ω respectively (based on equations 6.1 and 6.2). Similarly, for the inner section of the coupler, Z0o =68 Ω and Z0e =35 Ω were calculated.

Fig. 6.21 shows the structure of three sections directional coupler designed on High K material. Simulations have been carried out using Ansys HFSS. The gap between the two coupled transmission lines of the inner section of 2 mm width is set to 260 µm and that of outer section of width of 2.5 mm is 4.436mm. Bend lines of 50 Ω are added at the end of each ports.

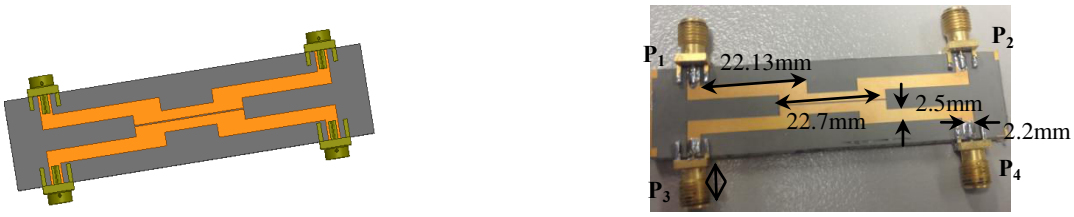

(a) (b)

Fig. 6.21 : Three sections directional coupler realized on High K material, (a) its simulated structure and (b) the fabricated device.

S parameters measurements of this coupler were performed on N5222A Agilent PNA using Ecal calibration. Fig. 6.21 and Fig. 6.22 respectively show the simulated and measured S parameters of this three sections MID directional coupler. The measurements are in good agreement with Ansys HFSS simulation results. From the measurements, a coupling factor of -10.85 dB is obtained at 1 GHz center frequency with a -1 dB bandwidth of 364 MHz. The -0.85 dB variation observed in the measurement result on coupling factor is due to the coupling gaps precision of less than 100µm in fabrication. The coupler exhibits a good impedance matching with S_{11} better than -20dB. In addition, insertion losses do not exceed 0.7 dB at 1 GHz. Insertion losses are mainly due to dielectric losses. A measured isolation better than -15 dB is shown across the complete frequency band from 0.2 GHz to 2 GHz.

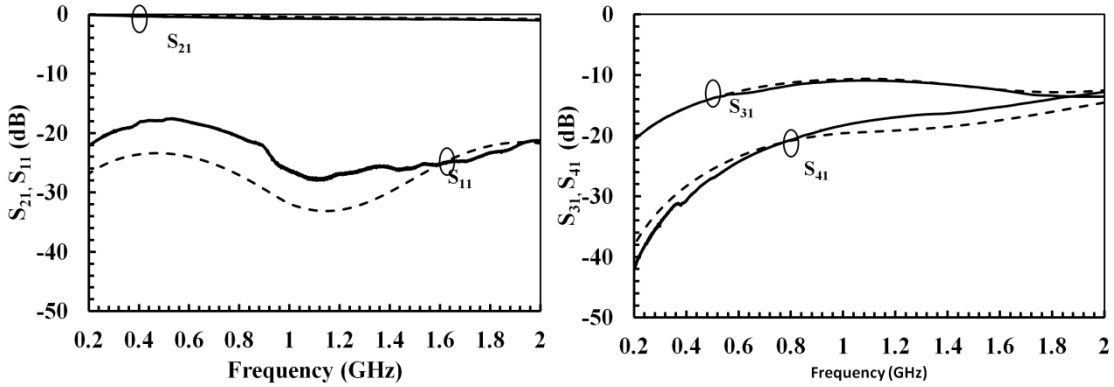

(a) (b)

Fig. 6.22 : Simulated and measured S parameters of three section directional coupler on high K thermoplastic material (a) return loss and insertion loss and (b) isolation and coupling.

Thus, the capability of MID technology in combination with LSS technique has proved in this chapter by the design and analysis of transmission lines and directional couplers.

6.4. Conclusion

This chapter studies the compatibility of MID polymers with LSS technique for RF applications. Mainly two thermoplastics are taken under study for their RF properties; LCP E130i and High K material. 50 Ω microstrip transmission lines on LCP E130i exhibit a quality factor of 56 at 2 GHz. The permittivity enhancement of molded thermoplastic substrate PE, PS and novel material were also carried out using additional charges. It was observed the enhancement in the substrate permittivities is observed in the novel substrate with permittivity of 8.5. The present work also discusses the RF potential of a novel high K material compatible with LSS technique. First of all, dielectric properties of this substrate were characterized based on cavity perturbation method. A dielectric permittivity of 8.5 and tangent loss of less than 7 $x10^{-3}$ were obtained. Two 50 Ω microstrip transmission lines have been realized by LSS. A quality factor of 117 was measured at 1 GHz. This substrate provides a high quality factor in comparison with the low cost classical MID substrates LCP Vectra E820i and LCP E130i. Then, a single section -10dB microstrip directional coupler is realized and measured. Experimental results of coupler show that the coupler exhibit a coupling accuracy of -10.8 dB at 1 GHz center frequency, an isolation and return loss of better than -20 dB across the complete frequency band from 0.2 GHz to 2 GHz. Further, a three sections -10 dB directional coupler at 1 GHz was also designed and implemented. The coupler provides a coupling of -10.8 dB at 1 GHz with a good matching and isolation better than 20 dB. A good agreement is obtained between measurement and simulation results, validating thus the potential of this novel high permittivity MID material in combination with LSS for RF applications.

References

[1] Y. Kawamura, K. Toyada, S. Namba, “Effective deep ultraviolet photoetching of polymethyl methacrylate by an excimer laser,” Applied Physics Letter, Vol. 40, pp.374–375.

[2] R. Srinivasan, V. Mayne-Banton, “Self-developing photoetching of polyethylene terephthalate films by far-ultraviolet excimer laser radiation, ” Applied Physics Letter, Vol. 41, pp.576–578.

[3] A. Yabe, “Laser Processing of Polymers, in Macromolecular Science and Engineering: New Aspects,” Springer,1999.

[4] R. Srinivasan, “In Photophysics and Photochemistry above 6 eV,” Elsevier, 1985.

[5] J.T.C. Yeh: J. Vac. Sci. Technology, 653 (1986)

[6] R. Srinivasan, B. Braren: Chem. Rev. 89, 1303 (1989)

[7] G. V. Steenberge, P. Geerinck, S. V. Put, J. V. Koetsem, H. Ottevaere, D. Morlion, H. Thienpont and P. V. Daele, “MT-compatible laser-ablated interconnections for optical printed circuit boards ,” Journal of Light wave Technology, vol. 22, no.9, pp. 2083-2090, 2004.

[8] N. Hendrickx, H. Suyal, G.V. Steenberge, A. McCarthy, A. Walker, H. Ottevaere, H. Thienpont, M. Taghizadeh, and P.V. Daele, “Laser Ablation and Laser Direct Writing as Enabling Technologies for the Definition of Micro-Optical Elements,” Proceedings SPIE, vol. 5956, '05.

[9] P. E. Dyer, “Excimer laser polymer ablation: Twenty years on,” Applied Physics A 77(2), pp. 167–173.

[10] K.C. Yung, S.M. Mei, and T. M. Yue, “Pulsed UV Laser Ablation of a Liquid Crystal Polymer,” Int. Journal on Advanced Manufacturing Tech., vol. 26, pp.1231-1236, 2005.

[11] A. M. Mangan, S. P. Voinigescu, M. T. Yang and M. Tazlauanu, “De-Embedding Transmission Line Measurements for Accurate Modeling of IC Designs,” IEEE Transactions on Electron Devices, vol. 53 (2006) 235-241.

[12] D. M. Pozar, Microwave Engineering, 2nd ed. John Wiley & Sons, Inc., 2005.

[13] R. K. Goyal, V. V. Madav, P. R. Pakankar and S. P. Butee, “Fabrication and Properties of Novel Polyetheretherketone/ Barium Titanate Composites with Low Dielectric Loss,” Journal of Electronic Materials, vol. 40, pp. 2240-2247, 2011.

[14] Vixtrex plc, Processing guide lines and material properties for Victrex PEEK 150GL30.

[15] J. N. Stanic, and A. Ploskic, “Bonding Strength between two injection molded polymers,” Master's thesis, June 2007.

[16] Damaskos, Material Measurement Solutions, [online] available at: http://www.damaskosinc.com/.

[17] C. I. Shie, J. C. Cheng, S. C. Chou and Y. C. Chiang, “Transdirectional coupled-line couplers implemented by periodical shunt capacitors,” IEEE Trans. Microwave Theory Tech. (2009), vol. 57, 2981-2988.

Chapter-7

General conclusion and future work

7.1. Thesis highlights

The objective of the thesis is to investigate the potential of MID technology in the RF field. This PhD thesis has contributed a collective study on the performance of various RF devices in several MID technologies. Corresponding to the thesis objectives listed in chapter 1, this chapter summarizes the analysis of the work done in terms of the achievement of its goal.

The whole thesis work has been divided into the characterization of molded thermoplastics and analysis of RF circuits based on various MID fabrication techniques. After a detailed presentation of the state of art of RF MID devices in chapter 2, the thesis has moved on to the characterization of molded thermoplastics and is presented in chapter 3. The low cost thermoplastics such as LCP (Liquid Crystal Polymer) Vectra E820i, LCP E130i, ABS PC (Acrylonitrile Butadiene Styrene Poly Carbonate) Cycoloy C1200HF, ABS PC Xantar LDS (Laser Direct Structuring) 3710, PC LDS Xantar 3730, PBT (PolyButylene Terephthalate) Pocan 7102 LDS, PBT Ultradur B4520, PPA (PolyPhthalAmide) LDS RTP 4099* 117359D and PA (polyamide) 66 Ultramid A3K have been characterized in terms of their dielectric properties and thermal properties. Some of the existing dielectric characterization methods have been reviewed in the chapter and resonance cavity method has chosen for the dielectric characterization since, this method provides characterization with high accuracy. The study of permittivity and losses of these thermoplastics show that thermoplastics provide low dielectric losses and LCP Vectra E820i presents low loss of 0.004 and high permittivity of nearly 4.4 among other characterized substrates. The chapter then flowed into the study of the thermal properties of the above listed thermoplastics. Thermal analysis has been done using Thermal Gravimetric Analysis (TGA) method. Analysis explains the high thermal stability of LCP Vectra E820i with a thermal stability at 511 ^{0}C. A brief study of the conductivity measurement of circuit metallization has also been carried out. For the two types of MID circuit metallization, a combination of nickel, gold and copper (Ni/Au/Cu) and silver ink, the conductivity measurements show that the MID metallization holds a conductivity in the order of 10^{06} S/m which is ten times less than the copper metallization.

This research exploited these promising electrical and thermal properties of molded thermoplastics to design the RF circuits. From chapter 4 to 6, the research has been focused in exploring the potential of the technology MID in the RF domain based on three different MID fabrication methods; Laser Direct Structuring (LDS), inkjet printing and laser ablation. Chapter 4 successfully presented MID RF performances based on LDS technology. LCP Vectra E820i, due to its high thermal stability and good electrical properties, has been chosen for the design of RF circuits in LDS technology. A comparison between coplanar waveguide (CPW), microstrip and stripline transmission line properties has been carried out. Results show that CPW lines exhibits more losses in signal transmission which in turns reduce the quality factor of the line. Quality factors of 31, 75 and 101 are respectively obtained from CPW, microstrip and stripline transmission lines at 1 GHz. In comparison with the classical substrates such as Rogers RO4003 and FR4, these MID lines exhibit high quality factor than FR4 lines and has less quality factor than a high quality high cost Rogers RO4003 lines. The research has then moved on to the design and analysis of passive devices such as antennas and filters. In this section, the thesis clearly presented the performances of MID microstrip patch antennas, low pass and band pass filters at different working frequencies. The research has also been focused onto the three dimensional antenna designs. An initial attempt has been made to study the three dimensional antenna design on MID by designing a bend patch antenna by fabricating the planar and bend part of the antenna separately and are pasted together with copper tape. Finally, an original three dimensional PIFA antenna has been successfully designed and fabricated.

Chapter 4 highlighted the potential use of inkjet printing for the realization of MID devices. Low-cost thermoplastic Acrylonitrile Butadiene Styrene PolyCarbonate (ABS PC) substrate is selected for its promising mechanical and thermal properties. The measurements of 50 Ω transmission lines in CPW and microstrip technologies allowed the extraction of relative permittivity, RF losses and quality factor. Inkjet printing of silver nano ink was used to fabricate those CPW and microstrip lines on the top of a 2 mm thick ABS PC. The results showed a nearly constant substrate relative permittivity at 2.8 from both technologies. Electrical characterization also showed that the conductive losses predominate dielectric losses and thus confirm the low loss property of the substrate. In order to reduce conductive losses, the conductor thickness should be increased. Based on these characterization results, an inkjet printed microstrip patch antenna and UWB antenna were designed and realized. Measurements are in good agreement with electromagnetic simulations for both antennas. The UWB antenna exhibits a -10dB reflection coefficient bandwidth from 3 GHz to 13 GHz

with a maximum gain of 4.2 dB. The focus of the research has been then into the study of the compatibility of low cost LCP E130i thermoplastic in inkjet printing fabrication. Since the surface roughness of LCP substrate is high (8-9µm), surface planarization has been adopted before moving on to the design of RF circuits on it. Planarization has been done with the help of UV/O_3 treatment. Surface planarized LCP substrate is then used for the design of transmission lines and low pass filters. Successful measurement responses have obtained from these inkjet fabricated devices, and have low quality factor compared to LDS lines.

Laser Subtractive Structuring (LSS), also called as laser ablation techniques was the yet another and final fabrication method of MID RF devices used in this thesis and chapter 6 dealt with its discussions and conclusions. As mentioned before in the thesis, LSS is an MID fabrication technique which does not require any special kind of thermoplastics for RF fabrication. The chapter discusses the realization of RF circuits using laser ablation technique on LCP E130i substrate. Similar to the studies discussed in chapter 4 and 5, RF properties' extraction have been carried out by taking into account two 50 Ω microstrip transmission lines on bare LCP E130i. The results showed a quality factor of 56 at 2 GHz, which is quite high value in comparison with that obtained from inkjet printed technology. In this chapter, a combination of special additive charges with classical thermoplastics such as PolyEthylene (PE), PolyStyrene (PS) have been introduced for the improvement of dielectric permittivity of the substrates. The characterized results of the newly developed substrates showed an improvement in the permittivities in all the experimented substrates. A novel High K thermoplastic material has got high permittivity value among the other experimented materials and is nearly of 8.5 which had further been used for the successful design of miniaturized directional coupler and transmission lines.

To conclude, the thesis work showed the possibility of choosing MID technology for RF applications. The thesis thus holds a collective record of information of MID RF performances, more into theoretical analysis and basic RF studies and some practical industrial application implementations.

7.2. Future work

The thesis can propose several ideas for MID technology in RF field as an extension to the work concluded in this chapter. If we start with one of the difficulties that have faced during this thesis, the complications to solder/paste the connectors with the MID devices, future work can be focused on to the development of integrated or implanted connectors

along with the devices to access the signal lines for measurement. The difficulties would be more if it comes to the inkjet printed MID devices. Since, soldering connectors in inkjet printed MID devices is not possible and de soldering of connectors in LDS devices may damage the circuit which leads to the proposition of such idea. Due to the time limitation of the thesis, the authors could not explore well the advantages of high permittivity thermoplastics and thus the thesis proposes the use of high permittivity materials for the development of three dimensional MID devices along with LDS fabrication technology. Scopes of developing three dimensional RF devices are more (the laboratory LCIS has already working on the implementation of RFID technology in combination with MID technology for the development of UHF RFID tags). The work can be further extended deeply to the miniaturized three dimensional RFID products. Immense scope of three dimensional device implementation is existing and lot more future RF MID products can be developed making the current thesis as a first book of basic studies on RF MID passive devices.

List of Publications

Peer-reviewed Publications Published

1. **Divya Unnikrishnan**, Darine Kaddour, Smail Tedjini, Eloise Bihar and Mohammed Saadaoui, "CPW-fed Inkjet Printed UWB Antenna on ABS-PC for Integration in Molded Interconnect Devices Technology, " IEEE Antennas and Wireless Propagation Letters (AWPL), 2014.

Peer-reviewed Publications Proposed

1. **Divya Unnikrishnan**, Darine Kaddour and Smail Tedjini, " A High Permittivity Thermoplastic Material for MID Technology and RF Applications," IEEE Microwave and Wireless Components Letters (submitted).
2. **Divya Unnikrishnan**, Darine Kaddour, Smail Tedjini, Eloise Bihar and Mohammed Saadaoui, "Inkjet Printed Molded Interconnected Devices on Planarized Liquid Crystal Polymer," Applied Physics Letters (APL) (to be submitted).
3. **Divya Unnikrishnan**, Darine Kaddour and Smail Tedjini, " Electrical Characterization of Molded Interconnect Devices by Laser Direct Structuring," Progress in Electromagnetics Research Symposium (PIERS) Proceedings (to be submitted).

Conferences Presented

1. **Divya Unnikrishnan**, Darine Kaddour and Smail Tedjini, " RF Circuit Design on Molded Interconnect Devices," International Symposium on Antennas and Propagation (APSYM), 17-19 December 2014, Cochin, India.
2. **Divya Unnikrishnan**, Darine Kaddour and Smail Tedjini, " Microstrip Transmission Lines and Antennas on Molded Interconnect Devices Materials", Mediterranean Microwave Symposium (MMS), 02-05 September 2013, Saida, Lebanon.
3. Ousamma Benzaim, Eloise Bihar, Darine Kaddour, **Divya Unnikrishnan**, Smail Tedjini and Mohammed Saadaoui, "Photonic Sintering and RF Performances of Inkjet Printed Transmission Lines," Large-Area, Organic and Printed Electronics Convention (LOPE-C), 12-13 June 2013, Munich, Germany.

4. **Divya Unnikrishnan**, Darine Kaddour and Smail Tedjini, " Performances RF de Circuits MIDs réalisés par LDS," Journées Nationales Microondes (JNM), 14-17 May 2013, Paris, France.

5. **Divya Unnikrishnan**, Darine Kaddour, Smail Tedjini, Eloise Bihar and Mohammed Saadaoui, " Ligne et Antenne MID réalisées par Impression Jet d'encre sur ABS PC"," Journées Nationales Microondes (JNM), 14-17 May 2013, Paris, France.

6. **Divya Unnikrishnan,** Darine Kaddour and Smail Tedjini, "Molded Interconnect Devices for RF Applications: Transmission Lines and Low Pass Filters", International Symposium on Signals, Systems and Electronics (ISSSE), 03-05 October 2012, Potsdam, Germany.

Conferences Proposed

1. **Divya Unnikrishnan**, Darine Kaddour and Smail Tedjini, " Facteur de qualité de lignes de transmission micro ruban sur la technologie MID," Journées Nationales Microondes (JNM), 02-05 June 2015 (submitted).

POTENTIEL DE LA TECHNOLOGIE MID POUR LES COMPOSANTS PASSIFS ET DES ANTENNES

Résumé :
La technologie MID (Molded Interconnect Device), fait de leur performance électrique, la flexibilité dans les circuits RF, le potentiel de réduire le nombre de composants, les étapes du processus et la miniaturisation du produit final, a conduit à de nouvelles contraintes à la RF (Radio Frequency) et le domaine des micro-ondes. Composants moulés sont interconnectées avec des substrats thermoplastiques et les pistes conductrices sont injectés sur la surface. L'objectif de cette thèse est d'étudier la compatibilité de MID pour les applications RF. Les avantages de la technologie MID dans le domaine RF est exploitée pour les lignes de transmission, filtres passifs, coupleurs directionnels et antennes réalisation. La caractérisation RF de différents matériaux de substrat MID et l'étude de la performance des composants RF ci-dessus sur la base de différentes technologies de fabrication MID sont inclus dans la thèse. Enfin, le concept d'une étude d'amélioration de la permittivité de certains thermoplastiques sont également étudiés.

Mots-clés : caractérisation de substrats thermoplastiques, lignes de transmission CPW, microruban et stripline, conception d'antennes 2D et 3D, filtres passifs et de coupleurs directionnels, différentes technologies de fabrication MID LDS, Impression jet d'encre et LSS, amélioration de la permittivité de thermoplastiques.

MID TECHNOLOGY POTENTIAL FOR RF PASSIVE COMPONENTS AND ANTENNAS

Abstract:
MID (Molded Interconnect Devices) technology, owing to their electrical performance, flexibility in RF circuits, its potential to reduce the number of components, process steps and miniaturization of the final product, has led to some new constraints to the RF (Radio Frequency) and microwave domain. Molded components are interconnected with thermoplastic substrates and conductive traces are injected on the surface. The objective of this thesis is to study the compatibility of MIDs for RF applications. The advantages of MID technology in the RF domain is exploited for transmission lines, passive filters, directional couplers and planar and 3D antennas realization. The RF characterization of various MID substrate materials and the study of the performance of the above RF components based on various MID fabrication technologies are included in the thesis. Finally, an permittivity improvement study of some thermoplastics are also studied.

Keywords: thermoplastic substrate characterization, transmission lines in CPW, microstrip and stripline, design of 2D and 3D antennas, passive filters and directional couplers, different MID fabrication techniques LDS, inkjet printing and LSS, thermoplastic permittivity improvement study.